

REPORT DOCUMENTATION PAGE

Form Approved
OMB No. 0704-0188

Public reporting burden for this collection of information is estimated to average 1 hour per response, including the time for reviewing instructions, searching existing data sources, gathering and maintaining the data needed, and completing and reviewing the collection of information. Send comments regarding this burden estimate or any other aspect of this collection of information, including suggestions for reducing this burden, to Washington Headquarters Services, Directorate for Information Operations and Reports, 1215 Jefferson Davis Highway, Suite 1204, Arlington, VA 22202-4302, and to the Office of Management and Budget, Paperwork Reduction Project (0704-0188), Washington, DC 20503.

1. AGENCY USE ONLY (Leave blank)			2. REPORT DATE	3. REPORT TYPE AND DATES COVERED
			9 Jan 97	
4. TITLE AND SUBTITLE			5. FUNDING NUMBERS	
The Effects of Secondary Flows on the Convective Heat Transfer from a Heated Block in an Airstream				
6. AUTHOR(S)				
Scott E. LeClaire				
7. PERFORMING ORGANIZATION NAME(S) AND ADDRESS(ES)			8. PERFORMING ORGANIZATION REPORT NUMBER	
University of Maine			96-132	
9. SPONSORING/MONITORING AGENCY NAME(S) AND ADDRESS(ES)			10. SPONSORING/MONITORING AGENCY REPORT NUMBER	
DEPARTMENT OF THE AIR FORCE AFIT/CIA 2950 P STREET WPAFB OH 45433-7765				
11. SUPPLEMENTARY NOTES				
12a. DISTRIBUTION AVAILABILITY STATEMENT			12b. DISTRIBUTION CODE	
Unlimited				
13. ABSTRACT (Maximum 200 words)				
<p style="text-align: right; margin-top: 100px;">19970117 124</p>				
14. SUBJECT TERMS			15. NUMBER OF PAGES	
			304	
			16. PRICE CODE	
17. SECURITY CLASSIFICATION OF REPORT	18. SECURITY CLASSIFICATION OF THIS PAGE	19. SECURITY CLASSIFICATION OF ABSTRACT	20. LIMITATION OF ABSTRACT	

**The Effects of Secondary Flows
on the Convective Heat Transfer from a
Heated Block in an Airstream**

by

Scott E. LeClair

A THESIS

Submitted in Partial Fulfillment of the
Requirements for the Degree of
Master of Science
(in Mechanical Engineering)

The Graduate School
University of Maine

May, 1996

Advisory Committee:

Michael T. Boyle, Associate Professor of Mechanical Engineering, Thesis Advisor
William C. Rivard, Professor of Mechanical Engineering
Justin H. Poland, Associate Professor of Mechanical Engineering
James Sucec, Professor of Mechanical Engineering

The Effects of Secondary Flows
on the Convective Heat Transfer from a
Heated Block in an Airstream

by Scott E. LeClair

An Abstract of the Thesis Presented in Partial
Fulfillment of the Requirements of the Degree of
Master of Science (in Mechanical Engineering)
May, 1996

A detailed investigation into the secondary flow effects on the convective heat transfer from a heated, low-profile, block in an airstream is presented. The block surfaces are heated by driving a direct current through stainless steel strips, adhered in a series circuit configuration on the block's surfaces. Measurements of the temperature distributions, on the front, top, rear, and lateral block surfaces, are taken via an automated data acquisition system equipped with 79 resistive type temperature sensors. The temperature sensors are installed between the stainless steel strips and the block substrate material. From the temperature measurements, local surface coefficient of heat transfer values are reduced, by performing an energy balance on a small region of stainless steel in the vicinity of each sensor. An overall, three-dimensional, convection heat transfer description for the block, at a Reynold's number (based on the block height) of approximately 21000 is presented. Also investigated are the heat transfer effects produced by varying freestream flow Reynold's number and average Grashof number. Further elaborating the flow field conditions present on the block's cover surface, flow visualization studies, using a modified ink-dot and oil of wintergreen method, are conducted. These studies are performed at freestream flow Reynold's numbers of 15000, 22000, 33000, and 51000.

Acknowledgments:

The author gratefully acknowledges the contributions of the University of Maine's Department of Mechanical Engineering community, without whom this work would not have been possible. K. A. Asante provided his skill in the construction of the heated block and board assembly. James Van Sandt and Peter Guyette provided their efforts and guidance in the creation and support of the computer data acquisition systems. Arthur Pete and Steve Webber facilitated the experimental equipment installations and the maintenance of the wind tunnel laboratory. Sincerest thanks are expressed to associate professor Michael Boyle for initiating the project, and providing enduring guidance and direction throughout the entire thesis process.

Lastly, the author would like to dedicate this work to his wife, Dina, and son, Alden. Their unconditional support and encouragement provided the drive required to pursue and accomplish this work.

Table of Contents:

	Acknowledgements.....	ii
I.	List of Tables	v
II.	List of Figures	vii
III.	Nomenclature	x
IV.	Introduction.....	1
V.	Background.....	3
VI.	Experimental Apparatus and Set-up	
	A. Experimental Block and Board Assembly	12
	B. Heat Transfer Data Monitoring and Recording Systems.....	17
	C. Flow Visualization Study Procedures.....	23
	D. Wind Tunnel Test Facility	25
VII.	Testing Conditions	28
VIII.	Data Reduction Scheme	30
IX.	Uncertainty.....	36
X.	Results	
	A. Block Cover Flow Visualization Testing	39
	B. Three-Dimensional Heat Transfer Description.....	47
	C. Effect of Reynold's Number.....	60
	D. Effect of Grashof Number.....	71
XI.	Conclusions	87
XII.	References	94
XIII.	Appendices	
	A. Miscellaneous Tables and Figures	96
	B. RTD Calibration Procedure and Data	100

C.	Detailed Uncertainty Analysis	111
D.	Data Acquisition and Calibration Software.....	118
E.	Equipment Listing.....	140
F.	Testing Data Tables and Figures	141
G.	Flow Visualization Test Modification	300
XIV.	Biography of the Author	304

I. List of Tables:

Table 1:	Experimental Testing Conditions.....	29
Table 2:	Test Data Uncertainty	38
Table 3:	Specific Average Uncertainties	38
Table A-1:	Property Analysis Table	99
Table B-1:	Hotbox Low Temperature Calibration Data	103
Table B-2:	Low Temperature Sensor Calibration Equations and Performance.....	105
Table B-3:	Hotbox High Temperature Calibration Data	107
Table B-4:	High Temperature Sensor Calibration Equations and Performance.....	109
Table C-1:	Uncertainty Analysis Summary	116
Table F-1:	Example Test Data Log	142
Table F-2 to F-7:	Testing Data Tables Test 10-25_1.....	143
Table F-8 to F-13:	Testing Data Tables Test 10-30_1.....	154
Table F-14 to F-19:	Testing Data Tables Test 11-01_1a.....	164
Table F-20 to F-25:	Testing Data Tables Test 11-02_1.....	174
Table F-26 to F-31:	Testing Data Tables Test 11-13_1.....	184
Table F-32 to F-37:	Testing Data Tables Test 11-14_1.....	194
Table F-38 to F-43:	Testing Data Tables Test 11-15_1.....	204
Table F-44 to F-49:	Testing Data Tables Test 11-21_1.....	214
Table F-50 to F-54:	Testing Data Tables Test 12-11_1.....	224

Table F-55 to F-59:	Testing Data Tables Test 12-12_1.....	233
Table F-60 to F-64:	Testing Data Tables Test 12-14_1.....	242
Table F-65 to F-69:	Testing Data Tables Test 12-14_2.....	251
Table F-70 to F-75:	Testing Data Tables Test 01-31_1.....	260
Table F-76 to F-81:	Testing Data Tables Test 02-01_1.....	270
Table F-82 to F-87:	Testing Data Tables Test 02-21_1.....	280
Table F-88 to F-93:	Testing Data Tables Test 02-27_1.....	290

II. List of Figures:

Figure 1:	Two-Dimensional Blunt Plate Set-up.....	3
Figure 2:	Three-Dimensional Qualitative Flow Description.....	11
Figure 3:	Block and Board Assembly - Top View	12
Figure 4:	Block and Board Assembly - Side View	12
Figure 5:	Block and Board Assembly - Front View	13
Figure 6:	RTD Mounting Detail.....	15
Figure 7:	Monitoring and Recording System Detail	17
Figure 8:	Model Orientation Detail.....	19
Figure 9:	Wind Tunnel Detail	25
Figure 10:	Wind Tunnel Test Section Detail.....	26
Figure 11:	Temperature Sensor Control Volume Detail.....	30
Figure 12:	Block Cover Flow Visualization $N_{Re} = 15030$, Freestream Velocity = 455 FPM	40
Figure 13:	Block Cover Flow Visualization $N_{Re} = 21802$, Freestream Velocity = 660 FPM	41
Figure 14:	Block Cover Flow Visualization $N_{Re} = 33034$, Freestream Velocity = 1000 FPM	42
Figure 15:	Block Cover Flow Visualization $N_{Re} = 51202$, Freestream Velocity = 1550 FPM	43
Figure 16:	Reattachment Length vs. Reynold's Number (Cover Surface)	45
Figure 17:	Coordinate System Detail	47
Figure 18:	3-D Composite Temperature Difference Surface Plot Tests 11-13, 14 (Cover Surface).....	48
Figure 19:	3-D Composite Nusselt Number Surface Plot Tests 11-13, 14 (Cover Surface).....	49
Figure 20:	Tests 11-13, 14: Composite Nusselt Number Contour Chart (Cover Surface)	50
Figure 21:	Test 01-31_1: Nusselt Number Contour Chart (Front Surface)	51

Figure 22:	Test 11-13_1: Nusselt Number Contour Chart (Left Lateral Surface).....	52
Figure 23:	Test 02-01_1: Nusselt Number Contour Chart (Rear Surface).....	53
Figure 24:	3-D Composite Nusselt Number Surface Plot Tests 11-01, 02 (Cover Surface)	61
Figure 25:	Tests 11-01, 02: Nusselt Number Contour Chart (Cover Surface)	62
Figure 26	Test 11-02_1: Nusselt Number Contour Chart (Left Lateral Surface)....	63
Figure 27:	Test 10-30_1: Nusselt Number Contour Chart (Front Surface)	64
Figure 28:	3-D Composite Nusselt Number Surface Plot Tests 11-15, 21 (Cover Surface)	65
Figure 29:	Tests 11-15, 21: Nusselt Number Contour Chart (Cover Surface)	66
Figure 30:	Test 11-21_1: Nusselt Number Contour Chart (Left Lateral Surface)....	67
Figure 31:	Standard Deviation in Nusselt Number vs. Reynold's Number.....	68
Figure 32:	Average Nusselt Number vs. Reynold's Number (Grashof Number Fixed at Approximately 3×10^7)	69
Figure 33:	3-D Composite Temperature Difference Surface Plot Tests 12-11, 02-21 (Cover Surface).....	72
Figure 34:	3-D Composite Nusselt Number Surface Plot Tests 12-11, 02-21 (Cover Surface).....	73
Figure 35:	Tests 12-11, 02-21: Nusselt Number Chart (Cover Surface)	74
Figure 36:	Test 02-21: Nusselt Number Chart (Left Lateral Surface)	75
Figure 37:	3-D Composite Temperature Difference Surface Plot Tests 12-12, 02-27 (Cover Surface).....	76
Figure 38:	3-D Composite Nusselt Number Surface Plot Tests 12-12, 02-27 (Cover Surface).....	77
Figure 39:	Tests 12-12, 02-27: Nusselt Number Contour Chart (Cover Surface)	78
Figure 40:	Test 02-27: Nusselt Number Contour Chart (Left Lateral Surface)	79

Figure 41:	Test 10-25_1: Nusselt Number Contour Chart (Front Surface)	80
Figure 42:	Standard Deviation in Nusselt Number vs. Grashof Number (Cover Surface)	81
Figure 43:	Average Grashof # vs. Average Nusselt # (Cover Surface)	82
Figure 44:	Standard Deviation in Nusselt Number vs. Grashof Number (Left Lateral Surface)	84
Figure 45:	Average Grashof # vs. Average Nusselt # (Left Lateral Surface).....	85
Figure A-1:	Electrical Wiring Diagram.....	97
Figure A-2:	Test Section Photograph	98
Figure C-1:	Heat Transfer Coefficient Uncertainty Contributions (For 3-D Heat Transfer Description Tests)	117
Figures F-1 to F-32:	Testing Data Temperature Distribution and Heat Transfer Coefficient Distribution Surface Plots.....	152
Figure G-1:	Un-Modified Flow Visualization Freestream Velocity = 455 FPM.....	301
Figure G-2:	Modified Flow Visualization Freestream Velocity = 455 FPM.....	302

III. Nomenclature:

Abbreviations:

A	Area (as noted)
CCW	Counter-Clockwise
deg	Degrees
Diff	Difference
F	Shape Factor
Fr	Front Face of Block
g	Acceleration of Gravity (32.174 ft/s ²)
h	Convection Heat Transfer Coefficient (Btu/hr-ft ² -'F)
H	Height of the Block
I	Current (amps)
K	Thermal Conductivity (Btu/hr-ft-'F)
L	Length of Block
N _{Re}	Reynold's Number
N _{Gr}	Grashof Number
N _{Nu}	Nusselt Number
q	Rate of Heat Transfer (Btu/hr)
R	Resistance (ohms)
RTD	Resistive Temperature Device
T	Temperature (as noted)
ΔT	Temperature Difference
Temp	Temperature (as noted)
U	Velocity (ft/s)
V	Voltage (volts)

W	Width of the block
β	Thermal Expansion Coefficient
ϵ	Emmissivity
ρ	Density (lbm/ft ³)
σ	Stefan-Boltzmann Constant (1.71234×10^{-9} Btu/hr-ft ² -'R ⁴)
μ	Absolute Viscosity (lbm/ft-s)

Subscripts:

ave	Average
back	Conduction, Through G-10 Block Substrate
cond	Conduction, in Stainless Steel Strip
conv	Convection, from Block Surface
film	At Film Conditions
fs	Freestream
FST	Freestream Temperature
gen	Generation
r	Reattachment
rad	Radiation
ss	Stainless Steel
tot	Total
xsect	Cross-Sectional
∞	of Bulk Unaffected Fluid

IV. Introduction:

In many practical engineering applications, designers must contend with the challenges of complex separating and reattaching secondary flows, resulting from bluff bodies immersed in a flow stream. The nature of the flow stream, and the geometrical shape of the body itself, both contribute to the structure and characteristics of the secondary flows produced in the vicinity of the body.

A common separating and reattaching flow scenario is that created when a floor mounted, low-profile rectangular block, is immersed in an airstream. One particularly prevalent example, is a semi-conductor chip mounted on a printed circuit board. In this setting, the chip acts as a block shaped thermal energy source, and the airstream a mechanism of heat dissipation. Considerable previous work has been conducted in areas of secondary flow research concerned with geometry similar to that of the above example. Little, however, can be classified as identical to the particulars of a semi-conductor chip's low-profile, rectangular, floor-mounted shape. Most past research deals with two-dimensional bluff plate flows, or three-dimensional cubic geometry flow scenarios. A few also include discussions concerning the effects complex secondary flows generate on the immersed body's heat transfer performance. The significance of past research, to the present work, is discussed herein.

More recently, advances in computing and instrumentation technology have expanded the capabilities of researchers, allowing them to deal with more complex three-dimensional flows, and the associated heat transfer. Often, research dealing with the rectangular block geometry similar to the electronic chip example is conducted solely by numerical modeling of the block and airstream conditions. It is the purpose of the present work, to provide a solid experimental foundation for the heated, low-profile, rectangular block scenario. The results presented provide detailed experimental data

describing the three-dimensional heat transfer performance of the block, along with effects observed in response to environmental changes in freestream Reynold's number and Grashof number. These fundamental results can form the basis of comparison for dynamically similar numerical research.

To attain the above results, an experimental investigation into the effects of secondary flows on the convection heat transfer from a heated, low-profile, block in an airstream is conducted. The experimental block surfaces are heated by driving a direct current through thin stainless steel strips, adhered in a series circuit configuration on the block surfaces. Measurements of the local surface temperatures, at various locations on the five exposed block surfaces (front, rear, top, and lateral sides), are taken via an automated data acquisition system equipped with 79 resistive type temperature sensors. The temperature sensors are installed between the stainless steel strips and the block's substrate material. With the surfaces' temperature distributions known, energy balances on small regions of stainless steel in the vicinity of each sensor are performed, and local surface coefficient of heat transfer values deduced. From the energy balance data, a three-dimensional convection heat transfer description for the entire block, at a Reynold's number based on the block height of approximately 21000, is constructed. Heat transfer effects produced by varying freestream flow Reynold's number and average Grashof number are also investigated and described.

To gain a better understanding of the flow field conditions present on the block's top surface, flow visualization studies are conducted. The studies are performed using a modified ink-dot and oil of wintergreen method, similar to that developed by Langston and Boyle (1982). These studies are performed at freestream flow Reynold's numbers of 15000, 22000, 33000, and 51000.

V. Background:

Background research provides relevant information pertaining to the structure of the secondary flows produced when a relatively uniform flow impinges upon a bluff object. The majority of applicable previous works can be broadly classified into three related bodies of research: two dimensional, rectangular bluff plate flows; three dimensional, cubic geometry flows; and three dimensional, low-profile rectangular package flows. Each of these bodies of work provides its own distinct set of findings, which when appropriately combined, provides insight into the factors important to the present work.

Two dimensional Separating Flows:

While it is difficult to obtain quantitative comparisons from two-dimensional rectangular bluff plate experiments, they do provide indications as to the qualitative nature and characteristics of flow over the rectangular, low-profile, block of the present work. Extensive research has been conducted for the thin rectangular plate object placed incident to incoming flow as shown below:

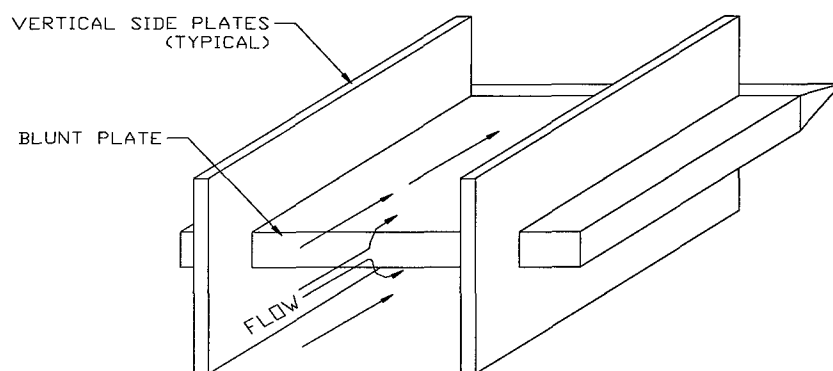


Figure 1

Two Dimensional Blunt Plate Set-up

In efforts to keep the flow field over the plate two-dimensional, most research incorporates the use of vertical endplates as shown. A detailed experiment was conducted by Djilali and Gartshore (1991), in which the above geometry was used and measurements of velocity field and surface static pressures were made using pulse wire anemometry and surface static pressure taps, respectively. The results of the experiment show the presence of a separation bubble structure beginning at the leading edge of the plate and extending to a reattachment line at approximately 4.7 plate thicknesses downstream. For Reynolds numbers including $25000 < N_{Re} < 90000$, based on plate thickness, Djilali and Gartshore found no significant change in the separation bubble reattachment length. The effect of Reynold's number on two-dimensional separated flow was further studied by Ota et. al. (1981), who also considered the effect of the plate's leading edge angle (also referred to as the separation angle). Ota et. al. observed three distinct flow regimes for bluff plate flow: (i) laminar separation - laminar reattachment, (ii) laminar separation - turbulent reattachment, and (iii) turbulent separation - turbulent reattachment. Shaw et. al. (1991) observed a bluff plate flow in regime (i) in which an increase in Reynold's number resulted in an increased separation bubble size, and thus reattachment length. Very little work has been done, and little is known about flows in regime (ii), but Ota et. al. did observe the presence of instabilities in the shear layer near separation, and a transition to turbulent flow at reattachment. Regime (iii) is the focus of much research, including the previously mentioned Djilali and Gartshore (1991) experiments. This regime has been characterized by a flow that becomes turbulent soon after separation, and a reattachment length that is independent of Reynold's number. In earlier work by Hillier and Cherry et. al. (1981), this transition of flow to regime (iii) was observed to occur for Reynold's number flows (based on plate height) of greater than 27000.

In the Hillier and Cherry et. al. paper, another factor found to have effect on the separation bubble structure is freestream turbulence. Their experiment observed a reduction in reattachment length from 4.88 plate thicknesses to 2.72 with an increase in the level of freestream turbulence intensity from 1.0 to 6.5 percent. This shortening of reattachment length with increases in freestream turbulence was further verified in two-dimensional works by Kiya and Sasaki (1983b) and Dziombia (1985). Dziombia further argued the observed turbulence effect could be better justified as an effective decrease in the separation angle. Later research on the issue of separation angle was expanded by Djilali (1992), where surface pressure distributions were measured as a function of separation angle. Results of the work show a 50 percent reduction in the separation bubble's reattachment length as the separation angle is decreased from 90 to 45 degrees.

Further two-dimensional studies on the blunt plate separating flow focused on the unsteadiness of the separation bubble structure. Studies by Hillier and Cherry (1981B), Hillier and Cherry et. al. (1983:1984), Kiya and Sasaki (1983b), and the previous Djilali and Gartshore (1991) observed the presence of a low frequency flapping of the shear layer near the leading edge, and a large scale shedding of vortices in pseudoperiodic bursts. Because of this unsteadiness, much of the literature reports a time-average separation line, defined as that series of points where the time-average of forward flow fractions equals 50 percent. To give a quantitative example, Djilali and Gartshore (1991) report of a broad region equal to 2.5 plate thicknesses about the time-average reattachment line where near wall flow can be moving instantaneously in either upstream or downstream directions.

It is important to note, the previously described two-dimensional flow research has some important differences that make quantitative comparisons between it and the

present work particularly difficult. Foremost is the absence of cross-stream velocity components present in this work's three-dimensional flow. The incorporation of vertical side plates in the blunt plate flows negate these components. Additionally, the bluff plate setup has flow both above and below the rectangular plate. This results in the absence of an incoming boundary layer, generated by the floor onto which the rectangular block setup is mounted. Both of these differences will undoubtedly affect the quantitative structure of the separation bubble.

Three Dimensional Separating Flows:

Another body of separating flow research has been conducted by experimenting with flows impinging on three-dimensional bluff objects. One example, applicable to the present work, is experimentation focused on separating flows produced when a cube is immersed in an airstream. While the geometry of a cube differs from that of the present work, the studies do provide insight into the structure of a three dimensional separating and reattaching flow field. A detailed experimental study, incorporating a wall mounted cube, was performed by Castro and Robbins (1977). Their study reveals a causal relationship between the incoming, upstream boundary layer thickness and the size of the separation bubble produced on the cube's cover. Results of surface pressure measurements taken in the experiment indicate a shortening of the separation bubble with an increase in the ratio of incoming boundary layer thickness to cube height. This result is particularly applicable to the present work, as a floor mounted, low-profile block experiences a similar build-up of upstream boundary layer thickness.

In another cubic geometry separating flow experiment, conducted by Chyu and Natarajan (1991), flow visualization by the oil-graphite method shows complex, interdependent surface flows produced by the interaction of the three-dimensional body,

mounting wall, and uniform freestream flow. Results of their experiment reveal the presence of a complex horseshoe shaped vortex system on the back side of the cube, and separating and reattaching flows initiated at the sharp leading edges of the cube's top and lateral surfaces. Closer examination of their results shows a significant difference between the separation bubble structure produced on the top surface of the three dimensional cube, and that produced on the surface of a two dimensional bluff plate. In particular, the three dimensional flow's separation bubble structure shows significant size variation in the cross-stream direction. The result is evident in the flow visualization, where the three dimensional separation bubble's reattachment line takes on the shape of an arch, with the ends of the arch near the corners of the leading edge, and its base near the stream-wise symmetry line. The previous two-dimensional studies, with flows contained within vertical side walls, lack any significant cross-stream variation in the separation bubble structure.

Some literature for three dimensional separating flow research performed on low aspect ratio rectangular blocks focuses on arrays of such objects. One such early work includes a numerical simulation study performed by Patankar (1977). Patankar's work resulted in a method for extrapolating flow data from an array subset to calculate periodic velocity correlations for the flow field around the entire object array. This work is particularly important to the rationale behind single object experimentation, such as the present work, since most applications dealing with rectangular blocks consist of many such objects arranged in various configurations within enclosures.

Another numerical simulation, focused on three dimensional flows produced by a low aspect ratio block in an airstream, was conducted by Shaw, Chen, and Chen (1991). The simulation provides a detailed description of the three dimensional secondary flows produced around the block, when immersed in a laminar uniform flow. Results show the

laminar flow field, around a three-dimensional block object, is substantially different than that found in two-dimensional simulations of the same geometry. This result is particularly evident on the rear surface of the block. Here, two-dimensional studies exhibit bounded recirculation regions, whereas the three-dimensional counterparts show initial recirculation, accompanied by a spiraling out of the fluid into the downstream flow.

Heat Transfer in Separating Flows:

Studies concerned with the heat transfer performance of bodies within a separating flow region have particular importance to the understanding of the present work. Two dimensional bluff plate flow experiments have experimenters attempting to investigate the effects of a separation bubble on the heat transfer characteristics from a plate in the stream-wise direction. In a paper by Ota and Kon (1974), a bluff rectangular heated plate was fitted with thermocouples to measure surface temperatures for determination of surface heat transfer coefficients. Results of the experiment show a separation bubble similar in structure to those described in the previous two dimensional experiments, with a reattachment length of approximately four times the plate thickness, for Reynold's number flows (based on plate thickness) in the 2720 to 17900 range. The results of the experiment also indicate the local heat transfer coefficient rises sharply from the plate's leading edge, to a maximum value at the location of flow reattachment. Beyond reattachment, the heat transfer coefficient steadily decreases, approaching the value for the turbulent boundary layer on a flat plate. The study also shows the average heat transfer coefficient to be 30 to 50 percent larger than that provided by the Colburn equation. This is postulated to be a result of increased turbulence intensity for the flow as compared to normal flat plate flow without separation and reattachment.

In Chyu and Natarajan's (1991) cubic geometry study, local Nusselt number distributions around the surfaces of a wall mounted cube are constructed, via an analogous naphthalene sublimation mass transfer experiment. Results of the experiment show the separation bubble structures present on the cover and lateral surfaces are the primary features of the flow field responsible for the transport characteristics around the cube. These surfaces are hypothesized to be completely engulfed in separation zones, and greatest transport rates are found on the upstream corners of the side surfaces. This important result cannot be investigated in two dimensional bluff plate flow experiments.

In Shaw, Chen, and Chen's (1991) three dimensional numerical prediction, calculations of the natural and mixed convection heat transfer environment and the effects of Reynold's and Grashof number variance are presented. The results concerned with Reynold's number effects, show significant enhancement of the overall heat transfer performance of the block surfaces produced by increases in the recirculation region coverage. Additionally, Grashof number changes are shown to modify the relative significance a particular block surface has on the overall heat transfer effectiveness. Most notably, for low Grashof numbers the cover surface of the block dominates heat transfer performance, followed by the front and lateral surfaces, respectively. As the Grashof number is increased (at a fixed Reynold's number), results show the lateral surfaces becomes the dominate heat transfer surfaces, followed by the front, and lastly, the cover.

Another study, by Wirtz (1994), includes direct measurement of the convective heat transfer distribution at 15 locations over the five exposed surfaces of a low profile (length to height ratio = 6) block. The block is part of an array of such objects, floor mounted in a low aspect ratio air flow channel. Results of the experiment are reported

for Reynold's numbers from 3000 to 7000. They show the average top surface heat transfer coefficient is close to the average for the entire package. The highest heat transfer rates indicated are present on the upstream face and sides. Additionally, the results show the local heat transfer coefficient on the cover is greatest near the upstream edge and steadily decreases in the direction of flow. It should be noted that arrays of blocks, in low Reynold's number ranges, do not exhibit a separation bubble on the cover surface. The work does, however, have important implications for the heat transfer characteristics of this experiment, particularly downstream of the cover's separation bubble.

The Wardwell (1993) Experiment:

One last study, whose flow field results are highly indicative of those further investigated in the present work, was performed by Wardwell (1993). Wardwell's study is focused on a detailed investigation of the separation bubble structure above the cover of a low profile rectangular block. Two dimensional velocity flow fields are mapped using laser Doppler velocimetry measurements. Results of the study reveal the presence of a single vortex separating at the leading edge of the block and reattaching at 1.43 block heights downstream on the symmetry plane, for a Reynold's number flow (based on block height) of 12600. The vortex is further characterized as the joining of two recirculation patterns, having their largest length on the symmetry plane and decreasing their reattachment lengths to zero at the block edges. A qualitative picture of three-dimensional flow described in Wardwell (1993) is shown in figure 2.

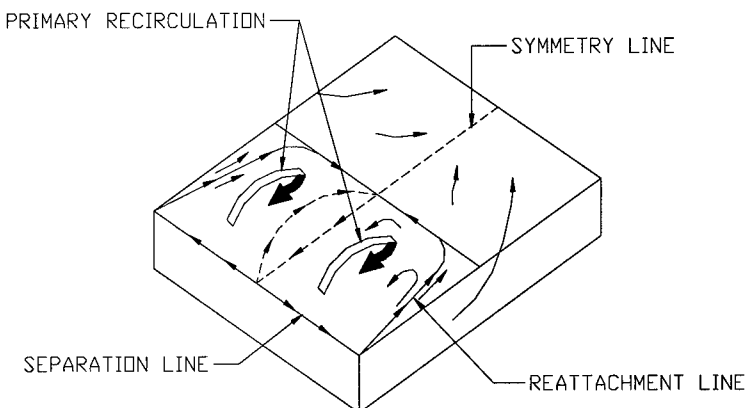


Figure 2

Three-Dimensional Qualitative Flow Description

The study goes on to show the dependence of the reattachment length on Reynold's number by investigating separation bubble structure changes for the Reynold's numbers 2300 and 12600. Additionally, the experimental block was studied for heated and unheated cases in efforts to describe the effects of Grashof number on the separation bubble. For the two Grashof numbers of investigation, 3.19×10^4 and zero, no noticeable effects were observed on the separation bubble structure or velocity distribution. Wardwell's work is of particular importance to this experiment, as the rectangular blocks subject to investigation are geometrically similar, and the exact same wind tunnel test section is used. Qualitative, as well as quantitative comparisons should reveal characteristically consistent results if the flow scenarios are also dynamically scaled.

VI(A). Experimental Block and Board Assembly:

The low profile block, surrounding heated board, and flow plate assemblies in the present work are detailed in figures 3 through 5.

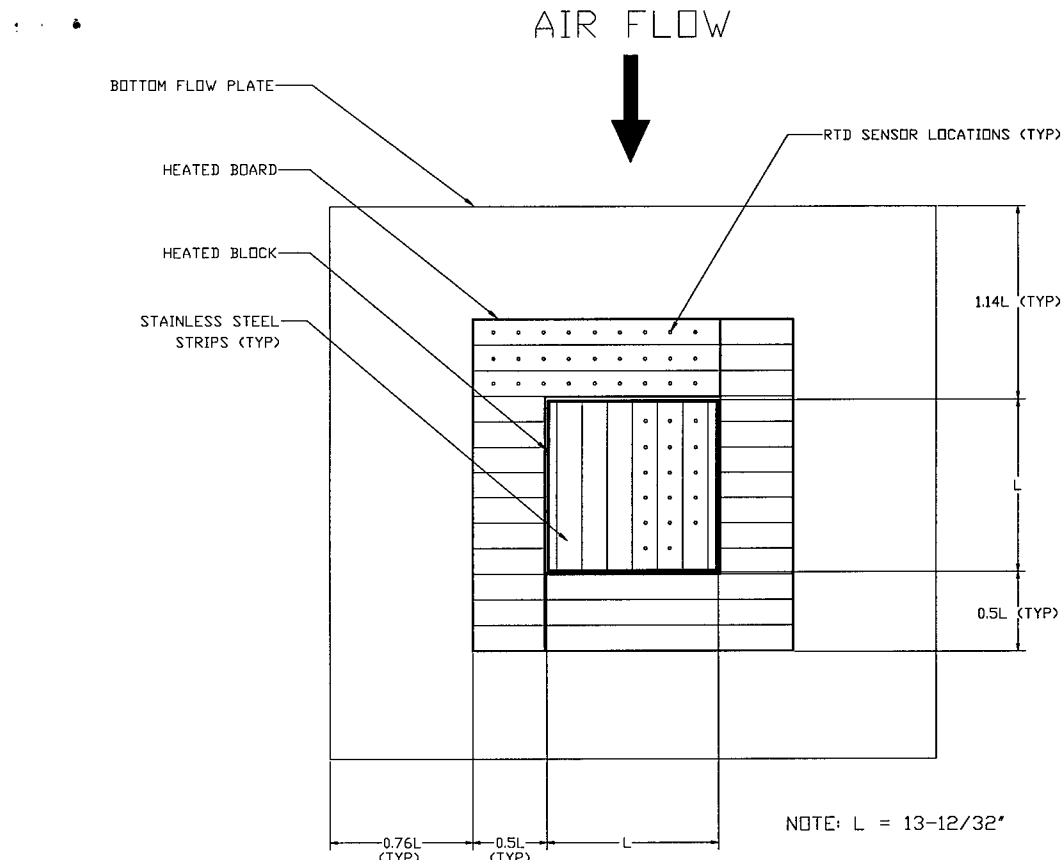


Figure 3
Block and Board Assembly - Top View

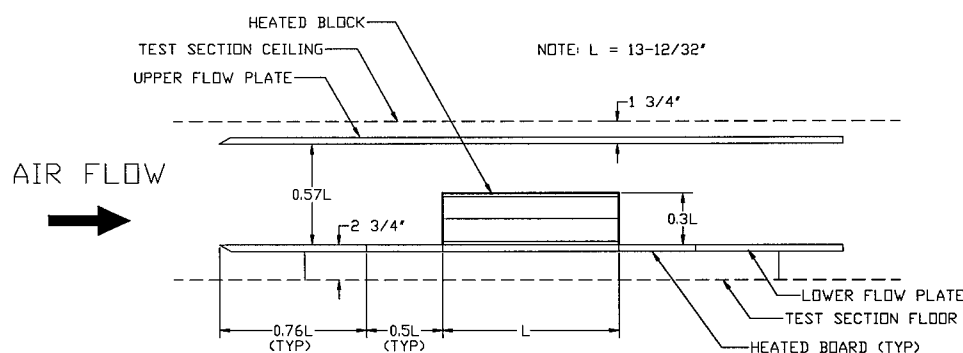


Figure 4
Block and Board Assembly - Side View

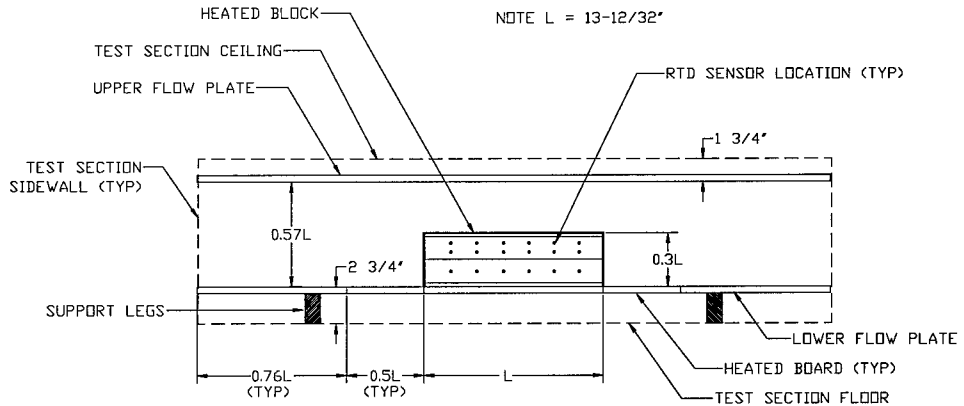


Figure 5

Block and Board Assembly - Front View

The entire assembly consists of an instrumented heated block, instrumented heated board assembly, top and bottom flow plates, and supporting floor framework.

The heated block is constructed similar to a hollow box, with exterior dimensions of 13-12/32 in wide x 13-12/32 in long x 4 in high. The block is mounted within a heated board assembly that wraps symmetrically around the entire box. A photograph of the block and lower flow plate assembly is located in Appendix A as figure A-2. The box is supported by a wooden structure attached to the floor of the wind tunnel test section. The support structure extends through the floor of the test section and allows for easy block height adjustment. The surrounding board structure is 6-22/32 inch wide and is electrically and thermally isolated from the heated box by a 1/32 inch thick plastic shim. The board assembly is supported off the wind tunnel's test section floor by 2 inch high wooden legs. A Plexiglas flow plate with sharp leading edge surrounds the board structure. With the addition of the floor plate, the entire bottom assembly dimensions become 43.5 in long by 47 in wide. Directly above the heated box, and surrounding bottom flow plate, is the upper flow plate. This plate is constructed of 3/4 in plywood, has a sharp leading edge, and dimensions identical to the bottom flow plate. The plate is supported by 1/2 inch diameter threaded rods attached to the wind tunnel's test section

ceiling. The threaded rods allow for precise adjustment of the vertical spacing between the upper flow plate and box top surface. For the purposes of the present work, the upper flow plate is adjusted to 7-20/32 inches above the bottom flow plate. At this height, the plate is 3-20/32 inches above the top surface of the heated block's cover. These dimensions were specifically chosen to ensure consistent geometric scaling of this experiment's block and board assembly with that of Wardwell's (1993).

The heated block structure itself is fabricated from rigid, 1/2 inch thick, G-10 fiberglass plates secured together with countersunk machine screws. The five exposed surfaces of the block are covered with stainless steel strips arranged in a series circuit configuration. The stainless steel strips are cut from 2 in wide by one thousandth of an inch thick roll stock. The strips are adhered to the surfaces of the block with 2 thousandths of an inch thick double sided adhesive strips manufactured by the 3M Corporation for high temperature applications. The strips of stainless steel are separated from each other along the block surfaces with gaps of approximately 1/16th of an inch. The strips are then jumpered together in a serpentine manner with 1/8 inch wide copper strips, completing the series circuit as designed. Micro-Measurements Group Inc. ETG-50B RTD's, with nickel foil sensing areas, are mounted between the block's G-10 substrate and stainless steel strips for measurement of the surface temperature distribution,. A cross-section diagram of the mounting installation is shown in figure 6:

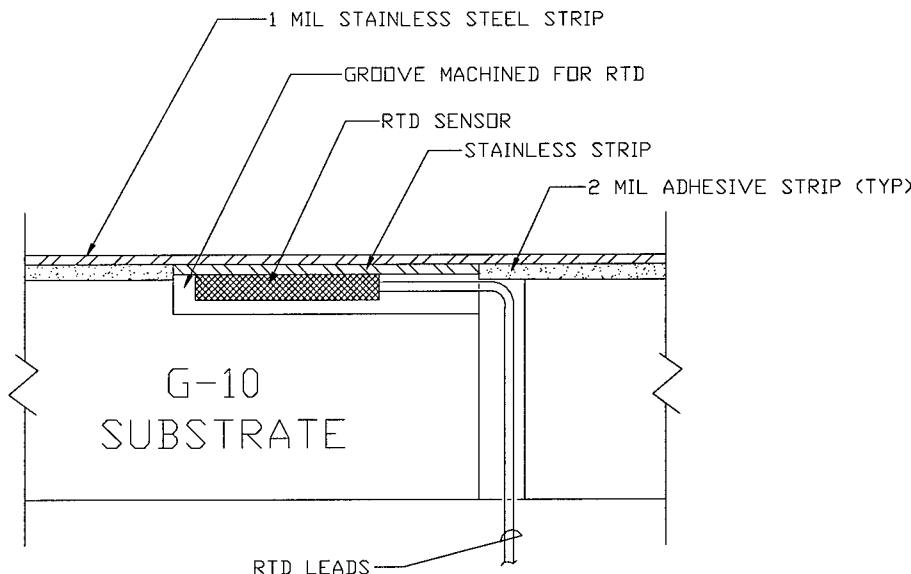


Figure 6

RTD Mounting Detail

The effective sensing area of each sensor is 0.1 inches x 0.1 inches. The RTD's are mounted similarly to the procedures used for mounting resistive type strain gauges. Each sensor is adhered to a small piece of stainless in direct contact with the stainless steel strips at the air flow surface. Additionally, small grooves are machined into the G-10 to provide mounting depressions and instrumentation wire raceways. This machining keeps the air flow surface of the block smooth. On the block surfaces, 41 RTD's are installed at locations on the cover and one side of the block as shown in figures 3 through 5. By rotating the block within the lower flow plate assembly, all five surfaces of the block can be fully investigated. An additional eight sensors are mounted on the inside surfaces of the block. The sensors mounted on the interior surfaces are provided for determination of the energy conducted transversely from the heated stainless through the G-10 material. RTD type temperature sensors are resistive in nature, and as such, respond not only to temperature change, but also mounting surface strain. For this reason each sensor is precisely calibrated for its own particular installation and

application. The calibration results in an accuracy, for each sensor, of +/- 0.5 degrees Fahrenheit. The calibration process and results is detailed in Appendix B.

The surrounding heated board structure is constructed similar to the heated box. The board assembly consists of two L-shaped sections that are fit around the heated box as illustrated. Each of the L-sections is covered by heated stainless steel strips arranged in a series circuit configuration. The strips are installed in the same manner as described above for the heated box. One of the L-sections is fitted with 27 RTD surface sensors located as shown in figure 3. Additionally, three RTD sensors are installed on the back side of the G-10 substrate for measurement of the backside temperatures. The L-sections are electrically coupled by 18 gauge insulated wiring. The final electrical arrangement puts each of the L-sections in series with each other, and the heated box, allowing for a direct current to be driven through all components at a constant rate. Figure A-1 of Appendix A presents an electrical wiring diagram of the entire circuit.

VI(B). Heat Transfer Data Monitoring and Recording Systems:

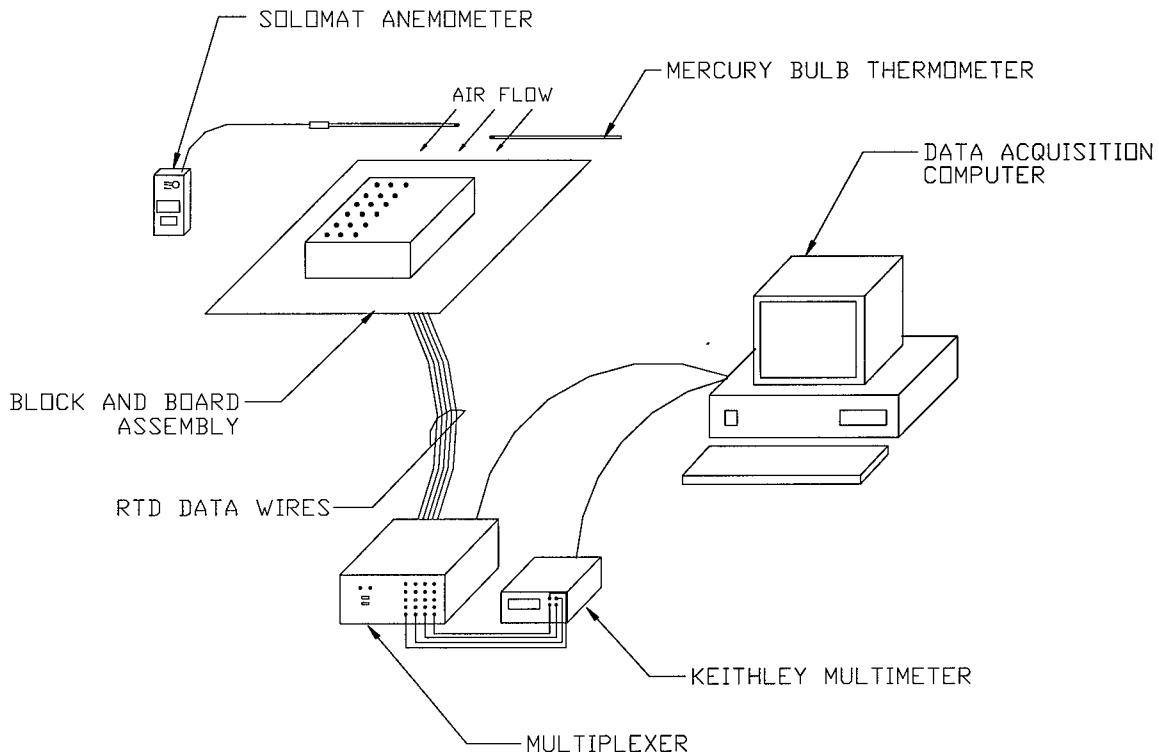


Figure 7

Monitoring and Recording System Detail

There are several systems involved in the monitoring and recording of data from each of the experimental tests performed with the heated block and board assembly. Figure 7 shows the major equipment pieces in their typical configuration layout. The basic purpose of the data monitoring and recording system is to obtain and record temperature measurements from each of the 79 RTD temperature sensors at known freestream flow conditions. With the block's temperature distribution and the ambient conditions defined, local heat transfer coefficients can be calculated as described in the data reduction section of this report.

Data Acquisition:

To obtain the required temperature measurements, each of the 79 RTD's is wired in a four wire configuration to an 80 channel, solid state, multiplexer switching unit. The multiplexer's switching mechanisms are controlled by a personal computer running computer software designed specifically for this experiment. The complete source code for this software is contained in Appendix D. The multiplexer unit can either scan successively through each of the 79 RTD's or switch to a user input sensor number. A Keithley, Model 196, 6-1/2 digit ohmmeter is used to read the resistance of each RTD during the switching. The Keithley unit has an accuracy of 100 micro-ohms in the range applicable to this experiment, and the four wire hook-up ensures lead resistances do not add to measurement error. The acquisition computer is also coupled to the Keithley's output channel, and the acquisition software records each RTD's resistance to an output data file. The software also has the capability of converting the recorded resistances to temperature measurements using the RTD manufacturer's correlation equation. The equation provided by the manufacturer is the following sixth order polynomial expression:

$$T = A + (BR) + (CR^2) + (DR^3) + (ER^4) + (FR^5) + (GR^6)$$

where:	R = Resistance	D = 3.47019E-03
	A = -387.148	E = -3.70193E-05
	B = 14.37356	F = 2.05767E-07
	C = -0.206576	G = -4.55192E-10

Because the RTDs respond to the mounting surface's strain at time of installation, the temperatures produced by the above equation need correction. This is accomplished by the use of an in-house calibration as described in Appendix B.

The source code for the calibration software is contained in Appendix D. The software first reads in calibration equations for each of the 79 RTDs from a calibration data file. The program then reads the temperature distribution data file created by the acquisition software, and applies the calibration equations to correct the temperature of each sensor. Temperature measurements produced by the software are measured repeatedly to better than 0.5 degrees Fahrenheit. The calibration software also prompts the user to enter the model rotation, freestream temperature, freestream velocity, and test resistor voltage drop for creation of an output file. The model rotation is obtained by visual inspection of the block's cover sensor locations. Zero degrees is defined as the model orientation as shown below:

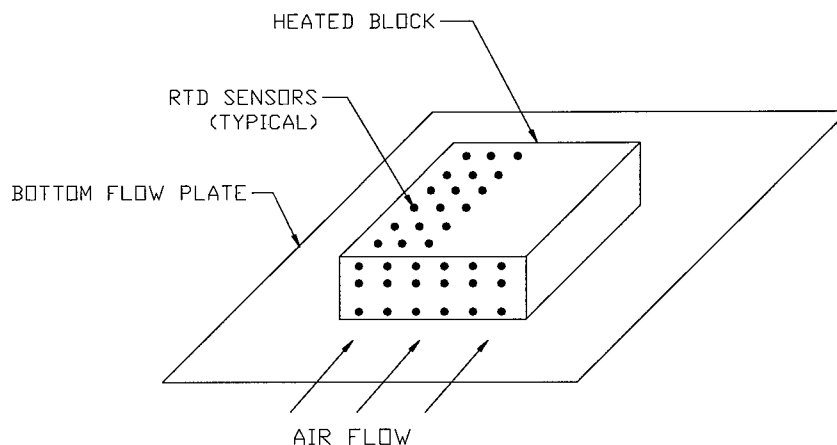


Figure 8

Model Orientation Detail

Freestream Property Measurements:

Free stream velocity is adjusted by closing off portions of the wind tunnel's supply fan inlet, or opening air bleeds located downstream of the fan. The tunnel control is described further in the Wind Tunnel Test Facility section of this report. The flow

velocity is measured by a Solomat Corporation Model MPM500e, hot-wire anemometer. The device is mounted through the side wall of the wind tunnel's test section, at block cover height, and eight inches upstream of the heated box as shown in figure 10. The anemometer has an accuracy of +/- 2.4 feet per minute over the applicable range. It also has the capability of taking flow readings once per second, and instantly averaging the multiple readings over a user defined time period. For the purposes of the present work, the device was allowed to average readings for twenty seconds before the freestream velocity was recorded. Averaging in this way resulted in freestream velocity readings within +/- 2 feet per minute.

Freestream temperature is measured using a mercury bulb thermometer, placed at block cover height, and eight inches upstream of the heated box as shown in figure 10. The thermometer is marked to a precision of 0.1 degrees Celsius.

Power Measurement:

The voltage drop across a test resistor placed in series with the heated box and board assembly is measured with a Hewlett Packard Model 3465A multimeter. The meter has an accuracy of +/- 0.01ohms, in the applicable range. The resistance was initially measured to be 0.102 ohms using the Keithley four wire ohmmeter described earlier. Because the resistor is in series with the box and board assembly, the current through the resistor is equal to that flowing through the box and board assembly. The resistor is ultimately provided to determine the power dissipated by the heated box and board assembly. During a test, the voltage drop across the test resistor is adjusted to test specifications via a rheostat on the direct current power supply. The voltage drop is measured and the current is determined using ohm's law. With the current through the box and board assembly known, the resistance at test recording time is measured with

the HP multimeter and the power dissipated by the box and board assembly calculated by power = I^2R .

Steady-State Monitoring:

An example of a test data log is included in Appendix F as table F-1. It is important to note that the computer acquired data files are obtained only when the block and board assembly have come to steady state heat transfer conditions. For the purposes of this experiment, steady state is defined to have been reached when the rate of change of temperature difference between the free stream and each of three temperature sensors drops to below 1/2 degree Fahrenheit in a 1/2 hour time period. The three sensors are numbers 1, 19, and 36, located on the block cover, side, and board respectively.

Testing Procedure:

In order to obtain consistent test results, the following test procedure is followed for each acquisition run:

- Power up acquisition and Calibration PC's and software
- Check heated box and board circuit continuity
- Power on (direct current) heated box and board assembly
- Adjust voltage drop across test resistor to spec with direct current rheostat
- Power on Wind Tunnel Fan
- Adjust tunnel flow velocity to spec

- Take temperature measurements of sensors 1, 19, and 36, freestream temperature, freestream velocity, and test resistor voltage drop every 5 minutes
- Calculate sensor temperature difference
- Continue monitoring until steady state conditions are reached
- Once steady state is reached, run complete sensor scan, final freestream temperature measurement, final temperature difference calculation, final freestream velocity measurement, and final test resistor voltage drop measurement.
- Drop out direct current power supply and quickly measure heated box and board assembly final resistance
- Run acquisition data file through calibration software routine
- Paste calibrated temperature distribution into data reduction spreadsheets

VI(C). Flow Visualization Study Procedure:

In order to better understand the secondary flows present on the cover of the block, flow visualization studies using a modification of a method designed by Langston and Boyle (1982) are conducted. The method consists of spraying wintergreen oil on the surface of a previously ink-dotted sheet and then starting the flow to be investigated. Portions of the ink dots are dissolved into the oil, which is being dragged by the air flow directly adjacent to it. The result is the production of an ink trail indicating the local surface flow direction. If ink dots are placed in a consistent pattern over the entire surface of the cover, the flow visualization test results in a complete two-dimensional representation of the cover's surface flow field. Examples of tests produced in this experiment are found in the Results section of this report. The one modification to Langston and Boyle's method made for this experiment was the thinning of wintergreen oil with oil-base paint thinner. Initial flow tests, using the ink dot method, resulted in pools of wintergreen oil being produced on the test sheet. This result is attributed to the relatively slow air flows of this study, not being able to evaporate the oil quickly enough to reduce pooling. The pools of oil build up enough thickness to modify the indicated direction of some surface flows on the block. The thinning modification reduces the oil's viscosity and increases its evaporation rate. The result is a reduction of oil pooling, and a more accurate investigation of this experiment's slow surface flows. Additional information on the details of the flow visualization method's modification, along with before and after comparisons, can be found in Appendix G.

For the purposes of the present work, the performance of flow visualization studies first entails masking of the block and board surfaces to protect them from the corrosive effects of wintergreen oil. This is accomplished by affixing strips of 2 inch wide ordinary masking tape to the exposed surfaces. A mylar test sheet is then

prepared by dotting it in a 1/2 inch by 1/2 inch grid pattern with a Staedtler Lumocolor permanent blue ink marker. The rear surface of the mylar is sprayed with repositionable adhesive, and affixed to the cover surface of the block. Careful attention is paid to affix the sheet as flat and as smoothly as possible, thereby limiting changes to the cover's surface flow field. Wintergreen oil is sprayed in a thin layer over the entire surface of the mylar test sheet. The wind tunnel, previously adjusted to the test flow specification, is then started and allowed to run until all oil on the test sheet has evaporated. This process takes anywhere from five to fifteen minutes depending on the velocity of the flow being investigated. The mylar is then removed from the box cover, and any oil sprayed off onto the block surface wiped clean.

It should be noted that the ink trails produced on the test sheets from the above method do fade after several months. For this reason, sheets to be retained for later records are photocopied soon after production.

VI(D). Wind Tunnel Test Facility:

The heated box and board assembly, including the lower and upper flow plates, is installed in the test section of the University of Maine Department of Mechanical Engineering's wind tunnel test facility. Diagrams of the wind tunnel and test sections are shown in figures 9 and 10.

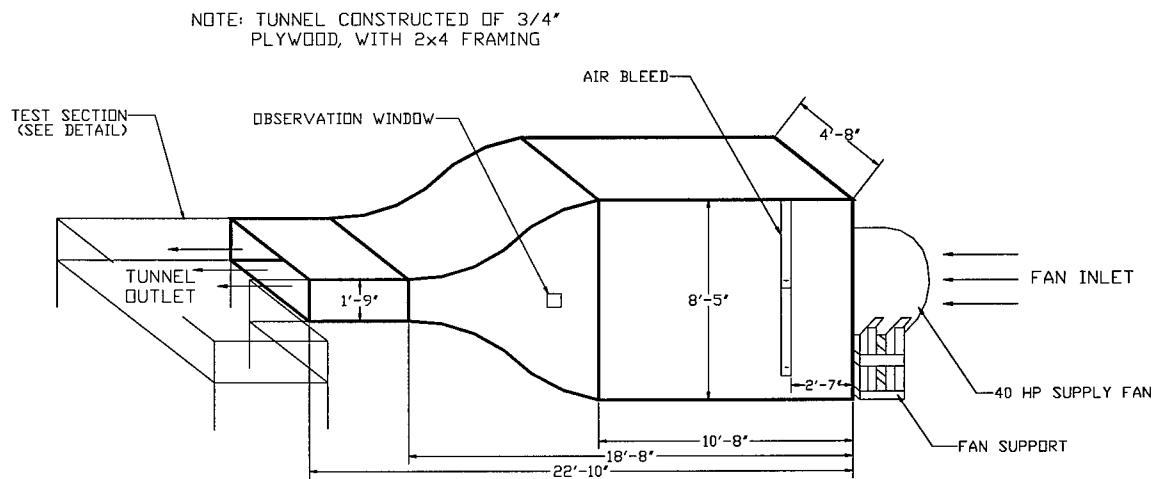


Figure 9

Wind Tunnel Detail

The wind tunnel is an open circuit design constructed of 3/4 inch plywood with an overall length of approximately 22'-10". Air flow is supplied by a 40 hp, inline type, vane-axial fan. Volumetric flow from the fan can be adjusted in several ways. One way is to adjust the pitch of the fan rotor vanes. This procedure was not used for the experiment as it requires a substantial effort. Another method of capacity control is to regulate the size of the fan inlet area. This is done by obstructing part of the inlet grating with cardboard sheets of varying sizes. This method was employed in the experiment for crude air flow adjustments. To fine tune the flow, air bleeds in the tunnel walls are provided at a location approximately 24 inches downstream of the fan outlet. The

bleeds can be adjusted to provide between zero and 6 square feet of bleed space for supply air to exit. The bleeds can be adjusted precisely, thus are used for tuning the flow to test specifications after crude adjustment is made by obstructing the fan inlet grating.

The wind tunnel contains several devices installed to control the turbulence intensity and velocity profile of the air stream provided to the test section. Additional detail as to the construction of these devices (and the tunnel itself) is provided in a paper by Boyle and Knaub (1988). The turbulence intensity at the test section entrance was measured to be approximately 1.2 to 1.5 percent by Wardwell (1993).

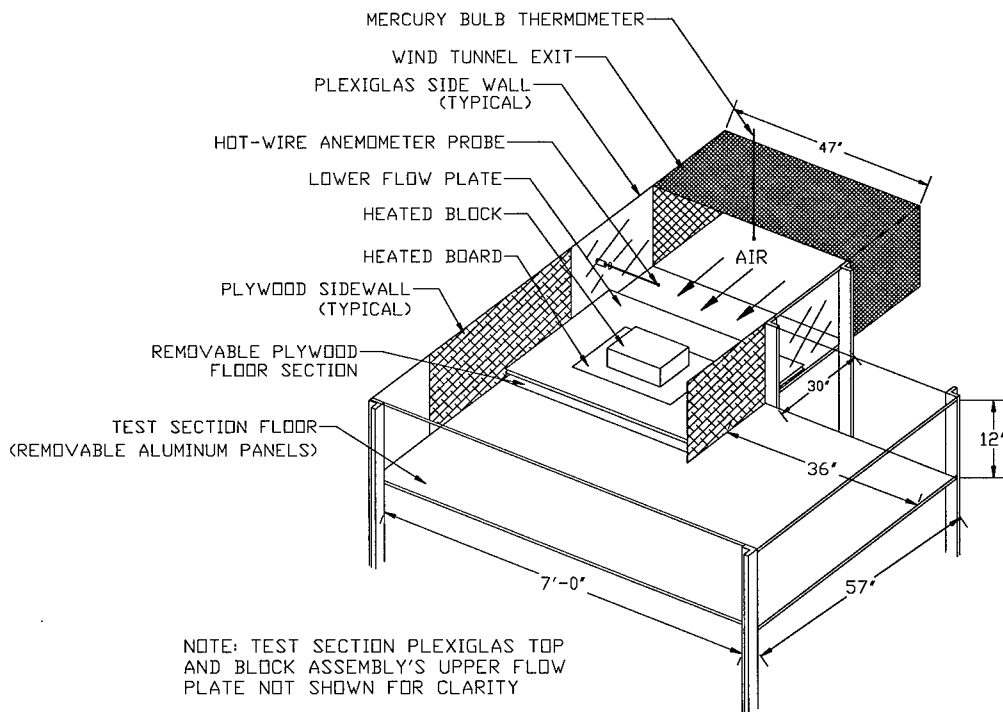


Figure 10

Wind Tunnel Test Section Detail

The tunnel facility's test section is attached to the end of the wind tunnel. Dimensions for the section are shown in figure 10. Its construction is of sections of

removable and reconfigurable aluminum, Plexiglas, and plywood plates. Detailed testing of the velocity profile in the test section can be found in work by Wardwell (1993). This experiment's heated box and board assembly is installed into the test section by removing a 47 inch x 48 inch floor plate and inserting the assembly in its place. The lower flow plate is then placed around the board, and the upper flow plate hung from the test section ceiling. Figures 9 and 10 illustrate the installation in more detail.

VII. Testing Conditions:

During the course of the experiment, several flow and heat transfer parameters are varied in efforts to determine their effects on secondary flows around the heated box, and heat transfer performance of the box surfaces. The flow and heat parameters varied include: adjustments to the freestream flow velocity, energy input to the heated box and board assembly, and horizontal orientation of the heated box.

Variation of the freestream flow's velocity is the vehicle by which the non-dimensional Reynold's number is adjusted. Likewise, changes to the electrical current driven through the box and board assembly, results in changes to the non-dimensional Grashof number. Because RTD sensors are located on only half the top cover and one side of the heated box, it must be rotated horizontally to obtain descriptions of the entire temperature distribution on all block surfaces.

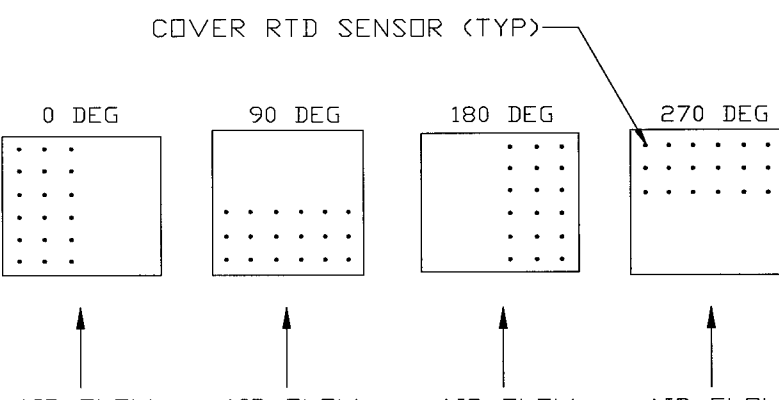
Table 1 presents the testing trials performed in the present work. The trials reported are conducted at three nominal Reynold's number values, and their associated Grashof numbers. All tests in the experiment are performed in the University of Maine at Orono, Department of Mechanical Engineering's wind tunnel facility. Freestream turbulence in the tunnel was previously reported by Wardwell (1993) as 1.2 to 1.5 percent. The orientation of the block's cover sensors in relation to the incoming airstream, corresponding freestream flow velocity, and input current to the block are also provided.

Table 1

Experimental Testing Conditions

*Reynold's Number	*Grashof Number (Ave)	Freestream Velocity (fpm)	Input Current (amps)	Box Orientation (deg CCW)	Test #
0	4.730E+07	0	2.21	90	12-14_2
0	9.441E+07	0	3.43	90	12-14_1
13964	4.195E+07	455	5.45	270	11-02_1
13979	3.121E+07	455	5.49	90	11-01_1a
14286	3.452E+07	455	5.54	0	10-30_1
19859	6.421E+07	660	6.96	270	02-27_1
19879	5.515E+07	660	7.03	0	10-25_1
20204	5.719E+07	660	7.02	90	12-12_1
20617	3.894E+07	660	5.43	270	11-13_1
20693	3.221E+07	660	5.42	0	01-31_1
20714	1.898E+07	660	4.22	270	02-21_1
20732	3.055E+07	660	5.42	180	02-01_1
21082	3.174E+07	660	5.42	90	11-14_1
21160	1.237E+07	660	4.22	90	12-11_1
50134	3.633E+07	1550	6.92	270	11-21_1
50493	2.811E+07	1550	6.98	90	11-15_1

- * - Reynold's number based on block height.
- Grashof number based on block length and average cover surface temperature.



Box Orientations

VIII. Data Reduction Scheme:

The process of data reduction in the experiment involves the determination of the local surface convection heat transfer coefficient distributions on the heated block surfaces, freestream flow Reynolds numbers, and average Grashof numbers for each testing trial.

The local surface coefficients are obtained by performing a first law energy balance on a control volume surrounding one RTD as shown in figure 11.

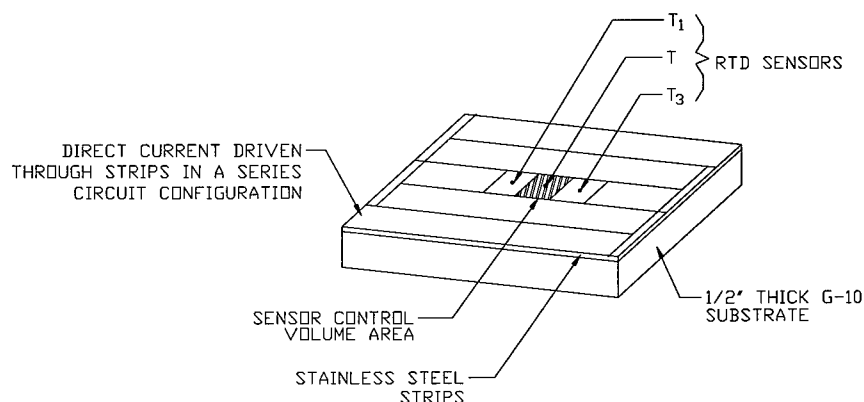


Figure 11

Temperature Sensor Control Volume Detail

In its most general sense, the first law equation for the above control volume under steady state conditions is written as:

$$q_{\text{cond},1-T} + q_{\text{cond},3-T} + q_{\text{gen}} - q_{\text{conv}} - q_{\text{back}} - q_{\text{rad}} = 0$$

The first two terms of the energy equation represent the heat transfer into, or out of, each side of the control volume transferred by conduction along the thin stainless steel strip. The driving temperature difference is given as the difference between the control volume RTD, and its two neighbors along the strip. The terms are expanded to:

$$q_{\text{cond},1 - T} = \frac{K_{ss} A_{\text{xsect, ss}}}{X_{1 - T}} (T_1 - T)$$

$$q_{\text{cond},3 - T} = \frac{K_{ss} A_{\text{xsect, ss}}}{X_{3 - T}} (T_3 - T)$$

The results of the test data, contained in Appendix F, reveal these terms to be negligible when compared to others in the energy equation. For this reason, these terms are neglected in the final surface coefficient of heat transfer determination.

The next term in the overall energy equation is the electrical generation term, q_{gen} . This term describes the amount of power being dissipated by the electrical current flowing through the thin, resistive control volume. Since our experimental procedure measures the resistance of the entire series circuit, we assume each square inch of stainless steel is dissipating an equal amount of power, and multiply by the appropriate area ratio. Incorporating this assumption, the generation term is written as:

$$q_{\text{gen}} = \frac{A}{A_{\text{tot, ss}}} (I^2 R_{\text{tot, ss}})$$

The fourth term in the energy balance equation represents the heat transferred by convection from the control volume surface. It is this term that contains the unknown surface coefficient of heat transfer value that will later be solved for. The term is written as:

$$q_{\text{conv}} = hA(T - T_{fs})$$

The fifth term describes the heat lost from the control volume by conduction heat transfer through the back of the control volume into the G-10 substrate material. Interior RTD sensors provide temperature measurements on the interior surface of the G-10, thus the driving temperature differential for this term is a known quantity. The backloss term is written as:

$$q_{\text{back}} = \frac{K_{\text{back}} A}{L_{\text{back}}} (T - T_{\text{back}})$$

The last term in the energy balance equation is the radiation heat transfer loss from the control volume. Its size quickly becomes significant with increases in temperature differentials between the control volume surface and surrounding environment. The term typically represents 2-10% of the total heat transfer from the control volume. The term in full detail is:

$$q_{\text{rad}} = \sigma A \varepsilon F (T^4 - T_{\text{fs}}^4)$$

Incorporating all of the above energy balance term equations into the general first law equation for the experimental control volume yields:

$$\frac{A}{A_{\text{tot, ss}}} (I^2 R_{\text{tot, ss}}) - hA(T - T_{\text{fs}}) - \frac{K_{\text{back}} A}{L_{\text{back}}} (T - T_{\text{back}}) - \sigma A \varepsilon F (T^4 - T_{\text{fs}}^4) = 0$$

Solving the above equation for the surface coefficient of heat transfer quantity yields:

$$h = \frac{I^2 R_{\text{tot, ss}}}{A_{\text{tot, ss}}(T - T_{fs})} - \frac{K_{\text{back}}}{L_{\text{back}}} \left(\frac{T - T_{\text{back}}}{T - T_{fs}} \right) - \sigma \varepsilon F \left(\frac{T^4 - T_{fs}^4}{T - T_{fs}} \right)$$

Calculations of the above equations, for each testing run, are performed using Microsoft Excel spreadsheet software. The results of the calculations are included in Appendix F.

The Reynold's number of a particular flow is defined by the following equation:

$$N_{\text{Re}} = \frac{\rho U_{\infty} L}{\mu}$$

For each of the testing trials in this experiment the flow Reynold's number is calculated using the heated block height as the length (L) value and the freestream velocity as U_{∞} . The calculations are performed by Microsoft Excel spreadsheet software, and are contained in Appendix A.

The Grashof number for a particular scenario is defined by the following equation:

$$N_{\text{Gr}} = \frac{g \rho^2 L^3 \Delta T \beta}{\mu^2}$$

The Grashof number determined for each of the testing trials in this experiment is an average value. This is based on the fact that the temperature difference used in the above calculation is the difference between the block cover's average surface temperature and the freestream temperature. Additionally, a film temperature, defined as the average between the average block surface temperature and freestream temperature is calculated. It is at this film temperature value that the quantities of density and viscosity are found using the B. Gebhart (1988) tables. The β quantity in the equation is also calculated as the reciprocal of the film temperature. The length quantity is defined as the length of the box cover. Incorporating these ideas into the Grashof number equation results in the following equation for this experiment's average Grashof number:

$$N_{Gr, \text{ave}} = \frac{g\beta^2 L^3 (T_{fs} - T_{avg})}{\mu^2 T_{film}}$$

The Grashof numbers, for each of the testing trials in the experiment, are calculated using Microsoft Excel spreadsheet software. The results of the calculations are included in Appendix A.

The Nusselt number is used for non-dimensionalization of the surface coefficient of heat transfer. The number is defined as:

$$N_{Nu} = \frac{hL}{k}$$

For the purposes of this experiment, an average Nusselt number is determined for a particular region of interest. For calculation of this value, the L value is the length of the cover surface, and the thermal conductivity, k, is evaluated at the film temperature. Taking the above into mind yields the following equation for average Nusselt number:

$$N_{\text{Nu, ave}} = \frac{h_{\text{ave}}L}{k_{\text{film}}}$$

IX. Uncertainty:

In experimentation, it is important to consider the cumulative effect of uncertainties in measured quantities upon the results. For the present work, the cumulative effect is quantified using the method developed by Kline and McKlintock (1953). The details of the entire uncertainty calculation, and specific contributions of its constituents can be found in Appendix C. A summary of the uncertainties associated with Reynolds, Grashof, and Nusselt numbers, for all tests conducted in this experiment, is presented in table 2. Additionally, some specific average uncertainties of concern are calculated in table 3.

The tables show the average uncertainty in the calculated Nusselt number, for a combination of all tests, is approximately ten percent. For only those tests included in the Three-Dimensional Heat Transfer Description Section (tests 11-13_1, 11-14_1, 01-31_1, and 02-01_1), the uncertainty drops to less than eight percent. The tables also show some trends in the effects of uncertainty. First, the tables show that as the freestream flow Reynold's number is increased, the uncertainty in that Reynold's number decreases, while uncertainty in Grashof and Nusselt numbers increases. More significant, however, is the effect of increasing Grashof number at a fixed freestream Reynold's number. In this scenario, uncertainty in Nusselt number drops dramatically. For the 660 foot per minute test cases, an approximately five-fold increase in the Grashof number results in a reduction of uncertainty in the Nusselt number from 21.5 to 4.15 percent. The results lead to the conclusion that optimal testing is conducted at minimum freestream Reynold's number and maximum Grashof number. Translating this to actual experimental quantities means performing the experiment at minimum freestream flow velocities and maximum power input to the block and board assembly. For the purposes of this experiment, however, both of these quantities are limited by the

physical capabilities of the experimentation hardware. The freestream flow velocity, while infinitely adjustable, becomes relatively unsteady at velocities below 455 feet per minute, and the block and board assembly is not thermally capable of conducting more than 7-8 amps without damage to the block's construction materials.

Table 2

Test Data Uncertainty

Test#	Model Orient.	F.S. NRe	NGr,ave	WRe	% Error NRe	WGr	% Error NGr	WNu	% Error NNu
10-25_1	0	19879.2	5.515E+07	208	1.049	1.695E+06	3.073	8	4.521
11-13_1	270	20617	3.894E+07	216	1.049	1.811E+06	4.651	11	6.678
11-14_1	90	21081.9	3.174E+07	221	1.049	1.903E+06	5.995	18	8.100
12-11_1	90	21159.5	1.237E+07	222	1.049	1.900E+06	15.358	70	21.508
12-12_1	90	20203.7	5.719E+07	212	1.049	1.765E+06	3.087	8	4.163
01-31_1	0	20693.1	3.221E+07	217	1.049	1.817E+06	5.641	16	7.859
02-01_1	180	20731.7	3.055E+07	217	1.049	1.824E+06	5.968	17	7.928
02-21_1	270	20714.7	1.898E+07	217	1.049	1.806E+06	9.514	28	17.396
02-27_1	270	19859.1	6.421E+07	208	1.049	1.718E+06	2.676	6	3.991
10-30_1	0	14286.3	3.452E+07	158	1.104	1.827E+06	5.293	14	6.572
11-01_1a	90	13979.2	3.121E+07	154	1.104	1.717E+06	5.502	17	8.717
11-02_1	270	13964.7	4.195E+07	154	1.104	1.740E+06	4.147	11	9.088
11-15_1	90	50492.8	2.811E+07	508	1.006	1.995E+06	7.096	47	12.076
11-21_1	270	50133.6	3.633E+07	504	1.006	1.971E+06	5.423	30	18.535
12-14_1	90	0	9.441E+07	69	n/a	2.091E+06	2.215	2	9.247
12-14_2	90	0	4.730E+07	72	n/a	2.120E+06	4.481	2	7.792

Table 3

Specific Average Uncertainties

Average Uncertainty in 3-D Heat Transfer Description = (Tests 11-13_1, 11-14_1, 01-31_1, and 02-01_1)	NRe	NGr	NNu
	1.05%	6.53%	10.03%
Average Uncertainty at 455 FPM Freestream Flow Velocity =	1.10%	4.82%	8.90%
Average Uncertainty at 660 FPM Freestream Flow Velocity =	1.05%	6.43%	8.99%
Average Uncertainty at 1550 FPM Freestream Flow Velocity =	1.01%	6.26%	15.31%
Average Uncertainty for Natural Convection Test =	n/a	3.35%	8.52%
Average Uncertainty for All Conducted Tests =	1.05%	5.55%	10.04%

X(A). Cover Flow Visualization Study Results:

Flow visualization studies, using a modified ink dot and oil of wintergreen method as described in the Flow Visualization Study Procedure Section, are performed on the cover surface of the experimental block. The goal of the studies is to provide a description of the surface flow field characteristics. The studies are conducted on an unheated block, at freestream Reynold's numbers, based on the block height, of approximately 15000, 22000, 33000, and 51000. These Reynold's numbers correspond to freestream flow velocities of 455, 660, 1000, and 1550 feet per minute, respectively. The results are presented in figures 12, 13, 14, and 15, respectively. Each study shows the existence of a three-dimensional separation bubble, separating from the leading edge of the block, and reattaching at a downstream distance of approximately one-third the length of the cover. In each figure, ink traces clearly exhibit the bubble as streaks of ink leading from the original dot, upstream, towards the leading edge of the cover. The bubble appears as a relatively symmetrical phenomena about the streamwise mid-line. The length of the bubble is greatest at the symmetry plane, and decreases to near zero at the edges of the cover surface. These qualities are consistent with the three-dimensional flow given in Wardwell (1993) by use of laser doppler velocimeter measurements on a smaller block at the same Reynold's number.

On the rear portion of the cover surface, downstream of the separation bubble, the flow visualization shows the existence of a three-dimensional flow field. Flow streamlines near the lateral edges of the cover show X-directed components converging toward the symmetry plane. In addition, near the symmetry plane reattachment area, the shear is relatively weak, as compared to flow near the lateral edge regions. This conclusion is based on ink streaks in this area being wide and irregular. The effect is most evident in the slower, 455 and 660 feet per minute, tests.

Block Cover Flow Visualization

$N_{Re} = 15030$, Freestream Velocity = 455 FPM

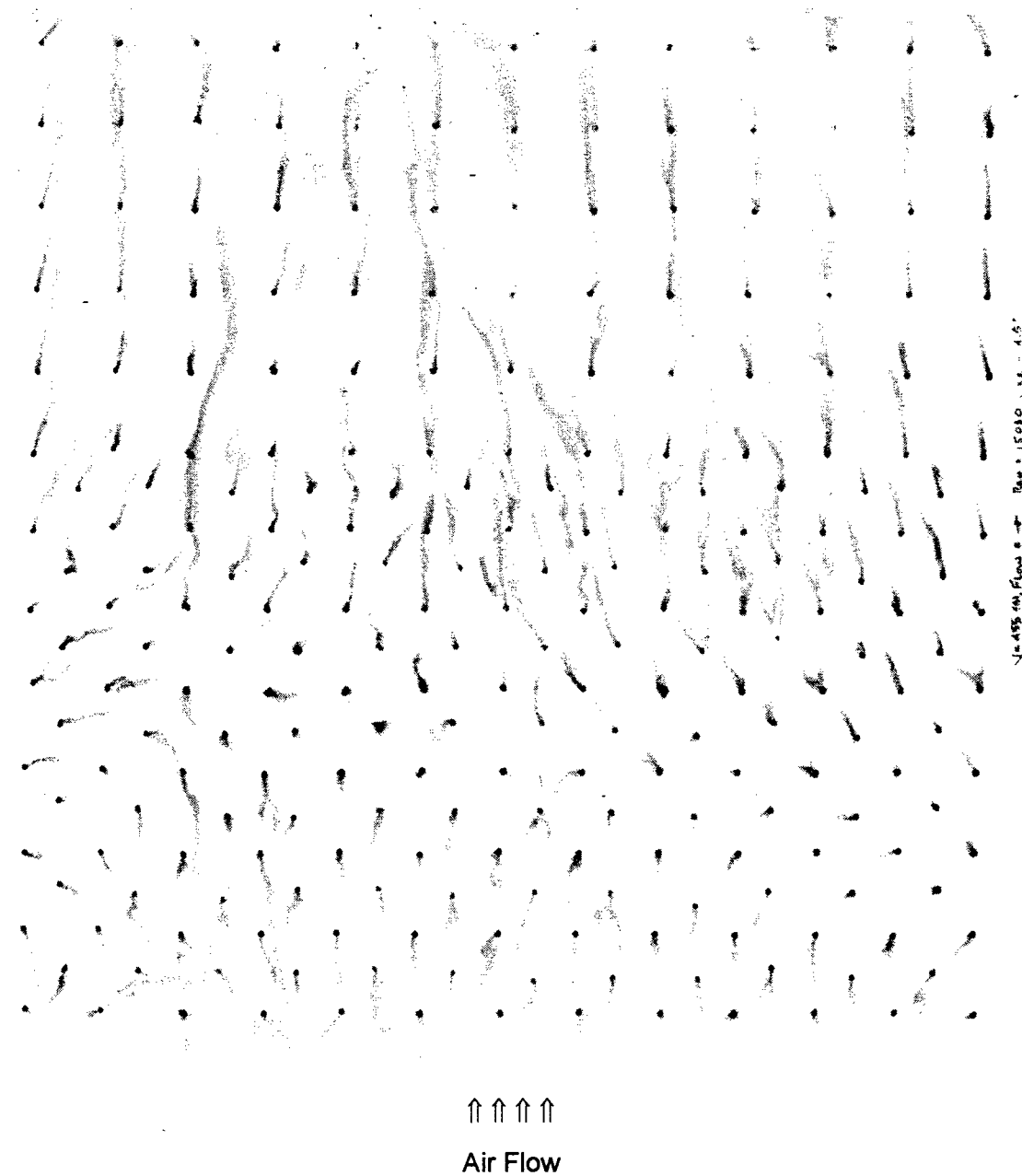


Figure 12

Block Cover Flow Visualization

$N_{Re} = 21802$, Freestream Velocity = 660 FPM

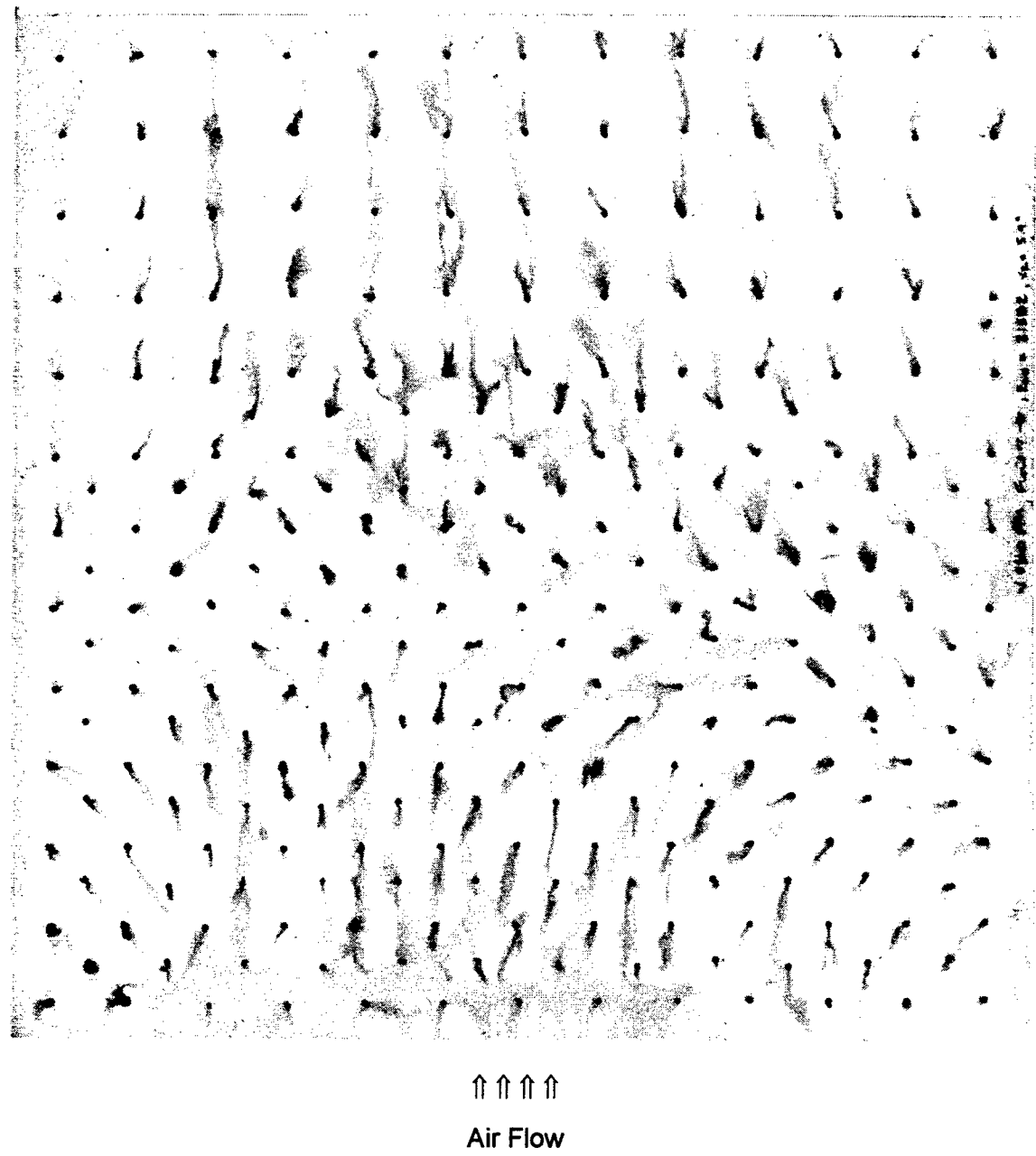


Figure 13

Block Cover Flow Visualization

$N_{Re} = 33034$, Freestream Velocity = 1000 FPM

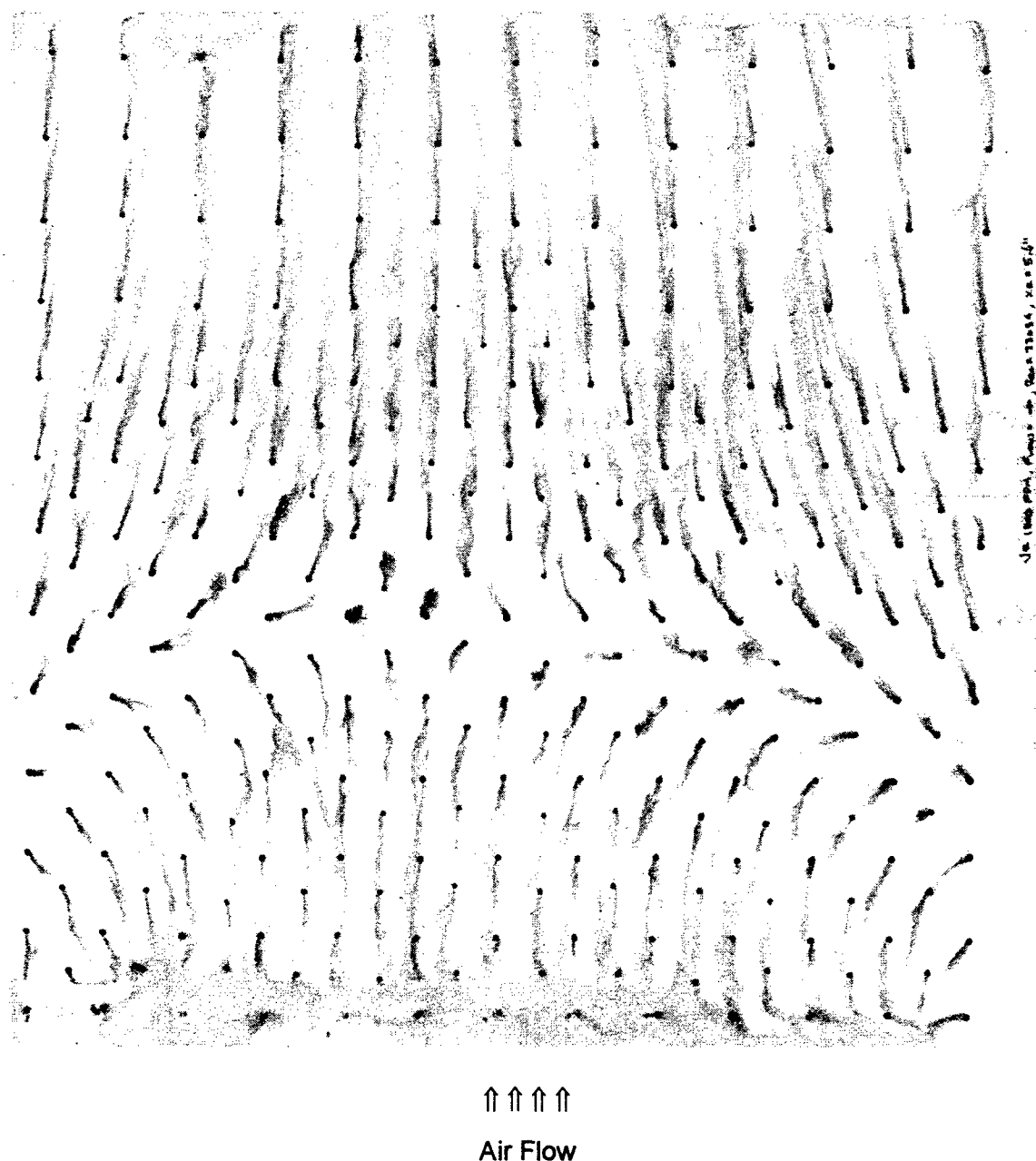


Figure 14

Block Cover Flow Visualization

$N_{Re} = 51202$, Freestream Velocity = 1550 FPM

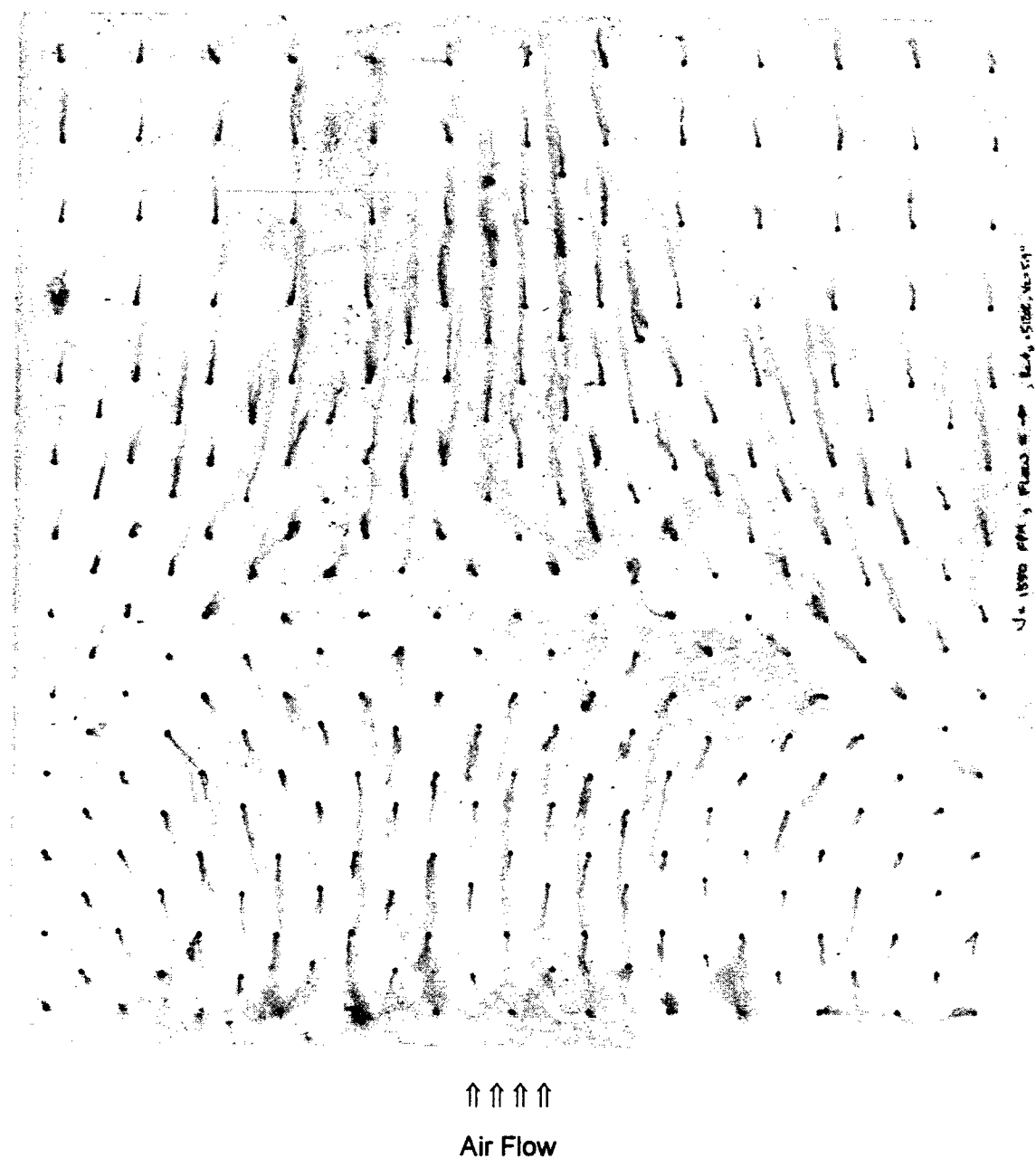


Figure 15

Figures 12 and 13 show the reattachment length of the separation bubble increases with Reynold's number. The dependence of the separation bubble reattachment length on Reynold's number was previously investigated for the blunt plate geometry by Ota et. al. (1981), and for the low-profile block by Wardwell (1993). For the two-dimensional case, Ota et. al. found reattachment length increases accompanied increases in Reynold's number, for flows with Reynold's numbers below 2.4×10^4 . Wardwell's work observed an increase in the reattachment length from 0.81^*H to 1.42^*H by increasing the flow Reynold's number from 2.3×10^3 to 1.26×10^4 . Additionally, Ota et. al. (1981) and Hillier and Cherry (1981a) both observed the existence of a threshold Reynold's number, above which, the reattachment length becomes independent of Reynold's number. Results of reattachment length versus freestream Reynold's number is shown in figure 16. The figure shows a marked break in the reattachment length's dependence on Reynold's number beginning at a threshold value of $N_{Re} = 21802$. This result is qualitatively consistent with earlier two-dimensional blunt plate studies, which also exhibited a Reynold's number independence threshold number.

It is known from the flow experiments of Dijali and Gartshore (1991) and Dijali (1991), that tunnel blockage ratio, and the separation angle (angle of the leading edge of the cover) both effect the size of the separation bubble. In particular an increase in blockage ratio, and decreases in the separation angle, are shown to reduce the separation bubble's length. These effects are qualitatively observed by comparing results from the present work with those in the dynamically similar experiment by Wardwell (1993). Comparing the separation bubble lengths, at a freestream Reynold's number of approximately 15000 (based on block height), reveals the bubble of the present work is approximately 30 percent shorter than that produced

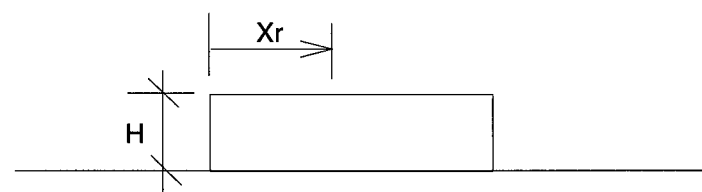
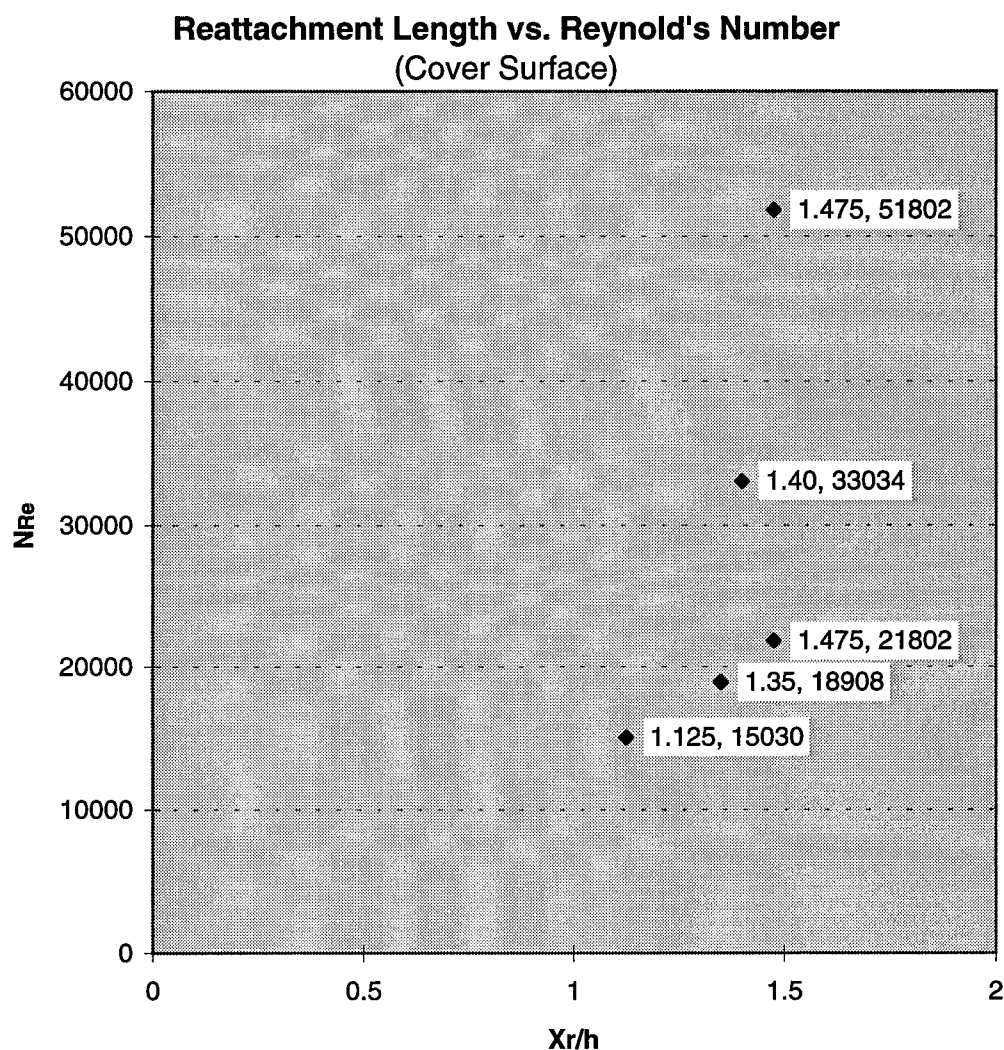


Figure 16

in Wardwell's experiment. This result is consistent with the blockage ratio and separation angle arguments above. The blockage ratio of Wardwell's experimental setup is approximately ten times smaller than that of the present experiment, and the leading edge of Wardwell's solid aluminum block is considerably closer to 90 degrees than that of the present experiment, being that aluminum can be machined to tighter tolerances than Fiberglas.

X(B): Three-Dimensional Heat Transfer Description Results:

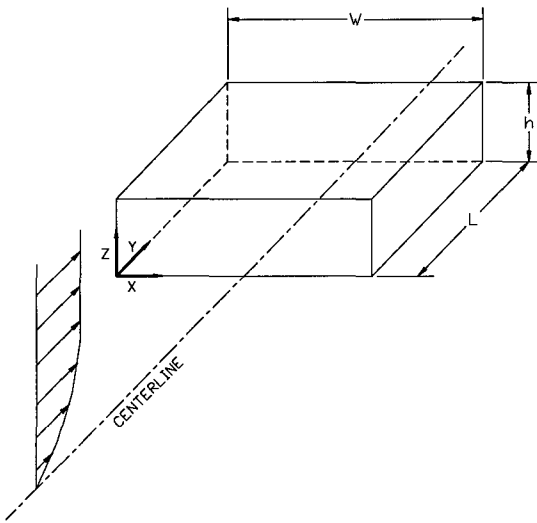


Figure 17

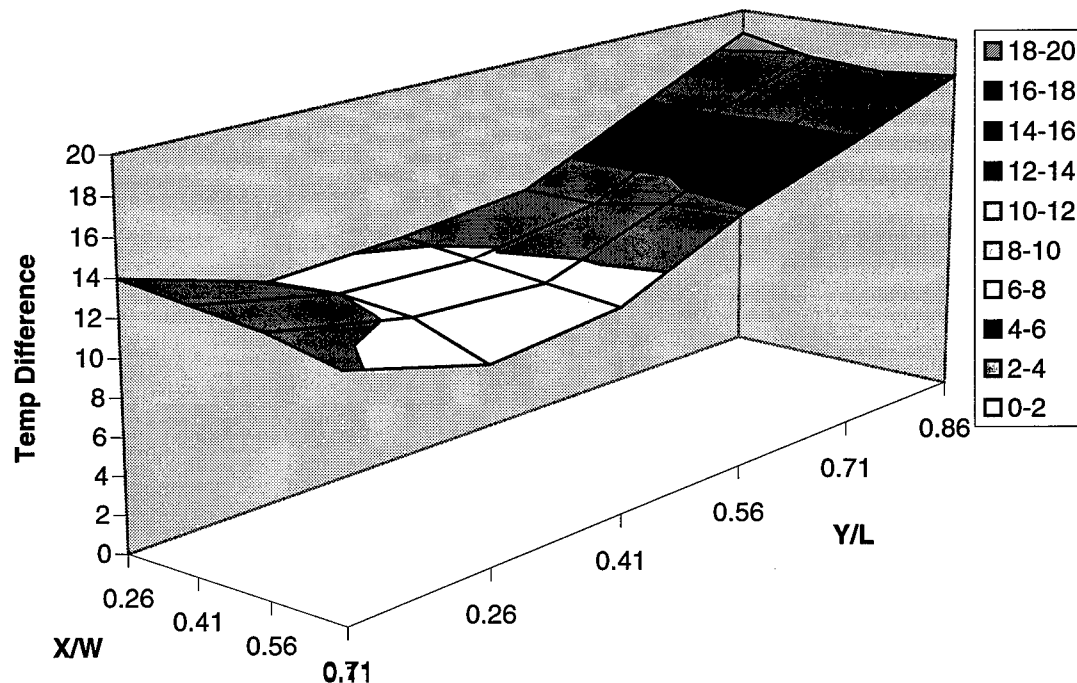
Coordinate System Detail

To facilitate the heat transfer description, the five exposed surfaces of the heated block are fitted with a coordinate system orientated to the freestream flow as shown in figure 17.

For the three Reynold's number flows investigated, the qualities of the surface heat transfer description are quite similar. For this reason, only the $N_{Re} \approx 21000$ flow scenario, representing a freestream flow velocity of 660 feet per minute, is presented in the full heat transfer description. Part C of these results discusses the quantitative effects produced by changes in the flow Reynold's number.

Figures 18 and 19 present surface plots of the cover's temperature difference and Nusselt number distributions. Figures 20 through 23 present the observed Nusselt numbers on the cover, lateral, front, and rear surfaces of the heated block, respectively. The figures display only those areas of the block for which RTD sensors are installed.

3-D Composite Temperature Difference Surface Plot
Tests 11-13,14 (Cover Surface)

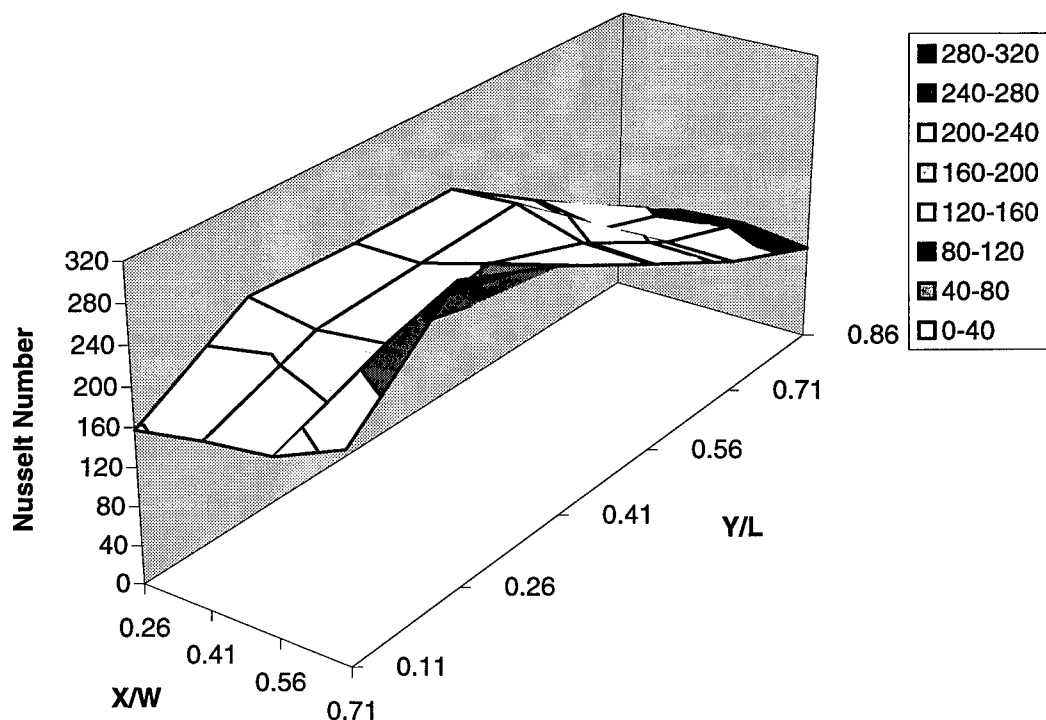


$NRe_{ave} = 20850, NGr_{ave} = 3.534 \times 10^7$

Figure 18

**Test 11-13,14: 3-D Nusselt Number Surface Chart
(Cover Surface)**

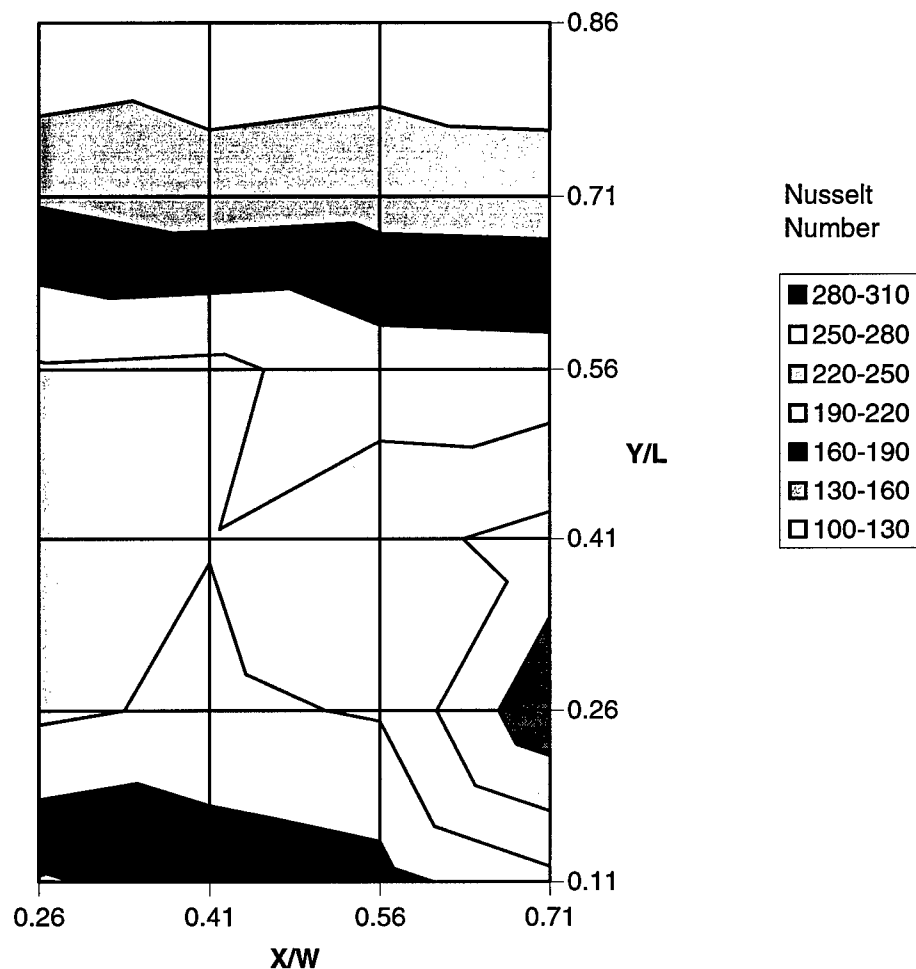
Note: Y/L=0 is upstream edge.



$$NRe_{ave} = 20850, NGr_{ave} = 3.534 \times 10^7$$

Figure 19

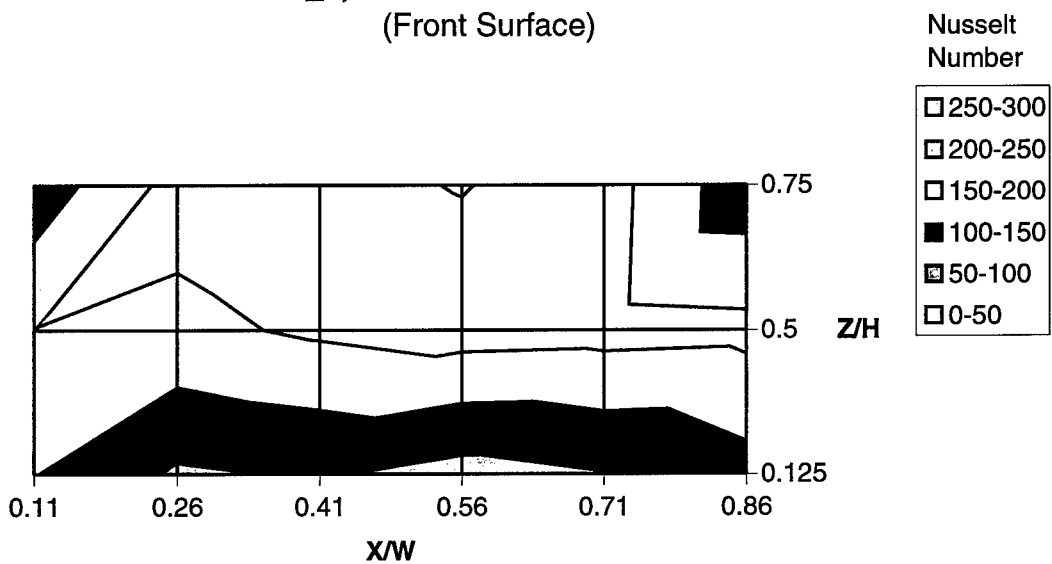
Composite Nusselt Number Surface Plot
Tests 11-13,14 (Cover Surface)



$NRe_{ave} = 20850$, $NGr_{ave} = 3.534 \times 10^7$

Figure 20

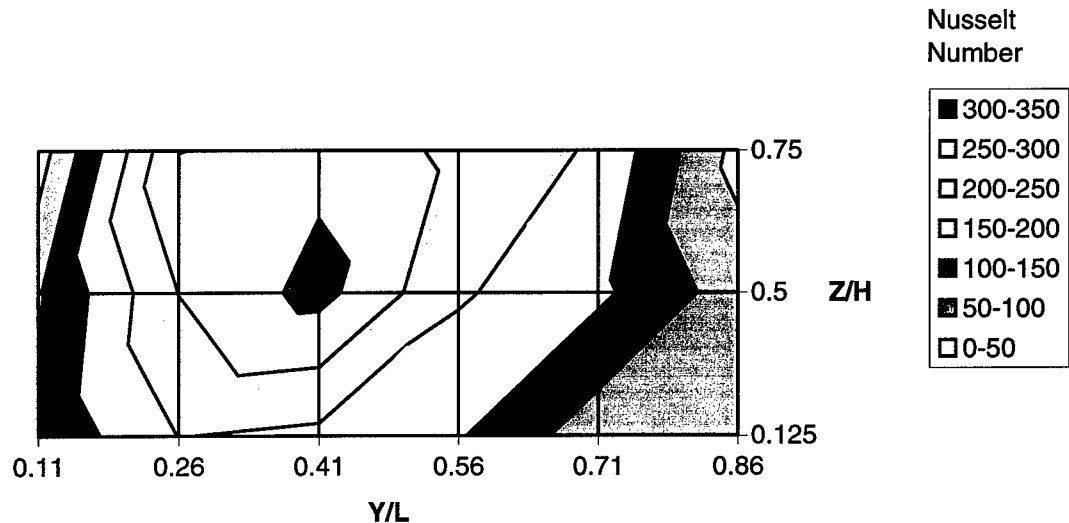
**Test 01-31_1, Nusselt Number Contour Chart
(Front Surface)**



$NRe = 20693, NGr,ave = 3.221 \times 10^7$

Figure 21

**Test 11-13_1, Nusselt Number Contour Chart
(Left Lateral Surface)**

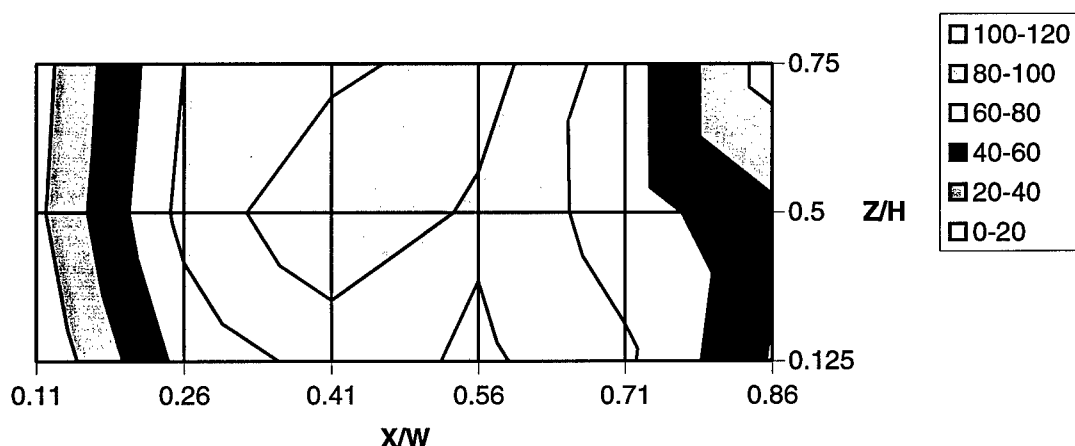


$NRe = 20617, NGr,ave = 3.894 \times 10^7$

Figure 22

**Test 02-01_1, Nusselt Number Surface Chart
(Rear Surface)**

Nusselt
Number



$$NRe = 20732, NGr,ave = 3.055 \times 10^7$$

Figure 23

Because of symmetry, only the left lateral surface ($X = 0$) results are characterized and included for discussion. All of the above results are associated with the $N_{Gr, ave} = 3.534 \times 10^7$ experimental test scenario.

Figures 19 and 20 show the Nusselt numbers, along the streamwise (Y) direction, increasing from the separation edge to a maximum at approximately $Y/L = 0.41$. The flow visualization shown in figure 13 reveals this maximum coincides with the region of the cover separation bubble's reattachment line. From this maximum, the Nusselt number steadily decreases in the downstream direction, to a minimum at the rear edge of the block. The three dimensional flow field measured by Wardwell (1993) can be used to interpret this Nusselt number distribution. The enhanced convection heat transfer, in regions engulfed by the separation bubble, is attributed to the vortex system's thermal and mass transport interaction with the adjacent freestream flow. Beyond the separation bubble reattachment line, near surface flow is heated as it travels along the cover surface in positive Y -direction. As a result of the heating, the temperature differential between the fluid and block surface is reduced, and local Nusselt number values are reduced.

The results described above, for the cover, are qualitatively consistent with the two-dimensional results obtained in the blunt plate heat transfer experiment performed by Ota and Kon (1974) and Shaw, Chen and Chen's (1991) laminar flow experiment. In particular, both studies show the existence of a rise in the Nusselt number, beginning at separation point, and peaking in the region corresponding to the cover separation bubble's reattachment line. The tailing off of Nusselt numbers beyond the reattachment region was also observed in Shaw, Chen and Chen (1991). Additionally, results in the domain of $0 < Y < H$ on the cover, are consistent with the qualitative transport description given by Chyu and Natarajan (1991) in their analogous mass transfer study based on a

cubic geometry. Quantitative comparisons between the present work and the above experiments, however, cannot be made directly as the structure and intensity of the separation bubbles produced on the cover surfaces are different for each. Studies by Wardwell (1993), Djilali and Gartshore (1991), and Chyu and Natarajan (1991) show the three-dimensional flow fields in each respective geometry and flow experiment are substantially different than those of the present work.

While it is obvious from the flow visualization that the cover flow field is highly three dimensional, cross-stream analysis of the Nusselt number distribution on the cover shows a relatively two dimensional phenomena. The Nusselt number distribution of figure 20 shows small variations in the cross-stream (X) direction from $0.26 < X/W < 0.71$. A slight rise is shown in the $0.11L < Y/L < 0.41$ domain at the outermost $X/W = 0.71$ sensor locations. The flow visualization of figure 13 shows the surface flow on the front half of the cover is slightly asymmetrical, with this domain exhibiting substantially larger X-components toward the block symmetry line. The Wardwell (1993) experiment shows these components are part of the three-dimensional nature of the separation bubble over the area. Increased convection heat transfer along the cover's edges was also previously observed on the cubic block by Chyu and Natarajan (1991). Downstream of $Y/L = 0.56$, beyond the separation bubble's reattachment region, the cross-stream variation in Nusselt number changes only slightly.

Nusselt numbers observed on the front face of the block in the present work are shown in figure 21. The figure shows good symmetry about the vertical mid-line of the surface. The data shows the Nusselt numbers are at a minimum near the bottom of the face, which corresponds to the $Z/H = 0.125$ sensor locations. This Nusselt number trend is consistent with that observed for three dimensional laminar flows by Shaw, Chen, and Chen (1991). The result is interesting, however, as data from Chyu and

Natarajan's (1991) mass transfer experiment shows a sharp increase in the mass transfer coefficient near the bottom of the cube's front surface. The discrepancy is speculated to be a result of the fact that Chyu and Natarajan's (1991) mass transfer experiment does not incorporate means to model energy transfer from the block to the surrounding floor board (i.e. no areas of the floor around the block are fitted with sublimation material). While convection heat transfer is still the largest contributor to energy transfer in this area, examination of the energy equation shows a significant contribution to the overall heat transfer from thermal conduction through the block's G-10 substrate, into the block interior. Because the surrounding floor area is also heated in the present work, it is a more realistic estimation of the complete heat transfer scenario.

Further up the block in the positive z-direction, the data shows a generally increasing trend in the Nusselt numbers, except in the top corners of the face. Data from sensors located at $Z/H = 0.5$ and 0.75 show the trend is monatomic, with the exception of the outermost sensors located at the $Z/H = 0.75$ height. These two locations, corresponding to the front face's top corners, reveal a sharp temperature rise, and thus decrease in the Nusselt number. Analyzing the Nusselt number distribution in the cross-stream direction shows relatively small Nusselt number variations from $0.26 < X/W < 0.71$, except for marked increases at the outermost sensors along the $Z/H = 0.125$ and $Z/H = 0.5$ heights. It is postulated that increased heat transfer near these two edges location sensors occurs from higher flow velocities in the region. The high velocities are created as a result of flow accelerating outward from the face's central high pressure region. Previous surface pressure measurements by Castro and Robbins (1977) support this conclusion, showing the lateral edges on the front face of a cube are low pressure regions as compared to the central portion of the face. Increased heat

transfer near the front face edges was also observed for laminar flow fields in Shaw, Chen, and Chen's (1991) experiment, and by Chyu and Natarajan (1991) on the cubic geometry.

Results concerning the block's left lateral surface are presented in figure 22. The figure shows the Nusselt numbers, along the streamwise (Y) direction, rise from the upstream edge to a peak at the $Y/L = 0.41$ sensor locations. From this peak, the Nusselt numbers steadily decrease to a minimum at sensor locations nearest the block's rear edge. Like the present work's turbulent flow results, laminar flow calculations by Shaw, Chen, and Chen (1991) produce similar streamwise results. Shaw, Chen, and Chen's (1991) calculations show portions of the flow on the lateral surface travel up onto the cover surface behind the cover's separation bubble area. Chyu and Natarajan's (1991) turbulent flow study on the cubic geometry observed the presence of a separation zone covering portions of the lateral surfaces' upstream halves. It is speculated that the flow field on the block's lateral surfaces in the present work, consists of a separated front half, followed by flow moving in the Y/L direction with a Z -component of velocity that forces portions of the flow up onto the rear of the cover surface. The Nusselt number distribution shown in figure 22 is consistent with this flow scenario. Vortex flow in the front separation region is expected to enhance cooling of the block surface there, similar to the enhanced heat transfer in the separated region on the cover surface. Downstream of reattachment, the flow picks up heat as it moves in the Y/L direction, thereby decreasing the temperature differential between the flow and block surface, and decreasing the local Nusselt number values.

Analyzing the lateral surface data from bottom to top (Z -direction), shows the Nusselt number values increase with respect to Z/H in the $0.11 < Y/L < 0.5$ domain. At approximately the vertical mid-line of the lateral face ($Y/L = 0.5$), the $Z/H = 0.5$ sensor

locations exhibit the greatest values of Nusselt number, although the difference between them and the $Z/H = 0.75$ locations is relatively small. Results of Chyu and Natarajan's (1991) mass transfer study, on the lateral surfaces of a cube, show qualitatively similar trends in this cross-stream(Z) direction. Their experiment also shows a strongly three dimensional convection heat transfer distribution on the lateral surface. One notable difference between their experiment, and the present work, is their observation of maximum mass transfer rates near the bottom edge of the front face where it meets the floor. This contradictory phenomena is likely to occur for the same reasons thought to have affected the front face's transport distribution (i.e. lack of sublimation material results in no conduction heat transfer modeling). It should be noted, however, that in the presents work, Nusselt number results reported at the extreme values of Y/L (0.11 and 0.86) on the lateral surface are of questionable accuracy. The question arises from the fact that the experimental block in use has relatively course internal surface temperature resolution near these locations. Conduction heat transfer calculations for the backloss term require using internal temperature sensors located at the $Y/L = 0.33$ and 0.66 locations.

The remaining heated surface, investigated in the present work, is the rear of the block. Traditionally, the heat transfer characteristics of this region are difficult to predict because of the highly complex recirculating structure of the area's flow field. Flow calculations by Shaw, Chen, and Chen (1991) describe a laminar flow field as one where portions of the flow passing along the lateral block surface flow into the region behind the block, travel up the rear face, and finally mix with flow passing over the cover surface. As the freestream Reynold's number is increased, it is expected the flow becomes increasingly complex. A summary of the turbulent flow field, behind a cubic block, is provided in Chyu and Natarajan (1991) based upon surface flow visualization.

Their summary includes mention of counter-rotating horseshoe vortices near the rear surface's base, and a large, inverted, U-shaped vortex within a separation cavity, engulfing most of the rear side. With such a complex flow system, one might think the heat transfer characteristics of the surface would be complex. However, the results found in the present work show a rather simple Nusselt number surface. Additionally, the average Nusselt number of the surface is the smallest for the entire block. Figure 23 presents Nusselt number distribution data on the rear surface. The figure exhibits a relatively symmetrical, with Z-direction variation greatest at the vertical symmetry line region and least near the outer edges. Deviation in across the face, in the (X) direction, consists of peak Nusselt numbers existing near the vertical mid-line of the surface, and then dropping relatively slowly, in each direction, out to the $X/W = 0.26$ and 0.71 sensor locations. The Nusselt numbers then drop rapidly when moving toward each edge of the rear surface. These results are consistent with that which might be expected from the complex vortex system described in the cubic geometry flow experiment by Chyu and Natarajan (1991).

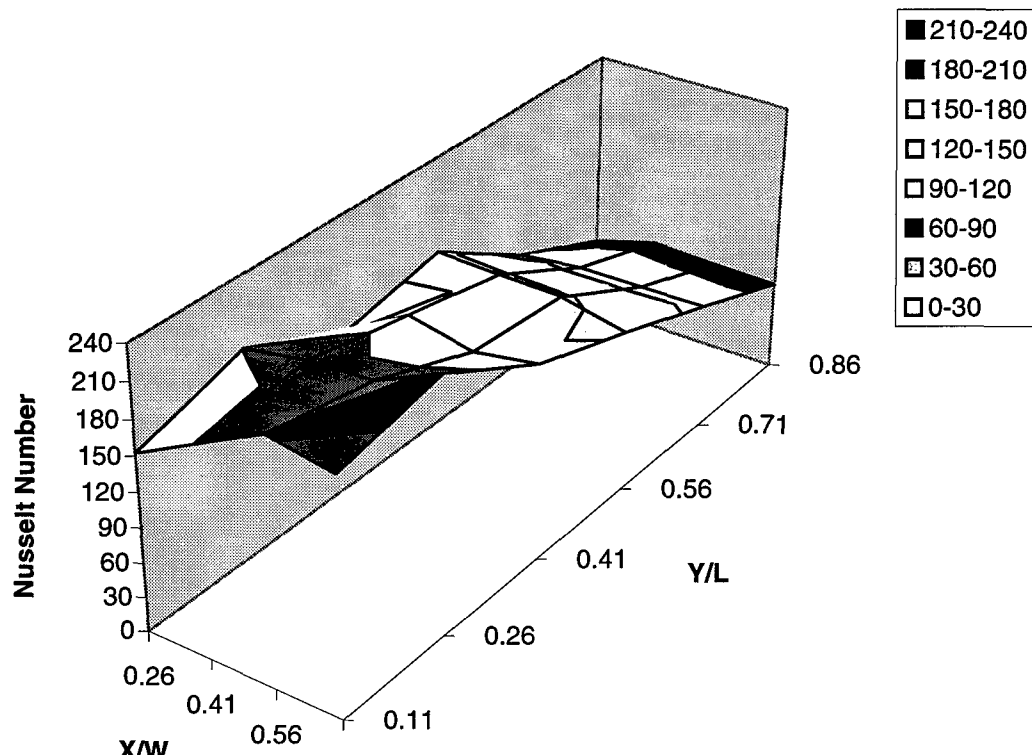
X(C). Effect of Reynold's Number:

In the present work, a change in Reynold's number is produced by changing the freestream flow velocity supplied to the control volume surrounding the heated block. To investigate the heat transfer effects, produced by these flow changes, it is helpful to first examine how varying the freestream velocity effects the flow field surrounding the block.

With an increase in the freestream Reynold's number, several structural changes to the flow field are observed, most notably is an increase in the separation bubble's reattachment length on the cover surface. This effect is found to be true for all Reynold's numbers below a threshold value as shown and discussed in the Flow Visualization Studies Section of this report. Another flow field effect, observed by Shaw, Chen, and Chen (1991) in their laminar flow simulation, is the enlargement of the recirculation regions on the rear and lateral surfaces of the block. These changes are sure to have corresponding effects on the convection heat transfer performance of the heated block surfaces.

To investigate the effects of a freestream Reynold's number change, Nusselt number distributions for freestream Reynold's numbers of approximately 14000 and 50000, based on block height, are produced. The results are presented in figures 24 through 30. The figures show the qualitative structure of the Nusselt number distribution, for a particular block surface, is relatively similar for the range of Reynold's numbers investigated. Comparison of the heat transfer data with the corresponding flow visualization, shows the maximum heat transfer location for the block cover (i.e. greatest Nusselt number) is located in the separation bubble's region of reattachment. This result holds true for all three freestream flow Reynold's numbers investigated. As mentioned earlier, this finding is

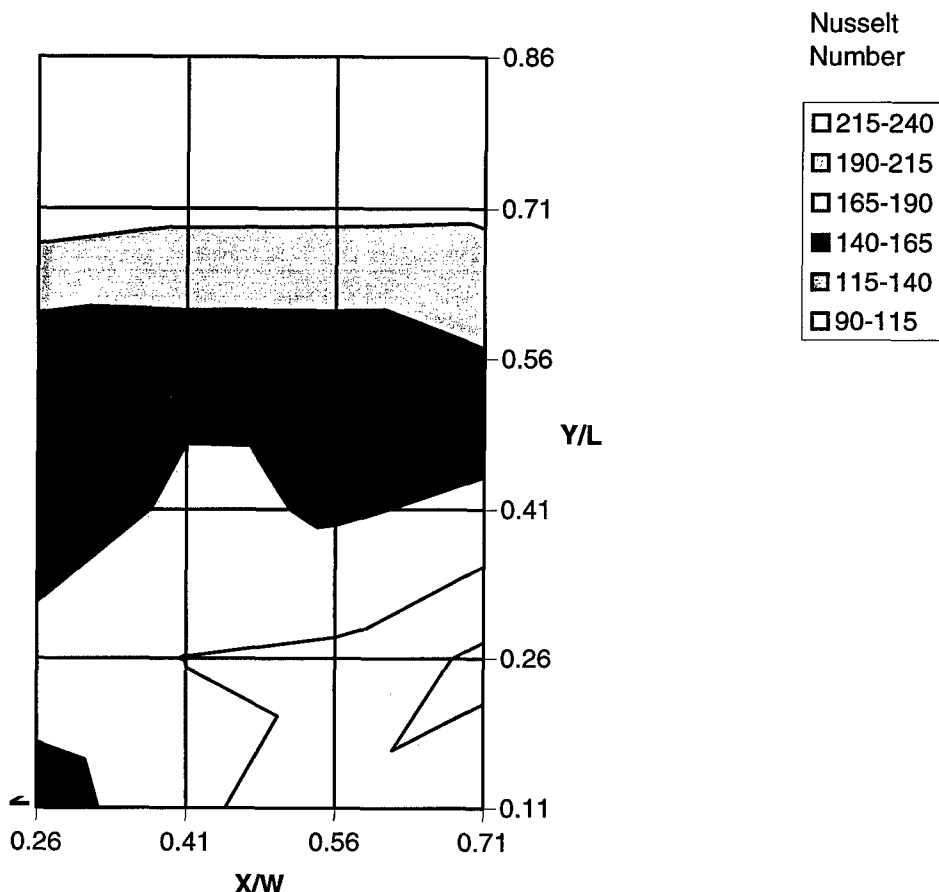
**Test 11-01, 02: 3-D Nusselt Number Surface Chart
(Cover Surface)**



$$NRe_{ave} = 13972, NGr_{ave} = 3.658 \times 10^7$$

Figure 24

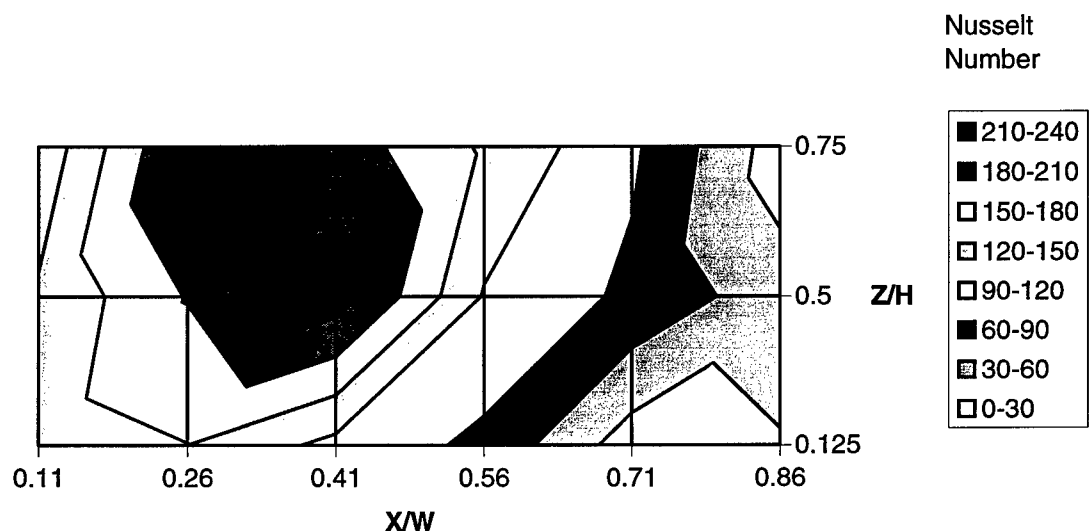
Composite Nusselt Number Contour Plot
Tests 11-01, 02 (Cover Surface)



$NRe_{ave} = 13972$, $NGr_{ave} = 3.658 \times 10^7$

Figure 25

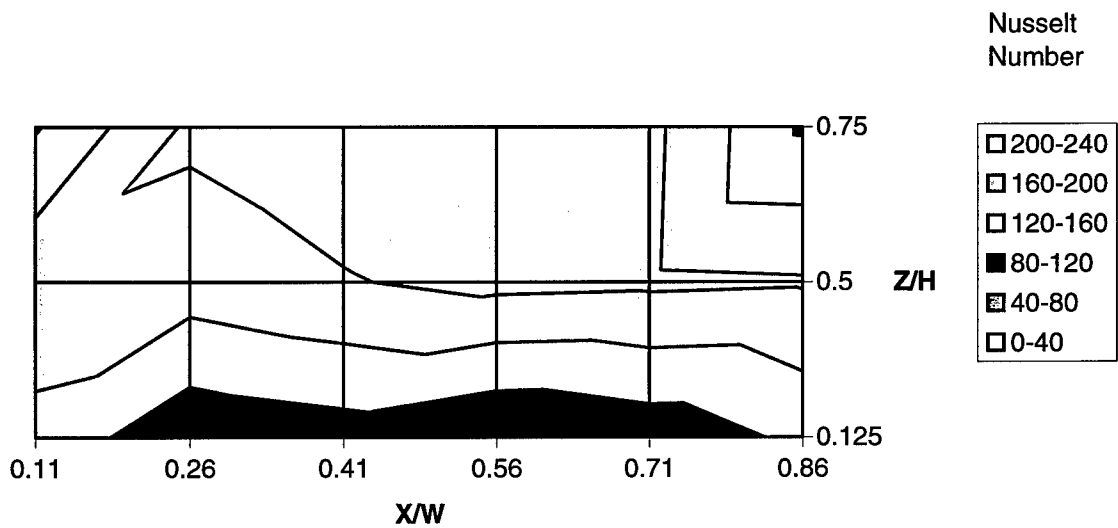
Test 11-02_1, Nusselt Number Contour Chart
(Left Lateral Surface)



$NRe = 13965, NGr,ave = 4.195 \times 10^7$

Figure 26

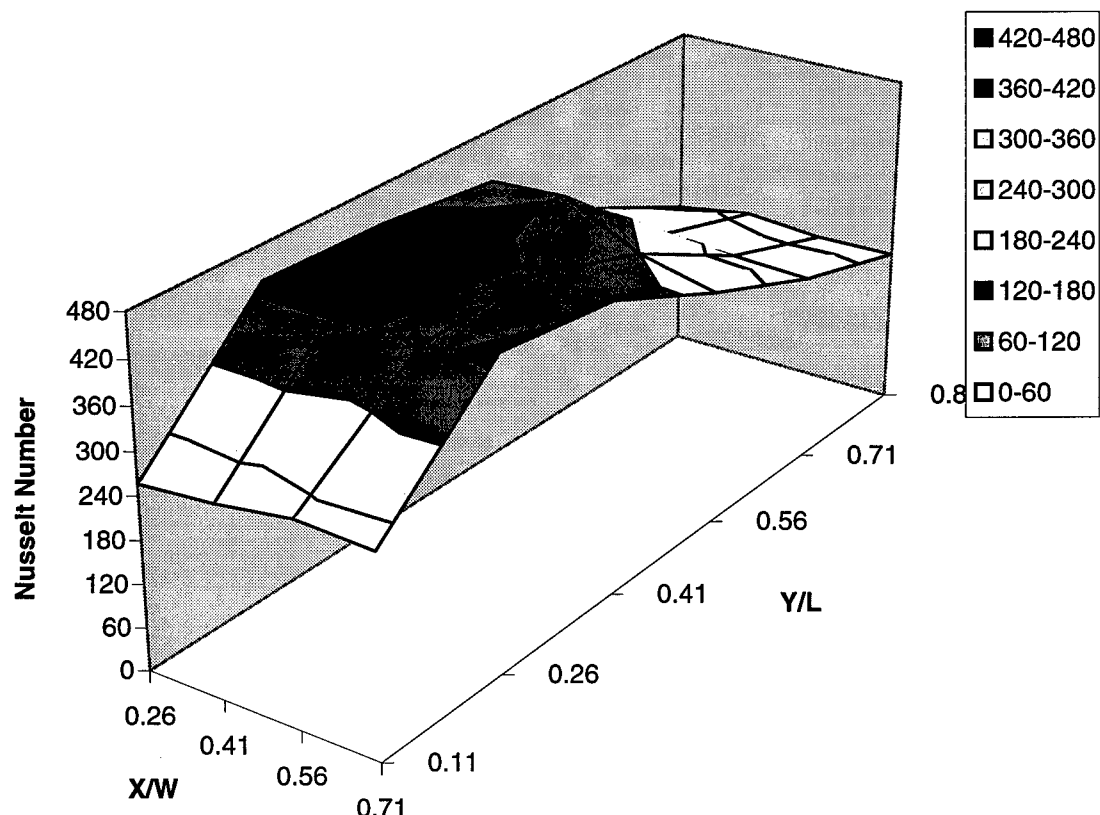
**Test 10-30_1, Nusselt Number Contour Chart
(Front Surface)**



$N_{Re} = 14286$, $N_{Gr,ave} = 3.452 \times 10^7$

Figure 27

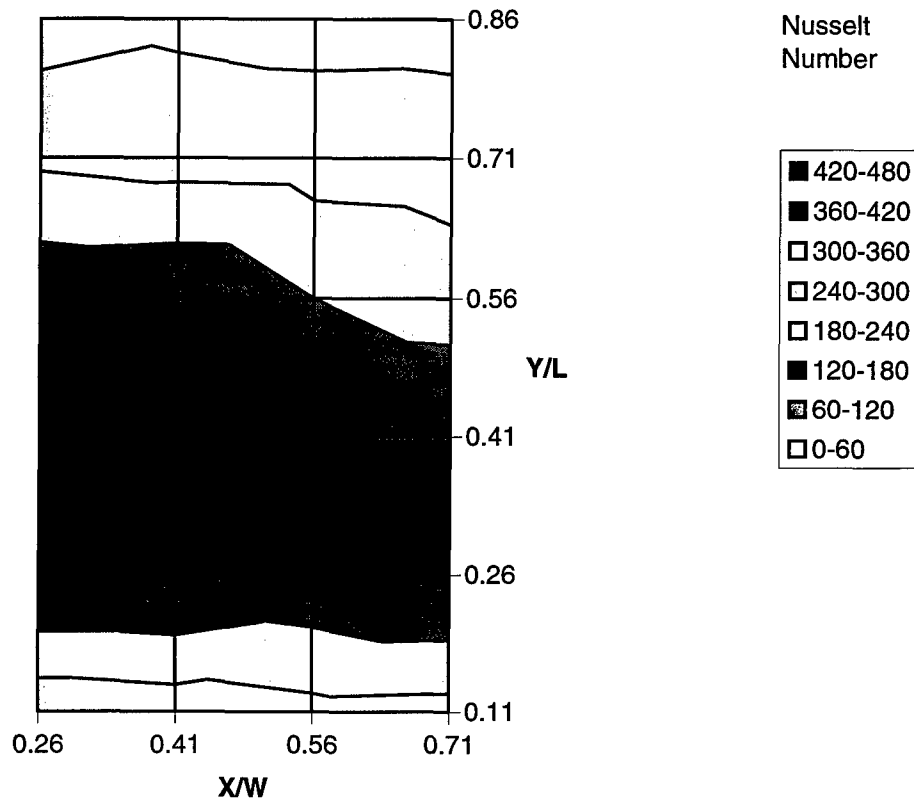
**Test 11-15, 21: 3-D Nusselt Number Surface Chart
(Cover Surface)**



$$NRe_{ave} = 50314, NGr_{ave} = 3.222 \times 10^7$$

Figure 28

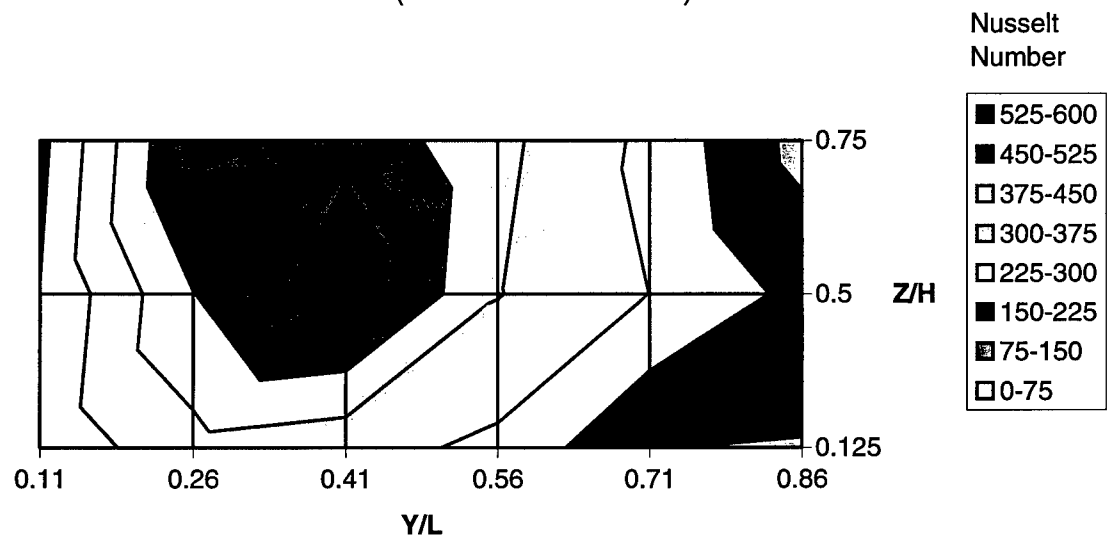
Composite Nusselt Number Contour Chart
Tests 11-15, 21 (Cover Surface)



$NRe_{ave} = 50314$, $NGr_{ave} = 3.222 \times 10^7$

Figure 29

Test 11-21_1, Nusselt Number Contour Chart
(Left Lateral Surface)



$N_{Re,ave} = 50134$, $N_{Gr,ave} = 3.633 \times 10^7$

Figure 30

consistent with previous blunt plate work by Ota and Kon (1974).

By comparing the shapes of the Nusselt number contour plots in figures 20, 25, and 29, an overall flattening of the Nusselt number distributions with Reynold's number decrease, is observed. To quantify this effect, a plot of the standard deviation in Nusselt numbers of each surface, along with other block surfaces, is presented in figure 31.

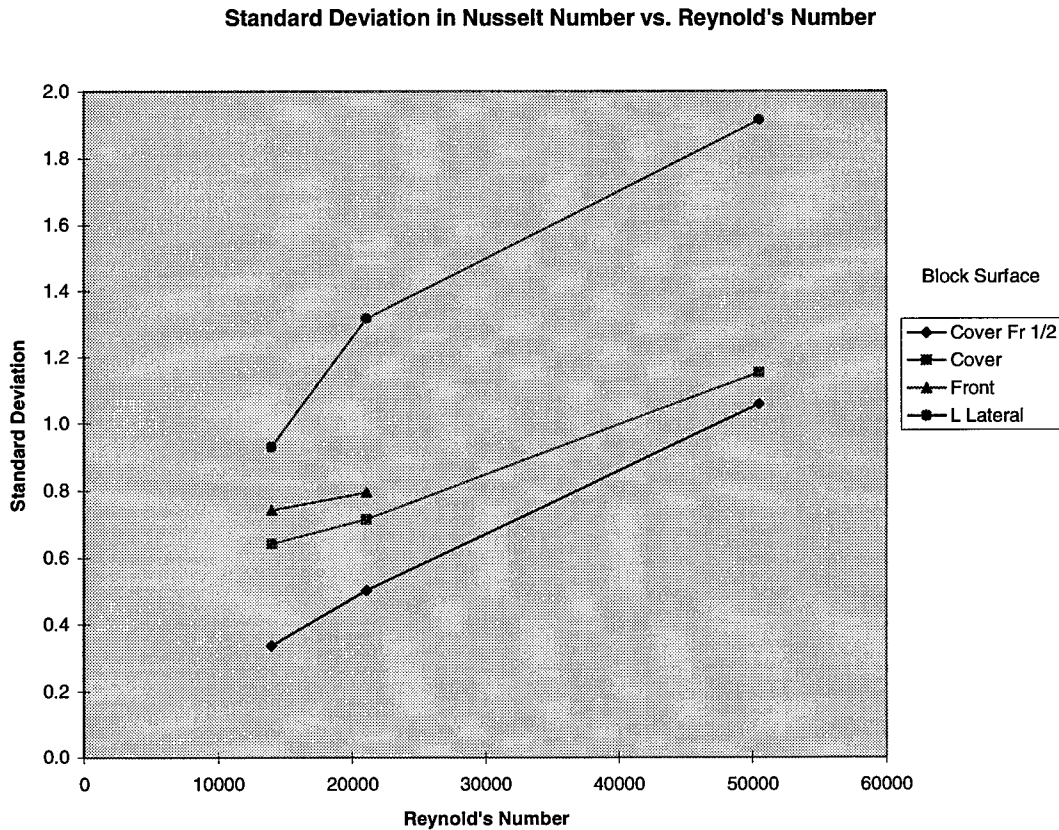


Figure 31

The figure presents a consistently increasing standard deviation in the Nusselt number, for a particular block surface, with increasing freestream flow Reynold's numbers. This translates to an overall increase in the Nusselt number surface's undulation as the freestream flow velocity is increased. The standard deviation increase on the front surface of the block is the smallest of all investigated surfaces. Examining figure 31 closely, shows the front surface of the block experiences only a slight increase

in the Nusselt number distribution's standard deviation, as compared to the cover and lateral surfaces. The result is expected, however, as the front surface's convection heat transfer is dominated by a flow field that lacks the Reynold's number dependent, separating flows found on the cover and lateral surfaces.

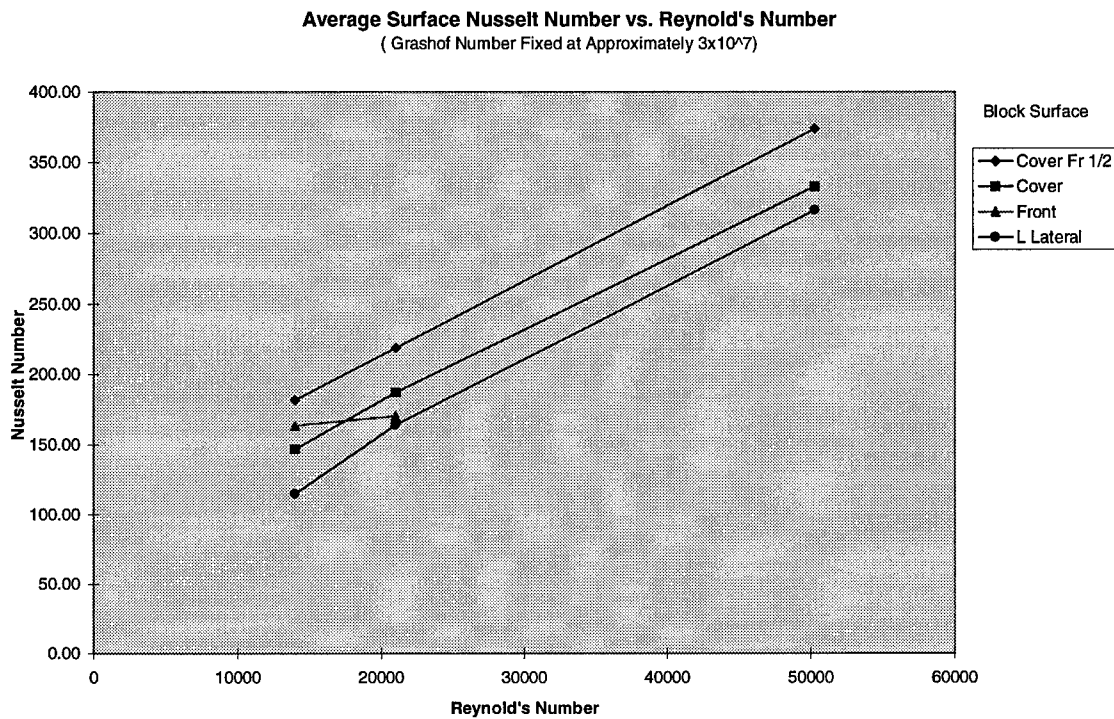


Figure 32

Figure 32 presents quantitative changes to the area based average Nusselt number of a block surface as freestream Reynold's number is changed. The results are associated with a fixed Grashof number of approximately 3×10^7 . Reducing the curves in figure 32 to exponential equations of the $N_{Nu} = N_{Re}^a$ form yields the following empirical relationships:

$$\text{Cover Front 1/2: } N_{Nu} = N_{Re}^{0.545}$$

$$\text{Full Cover: } N_{Nu} = N_{Re}^{0.529}$$

$$\text{Front: } N_{Nu} = N_{Re}^{0.525}$$

$$\text{Rear: } N_{Nu} = N_{Re}^{0.422}$$

$$\text{Lateral: } N_{Nu} = N_{Re}^{0.514}$$

The figure shows consistently increasing average Nusselt numbers with increases in freestream Reynold's number on the cover and lateral surfaces. Additionally, both surfaces increase at approximately the same rate.

This result is expected as higher heat transfer is commonly associated with increasing Reynold's number, even for non-separating flow fields. Additionally, increased heat transfer on the cover is also attributed to a larger vortex system, as flow visualization shows increased reattachment length and separation bubble intensity with the higher Reynold's numbers.

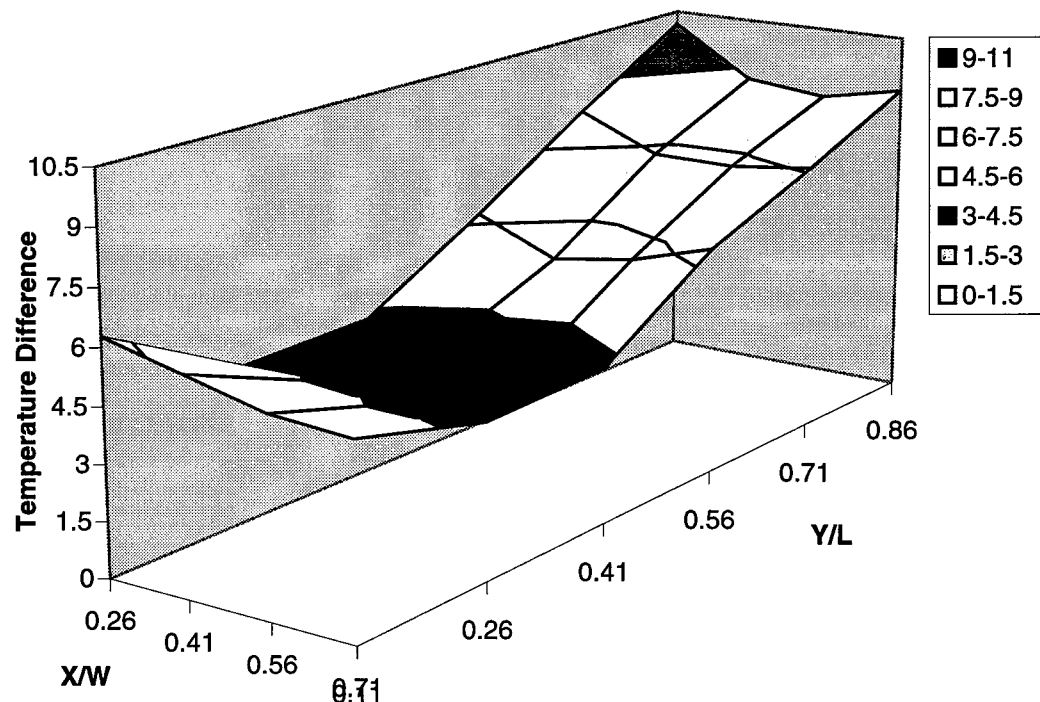
Although only two data points are available for the front surface of the block, the data show the surface is less affected by Reynold's number changes. Figure 32 shows only a relatively slight increase in average Nusselt number when freestream Reynold's number is increased from approximately 14000 to 21000.

X(D). Effect of Grashof Number:

In the present work, the method by which Grashof number changes are induced is by varying the current driven through the heated block. Tests are conducted at three Grashof numbers at a fixed freestream Reynold's number of approximately 21000. Figures 33-35 present the temperature distribution and Nusselt number distribution on the cover of the block at a Grashof number of 1.568×10^7 . Figure 36 shows the Nusselt number distribution on the left lateral block surface at a Grashof number of 1.898×10^7 . Figures 37-39 present the temperature distribution and Nusselt number distribution on the cover of the block at a Grashof number of 6.07×10^7 . Figures 40 and 41 show the Nusselt number distributions on the left lateral and front surfaces of the block at Grashof numbers of 6.421×10^7 and 5.515×10^7 , respectively. These figures, when combined with those presented in the Three-Dimensional Heat Transfer Description Section, provide three separate Grashof number scenarios on the cover, lateral, and front surfaces of the block.

Qualitatively comparing the shapes of the Nusselt number distribution surfaces on the cover of the block shows relatively similar features for all three Grashof numbers. Upon quantitative scrutiny, however, several significant changes are observed. One such important change is the relative deviation of the Nusselt number distribution with respect to an average for the entire surface. The deviation is best expressed by analyzing changes in the surface's standard deviation. Figure 42 presents the standard deviation in the cover surface's Nusselt number distribution at three average Grashof numbers, for a fixed freestream Reynold's number of approximately 14000. Also included in the figure, are data points representing the standard deviations for the cover at Reynold's numbers of approximately 21000 and 50000, at a single average Grashof number.

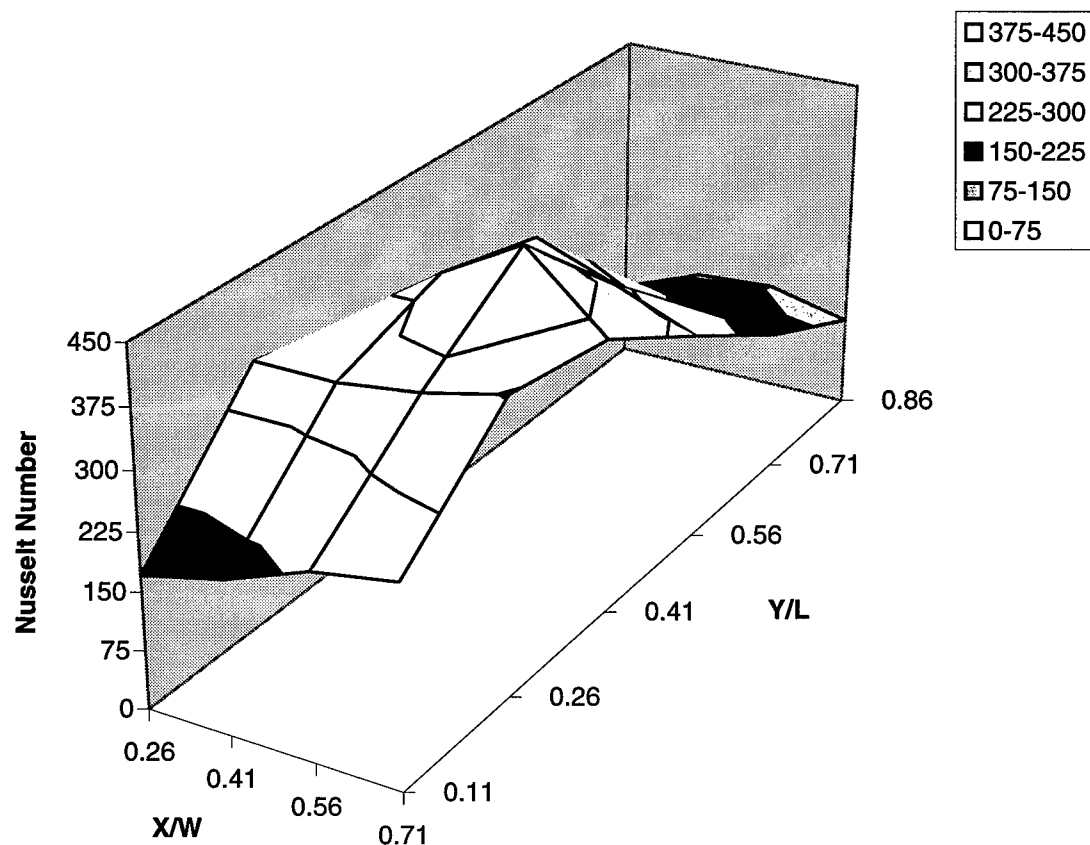
Composite Temp Diff Surface Plot
Tests 12-11, 02-21 (Cover Surface)



$NRe = 20937, NGr = 1.568 \times 10^7$

Figure 33

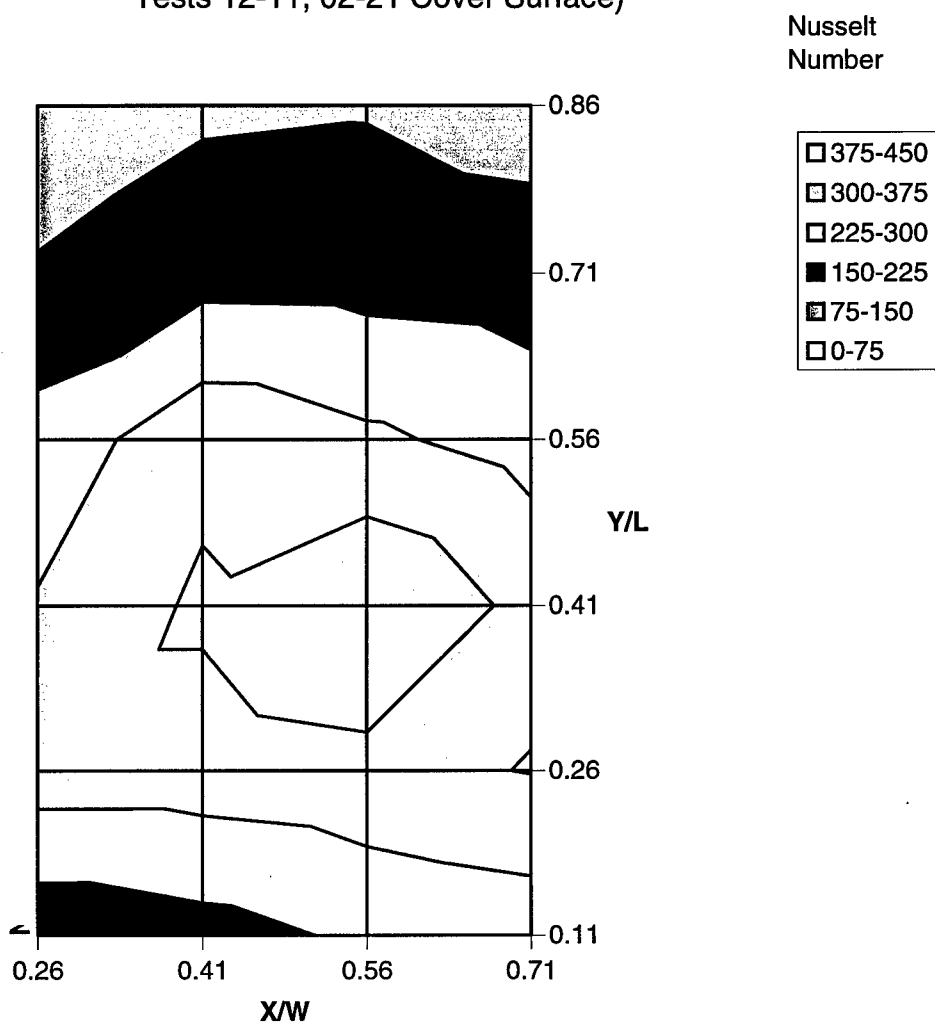
**Test 12-11, 02-21: 3-D Nusselt Number Surface Plot
(Cover Surface)**



$N_{Re,ave} = 20937$, $N_{Gr,ave} = 1.568 \times 10^7$

Figure 34

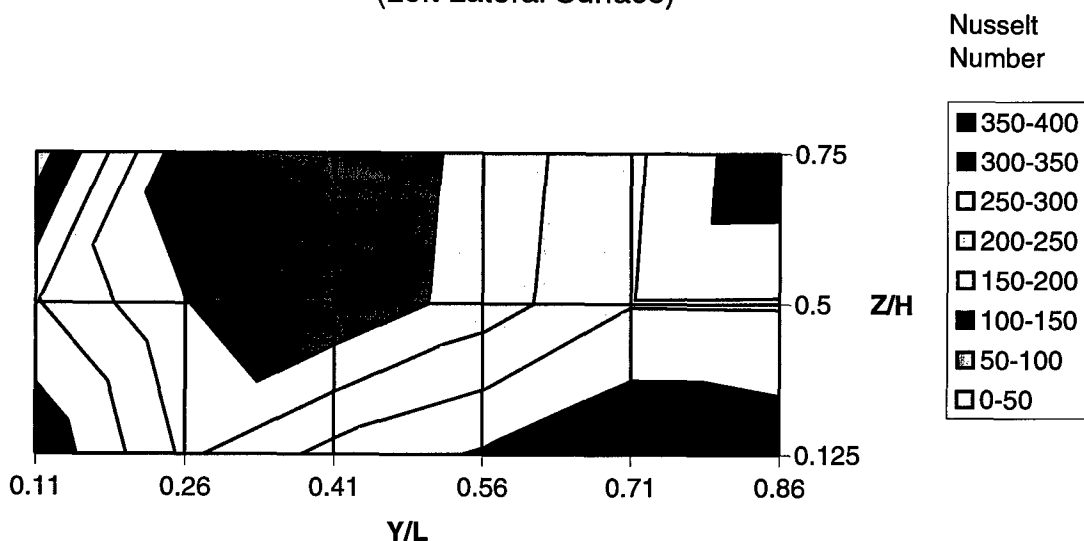
Composite Nusselt Number Contour Plot
 Tests 12-11, 02-21 Cover Surface)



N_{Re},ave = 20937, N_{Gr},ave = 1.568x10⁷

Figure 35

**Test 02-21_1, Nusselt Number Contour Chart
(Left Lateral Surface)**



$N_{Re} = 20715$, $N_{Gr,ave} = 1.898 \times 10^7$

Figure 36

3-D Composite Temperature Difference Surface Plot
Tests 12-12, 02-27 (Cover Surface)

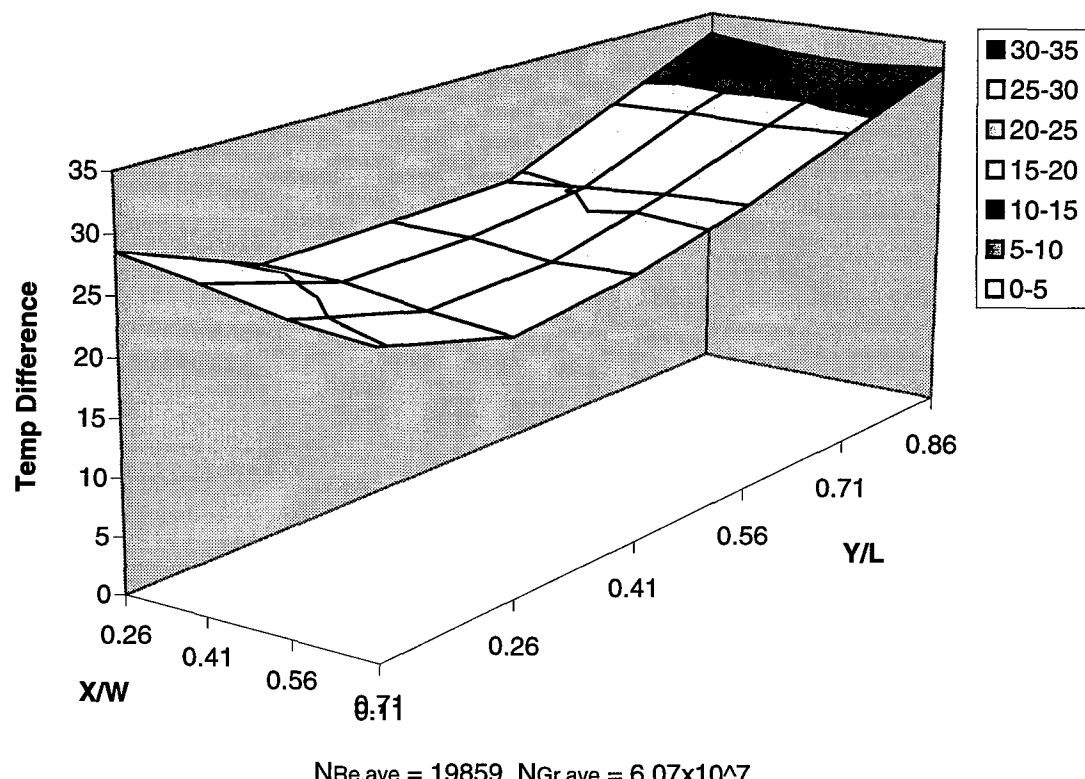
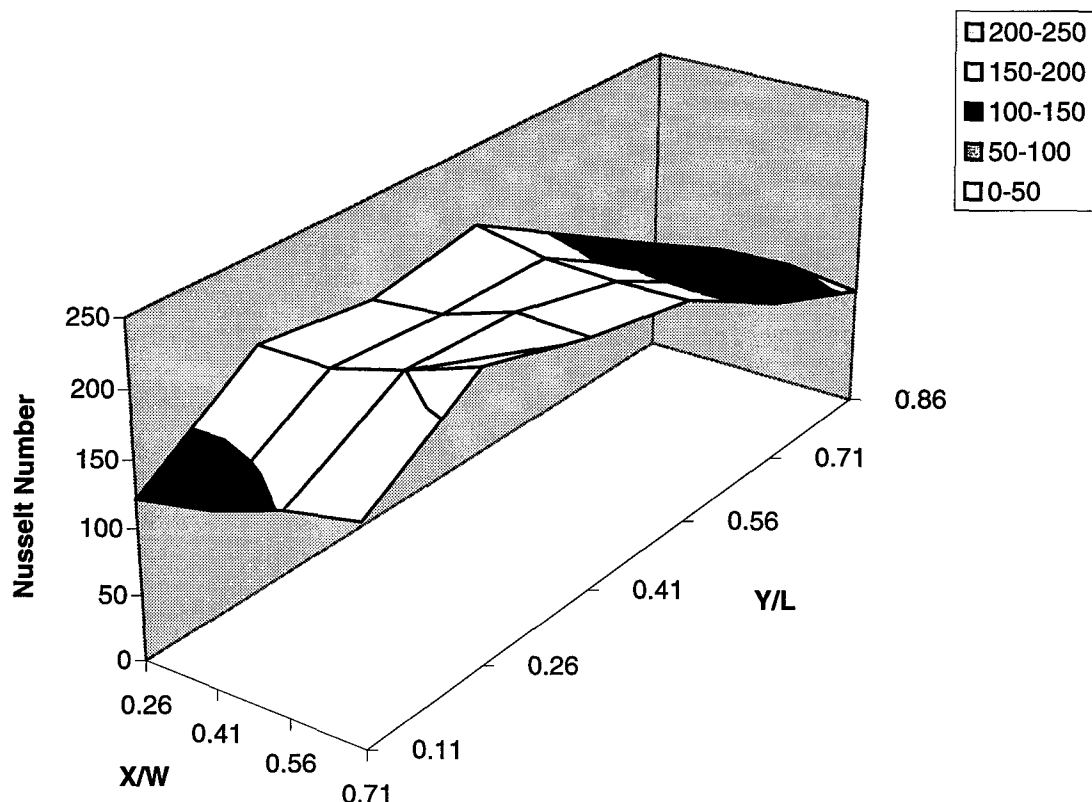


Figure 37

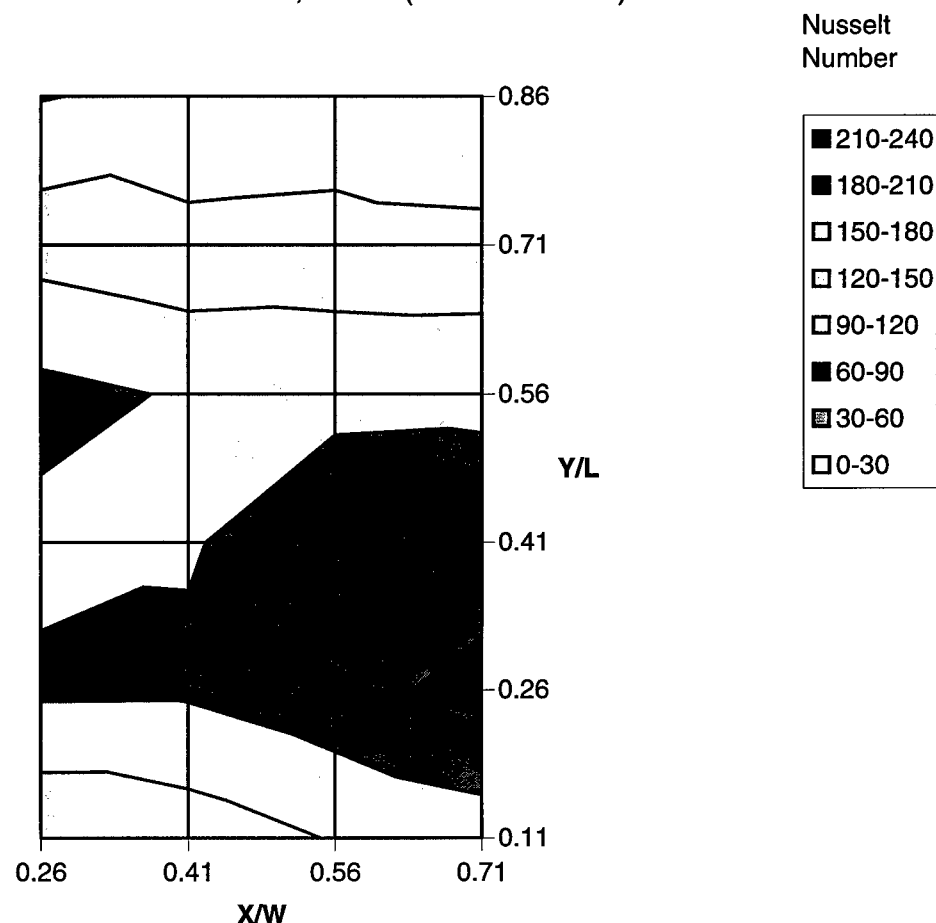
**Tests 12-12, 02-27: 3-D Nusselt Number Surface Chart
(Cover Surface)**



$N_{Re,ave} = 19859, N_{Gr,ave} = 6.07 \times 10^7$

Figure 38

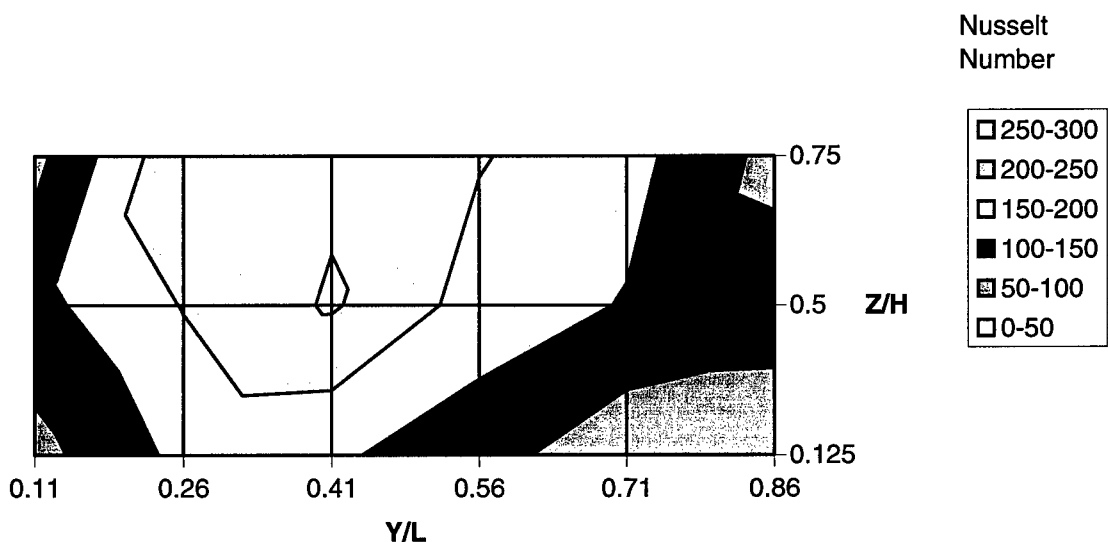
Composite Nusselt Number Contour Chart
Tests 12-12, 02-27 (Cover Surface)



$NRe_{ave} = 19859$, $NGr_{ave} = 6.07 \times 10^7$

Figure 39

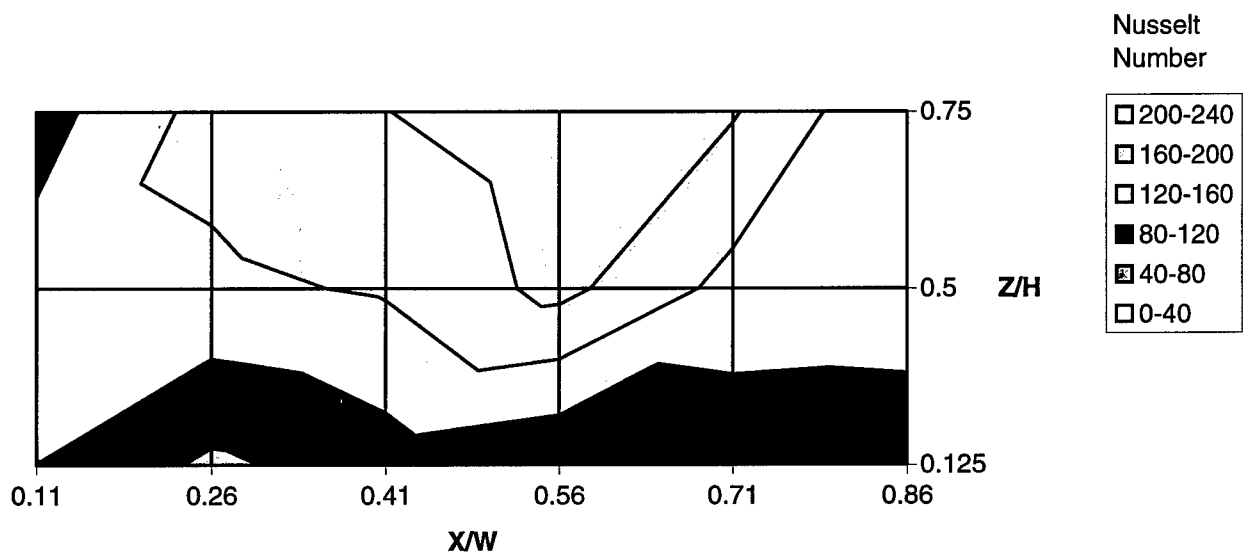
Test 02-27_1, Nusselt Number Contour Chart
(Left Lateral Surface)



$$NRe_{ave} = 19859, NGr_{ave} = 6.421 \times 10^7$$

Figure 40

**Test 10-25_1, Nusselt Number Contour Chart
(Front Surface)**



$NRe_{ave} = 19879, NGr_{ave} = 5.515 \times 10^7$

Figure 41

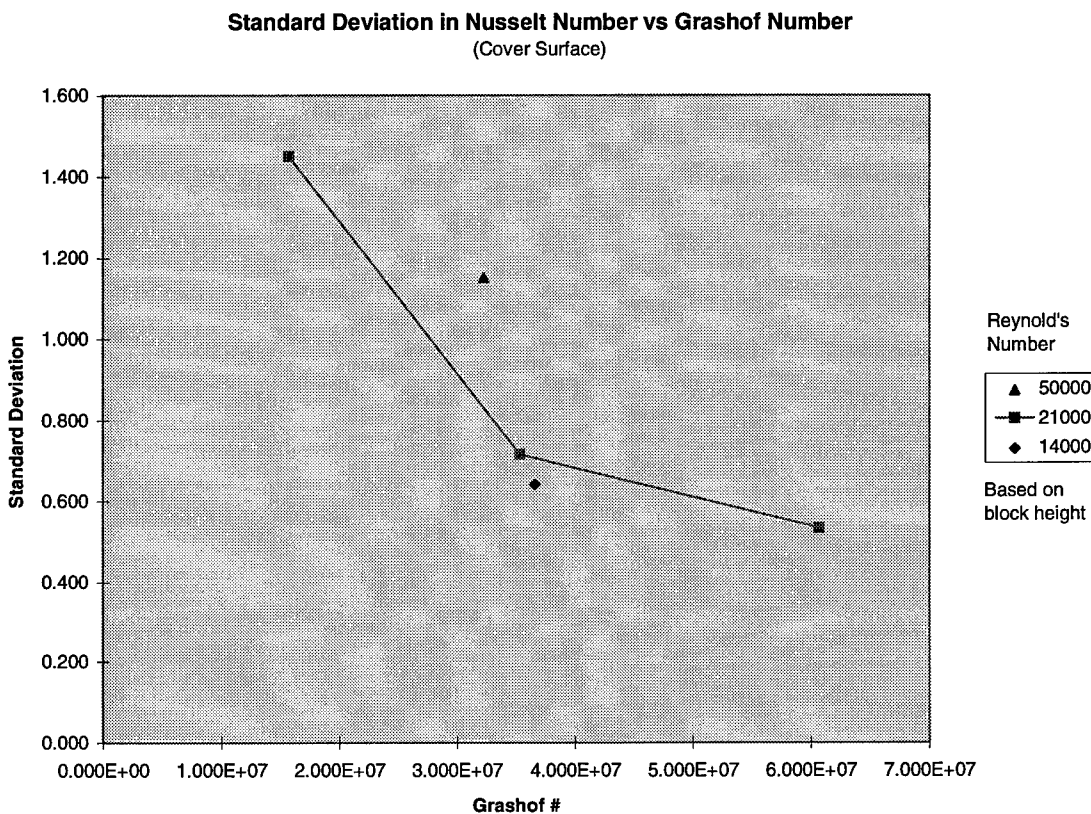


Figure 42

The figure shows the standard deviation in the Nusselt number consistently decreases with increasing Grashof number, resulting in an overall flattening of the surface distribution as the influence of buoyancy grows. This effect is attributed to the fact that buoyancy forces increase the strength of natural convection heat transfer in regions of relatively stagnant flow, bringing the regions heat transfer performance closer to that of surrounding forced convection counterparts. Additionally, it is argued in Shaw, Chen, and Chen (1991), that the upward directed forces of buoyancy cause fluid moving over the separation bubble region to flow upward, reducing the intensity of the vortex system's heat dissipation. This effect would serve the purpose of flattening the front portion of the cover, bringing it closer to the heat transfer performance of the non-separating rear portion.

The overall quantitative effect to the cover's average Nusselt number, of increasing the average Grashof number, is shown in figure 43.

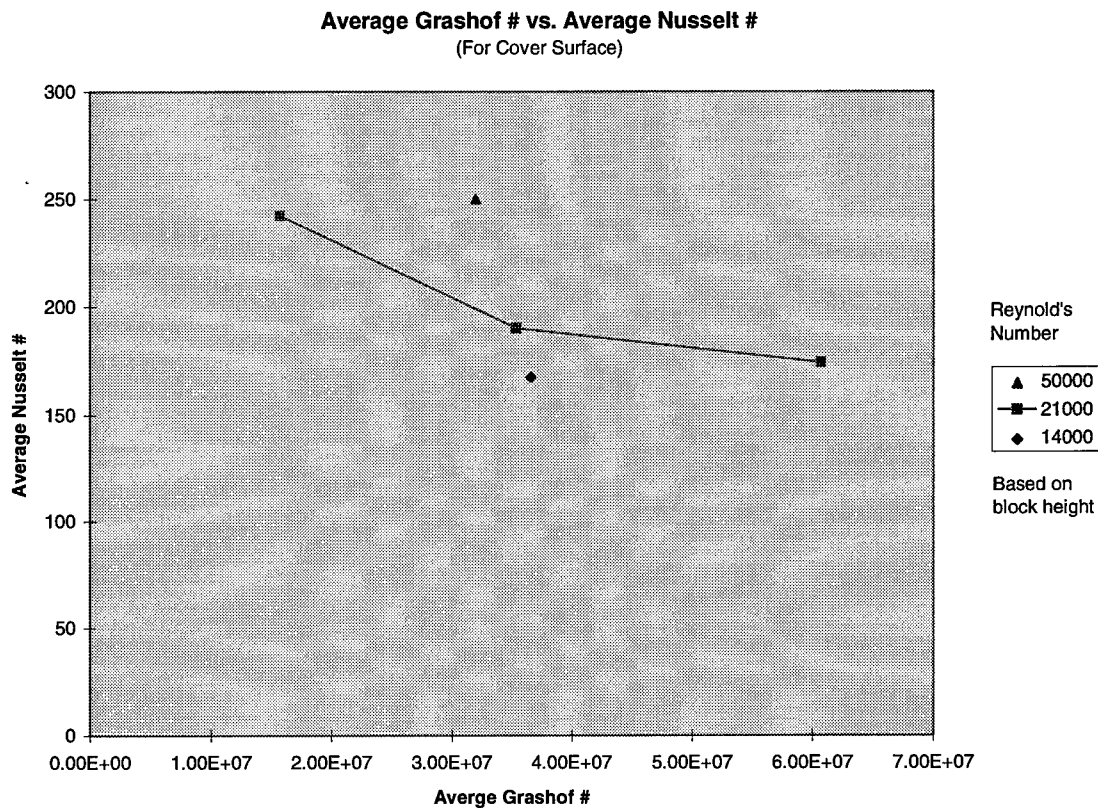


Figure 43

The figure shows the average Nusselt number decreases with increases in the average Grashof number. Additionally, the rate of decrease diminishes with increasing Grashof number. While the Nusselt number effects produced by the increased buoyancy forces described earlier certainly affect the average Nusselt number for the cover, the influence of upstream flow changes produced by the surrounding heated board are also important. Because the board upstream of the block is heated, portions of the boundary layer flow, which impinges on the block front face and moves up onto its cover, is heated to higher temperatures as the Grashof number is increased. The higher temperature air (in effect the cooling supply to the block) results in a smaller

temperature difference between the freestream flow and block surface, and can not cool the block surfaces as effectively. The reduction in average Nusselt number may further be explained by realizing the region of greatest convection heat transfer lies at the reattachment line of the separation bubble. In this region, relatively cool freestream flow is being forced down to the surface of the cover by pressure differentials in the flow field. The force of buoyancy inhibits this phenomena, as it operates in exactly the opposite direction of the pressure forces. While these results seem contrary to many non-separating flow findings, they are supported by Shaw, Chen, and Chen's (1991) simulation involved with similar laminar separating flows. In their observations, the average Nusselt number on the cover surface decreased by approximately eight percent when the Grashof number was increased ten-fold ($N_{Gr} = 10000 - 100,000$, $N_{Re} = \text{fixed} = 100$). In the present work, a 287 percent increase in the Grashof number (1.156×10^7 to 6.07×10^7) results in an average Nusselt number drop for the cover surface of 26 percent. The greater Nusselt reduction in the present work is attributed to the fact that the heated board surrounding the block emits the same heat flux as the block itself (due to the equal current passing through both devices), thereby simulating perfect thermal conductivity in the heated board. Shaw, Chen, and Chen's computer simulation allowed for more realistic conduction heat transfer modeling.

Figures 36 and 40, along with figure 16 from the Three-Dimensional Heat Transfer Description Section, provide three separate Grashof number results for the left lateral surface of the block. Generally speaking, the three figures show a relatively similar picture of the Nusselt number distribution. The surface seems less influenced by the effects of Grashof number variation than exhibited by the cover surface. Figure 44 presents the standard deviation in the Nusselt number distribution for each of the three Grashof number (based on the cover calculations) scenarios.

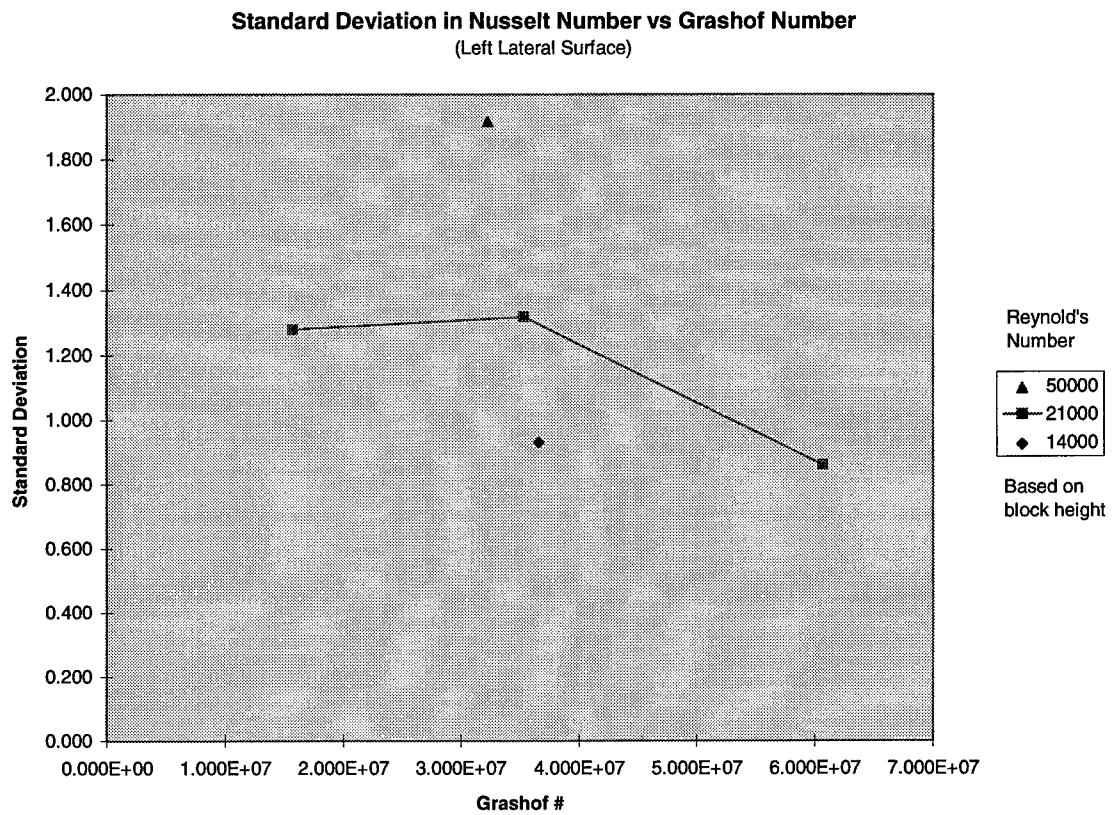


Figure 44

The figure shows the standard deviation in Nusselt number changes relatively little with an increase in the cover Grashof number from 1.898×10^7 to 3.5×10^7 , and a fixed freestream flow velocity of 660 feet per minute. As the cover Grashof number is further increased to 6.4×10^7 , the standard deviation on the left lateral surface drops by approximately 33 percent.

Quantitative changes produced by Grashof number variation on the left lateral surface's Nusselt number average are shown in figure 45.

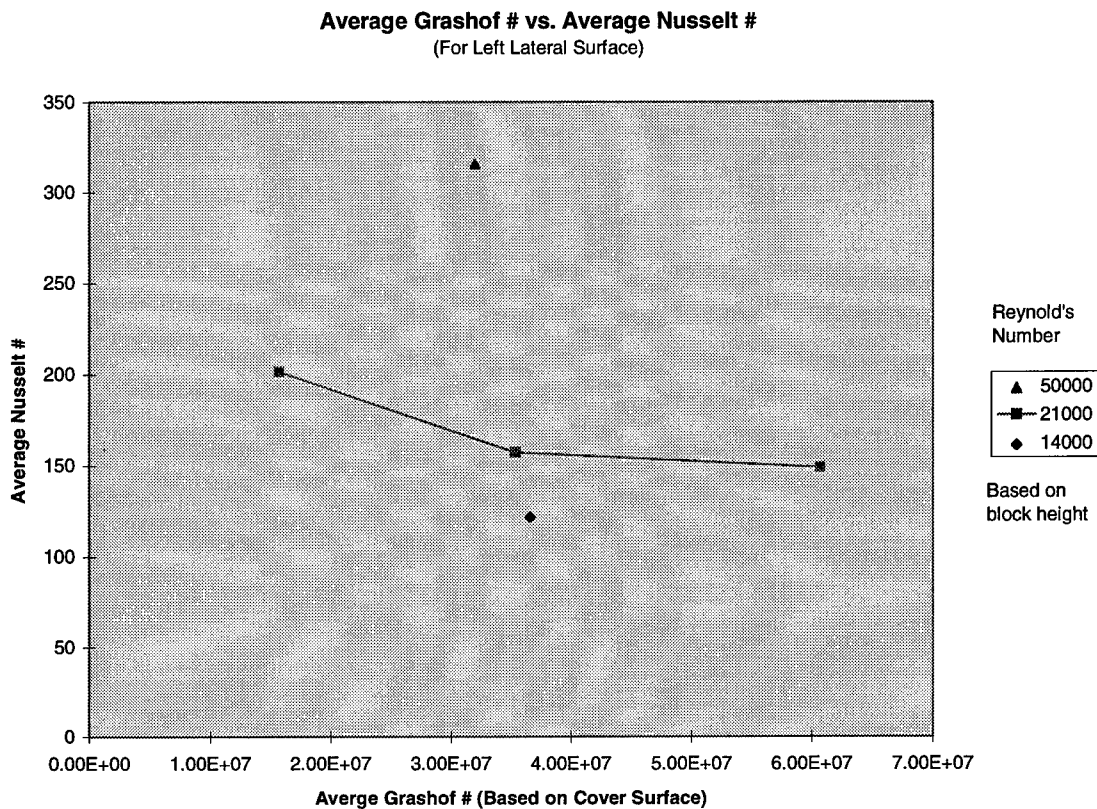


Figure 45

The figure shows the average surface Nusselt number decreases with increasing Grashof number. Additionally, the rate of decrease appears to be diminishing towards a limiting value. These changes are almost identical, in trends and magnitude, to those found on the block's cover surface. The similarity is attributed to the fact that both surfaces experience the same increase in incoming boundary layer flow temperature from the upstream board heating.

Figures 15 and 41 present Nusselt number distributions on the front face of the block at average cover Grashof numbers of 3.221×10^7 and 5.515×10^7 , respectively. Comparing the two figures shows the surface is substantially less sensitive to Grashof number variation than either the left lateral or cover surfaces. The Grashof number change produces relatively little qualitative change in the structure of the surface

distribution, but results in a quantitative decrease in the average Nusselt number on the surface of approximately six percent . Additionally, the Nusselt number, located near the centerline of the upper row of RTD sensors, drops approximately 10 percent. The drop in average Nusselt number is again attributed to the upstream boundary layer flow effects produced by the heated board surface.

XI. Conclusions:

The goal of the present work is to investigate and describe the effects of secondary flows on the convective heat transfer from the surfaces of a heated block immersed in an airstream. A complete three dimensional heat transfer description is produced, along with description of the effects observed in response to changes in the freestream Reynold's number and Grashof number. The experimental foundation of low-profile block data constructed provides a detailed base for comparisons with contemporary dynamically similar numerical research. Additionally, the data reported furnishes convective boundary conditions for traditional thermal modeling of solid components.

Results of the three dimensional heat transfer description show Nusselt number distributions, on each of the exposed block surfaces, are highly influenced by the nature and characteristics of the three dimensional flow fields in which they exist. The predominant characteristic of the convection heat transfer, on the cover surface of the block, is the influence of a separating and reattaching flow field. The present work shows this feature influences the heat transfer performance on the cover by significantly increasing convection heat transfer from the surface regions on which the bubble interacts. Additionally, the maximum Nusselt numbers on the surface are located in the region of the separation bubble reattachment line. Beyond the reattachment region, the Nusselt number distribution on the cover behaves similar to typical flat plate flows, exhibiting a steady decrease in the streamwise (Y) direction. The result is attributed to the diminishing temperature difference between the cooling fluid and block surface as it picks up energy, flowing along the heated cover surface.

Interestingly, the Nusselt number distribution on the cover shows regions with significant three dimensional features, and regions with predominantly two dimensional

shape. While flow visualization studies conducted in the present work, Wardwell (1993), and Shaw, Chen, and Chen (1991) all show considerably three dimensional flow fields, the resulting Nusselt number distributions do not reflect this same significance. Cross-stream (X-direction) variations in the heat transfer coefficient are quantitatively significant only in the regions engulfed by the separation bubble.

The results of the Nusselt number distributions on the lateral surfaces of the block show three dimensional trends that exhibit separating and reattaching flow fields stemming from the surfaces' sharp leading edges. Likewise, the Nusselt number distributions show an increase in convection heat transfer from the leading edge of the surface, up to a maximum near the approximate streamwise (Y-direction) mid-line. It is speculated this maximum corresponds with a reattachment line region present on the lateral surfaces. Beyond the Nusselt number maximum, surface flow picks up heat as it moves along the streamwise direction, thereby reducing the temperature difference between the fluid and block surfaces, reducing the Nusselt number values to a minimum at the rear edge of the lateral surface.

Unlike the cover surface, the lateral surfaces exhibit considerable variation in the cross-stream (Z) direction. Results show the Nusselt number distribution, on the upstream half of the surface, increases from the bottom of the surface, to a maximum near the $Z/H = 0.5$ sensor line, and then drops slightly to the $Z/H = 0.75$ location. The downstream half of the surface shows smaller variations. Bottom to top variation there consistently increases, but the differences between the Nusselt number values at $Z/H = 0.125$, 0.5, and 0.75 sensor lines locations are less significant than those on the upstream half.

The Nusselt number distribution results on the front surface of the block shows a generally increasing trend from bottom to top (Z-direction). This is consistent with the

numerical simulation data presented by Shaw, Chen, and Chen (1991). The surface also exhibits good symmetry about the vertical mid-line of the face. Nusselt number distribution is relatively flat in the cross-stream (X) direction, except for the outermost sensors near the face's lateral edges. Near both edges of the face, the $Z/H = 0.125$ and $Z/H = 0.5$ sensors exhibit an increase in the convection heat transfer. This result is attributed to the increased flow velocities in those areas, produced from the accelerating flows, moving outward from the central impingement region.

The flow experiments by Chyu and Natarajan (1991) and Shaw, Chen, and Chen (1991) both indicate highly complex, recirculating, multiple vortex systems exist on the rear surface of a cube and low-profile block, respectively. Results of the present work show a Nusselt number distribution, on the rear surface, consistent with these flows. Variation of the Nusselt number in the X-direction shows a clearly defined, inverted, horseshoe shaped Nusselt number distribution, with its maximum at the top of the surface's vertical mid-line. Additionally, plots of the local Nusselt numbers exhibit relatively minimal Z-direction variation, with all three horizontal lines of RTD sensors showing similar values.

For cover, lateral, and front surfaces of the block, the Nusselt number distribution is investigated at three different freestream Reynold's numbers (15000, 22000, and 51000 based on block height). In all cases, the observed effect of increasing the freestream Reynold's number is a corresponding increase in the convection heat transfer rate.

The cover and lateral surface's Nusselt number distributions are significantly influenced by increases in freestream Reynold's number. Results of the present work show increases in the surfaces' average Nusselt number of 16.75 and 27.9 percent as the freestream Reynold's number (based on block height) is increased from 15000 to

21000, respectively. Additionally, both surfaces' convection heat transfer rates more than double when the freestream Reynold's number is increased from 15000 to 51000. The trend of these results is consistent with that found by Shaw, Chen, and Chen (1991) in their simulation experiment performed at much lower Reynold's numbers (100 to 500 based on block height). The flow visualization testing in the present work, and a previous flow study by Wardwell (1993), both show the reattachment length of the cover's separation bubble increases in size for Reynold's numbers below a threshold value. Additionally, results from the present work show an increase in freestream Reynold's number produces a more intense, and undulated, Nusselt number distribution on the cover, particularly in the separation zone area. Because the separation zones are the regions of greatest convection heat transfer, the observed average Nusselt number increases are attributed to the presence of larger, more intense separation bubbles. Previous flow studies by Chyu and Natarajan (1991) infer a separation bubble phenomena on the lateral surfaces of a cube. It is reasonable to expect that separation bubbles exist on the lateral surfaces of the block in the present work. Increases in the average Nusselt number on the surfaces (with increased Reynold's number), are attributed to separation zone structure changes similar to those described earlier for the cover.

Unlike the cover and lateral surfaces, the front surface of the block exhibits a relatively modest increase in average Nusselt number as freestream Reynold's number is increased. For the Reynold's number increase of 15000 to 21000, the surface Nusselt number increases by only 2.5 percent. This result is qualitatively consistent with the results observed in the simulation by Shaw, Chen, and Chen (1991). The result is expected as the front surface flow is dominated by a strong flow into a central

impingement area, whose structure does not significantly change with increased flow velocity.

The convection heat transfer effects produced by Grashof number variations are also investigated. Traditionally, the purpose for examining Grashof number effects is to determine the significance of buoyancy forces. The present work investigates three different Grashof number scenarios, at a fixed freestream Reynold's number of approximately 21000 (based on block height). Results show increases in the Grashof number cause the Nusselt number distribution, on the cover of the block, to flatten and become more uniform. The standard deviation of the distribution's surface drops approximately 50 percent as Grashof number is increased from 1.568×10^7 to 3.534×10^7 . Increasing the Grashof number further, to 6.07×10^7 , results in a an additional standard deviation drop of 26 percent. The change in the distribution's shape is attributed to the forces of buoyancy. Because buoyancy forces act in the positive Z-direction, they are in direct competition with the forces created by the pressure differential in the reattachment region of the cover's separation bubble. This opposition decreases the cooling effectiveness of the separation. Since the separation bubble is a convection enhancing phenomena, and the reattachment region is the location of maximum convection heat transfer, a drop of the Nusselt number for the entire separation zone area results. Additionally, forces of buoyancy in the non-separating rear section of the cover tend to lift the fluid off the surface, along with the heat it has absorbed as it moves over the surface. This effect tends to increase the heat transfer effectiveness of the cover's rear portion, bringing the local Nusselt number values closer to those present on the front half.

From the above arguments concerning the qualitative effects of increasing Grashof number, it is evident buoyancy forces serve both to increase, and decrease, the

convection heat transfer on the cover surface of the block. Normally, quantitative comparisons of the entire surface's average Nusselt number would provide insight into the more dominate effect. Results of quantitative comparisons of the Nusselt number for the entire cover surface show the value decreases with increasing Grashof number. If buoyancy were the only factor affecting the convection heat transfer this would lead to the conclusion that the separation bubble structure changes described are the dominant convection effect. In the present work, however, changes in the Grashof number are also accompanied by changes in the properties of the incoming freestream flow and boundary layer. When input current to the heated block is increased, so is current to the upstream heated board sections. This results in higher temperature, and thus lower cooling capacity, fluid initially impinging upon the block surfaces. Because of this, we must look to the effects produced on other block surfaces, as a result of the Grashof number change, for further insight. This "big picture" analysis leads to different conclusions. In particular, examination of the average surface convection performance for the lateral and front face show Grashof number increases produce Nusselt number decreases, albeit not as great as those produced on the cover surface. Since these surfaces are oriented in the same direction as the forces of buoyancy, their convection heat transfer performance intuitively would exhibit an increase with increased Grashof number. This result leads to the conclusion that the changes to the upstream freestream flow properties dominate the convection performance effects, and cause the overall reduction in average Nusselt numbers on the investigated surfaces.

The data described herein provides both a qualitative and quantitative description of the heat transfer from a heated block, along with discussions concerning the effects of the local three dimensional flow field. Near surface flow on the cover of the block, is elaborated by flow visualization. Lastly, the effects generated by changes

to the freestream Reynold's number and average Grashof number are explained, further characterizing the heat transfer performance of the block in various environmental conditions.

XII. References:

Boyle, M. T., and Wardwell, S., 1995, "The Three-Dimensional Vortex System Near the Cover of a Rectangular Package Shape Mounted in a Duct," *Proceedings of the 30th ASME Heat Transfer Conference*, Vol. 1, pp. 17-25.

Castro, I. P., and Robins, A. G., 1977, "The Flow Around a Surface-Mounted Cube in Uniform and Turbulent Streams," *Journal of Fluid Mechanics*, Vol. 79, pp. 307-355.

Cherry, N. J., Hillier, R., and Latour, M. E. M. P., 1983a, "The Unsteady Structure of Two-Dimensional Separated and Reattaching Flows," *Journal of Wind Engineering and Industrial Aeronautics*, Vol. 11, pp. 95-105.

Cherry, N. J., Hillier, R., and Latour, M. E. M. P., 1983b, "Unsteady Measurements in a Separated and Reattaching Flow," *Journal of Fluid Mechanics*, Vol. 144, pp. 13-46.

Chyu, M. K., and Natarajan, V., 1991, "Local Heat/Mass Transfer Distributions on the Surface of a Wall-Mounted Cube," *Journal of Heat Transfer*, Vol. 113, pp. 851-857.

Djilali, N., and Gartshore, I. S., 1991, "Turbulent Flow Around a Bluff Rectangular Plate. Part I: Experimental Investigation," *Journal of Fluids Engineering*, Vol. 113, pp. 51-59.

Djilali, N., "Effects of Leading Edge Geometry on a Turbulent Separation Bubble," *AIAA Journal*, Vol. 30, N. 2, pp. 559.

Dziomba, B., 1985, "Experimental Investigations of Bluff Body Separation Regions," Presented at CASI Aerodynamics Symposium, Montreal.

Gebhart, B., 1988, *Buoyancy-Induced Flows and Transport*, Hemisphere Publications Inc., pp. 937-938.

Hillier, R., and Cherry, N. J., 1981a, "The Effect of Freestream Turbulence on Separation Bubbles," *Journal of Wind Engineering and Industrial Aeronautics*, Vol. 8, pp. 49-58.

Hillier, R., and Cherry, N. J., 1981b, "Pressure Fluctuations Under a Turbulent Shear Layer," Proceedings of the 3rd Symposium on Turbulent Shear Flows, University of California, Davis, pp. 16.23-16.29.

Kiya, M., and Sasaki, K., 1983, "Freestream Turbulence Effects on a Separation Bubble," *Journal of Wind Engineering and Industrial Aeronautics*, Vol. 14, pp. 375-386.

Langston, L.S., and Boyle, M.T., 1982, "A New Surface Streamline Flow Visualization Technique," *Journal of Fluid Mechanics*, Vol. 125, pp. 53-58.

Ota, T., Asano, Y., and Ikawa, J., 1981, "Reattachment Length and Transition of the Separated Flow Over Blunt Flat Plates," *Bulletin. Japanese Society of Mechanical Engineers*, Vol. 24(192), pp. 941-947.

Ota, T., and Kon N., 1974, "Heat Transfer in the Separated and Reattached Flow on a Blunt Flat Plate," *Journal of Heat Transfer*, pp. 459-462.

Patankar, S. V., Liu, C. H., and Sparrow, E. M., 1977, "Fully Developed Flow and Heat Transfer in Ducts Having Streamwise-Periodic Variations of Cross-Sectional Area," *Journal of Heat Transfer*, Vol. 99, pp. 180-186.

Shaw, H. J., Chen, W. L., and Chen, C. K., 1991, "Study on the Laminar Mixed Convective Heat Transfer in a Three-Dimensional Channel with a Thermal Source," *Journal of Electronic Packaging*, Vol. 113, pp. 40-49.

Wardwell, Scott E., 1993, "An Investigation of the Vortex Above the Cover of a Three-Dimensional Electronics Package Shape," Master's Thesis, University of Maine.

Wirtz, R. A., and Mathur, A., 1994, "Convective Heat Transfer Distribution on the Surface of an Electronic Package," *Journal of Electronic Packaging*, Vol. 116, pp. 49-54.

XIII(A). Miscellaneous Tables and Figures

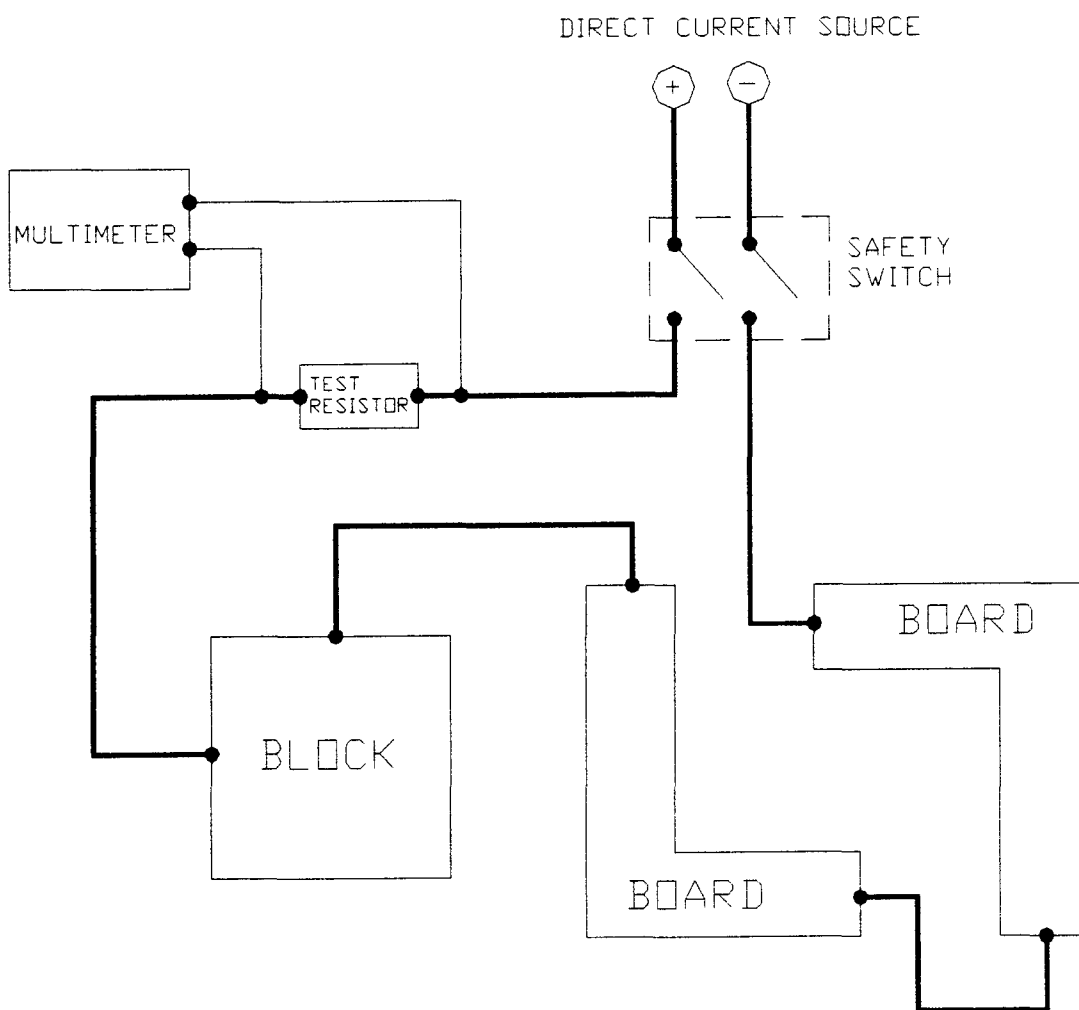
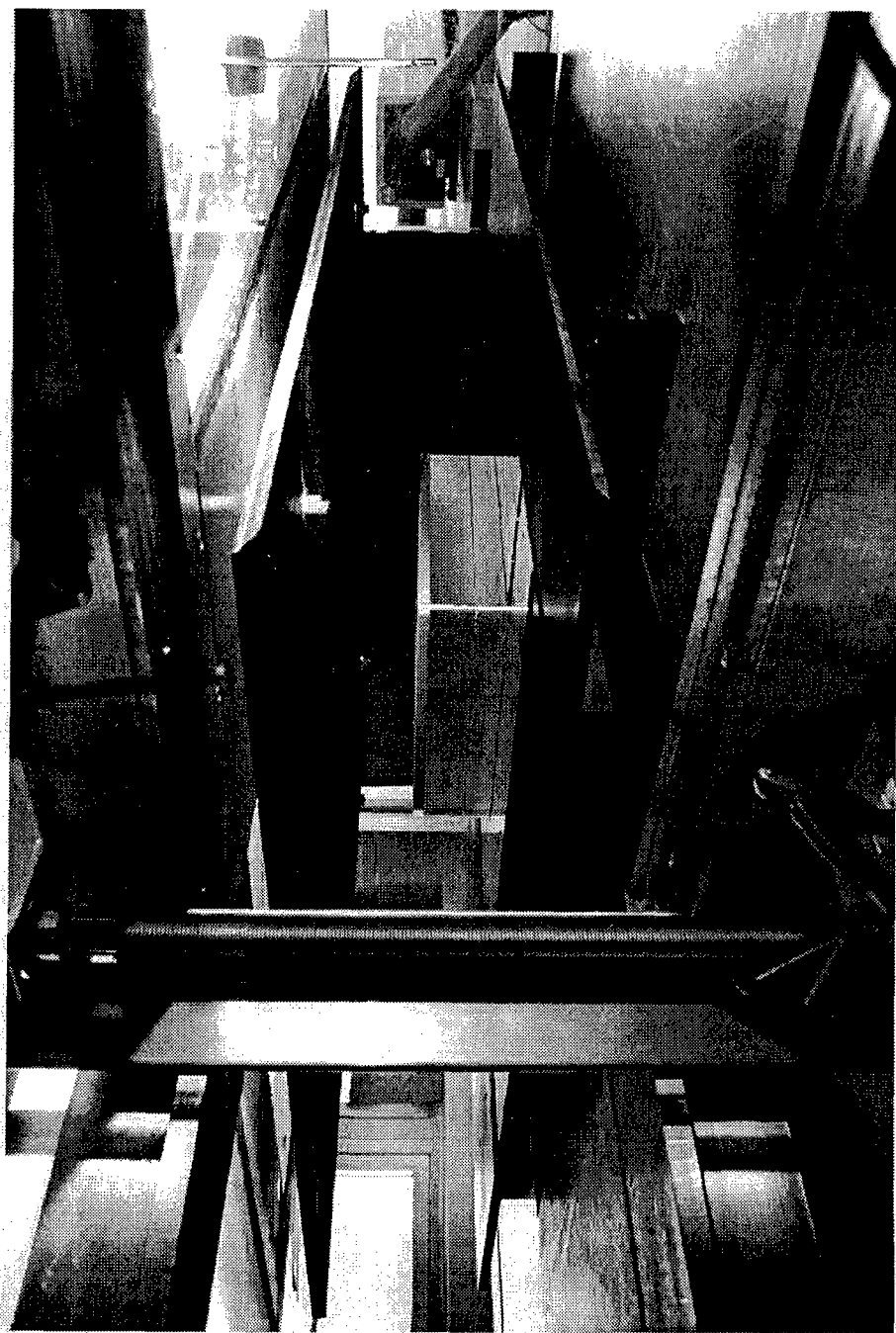


Figure A-1

Electrical Wiring Diagram



Test Section Photograph

Figure A-2

Table A-1

Property Analysis Table
(For Corresponding Cover Area)

Test#	Model	Orient.	Velocity	F.S.	Temp	Delta V	Test Resist	Tot. SS	Ave 1/2	Ave 1/2	Delta T	Ave 1/2	h	Back T	File	Cond	Viscosity	Density	Properties (at Film Temp)		Ref(h)	Grav(e)	Nu(e)	
																			Kin. Visc.	Ref(e)				
12-11_1	90	680	547.4	0.450	544.4	0.553	10,450	552.4	4,632	4,483	12,063	3,059	555,517	549,750	0.0154	1,2578E-05	7,230E-02	1,7397E-04	21160	1,237E-07	3,246E-02	2,121E-02	1,870E-02	
11-14_1	90	680	544.4	0.553	551.8	0.718	10,240	576.3	24,511	2,835	576,208	584,050	0.01671	1,2827E-05	7,210E-02	1,7461E-04	21082	3,174E-07	3,174E-02	2,0204	6,719E-07	1,870E-02		
12-12_1	90	680	566.8	0.717	10,240	581.4	24,633	2,690	580,098	589,100	0.01688	1,2914E-05	6,974E-02	1,8611E-04	19879	6,616E-07	6,616E-02	1,818E-02						
10-25_1	0	680	549.78	0.553	10,530	562.8	12,848	2,913	561,264	568,204	0.01657	1,2891E-05	7,134E-02	1,7786E-04	20693	2,086E-07	2,086E-02	2,0221E-02						
01-31_1	0	680	649.4	0.653	10,630	661.6	12,118	3,041	561,210	635,459	0.01677	1,2678E-05	7,140E-02	1,7756E-04	20732	3,056E-07	2,160E-02							
02-01_1	180	680	549.6	0.554	10,420	585.3	15,721	2,232	564,568	557,461	0.01568	1,2713E-05	7,120E-02	1,7855E-04	20817	3,894E-07	1,956E-02							
11-13_1	270	680	552.3	0.430	10,930	559.8	7,517	2,232	558,870	558,059	0.01558	1,2688E-05	7,140E-02	1,7771E-04	20716	1,898E-07	1,599E-02							
02-21_1	270	680	555	0.710	10,450	583.9	28,860	2,232	562,825	569,430	0.0154	1,2820E-05	6,970E-02	1,8635E-04	19859	6,421E-07	1,620E-02							
02-27_1	270	680	455	0.580	559.0	10,400	572.1	13,183	2,780	670,102	565,650	0.01568	1,2853E-05	7,080E-02	1,8154E-04	13079	3,121E-07	1,948E-02						
11-01_1a	90	455	548.9	0.580	554.3	0.556	10,400	562.6	13,729	2,984	563,380	555,784	0.01577	1,2683E-05	7,140E-02	1,7764E-04	14286	3,452E-07	2,095E-02					
10-30_1	0	455	554.3	0.556	572.0	17,756	1,773	569,550	563,168	0.01574	1,2812E-05	7,050E-02	1,8173E-04	13965	4,195E-07	1,2568E-02								
11-02_1	270	455	1550	539.2	0.712	10,500	549.3	10,140	6,305	545,589	544,250	0.01627	1,2482E-05	7,290E-02	1,7121E-04	50493	2,811E-07	3,874E-02						
11-15_1	90	1550	539.7	0.706	10,250	553.1	13,388	2,232	548,640	546,394	0.01532	1,2519E-05	7,280E-02	1,7244E-04	50134	3,633E-07	1,824E-02							
11-21_1	270	1550	0	531.3	0.350	10,740	568.0	36,350	568,743	549,650	0.01539	1,2576E-05	7,230E-02	1,7395E-04	0	9,441E-07	2,654E-01							
12-14_1	90	0	530.5	0.225	10,700	546.9	16,362	0.346	546,623	538,700	0.01513	1,2384E-05	7,370E-02	1,6803E-04	0	4,730E-07	2,546E-01							
12-14_2	90	0																						

XIII(B). RTD Calibration Procedure

The local temperature distribution measurements in this experiment are obtained using Micro-Measurements Group Inc's ETG-50B resistive type temperature devices (RTD's). These surface temperature measurement devices are similar in design, and operation, to resistive type strain gauges. The devices consist of a thin nickel foil sensing grid, adhered to a flexible substrate material. The sensors are installed by adhering the substrate material with high temperature strain gauge mounting epoxy, to the surface on which temperature measurements are required.

In operation, as the temperature of the mounting surface changes, so does the materials surface strain. The RTD reacts to the mounting strain via elongation of the sensing grid. The elongation changes the electrical resistance of the nickel grid, and the change in resistance is correlated to the corresponding mounting surface's temperature change.

The operational nature of the RTD requires it to be individually calibrated for its particular mounting surface, thereby incorporating the material's specific surface strain characteristics. Typically, the RTD manufacturer provides this material specific calibration equation for the device, along with the environmental factors under which this equation was developed. For the RTD's in this experiment, Micro-Measurements Inc. provided the following sixth-order polynomial calibration equation for 1018 steel surface mounting, at 75 degrees Fahrenheit:

$$T = A + (BR) + (CR^2) + (DR^3) + (ER^4) + (FR^5) + (GR^6)$$

where:	R = Resistance	D = 3.47019E-03
	A = -387.148	E = -3.70193E-05
	B = 14.37356	F = 2.05767E-07
	C = -0.206576	G = -4.55192E-10

For the exact installation described above, the gauges have a manufacturer's stated resistance of 50.0 ohms +/- 0.3%. Since this experiment's RTD installation is not exactly as stated in the above conditions, another RTD calibration was required. This was accomplished after mounting all gauges and assembling the heated block and board assembly.

The new RTD calibration procedure involved the production of two linear calibration equations, one for temperatures between 75 and 120 'F, and one for temperatures between 120 and 136 'F. The equations were developed by linear curve fitting of temperature data obtained by placing the entire block and board assembly in a heated, insulated, test room and recording each sensors' manufacturer's equation temperature at various known room temperatures. The various room temperatures were produced using a constant wattage, resistive type, floor heater attached to a variable rheostat. For the purposes of this calibration, it is important for the room and block and board assembly to be at a steady state temperature conditions before calibration data is recorded. To accomplish this, the test room was fitted with an oscillating axial fan to mix the room air flow, and the calibration temperature data was recorded only after several hours of constant room temperature conditions.

The calibration temperature data for the room was recorded using an Omega OM-202 temperature logger equipped with ten thermocouple channels, five of which were used. The five thermocouples were located at various locations adjacent to the block and board assembly, and the channels were averaged to produce the known room temperature value. Typically, the five channels all displayed the same temperature value, to the nearest one-half degree Fahrenheit. The RTD sensor temperatures were recorded using the *HOTBOX2A.EXE* data acquisition software

described in Appendix D. Results of the calibration data acquisition, for each sensor, are presented in tables B-1 and B-3.

Once the calibration data was obtained for 12 known room temperatures between 75 and 136 degrees Fahrenheit, the data was curve fit using the least squares method, producing two calibration curves. The slope-intercept values for sensor's two curves, is provided in tables B-2 and B-4. The first curve, for low temperatures, produces calibrated temperatures between 75 and 120 degrees Fahrenheit to an average accuracy of approximately +/- 0.25 degree Fahrenheit, and a standard deviation average of 0.232. This translates to a average percent difference in actual - calibrated temperature of +/- 0.24%. The second, high temperature curve, produces calibrated temperatures between 120 and 136 degrees Fahrenheit to an average accuracy of approximately +/- 0.11 degree Fahrenheit, and a standard deviation average of 0.223. This translates to a average percent difference in actual - calibrated temperature of +/- 0.08%.

Table B-1
Hotbox Low Temperature Calibration Data

Sensor #	Uncalibrated Sensor Temps, at Known Room:(°F)									
	75	81	83	90	100	106	109	110	120	
1	88.825	94.220	96.141	102.683	112.142	116.838	120.140	120.301	129.998	
2	88.838	94.779	96.798	103.657	113.496	118.410	121.841	121.841	132.104	
3	89.655	95.244	97.183	103.664	113.106	117.828	121.159	121.068	131.004	
4	89.033	94.918	96.951	103.677	113.613	118.572	121.970	121.957	132.307	
5	89.314	94.938	96.918	103.703	113.613	118.565	121.957	121.944	132.288	
6	88.838	94.726	96.765	103.703	113.177	118.145	121.564	121.481	131.786	
7	88.865	94.752	96.752	103.598	113.379	118.332	121.783	121.712	132.066	
8	88.879	94.765	96.758	103.605	113.392	118.352	121.796	121.732	132.085	
9	88.892	94.765	96.745	103.098	112.579	117.414	120.695	120.656	130.673	
10	88.919	95.038	96.758	103.796	113.658	118.610	122.002	122.060	132.396	
11	86.377	92.368	94.326	101.140	111.008	115.950	119.379	119.372	129.750	
12	87.068	92.974	94.832	101.489	111.021	115.957	119.372	119.366	129.450	
13	88.838	94.712	96.559	103.276	112.845	117.757	121.094	121.094	131.284	
14	90.632	96.354	98.250	104.762	114.100	118.869	122.137	122.131	132.021	
15	88.979	94.805	96.725	103.440	113.099	117.938	121.339	121.313	131.513	
16	89.608	95.477	97.296	104.078	113.782	118.778	122.272	122.189	132.504	
17	90.592	96.606	98.356	105.091	114.945	119.895	123.333	123.307	133.596	
18	89.943	95.716	97.501	104.092	113.678	118.526	121.950	121.867	131.920	
19	92.621	98.482	100.228	106.928	116.527	121.487	124.905	124.815	134.977	
20	89.970	95.729	97.515	104.157	113.626	118.559	121.938	121.822	131.952	
21	98.634	103.025	104.164	111.171	118.675	126.026	130.699	131.220	142.824	
22	90.003	95.736	97.428	103.980	113.444	118.261	121.609	121.513	131.519	
23	91.560	97.428	99.150	105.866	115.444	120.411	123.866	123.750	134.008	
24	89.782	95.464	97.117	103.493	112.637	117.388	120.643	120.643	130.355	
25	92.081	97.906	99.554	106.056	115.418	120.250	123.590	123.660	133.513	
26	91.680	97.203	98.780	105.045	114.074	118.752	121.983	121.938	131.513	
27	89.756	95.716	97.349	104.039	113.632	118.739	121.996	121.957	132.225	
28	91.193	97.137	98.899	105.557	115.230	120.205	123.628	123.622	133.792	
29	92.181	98.177	99.891	106.699	116.449	121.500	124.988	125.008	135.274	
30	0.000	0.000	0.000	0.000	0.000	0.000	0.000	0.000	0.000	
31	92.208	98.151	99.501	105.977	115.334	120.069	123.506	123.410	133.215	
32	90.317	95.816	97.647	103.986	113.223	117.938	121.217	121.094	130.877	
33	90.698	96.247	98.071	104.427	113.626	118.371	121.648	121.577	131.367	
34	90.685	96.274	98.098	104.972	114.620	119.514	122.889	122.896	133.069	
35	90.698	96.699	98.647	105.491	115.308	120.359	123.776	123.808	134.223	
36	88.007	93.607	95.397	101.865	111.165	115.963	119.276	119.237	129.144	
37	91.927	97.892	99.686	106.469	116.261	121.307	124.732	124.802	135.141	
38	90.083	96.028	97.866	104.637	114.425	119.353	122.748	122.838	133.126	
39	90.384	96.367	98.190	104.992	114.763	119.695	123.127	123.191	133.589	
40	92.741	98.773	100.777	107.675	117.608	122.600	126.052	126.045	136.507	
41	90.043	95.763	97.680	104.322	113.873	118.707	122.111	122.143	132.237	
42	92.234	98.091	99.898	106.607	116.235	121.133	124.495	124.501	134.679	
43	90.050	95.869	97.694	104.315	113.827	118.688	122.053	121.944	132.034	
44	0.000	0.000	0.000	0.000	0.000	0.000	0.000	0.000	0.000	
45	89.582	95.304	97.024	103.499	112.819	117.550	120.824	120.824	130.616	
46	90.157	96.141	98.025	104.841	114.633	119.650	123.063	123.166	133.513	
47	90.979	96.858	98.667	105.360	114.997	119.850	123.179	123.172	133.253	
48	94.519	100.109	101.773	108.231	117.408	122.240	125.693	125.456	135.413	
49	93.448	98.978	100.763	107.216	116.514	121.384	124.879	124.693	134.698	
50	94.533	100.400	102.076	108.644	118.022	123.031	126.557	126.353	136.412	
51	93.501	99.117	100.710	107.072	116.028	120.920	124.315	124.052	133.748	
52	96.427	102.301	103.967	110.584	119.985	124.988	128.494	128.334	138.400	
53	95.371	101.146	102.828	109.304	118.539	123.525	127.005	126.800	136.734	

Table B-1
 Hotbox Low Temperature Calibration Data

Sensor #	Uncalibrated Sensor Temps, at Known Room:(F)									
	75	81	83	90	100	106	109	110	120	
54	91.814	97.647	99.263	105.859	115.204	120.224	123.776	123.564	133.577	
55	95.829	101.668	103.308	109.892	119.276	124.347	127.887	127.695	137.757	
56	94.706	100.644	102.327	108.984	118.539	123.590	127.184	126.941	137.132	
57	95.244	100.658	102.320	108.415	117.207	121.996	125.392	125.085	134.565	
58	96.015	101.951	103.624	110.284	119.882	124.988	128.570	128.379	138.589	
59	94.998	100.618	102.169	108.369	117.252	122.047	125.411	125.226	134.787	
60	96.108	101.997	103.611	110.166	119.514	124.527	127.996	127.823	137.820	
61	0.000	0.000	0.000	0.000	0.000	0.000	0.000	0.000	0.000	
62	93.667	99.673	101.344	107.983	117.453	122.607	126.135	125.924	136.115	
63	107.826	112.637	113.522	119.702	124.443	134.508	138.286	138.627	150.015	
64	90.237	96.115	97.906	104.578	114.295	119.211	122.542	122.677	132.828	
65	0.000	0.000	0.000	0.000	0.000	0.000	0.000	0.000	0.000	
66	90.839	96.639	98.455	105.064	114.627	119.482	122.793	122.896	132.942	
67	91.320	96.666	98.157	104.729	114.165	118.991	122.780	122.922	132.955	
68	90.605	96.659	98.436	105.268	115.081	120.037	123.461	123.545	133.868	
69	0.000	0.000	0.000	0.000	0.000	0.000	0.000	0.000	0.000	
70	89.849	95.895	97.621	104.394	114.295	119.243	122.677	122.754	133.056	
71	87.464	93.181	95.038	101.555	110.982	115.820	119.146	119.205	129.132	
72	89.501	95.497	97.309	104.111	113.983	118.953	122.311	122.446	132.784	
73	90.585	96.148	97.879	104.138	113.522	118.235	121.474	121.532	131.208	
74	88.189	94.080	95.942	102.709	112.474	117.323	120.701	120.817	131.182	
75	90.164	96.048	97.886	104.703	114.516	119.456	122.909	123.012	133.310	
76	89.153	95.178	97.030	103.855	113.769	118.752	122.195	122.336	132.688	
77	89.736	95.703	97.495	104.269	114.074	118.875	122.214	122.356	132.688	
78	90.210	96.320	98.230	105.058	114.971	119.973	123.320	123.487	133.805	
79	88.624	94.579	96.460	103.295	113.203	118.184	121.558	121.732	132.085	

Table B-2**Low Temperature Sensor Calibration Equations and Performance**

Sensor #	Linear Fit Calibration Eq		Calculated Temps Using Linear Calibration Equation								
	Slope	Intercept	75	81	83	90	100	106	109	110	120
1	1.09612	-22.40150	74.9617	80.8753	82.9810	90.1518	100.5201	105.6675	109.2869	109.4633	120.0924
2	1.04759	-18.32959	74.7366	80.9604	83.0754	90.2609	100.5682	105.7161	109.3103	109.3103	120.0618
3	1.09588	-23.42470	74.8263	80.9512	83.0761	90.1785	100.5257	105.7005	109.3509	109.2511	120.1398
4	1.04729	-18.43968	74.8037	80.9670	83.0962	90.1402	100.5461	105.7396	109.2983	109.2847	120.1242
5	1.05138	-18.91966	74.9837	80.8967	82.9784	90.1120	100.5313	105.7377	109.3040	109.2903	120.1659
6	1.05763	-19.24961	74.7079	80.9352	83.0917	90.4295	100.4495	105.7037	109.3198	109.2320	120.1308
7	1.04951	-18.47931	74.7853	80.9637	83.0627	90.2477	100.5129	105.7111	109.3330	109.2585	120.1251
8	1.04928	-18.46906	74.7902	80.9663	83.0575	90.2419	100.5113	105.7157	109.3294	109.2623	120.1255
9	1.08891	-22.12665	74.6688	81.0640	83.2200	90.1378	100.4618	105.7267	109.2994	109.2569	120.1646
10	1.04346	-18.04514	74.7386	81.1235	82.9183	90.2622	100.5528	105.7200	109.2595	109.3200	120.1052
11	1.04646	-15.63537	74.7545	81.0238	83.0728	90.2033	100.5298	105.7014	109.2897	109.2823	120.1425
12	1.07087	-18.48671	74.7517	81.0763	83.0659	90.1947	100.4022	105.6881	109.3451	109.3387	120.1373
13	1.06976	-20.26064	74.7748	81.0586	83.0345	90.2201	100.4566	105.7113	109.2811	109.2811	120.1819
14	1.09694	-24.68050	74.7374	81.0141	83.0939	90.2372	100.4804	105.7117	109.2965	109.2900	120.1387
15	1.06662	-20.11690	74.7902	81.0044	83.0523	90.2147	100.5172	105.6786	109.3062	109.2784	120.1580
16	1.05658	-19.81527	74.8628	81.0639	82.9858	90.1515	100.4046	105.6833	109.3750	109.2873	120.1859
17	1.05471	-20.74945	74.7989	81.1420	82.9877	90.0912	100.4843	105.7051	109.3312	109.3038	120.1557
18	1.07927	-22.23106	74.8415	81.0721	82.9986	90.1121	100.4579	105.6902	109.3856	109.2960	120.1459
19	1.07010	-24.28250	74.8315	81.1033	82.9717	90.1414	100.4133	105.7210	109.3786	109.2823	120.1567
20	1.08006	-22.32742	74.8454	81.0654	82.9944	90.1681	100.3952	105.7231	109.3726	109.2474	120.1883
21	1.01286	-22.90541	76.9967	81.4441	82.5978	89.6949	97.2953	104.7408	109.4739	110.0016	121.7548
22	1.09195	-23.42704	74.8516	81.1118	82.9593	90.1138	100.4480	105.7079	109.3637	109.2589	120.1850
23	1.06873	-22.99992	74.8527	81.1240	82.9644	90.1419	100.3782	105.6866	109.3790	109.2551	120.2181
24	1.11901	-25.67198	74.7951	81.1533	83.0030	90.1378	100.3700	105.6865	109.3288	109.2888	120.1967
25	1.09546	-26.07026	74.8004	81.1815	82.9868	90.1094	100.3651	105.6583	109.3172	109.3939	120.1874
26	1.13834	-29.49352	74.8695	81.1565	82.9517	90.0834	100.3615	105.6866	109.3646	109.3134	120.2130
27	1.06901	-21.12235	74.8276	81.1989	82.9446	90.0963	100.3513	105.8107	109.2925	109.2508	120.2274
28	1.06484	-22.30095	74.8054	81.1349	83.0111	90.1009	100.4011	105.6987	109.3437	109.3373	120.1668
29	1.05186	-22.11918	74.8423	81.1493	82.9521	90.1132	100.3688	105.6818	109.3507	109.3717	120.1701
30	#NUM!	#NUM!	#NUM!	#NUM!	#NUM!	#NUM!	#NUM!	#NUM!	#NUM!	#NUM!	#NUM!
31	1.10688	-27.27372	74.7692	81.3674	82.8617	90.0298	100.3869	105.6279	109.4323	109.3260	120.1789
32	1.11717	-26.04040	74.8593	81.0026	83.0481	90.1299	100.4492	105.7167	109.3799	109.2425	120.1718
33	1.11520	-26.30876	74.8380	81.0263	83.0604	90.1486	100.4074	105.6990	109.3536	109.2744	120.1922
34	1.06599	-21.68914	74.9798	80.9376	82.8820	90.2096	100.4942	105.7111	109.3088	109.3163	120.1606
35	1.04299	-19.82099	74.7764	81.0354	83.0671	90.2053	100.4444	105.7126	109.2765	109.3098	120.1726
36	1.10225	-22.13531	74.8704	81.0430	83.0160	90.1454	100.3963	105.6849	109.3367	109.2937	120.2137
37	1.04971	-21.64842	74.8486	81.1101	82.9933	90.1135	100.3923	105.6891	109.2844	109.3579	120.2109
38	1.05439	-20.17250	74.8100	81.0783	83.0163	90.1555	100.4759	105.6719	109.2516	109.3465	120.1940
39	1.05177	-20.25419	74.8087	81.1015	83.0188	90.1730	100.4498	105.6371	109.2468	109.3141	120.2503
40	1.03695	-21.42135	74.7465	81.0014	83.0794	90.2323	100.5324	105.7088	109.2884	109.2811	120.1297
41	1.07460	-21.91590	74.8440	80.9907	83.0507	90.1882	100.4517	105.6463	109.3042	109.3386	120.1856
42	1.06887	-23.77536	74.8112	81.0716	83.0030	90.1741	100.4652	105.7006	109.2941	109.3006	120.1796
43	1.08070	-22.54306	74.7738	81.0624	83.0347	90.1900	100.4696	105.7228	109.3594	109.2416	120.1458
44	#NUM!	#NUM!	#NUM!	#NUM!	#NUM!	#NUM!	#NUM!	#NUM!	#NUM!	#NUM!	#NUM!
45	1.10561	-24.26535	74.7773	81.1036	83.0053	90.1641	100.4684	105.6990	109.3188	109.3188	120.1449
46	1.04698	-19.59052	74.8017	81.0668	83.0393	90.1755	100.4275	105.6801	109.2535	109.3613	120.1944
47	1.07276	-22.83675	74.7615	81.0683	83.0089	90.1889	100.5270	105.7331	109.3043	109.2968	120.1112
48	1.10865	-29.87158	74.9170	81.1144	82.9592	90.1188	100.2929	105.6499	109.4781	109.2154	120.2542
49	1.09772	-27.61095	74.9688	81.0392	82.9986	90.0822	100.2888	105.6347	109.4712	109.2670	120.2497
50	1.08284	-27.53917	74.8249	81.1780	82.9928	90.1049	100.2598	105.6837	109.5018	109.2809	120.1732
51	1.12601	-30.43612	74.8469	81.1706	82.9643	90.1280	100.2125	105.7210	109.5438	109.2476	120.1654
52	1.08033	-29.34540	74.8278	81.1737	82.9735	90.1221	100.2783	105.6832	109.4708	109.2980	120.1726
53	1.09618	-29.71132	74.8327	81.1631	83.0069	90.1058	100.2290	105.6946	109.5093	109.2846	120.1741
54	1.08470	-24.72828	74.8624	81.1895	82.9424	90.0971	100.2336	105.6788	109.5317	109.3017	120.1628
55	1.08051	-28.66772	74.8768	81.1859	82.9579	90.0720	100.2116	105.6909	109.5159	109.3084	120.1806
56	1.06817	-26.32707	74.8347	81.1775	82.9752	90.0860	100.2923	105.6877	109.5267	109.2671	120.1528
57	1.15161	-34.79697	74.8869	81.1217	83.0356	90.0547	100.1796	105.6947	109.6056	109.2520	120.1693
58	1.06400	-27.29189	74.8680	81.1839	82.9639	90.0502	100.2624	105.6952	109.5065	109.3032	120.1667
59	1.14052	-33.52578	74.8210	81.2307	82.9996	90.0708	100.2020	105.6708	109.5075	109.2965	120.2010
60	1.08725	-29.68234	74.8115	81.2144	82.9692	90.0961	100.2598	105.7102	109.4819	109.2938	120.1631
61	#NUM!	#NUM!	#NUM!	#NUM!	#NUM!	#NUM!	#NUM!	#NUM!	#NUM!	#NUM!	#NUM!
62	1.06887	-25.32250	74.7957	81.2153	83.0014	90.0976	100.2199	105.7288	109.4998	109.2743	120.1672
63	1.06310	-37.49721	77.1328	82.2474	83.1883	89.7582	94.7984	105.4985	109.5149	109.8774	121.9840
64	1.06496	-21.26331	74.8351	81.0949	83.0022	90.1076	100.4558	105.6911	109.2385	109.3822	120.1926
65	#NUM!	#NUM!	#NUM!	#NUM!	#NUM!	#NUM!	#NUM!	#NUM!	#NUM!	#NUM!	#NUM!
66	1.07761	-23.07107	74.8182	81.0683	83.0253	90.1472	100.4524	105.6842	109.2522	109.3632	120.1889
67	1.08331	-23.58031	75.3479	81.1393	82.7546	89.8741	100.0962	105.3243	109.4290	109.5828	120.4517
68	1.04958	-20.32041	74.7767	81.1308	82.9959	90.1666	100.4661	105.6679	109.2616	109.3498	120.1846
69	#NUM!	#NUM!	#NUM!	#NUM!	#NUM!	#NUM!	#NUM!	#NUM!	#NUM!	#NUM!	#NUM!
70	1.04999	-19.52912	74.8113	81.1596	82.9718	90.0834	100.4794	105.6747	109.2804	109.3612	120.1782
71	1.08846	-20.38498	74.8162	81.0389	83.0602	90.1537	100.4146	105.6806	109.3008	109.3650	120.1702
72	1.04857	-19.03532	74.8131	81.1003	83.0003	90.1327	100.4843	105.6957	109.2168	109.3583	120.1985

Table B-2
Low Temperature Sensor Calibration Equations and Performance

Sensor #	Linear Fit Calibration Eq		Calculated Temps Using Linear Calibration Equation									
	Slope	intercept	75	81	83	90	100	106	109	110	120	
73	1.11462	-26.08149	74.8861	81.0868	83.0162	89.9925	100.4521	105.7053	109.3156	109.3802	120.1652	
74	1.05691	-18.37625	74.8319	81.0581	83.0261	90.1782	100.4990	105.6240	109.1942	109.3168	120.2717	
75	1.05056	-19.85135	74.8711	81.0525	82.9835	90.1451	100.4542	105.6440	109.2715	109.3797	120.1984	
76	1.04221	-18.10555	74.8103	81.0896	83.0198	90.1328	100.4653	105.6586	109.2469	109.3939	120.1828	
77	1.05843	-20.18798	74.7916	81.1072	83.0040	90.1738	100.5517	105.6333	109.1674	109.3177	120.2534	
78	1.04170	-19.25549	74.7164	81.0812	83.0708	90.1836	100.5100	105.7205	109.2071	109.3811	120.1294	
79	1.04362	-17.65440	74.8352	81.0499	83.0130	90.1461	100.4863	105.6845	109.2057	109.3873	120.1919	
Average Calibrated Temp ('F) ==>			74.8907	81.1075	83.0029	90.1313	100.2920	105.6718	109.3501	109.3301	120.2237	
Average Calibrated - Actual ==>			-0.1093	0.1075	0.0029	0.1313	0.2920	-0.3282	0.3501	-0.6699	0.2237	
Average Percent Difference ==>			0.1478	0.1320	0.0040	0.1468	0.2944	0.3090	0.3213	0.6101	0.1855	
Standard Deviation ==>			0.374764	0.164112	0.079768	0.098129	0.749537	0.123473	0.098272	0.117567	0.281298	
Average Uncertainty in Calibrated Temperature Using Low-Temp Curve ==>										0.246095 'F		

Table B-3
 Hotbox High Temperature Calibration Data

Sensor #	120	132	134	136
1	129.998	142.786	143.676	146.131
2	132.104	145.214	146.181	148.959
3	131.004	143.588	144.382	147.073
4	132.307	145.382	146.188	149.021
5	132.288	145.064	145.713	148.555
6	131.786	144.889	145.720	148.548
7	132.066	145.164	145.957	148.778
8	132.085	145.176	145.982	148.791
9	130.673	143.325	144.195	146.811
10	132.396	145.457	146.250	149.021
11	129.750	142.861	143.688	146.499
12	129.450	142.341	143.043	145.832
13	131.284	144.139	144.845	147.571
14	132.021	144.551	145.245	147.982
15	131.513	144.533	145.232	147.982
16	132.504	145.551	146.568	149.220
17	133.596	146.680	147.565	150.362
18	131.920	144.714	145.726	148.374
19	134.977	147.883	148.766	151.497
20	131.952	144.801	145.844	148.411
21	142.824	160.365	163.133	165.963
22	131.519	144.189	144.895	147.683
23	134.008	146.880	147.565	150.393
24	130.355	142.642	143.369	146.038
25	133.513	146.119	146.861	149.605
26	131.513	143.713	144.526	147.017
27	132.225	145.189	146.007	148.586
28	133.792	146.736	147.378	150.250
29	135.274	148.449	149.176	151.924
30	0.000	0.000	0.000	0.000
31	133.215	145.763	146.562	149.002
32	130.877	143.193	143.832	146.487
33	131.367	143.744	144.408	147.036
34	133.069	145.950	146.213	149.251
35	134.223	147.391	147.677	150.641
36	129.144	141.695	141.557	144.614
37	135.141	148.331	148.225	151.410
38	133.126	146.244	145.988	149.220
39	133.589	146.668	146.487	149.785
40	136.507	149.667	150.275	153.186
41	132.237	145.033	145.001	148.281
42	134.679	147.528	148.312	150.970
43	132.034	144.745	145.769	148.281
44	0.000	0.000	0.000	0.000
45	130.616	143.106	143.776	146.524

Table B-3

Hotbox High Temperature Calibration Data

Sensor #	120	132	134	136
46	133.513	146.593	146.543	149.822
47	133.253	146.144	146.531	149.524
48	135.413	148.051	147.839	151.032
49	134.698	147.372	147.366	150.381
50	136.412	149.207	150.747	153.075
51	133.748	146.144	147.428	149.779
52	138.400	151.230	152.722	155.032
53	136.734	149.412	150.654	153.149
54	133.577	146.450	147.970	150.269
55	137.757	150.647	151.955	154.415
56	137.132	150.114	151.224	153.927
57	134.565	146.711	147.870	150.257
58	138.589	151.608	152.673	155.352
59	134.787	147.060	148.169	150.554
60	137.820	150.616	151.658	154.273
61	0.000	0.000	0.000	0.000
62	136.115	149.189	150.288	152.840
63	150.015	163.627	165.477	172.453
64	132.828	145.782	146.574	149.325
65	0.000	0.000	0.000	0.000
66	132.942	145.720	146.425	149.263
67	132.955	145.732	146.967	149.257
68	133.868	146.986	147.677	150.635
69	0.000	0.000	0.000	0.000
70	133.056	146.156	146.873	149.630
71	129.132	141.752	142.410	145.170
72	132.784	145.844	146.150	149.220
73	131.208	143.563	143.826	146.873
74	131.182	143.957	143.651	147.210
75	133.310	146.406	146.131	149.667
76	132.688	145.876	145.270	149.089
77	132.688	145.857	145.282	149.064
78	133.805	146.867	147.372	150.486
79	132.085	145.220	145.058	148.536

Table B-4

High Temperature Sensor Calibration Equations and Performance

Sensor #	Linear Fit Calibration Eq		Calculated Temps Using Linear Calibration			
	Slope	Intercept	120	132.5	133.5	136
1	0.99085	-8.86037	119.9477	132.6187	133.5005	135.9331
2	0.95530	-6.21699	119.9817	132.5056	133.4294	136.0832
3	1.00123	-11.18558	119.9793	132.5788	133.3738	136.0681
4	0.96327	-7.46405	119.9835	132.5783	133.3547	136.0836
5	0.99002	-10.97828	119.9890	132.6374	133.2800	136.0936
6	0.96049	-6.59619	119.9829	132.5682	133.3663	136.0826
7	0.96284	-7.17727	119.9808	132.5920	133.3555	136.0717
8	0.96307	-7.22766	119.9799	132.5875	133.3637	136.0690
9	0.99543	-10.10512	119.9704	132.5645	133.4305	136.0346
10	0.96689	-8.03675	119.9754	132.6039	133.3707	136.0499
11	0.96075	-4.67692	119.9803	132.5767	133.3712	136.0719
12	0.98168	-7.09796	119.9799	132.6347	133.3238	136.0617
13	0.98608	-9.48340	119.9729	132.6489	133.3451	136.0331
14	1.00839	-13.14428	119.9838	132.6189	133.3187	136.0786
15	0.97472	-8.21779	119.9710	132.6619	133.3433	136.0238
16	0.96107	-7.37566	119.9698	132.5089	133.4863	136.0350
17	0.96018	-8.29444	119.9815	132.5445	133.3942	136.0798
18	0.97769	-9.00037	119.9766	132.4852	133.4746	136.0636
19	0.97390	-11.47587	119.9782	132.5474	133.4073	136.0671
20	0.97535	-8.73368	119.9662	132.4985	133.5158	136.0195
21	0.68989	21.44771	119.9810	132.0824	133.9921	135.9445
22	0.99628	-11.04352	119.9867	132.6096	133.3130	136.0906
23	0.98238	-11.66124	119.9851	132.6303	133.3032	136.0814
24	1.02642	-13.81562	119.9833	132.5949	133.3411	136.0806
25	1.00043	-13.58688	119.9839	132.5954	133.3377	136.0829
26	1.03494	-16.14254	119.9651	132.5913	133.4328	136.0108
27	0.97847	-9.42294	119.9553	132.6402	133.4405	135.9640
28	0.97817	-10.88405	119.9876	132.6490	133.2770	136.0863
29	0.96350	-10.36876	119.9673	132.6614	133.3618	136.0095
30	#NUM!	#NUM!	#NUM!	#NUM!	#NUM!	#NUM!
31	1.01255	-14.93785	119.9487	132.6542	133.4632	135.9338
32	1.02956	-14.76838	119.9776	132.6577	133.3156	136.0491
33	1.02486	-14.66044	119.9729	132.6576	133.3381	136.0314
34	0.99447	-12.32686	120.0066	132.8164	133.0779	136.0991
35	0.97696	-11.14191	119.9880	132.8525	133.1319	136.0276
36	1.03624	-13.79857	120.0252	133.0310	132.8880	136.0558
37	0.98531	-13.13480	120.0205	133.0167	132.9123	136.0505
38	0.99504	-12.43228	120.0337	133.0866	132.8319	136.0479
39	0.99195	-12.47141	120.0417	133.0153	132.8358	136.1072
40	0.96450	-11.67513	119.9853	132.6781	133.2645	136.0721
41	1.00506	-12.85989	120.0464	132.9071	132.8750	136.1716
42	0.98503	-12.69556	119.9669	132.6235	133.3957	136.0139
43	0.98729	-10.39388	119.9624	132.5119	133.5228	136.0029
44	#NUM!	#NUM!	#NUM!	#NUM!	#NUM!	#NUM!
45	1.01200	-12.19745	119.9858	132.6257	133.3037	136.0847
46	0.98673	-11.70540	120.0360	132.9424	132.8931	136.1286
47	0.98955	-11.85947	120.0009	132.7572	133.1401	136.1018

Table B-4

High Temperature Sensor Calibration Equations and Performance

Sensor #	Linear Fit Calibration Eq		Calculated Temps Using Linear Calibration			
	Slope	Intercept	120	132.5	133.5	136
48	1.02808	-19.17120	120.0437	133.0365	132.8186	136.1012
49	1.02258	-17.72698	120.0122	132.9723	132.9662	136.0493
50	0.96182	-11.23390	119.9698	132.2762	133.7574	135.9966
51	1.00064	-13.86641	119.9666	132.3704	133.6553	136.0077
52	0.96263	-13.26485	119.9631	132.3136	133.7498	135.9735
53	0.97893	-13.87957	119.9733	132.3842	133.6000	136.0425
54	0.95886	-8.11968	119.9626	132.3060	133.7635	135.9679
55	0.96313	-12.71174	119.9667	132.3815	133.6413	136.0106
56	0.95895	-11.51987	119.9829	132.4320	133.4965	136.0885
57	1.02366	-17.77760	119.9709	132.4043	133.5907	136.0342
58	0.95962	-13.01598	119.9764	132.4696	133.4916	136.0624
59	1.01746	-17.17669	119.9637	132.4510	133.5793	136.0060
60	0.97721	-14.70479	119.9738	132.4781	133.4964	136.0518
61	#NUM!	#NUM!	#NUM!	#NUM!	#NUM!	#NUM!
62	0.95872	-10.53554	119.9608	132.4951	133.5487	135.9954
63	0.74851	8.57369	120.8607	131.0494	132.4341	137.6557
64	0.97452	-9.46708	119.9760	132.5998	133.3717	136.0525
65	#NUM!	#NUM!	#NUM!	#NUM!	#NUM!	#NUM!
66	0.98726	-11.25886	119.9901	132.6053	133.3014	136.1032
67	0.97973	-10.31456	119.9456	132.4636	133.6736	135.9172
68	0.96168	-8.74332	119.9951	132.6104	133.2749	136.1196
69	#NUM!	#NUM!	#NUM!	#NUM!	#NUM!	#NUM!
70	0.96846	-8.88916	119.9702	132.6570	133.3514	136.0214
71	1.00315	-9.55537	119.9830	132.6427	133.3028	136.0715
72	0.97939	-10.04207	120.0053	132.7962	133.0959	136.1026
73	1.03091	-15.23666	120.0265	132.7634	133.0345	136.1757
74	1.00821	-12.16158	120.0973	132.9772	132.6687	136.2569
75	0.98608	-11.37552	120.0786	132.9923	132.7211	136.2079
76	0.98340	-10.35304	120.1323	133.1013	132.5054	136.2610
77	0.98477	-10.54121	120.1257	133.0941	132.5279	136.2523
78	0.96846	-9.57023	120.0140	132.6640	133.1531	136.1689
79	0.98073	-9.47477	120.0653	132.9472	132.7883	136.1993
Average Calibrated Temp ('F) ==>			120.0037	132.6241	133.2859	136.0863
Average Calibrated - Actual ==>			0.0037	0.1241	-0.2141	0.0863
Average Percent Difference ==>			0.0031	0.0937	0.1604	0.0634
Standard Deviation ==>			0.107609	0.280038	0.308293	0.19744

Average Uncertainty in Calibrated Temperature Using High-Temp Curve ==> 0.10707

XIII(C). Detailed Uncertainty Analysis:

The propagation of experimental measurement uncertainty through the results of this experiment are best calculated through the proven methods of Kline and McClintock (1953). This method defines an uncertainty for a given result by the following equation:

$$W_R = \left[\left(\frac{\partial R}{\partial W_1} W_1 \right)^2 + \left(\frac{\partial R}{\partial W_2} W_2 \right)^2 + \dots \left(\frac{\partial R}{\partial W_n} W_n \right)^2 \right]^{\frac{1}{2}}$$

Where W_r , W_1 , W_2 , and W_i are the uncertainties in the final result and associated independent variables, respectively. The final uncertainty can be converted to a percent basis by:

$$\text{Percent Uncertainty} = \frac{W_R}{R} * 100\%$$

For the purposes of this experiment the following quantities require an uncertainty analysis:

- Reynold's Number
- Grashof Number
- Nusselt Number
- Surface Coefficient of Heat Transfer

Reynold's number is defined by the following equation:

$$N_{Re} = \frac{\rho U_{fs} L}{\mu}$$

The uncertainty in this quantity is written as:

$$W_{Re} = \left[\left(\frac{U_{fs} L}{\mu} W_\rho \right)^2 + \left(\frac{\rho L}{\mu} W_{U_{fs}} \right)^2 + \left(\frac{U_{fs} \rho}{\mu} W_L \right)^2 \right]^{\frac{1}{2}}$$

The length quantity in the equation is the height of the box above the board assembly. This is measured to be 0.3012 feet + or - 3.33x10⁻³ feet. Freestream velocity is measured with a Solomat hot-wire anemometer to within an uncertainty of + or - 2.4 feet per minute. Density and kinematic viscosity values are obtained from tables provided by B. Gerbert et. al. (1988). The uncertainty in these values is assumed to provide a negligible contribution to overall Reynold's number uncertainty

The Grashof number for a particular test is defined as:

$$N_{Gr} = \frac{g\beta L^3 \rho^2 \Delta T}{\mu^2}$$

The length quantity in this equation is the length of the cover surface. This surface is measured with a steel rule to 1.115 feet + or - 3.33x10⁻³ feet. The temperature difference term is defined as the difference between the average surface and free stream temperatures. The surface temperature is found with the acquisition sensors with an uncertainty of 0.5 degrees Fahrenheit. The freestream temperature is measured with the mercury bulb thermometer to an uncertainty of 0.5 degrees Fahrenheit. These uncertainty in these measurements combines to produce the following equation for the temperature difference uncertainty:

$$W_{\Delta T} = \left[(W_{T_{surf}})^2 + (W_{fst})^2 \right]^{\frac{1}{2}}$$

The next value in the Grashof number equation is β . β for this experiment is written as the reciprocal of the film temperature. Film temperature is defined as the average of the freestream and surface temperatures. Thus the uncertainty in the film temperature and β are:

$$W_{\text{film}} = \left[\left(\frac{1}{2} W_{\text{surf}} \right)^2 + \left(\frac{1}{2} W_{\text{fst}} \right)^2 \right]^{\frac{1}{2}}$$

$$\beta = \frac{1}{T_{\text{film}}^2}$$

$$W_\beta = \left[\left(\frac{1}{T_{\text{film}}^2} W_{\text{film}} \right)^2 \right]^{\frac{1}{2}}$$

The remaining values of acceleration due to gravity, density, and absolute viscosity are found from the B. Gebhart et. al. tables and assumed to have negligible contributions to the Grashof number uncertainty in this experiment. With the intermediate uncertainties defined, the total uncertainty in the Grashof number calculation is:

$$W_{\text{Gr}} = \left[\left(\frac{\Delta T g L^3 \rho^2}{\mu^2} W_\beta \right)^2 + \left(\frac{\beta g L^3 \rho^2}{\mu^2} W_{\Delta T} \right)^2 + \left(\frac{3 \beta \Delta T g L^2 \rho^2}{\mu^2} W_L \right)^2 + \left(\frac{2 \beta \Delta T g L^3 \rho}{\mu^2} W_\rho \right)^2 \right]^{\frac{1}{2}}$$

The Nusselt number is defined as:

$$N_{\text{Nu}} = \frac{hL}{k}$$

In order to determine the uncertainty associated with this non-dimensional number, it is helpful to first determine the uncertainty in the heat transfer coefficient. As outlined in the Data Reduction section of this report, the heat transfer coefficient is determined by taking a first law energy balance on a portion of the thin stainless steel strip above a single RTD temperature sensor. The overall equation for determination of the heat transfer coefficient is (with stainless steel conduction terms omitted):

$$h = \frac{I^2 R_{\text{tot, ss}}}{A_{\text{tot, ss}}(T - T_{\text{fs}})} - \frac{k_{\text{back}}}{L_{\text{back}}} \left(\frac{T - T_{\text{back}}}{T - T_{\text{fs}}} \right) - \sigma \varepsilon F \left(\frac{T^4 - T_{\text{fs}}^4}{T - T_{\text{fs}}} \right)$$

Using the above equation yields the following uncertainty calculation for the surface coefficient of heat transfer:

$$W_h = \left[\left(\frac{\partial h}{\partial I} W_I \right)^2 + \left(\frac{\partial h}{\partial R_{tot, ss}} W_{R_{tot, ss}} \right)^2 + \left(\frac{\partial h}{\partial A_{tot, ss}} W_{A_{tot, ss}} \right)^2 + \left(\frac{\partial h}{\partial T} W_T \right)^2 + \left(\frac{\partial h}{\partial T_{fs}} W_{T_{fs}} \right)^2 \right]^{\frac{1}{2}}$$

$$+ \left(\frac{\partial h}{\partial k_{back}} W_{k_{back}} \right)^2 + \left(\frac{\partial h}{\partial L_{back}} W_{L_{back}} \right)^2 + \left(\frac{\partial h}{\partial T_{back}} W_{T_{back}} \right)^2 + \left(\frac{\partial h}{\partial \varepsilon} W_\varepsilon \right)^2 \right]$$

Where the partial terms in the above equation are:

$$\frac{\partial h}{\partial I} = \frac{2IR_{tot, ss}}{A_{tot, ss}(T - T_{fs})}$$

$$\frac{\partial h}{\partial R_{tot, ss}} = \frac{I^2}{A_{tot, ss}(T - T_{fs})}$$

$$\frac{\partial h}{\partial A_{tot, ss}} = \frac{-I^2 R_{tot, ss}}{A_{tot, ss}^2 (T - T_{fs})}$$

$$\frac{\partial h}{\partial k_{back}} = \frac{-(T - T_{back})}{L_{back}(T - T_{fs})}$$

$$\frac{\partial h}{\partial L_{back}} = \frac{k_{back}(T - T_{back})}{L_{back}^2(T - T_{fs})}$$

$$\frac{\partial h}{\partial \varepsilon} = \frac{-\sigma F(T^4 - T_{fs}^4)}{(T - T_{fs})}$$

$$\frac{\partial h}{\partial T} = \frac{-I^2 R_{tot, ss}}{A_{tot, ss}(T - T_{fs})^2} - \frac{k_{back}}{L_{back}(T - T_{fs})} + \frac{k_{back}(T - T_{back})}{L_{back}(T - T_{fs})^2} - \frac{\sigma \varepsilon F(4T^3)}{(T - T_{fs})} + \frac{\sigma \varepsilon F(T^4 - T_{fs}^4)}{(T - T_{fs})^2}$$

$$\frac{\partial h}{\partial T_{fs}} = \frac{I^2 R_{tot, ss}}{A_{tot, ss}(T - T_{fs})^2} - \frac{k_{back}(T - T_{back})}{L_{back}(T - T_{fs})^2} + \frac{\sigma \varepsilon F(4T_{fs}^3)}{(T - T_{fs})} - \frac{\sigma \varepsilon F(T^4 - T_{fs}^4)}{(T - T_{fs})^2}$$

$$\frac{\partial h}{\partial T_{back}} = \frac{k_{back}}{L_{back}(T - T_{fs})}$$

and the uncertainties in the measured quantities are:

$$W_I = \left[\left(\frac{\partial}{\partial V} W_V \right)^2 + \left(\frac{\partial}{\partial R} W_R \right)^2 \right]^{\frac{1}{2}}$$

$$W_V = 5 \times 10^{-4} \text{ volts}$$

$$W_R = 5 \times 10^{-5} \text{ ohms}$$

$$I = V/R$$

$$W_I = \left[\left(\frac{1}{R} 5 \times 10^{-4} \right)^2 + \left(\frac{-V}{R^2} 5 \times 10^{-5} \right)^2 \right]^{\frac{1}{2}}$$

$$W_{R_{tot,ss}} = 0.01 \text{ ohms}$$

$$W_{A_{tot,ss}} = \left[(L * W_W)^2 + (W * W_L)^2 \right]^{\frac{1}{2}}$$

$$W_W = 3.33 \times 10^{-3} \text{ feet}$$

$$W_L = 3.33 \times 10^{-3} \text{ feet}$$

$$W_{A_{tot,ss}} = \left[(38.0 \text{ ft} * 3.33 \times 10^{-3} \text{ ft})^2 + (0.1667 \text{ ft} * 3.33 \times 10^{-3} \text{ ft})^2 \right]^{\frac{1}{2}}$$

$$W_{A_{tot,ss}} = 0.127 \text{ feet}^2$$

$$W_T = 0.5 \text{ } ^\circ\text{F}$$

$$W_{Tfs} = 0.5 \text{ } ^\circ\text{F}$$

$$W_{kback} = 0.026 \text{ Btu/hr-ft-'R}$$

$$W_{Lback} = 3.33 \times 10^{-3} \text{ feet}$$

$$W_{Tback} = 0.5 \text{ } ^\circ\text{F}$$

$$W_\epsilon = 0.01$$

The uncertainty in the Nusselt number can now be determined as:

$$W_{Nu} = \left[\left(\frac{L}{k} W_h \right)^2 + \left(\frac{h}{k} W_L \right)^2 + \left(-\frac{hL}{k^2} W_k \right)^2 \right]^{\frac{1}{2}}$$

Table C-1
Uncertainty Analysis Summary

Test#	Surface Coefficient of Heat Transfer Uncertainty Contributions (%)										h (W/mK)	% Error Net
	W(FanD)	W(Baro)	W(DuctT)	W(Re)	W(G)	% Error Re*	W(G)	% Error Gr*	W(U)	% Error h*		
12-11_1	3.536E-01	1.170E-08	7.070E-01	2.219E-02	1.048	1.000E+08	15.356	5.320E-03	2.503E-04	3.506E-05	2.471E-01	21.51
11-14_1	3.536E-01	1.167E-08	7.071E-01	2.211E-02	1.048	1.003E+08	5.985	5.570E-03	6.919E-05	1.497E-05	2.478E-01	8.10
12-12_1	3.536E-01	1.111E-06	7.071E-01	2.118E-02	1.048	1.000E+08	3.087	5.980E-03	1.745E-06	2.206E-02	2.377E-04	4.16
10-25_1	3.536E-01	1.082E-06	7.071E-01	2.064E-02	1.049	1.008E+08	3.073	5.990E-03	1.010E-05	4.281E-03	4.195E-03	4.15
01-31_1	3.536E-01	1.082E-06	7.071E-01	2.170E-02	1.048	1.000E+05	3.073	5.090E-03	3.069E-05	4.250E-03	4.145E-03	4.52
02-01_1	3.536E-01	1.143E-06	7.071E-01	2.174E-02	1.049	1.014E+06	5.641	5.570E-03	6.128E-05	2.148E-02	2.148E-02	7.85
11-13_1	3.536E-01	1.138E-06	7.071E-01	2.174E-02	1.049	1.024E+06	5.948	5.570E-03	1.304E-05	2.277E-02	2.277E-02	7.93
02-21_1	3.536E-01	1.143E-06	7.071E-01	2.172E-02	1.048	1.015E+06	4.651	5.570E-03	7.020E-05	2.020E-02	2.515E-02	2.409E-01
02-27_1	3.536E-01	1.090E-06	7.071E-01	2.082E-02	1.048	1.000E+06	9.514	5.320E-03	1.395E-05	6.179E-03	6.179E-03	6.67
11-01_1*	3.536E-01	1.105E-06	7.071E-01	1.543E-02	1.104	1.017E+06	5.502	5.582E-03	1.321E-05	5.753E-03	5.753E-03	6.68
10-30_1	3.536E-01	1.144E-06	7.071E-01	1.577E-02	1.104	1.027E+06	5.233	5.582E-03	5.401E-05	1.203E-05	1.348E-02	8.72
11-02_1	3.536E-01	1.115E-06	7.071E-01	1.541E-02	1.104	1.140E-06	4.147	5.580E-03	3.179E-05	7.003E-06	7.003E-06	6.57
11-15_1	3.536E-01	1.194E-06	7.071E-01	5.070E-02	1.006	1.089E+06	7.046	5.570E-03	5.809E-05	1.879E-04	5.286E-02	12.07
11-21_1	3.536E-01	1.184E-06	7.071E-01	5.042E-02	1.006	1.071E-06	5.423	5.602E-03	9.084E-05	3.198E-05	4.048E-02	4.048E-02
12-14_1	3.536E-01	1.170E-06	7.071E-01	6.940E-01	#DIV/0!	2.091E-06	2.216	5.180E-03	2.704E-06	5.528E-07	4.567E-04	2.362E-00
12-14_2	3.536E-01	1.216E-06	7.071E-01	7.105E-01	#DIV/0!	2.120E-06	4.481	5.020E-03	5.210E-06	2.197E-07	7.047E-06	9.25

Heat Transfer Coefficient Uncertainty Contributions
For 3-D Heat Transfer Description Tests

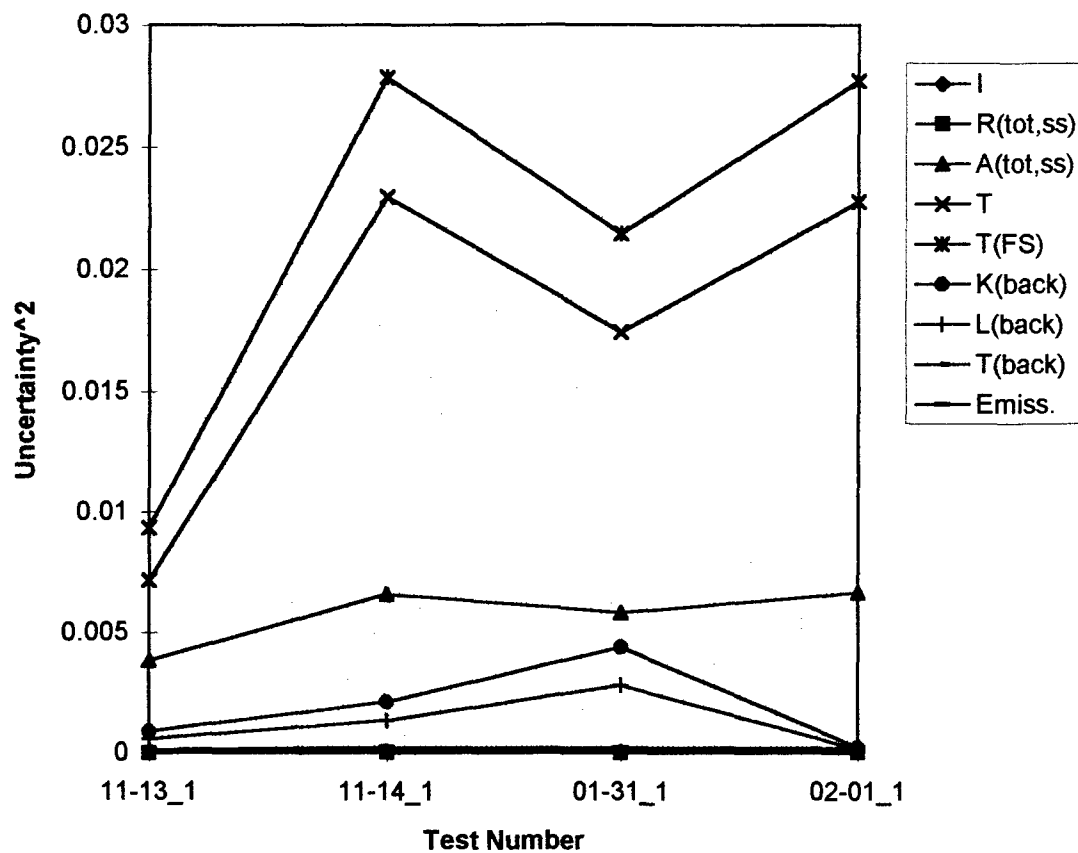


Figure C-1

XIII(D). Data Acquisition and Calibration Software:

Several pieces of software, designed specifically for this experiment, were used for the acquisition and calibration of experimental data. A typical testing run consisted of collecting the temperature data, via the RTD sensors, using acquisition software. The raw data is then run through another piece of software which calibrates the data for each individual sensor.

For the purposes of acquisition, the software used is entitled, *HOTBOX2A.EXE*. This code interfaces with the multiplexer switching unit and the Keithley ohmmeter. The code switches the multiplexer through each of the RTD sensors, each time pausing to read resistance information from the Keithley output channel. The code stores the information in arrays and prints it to the screens during runtime. The code then produces an output data file consisting of three columns of numbers. The first column is the sensor number; the second, the RTD resistance value; and the third, the temperature calculated using the manufacturer's equation provided in the Experimental Block and Board Assembly section. This data file is named using the following naming convention:

month-day_test#.dat

The calibration software, entitled, *HEAT_R4.EXE* is then run to calibrate the raw data. This code first reads information about the overlay file path, dual calibration curve breakpoint, and the test resistor resistance from a configuration file named *HEAT.CFG*. The code then prompts the user to input the raw data file path, and reads the file into a C++ style structure. After reading all raw data, the code then opens and reads another data file, entitled *CALIBR.OV2*. This file contains the slope and offset information for each sensors' calibration curves. Details on the construction of these

calibration curves can be found in Appendix B. The slope and offset information is also stored in the C++ structure. The code then performs the necessary calibration algorithms, and writes a calibrated temperature back to the structure. With all calibration procedures now complete, the user is prompted to enter a pathname for a calibrated temperature output file, along with various other specific test information. *HEAT_R4.EXE* then creates the output file. All output files were named using the following naming convention:

month-day_test#.cal

/* HEAT_r4.CPP

This program reads data from the HOTBOX2A.EXE's output data file and modifies the sensor temperature to account for a calibration offset. The program then writes the sensor number, resistance, and corrected temperature to a user defined data file.

NOTE: The input data file must be in columnar text in the following form:

Sensor# Resistance Temperature

The offset data file must be a single column of offset values corresponding to each sensor */

```
#include <stdlib.h>
#include <stdio.h>
#include <conio.h>
#include <io.h>
#include <dos.h>
```

```
#define NUM_SENS 79
#define DEFAULT_CONFIG "a:\\heat.cfg"
```

```
struct SensData {
    int sens_num;
    float temp;
    float resist;
    float h_value;
    float lowslope, highslope;
    float lowintercept, highintercept;
    float caltemp;
};
```

```
SensData *ModifyTemp( SensData Sensor[], char calibration_file[], float cal_breakpt );
void OutputFunc( SensData Sensor[], char input_file[], float test_resist );
```

```
main()
{
```

```
    int i=0;
    char input_file[100];
    char calibration_file[100];
    char config_file[100] = DEFAULT_CONFIG;
    char more = 'N';
    FILE *fp;
    SensData Sensor[NUM_SENS];
    SensData *Sensor_ptr;
    float cal_breakpt;
    float test_resist;
```

```
    clrscr();
```

```
    /* Check for configuration path change */
```

```

while( more == 'N' ) {

printf( "\n\n\nUse default configuration file path ? Y/N ==> ");
more = getche();
if(more == 'n'){
    more = 'N';
    printf( "\n\nEnter the path and filename to configuration file ==> ");
    scanf( "%s", config_file );
    break;
}
}

if ( ( fp = fopen( config_file, "rb" ) ) == NULL ) {
    clrscr();
    printf( "\n\n%s could not be opened !!", config_file );
    exit( 0 );
}
else
    fscanf( fp, "%s %f %f", calibration_file, &cal_breakpt, &test_resist );
    printf( "\n\n%s found and opened.", config_file );

/* Enter input data file name and path */

printf( "\n\nEnter the input data file name ==> ");
scanf( "%s", input_file );

if ( ( fp = fopen( input_file, "rb" ) ) == NULL ) {
    clrscr();
    printf( "\n\n%s could not be opened !!", input_file );
    exit( 0 );
}
else
    printf( "\n\n%s found and opened.", input_file );

/* Read in data from input_file */

printf( "\n\nReading %s data ... ", input_file );
while ( !feof( fp ) ) {
    fscanf( fp, "%d %f %f", &Sensor[i].sens_num, &Sensor[i].resist, &Sensor[i].temp );
    printf( "\nSensor #%d\tResist = %f\tTemp = %f", Sensor[i].sens_num, Sensor[i].resist,
Sensor[i].temp );
    i++;
}
fclose( fp );
printf( "\n\nData read complete." );

/* Call ModifyTemp function and pass the structure array Sensor[] argument */

Sensor_ptr = ModifyTemp( Sensor, calibration_file, cal_breakpt );

/* Call OutputFunc function and pass the structure array Sensor[], and input_file arguments */

OutputFunc( Sensor_ptr, input_file, test_resist );

printf( "\n\nProgram terminated." );

```

```

        return( 0 );
    } //End of main()

/* Function Modify_Temp is passed the array of structures, from which it calculates
   the correct temperatures using the calibration slope and intercepts (both high
   and low) for each sensor. The function then returns the updated Sensor structure array */

SensData *ModifyTemp( SensData Sensor[], char calibration_file[], float cal_breakpt )
{
    int i = 0;
    FILE *ofp;

    /* Initialize calibration slope and intercept (both high and low) from file */

    if ( ( ofp = fopen( calibration_file, "rb" ) ) == NULL ) {
        clrscr();
        printf( "\n\nCould not open %s calibration file !!", calibration_file );
        exit( 0 );
    }

    while ( !feof( ofp ) ) {
        fscanf( ofp, "%f %f %f %f", &Sensor[i].lowslope, &Sensor[i].lowintercept,
&Sensor[i].highslope, &Sensor[i].highintercept );
        printf( "\nSensor #%-d\tLow Slope ==> %f\tLow Intercept ==> %f", i+1, Sensor[i].lowslope,
Sensor[i].lowintercept );
        printf( "\nSensor #%-d\tHigh Slope ==> %f\tHigh Intercept ==> %f", i+1, Sensor[i].highslope,
Sensor[i].highintercept );
        i++;
    }
    fclose( ofp );
    printf( "\n\nCalibration read complete." );

    /* Calculate correct temps and output to screen */

    printf( "\n\nCalculating corrected temps and printing to screen ... ");
    printf( "\n\n" );

    for( i = 0; i <= ( NUM_SENS - 1 ); i++ ) {
        Sensor[i].caltemp = Sensor[i].temp * Sensor[i].lowslope + Sensor[i].lowintercept ;
        if ( Sensor[i].caltemp >= cal_breakpt )
            Sensor[i].caltemp = Sensor[i].temp * Sensor[i].highslope + Sensor[i].highintercept ;
        printf( "\nSensor #%-d\tCorrect Temp = %f", Sensor[i].sens_num, Sensor[i].caltemp );
    }
    return( Sensor );
} //End of ModifyTemp function

void OutputFunc( SensData Sensor[], char input_file[], float test_resist )
{
    int i;
    float voltage;
    float rotation;
    float air_velocity;
    float air_temp;
    char io_buf[BUFSIZ];
    char new_file[100];
    char user_name[50];

```

```

FILE *nfp;
struct time t;
union REGS reg; //for date field

char *months[] = {
    "",
    "January", "February", "March", "April", "May", "June", "July", "August",
    "September", "October", "November", "December" };

char *days[] = {
    "Sunday", "Monday", "Tuesday", "Wednesday", "Thursday", "Friday", "Saturday" };

/* Input new output data file name and open */

printf( "\n\n\nEnter the new output data file name ==> " );
scanf( "%s", new_file );
if ( ( nfp = fopen( new_file, "ab" ) ) == NULL ) {
    clrscr();
    printf( "\n\n%s could not be opened !!", new_file );
    exit( 0 );
}

/* Input the test conditions to appear on output file header */

printf( "\n\nEnter the user name to appear on output file header (No Spaces) ==> " );
scanf( "%s", user_name );

printf( "\n\nEnter the test resistor voltage drop ==> " );
scanf( "%f", &voltage );

printf( "\n\nEnter the model rotation CCW (degrees) ==> " );
scanf( "%f", &rotation );

printf( "\n\nEnter the airstream velocity (FPM) ==> " );
scanf( "%f", &air_velocity );

printf( "\n\nEnter the airstream temperature (deg F) ==> " );
scanf( "%f", &air_temp );

/* Create and write output file header */

setbuf( nfp, io_buf );

printf( "\n\nWriting to output file %s ...", new_file );
fprintf( nfp, "\n\nOutput Filename ==> %s", new_file );
fprintf( nfp, "\n\n( Created from input file ==> %s)", input_file );

reg.x.ax = 0x2A00; //Set up call code for int. 0x21
intdos( &reg, &reg ); //Get date & weekday
fprintf( nfp, "\n\nCurrent Date:\t%s, %s %d, %d", days[reg.h.al], months[reg.h.dh], reg.h.dl,
reg.x.cx );

gettime( &t );
fprintf( nfp, "\nCurrent Time:\t%2d:%2d hrs", t.ti_hour, t.ti_min );

fprintf( nfp, "\nUser Name:\t%s", user_name );

```

```
fprintf( nfp, "\n\nInput Current ==>\t %5.2f amps ", voltage/test_resist );

fprintf( nfp, "\nModel Rotation ==>\t %5.1f deg's ", rotation );

fprintf( nfp, "\nAirstream Velocity ==>\t %6.2f fpm ", air_velocity );

fprintf( nfp, "\nAirstream Temp ==>\t %6.1f deg F ", air_temp );

/* Write output data to file */

fprintf( nfp, "\n\nSensor\tResist\tTemp");
fprintf( nfp, "\nNum\t(ohms)\t(deg 'F)\n\n" );

for( i = 0; i <= ( NUM_SENS - 1 ); i++ ) {
    fprintf( nfp, "%d\t%f\t%f\n", Sensor[i].sens_num, Sensor[i].resist, Sensor[i].caltemp );
}
fclose( nfp );
printf( "\n\nOutput file %s created without errors.", new_file );
return;
} //End of OutputFunc Function
```

/ HEAT.CFG */*

a:\calibr.ov2
120.0
0.102

/*CALIBR.OV2 */

1.096124	-22.4015	0.990847	-8.86037
1.047594	-18.3296	0.955298	-6.21699
1.095879	-23.4247	1.001228	-11.1856
1.04729	-18.4397	0.963271	-7.46405
1.051384	-18.9197	0.990016	-10.9783
1.057627	-19.2496	0.960489	-6.59619
1.049509	-18.4793	0.962837	-7.17727
1.049283	-18.4691	0.963073	-7.22766
1.088911	-22.1266	0.995427	-10.1051
1.043463	-18.0451	0.966888	-8.03675
1.046457	-15.6354	0.960749	-4.67692
1.070869	-18.4867	0.981675	-7.09796
1.069762	-20.2606	0.986078	-9.4834
1.096941	-24.6805	1.008386	-13.1443
1.066624	-20.1169	0.974724	-8.21779
1.056581	-19.8153	0.961069	-7.37566
1.054711	-20.7494	0.960178	-8.29444
1.079268	-22.2311	0.977691	-9.00037
1.070102	-24.2825	0.9739	-11.4759
1.080058	-22.3274	0.975354	-8.73368
1.012857	-22.9054	0.689893	21.44771
1.091949	-23.427	0.996284	-11.0435
1.068727	-22.9999	0.982377	-11.6612
1.119011	-25.672	1.02642	-13.8156
1.095456	-26.0703	1.000433	-13.5869
1.13834	-29.4935	1.034937	-16.1425
1.069009	-21.1223	0.97847	-9.42294
1.064845	-22.301	0.978172	-10.8841
1.05186	-22.1192	0.963497	-10.3688
0	0	0	0
1.106877	-27.2737	1.012548	-14.9379
0	0	0	0
1.115204	-26.3088	1.024864	-14.6604
1.065986	-21.6891	0.994472	-12.3269
1.042993	-19.821	0.976955	-11.1419
1.10225	-22.1353	1.036237	-13.7986
1.049713	-21.6484	0.985307	-13.1348
1.054388	-20.1725	0.995042	-12.4323
1.051767	-20.2542	0.991946	-12.4714
1.036951	-21.4214	0.964496	-11.6751
1.074597	-21.9159	1.005061	-12.8599
1.068874	-23.7754	0.985027	-12.6956
1.080698	-22.5431	0.987293	-10.3939
0	0	0	0
1.105609	-24.2654	1.011999	-12.1975
1.046976	-19.5905	0.986731	-11.7054
1.072756	-22.8367	0.989549	-11.8595
1.108651	-29.8716	1.028076	-19.1712

1.09772	-27.6109	1.022578	-17.727
1.08284	-27.5392	0.961819	-11.2339
1.12601	-30.4361	1.000635	-13.8664
1.080332	-29.3454	0.962629	-13.2648
0	0	0	0
1.084701	-24.7283	0.958864	-8.11968
1.080513	-28.6677	0.963134	-12.7117
1.068167	-26.3271	0.958951	-11.5199
1.151609	-34.797	1.023658	-17.7776
1.063999	-27.2919	0.959617	-13.016
1.140516	-33.5258	1.01746	-17.1767
1.087255	-29.6823	0.977206	-14.7048
1.068167	-26.3271	0.958951	-11.5199
0	0	0	0
0	0	0	0
1.064956	-21.2633	0.974516	-9.46708
0	0	0	0
1.077613	-23.0711	0.987265	-11.2589
1.083314	-23.5803	0.979731	-10.3146
1.049579	-20.3204	0.961682	-8.74332
0	0	0	0
1.049989	-19.5291	0.968459	-8.88916
1.088461	-20.385	1.003147	-9.55537
1.048574	-19.0353	0.979391	-10.0421
1.114618	-26.0815	1.030906	-15.2367
1.056913	-18.3762	1.008209	-12.1616
1.050557	-19.8513	0.986079	-11.3755
1.042207	-18.1056	0.983399	-10.353
1.058433	-20.188	0.984768	-10.5412
1.041701	-19.2555	0.968456	-9.57023
1.043618	-17.6544	0.980732	-9.47477

```

PROGRAM HOTBOX2A.EXE;
{$N+}
uses dos, crt, printer;

type
  sdesc = RECORD len : byte; address : integer; END;

{ PC488SEG is called with the segment address of the firmware ROM.
  It returns TRUE if no board is found (an error condition) }
function pc488seg (seg : word) : boolean; external;

procedure initialize (var myaddr, level : integer); external;
procedure transmit (var st : sdesc; var status : integer); external;
procedure receive (var st : sdesc; var len,status : integer); external;
procedure spoll (var address,poll,status : integer); external;
procedure ppoll (var poll : integer); external;
procedure send (var address : integer; var st : sdesc; var status : integer); external;
procedure enter (var st : sdesc; var len,address,status : integer); external;
procedure tarray (var seg,ofs,count : word; var eoi,status : integer); external;
procedure rarray (var seg,ofs,count,len : word; var status : integer); external;
procedure dma2 (var seg,ofs,count,mode : word; var status : integer); external;

{ The routines below are place-holders, for older IEEE-488 subroutines, which
  have been replaced by tarray, rarray, dma2... However, the old routines
  are still available }

procedure xmita (var a,b,c : integer); external;
procedure recva (var a,b,c,d : integer); external;
procedure dma (var a,b,c,d : integer); external;

{$L c:\tp\hbox\turbo4}
{-----}

CONST
  sensor_count      = 79;      {-- total number of sensors - 1 ---}
  BAD_LIST          = [17,21,23,44]; {-- LIST OF BAD SENSORS --}

TYPE
  s80 = string[80];
  s10 = string[10];

  point = record
    x      : real;
    y      : real;
    z      : real;
  end;

  data_rec = record
    sens_loc   : point;
    high_res   : real;
    low_res    : real;
    avg_res    : real;
    high       : real;
    low        : real;
    average    : real;
  END;

```

```

var
  g_address, g_status : integer;      {--- static variables ---}
  g_length, g_level   : integer;      {--- IEEE 488 drivers ---}
  g_s80                : s80;
  g_sdesc              : sdesc;
  my_address, level    : integer;
  fvar                 : text;
  data                 : array[0..SENSOR_COUNT] of data_rec;
  sensor_loc          : array[0..sensor_count] of point;

  avg_count            : byte;        {-- sample count for meter --}
  velocity             : real;
  watts                : real;
  volts                : real;
  current              : real;
  box_hgt              : real;
  atmos_pres           : real;
  air_temp              : real;
  model_rotation       : real;

  file_count            : byte;
  date_stg, time_stg  : string;
  run_hi, run_low       : real;

{-----}
procedure send_it(address : integer; cmd : s80);
begin
  g_address := address;
  g_s80    := cmd;
  g_sdesc.len := length(g_s80); { (build string descriptor) }
  g_sdesc.address := ofs(g_s80)+1;
  send (g_address,g_sdesc,g_status);
end;
{-----}
procedure receive_it(address : integer; var ans : s80);
begin
  g_s80  := ans;
  g_address := address;
  g_sdesc.len := 80;      { receive up to 80 characters from device }
  g_sdesc.address := ofs(g_s80)+1;
  enter (g_sdesc, g_length, g_address, g_status);
  g_s80[0] := char(g_length); { trim string to received length }
  ans  := g_s80;
end;
{-----}
procedure meter_msg(msg : s10; time : integer);
var
  j : integer;
  tmp : s80;

begin
  tmp := msg;
  for j := 1 to length(tmp) do if tmp[j] = ' ' then tmp[j] := '@';

```

```

tmp := 'D' + tmp + 'X';

send_it(7, tmp);
delay(time);
send_it(7,'DX');
end;

{-----}
procedure strip_string(var data : s80);
var
  temp  : s80;
  start, finish : integer;
  j      : integer;

begin
  start := 0;
  finish := 0;

  for J := 1 to length(data) do
  begin
    if (data[j] in ['+', '-']) and (start = 0) then start := j;
    if data[j] = ',' then finish := j;
  end;

  if finish = 0 then finish := length(data) + 1;

  temp := copy(data, start, (finish - start));
  data := temp;
end;

{-----}
function power(stuff, ep : extended) : extended;
begin
  power := exp((ln(abs(stuff)) * ep));
end;
{-----}
procedure select_channel(ch : byte);
begin
  write(lst , char(ch));
  delay(50);
end;
{-----}
function convert(R : real) : extended;
const
  A = -387.148;
  B = 14.37356;
  C = -0.206576;
  D = 3.47019e-3;
  E = -3.70193e-5;
  F = 2.05767e-7;
  G = -4.55192e-10;

var
  temp : extended;

begin

```

```

temp := A + (B * R) + c * power(r, 2.0) + d * power(R, 3.0);
temp := temp + e * power(R, 4.0) + f * power(R, 5.0) + g * power(R, 6.0);
convert := temp;
end;

{-----}
function read_meter(mode : byte): real;
var
  recv  : s80;
  err   : integer;
  treal : real;

begin
  case mode of
    1 : send_it(7, 'U6X');    {-- send high buffer value --}
    2 : send_it(7, 'U5X');    {-- send low buffer value ---}
    3 : send_it(7, 'U4X');    {-- send average buffer value --}
  end;

  receive_it(7, recv);
  strip_string(recv);

  val(recv, treal, err);
  read_meter := treal;
end;
{-----}

procedure do_average;
var
  s : string[3];
begin
  str(avg_count, s);
  send_it(7, 'I'+ s + 'T4X'); {-- avg_count samples trigger on execute --}
end;
{-----}

procedure display_data(cnt : byte);
var
  cable  : char;
  gage   : byte;

begin
  with data[cnt] do
  begin
    cable := chr(cnt div 16 + 65);
    gage := cnt mod 16 + 1;
    gotoxy(34, 3); write(cnt);
    gotoxy(47, 3); write(cable);
    gotoxy(58, 3); write(gage, ' ');
    gotoxy(32, 5); write(sens_loc.x:4:2);
    gotoxy(32, 7); write(sens_loc.y:4:2);
    gotoxy(32, 9); write(sens_loc.z:4:2);
    gotoxy(32,11); write(high:5:3);
    gotoxy(32,13); write(low:5:3);
    gotoxy(32,15); write(average:5:3);
    gotoxy(32,21); write(run_hi:5:2);
    gotoxy(32,23); write(run_low:5:2);
  end;
end;

```

```

writeln;
end;

{-----}
procedure Get_data(data_count : byte);
begin
  with data[data_count] do
  begin
    select_channel(data_count);
    do_average;           { tell meter to average }

    sens_loc := sensor_loc[data_count];
    high_res := read_meter(1);
    low_res := read_meter(2);
    avg_res := read_meter(3);

    high := convert(high_res);
    low := convert(low_res);
    average := convert(avg_res);

    if average > run_hi then run_hi := average;
    if average < run_low then run_low := average;
  end;

  display_data(data_count);
end;
{-----}
PROCEDURE FILL_BAD_NODE(NODE_NUM : BYTE);
begin
  with data[NODE_NUM] do      { Fill element in data array for bad sensor }
  begin
    sens_loc := sensor_loc[node_num];
    high_res := 0.0;
    low_res := 0.0;
    avg_res := 0.0;

    high := 0.0;
    low := 0.0;
    average := 0.0;
  end;
END;
{-----}
procedure set_up_display;
begin
  clrscr;

  writeln('----- HOTBOX HEATER DATA ',
         '-----');

  writeln;
  writeln(' Current data set for Address     Cable     Gage');
  writeln('-----');
  writeln(' Location X.....');
  writeln;
  writeln(' Location Y.....');
  writeln;

```

```

writeln(' Location Z.....');
writeln;
writeln(' High Reading.....');
writeln;
writeln(' Low Reading.....');
writeln;
writeln(' Average Reading.....');
writeln;
writeln(' Input power to strips....',watts:3:2);
writeln;
writeln(' Number of averages.....',avg_count);
writeln;
writeln(' Current run High Temp....');
writeln;
writeln(' Current run Low Temp....');
end;
{-----}
procedure load_locations;
var
  j   : byte;
  fvar : text;

begin
  assign(fvar, 'C:\TP\HBOX\DATA\rtdbox2.dat');
  reset(fvar);
  for j := 0 to sensor_count do
  begin
    with sensor_loc[j] do
    begin
      readln(fvar, x, y, z);
    end;
  end;
  close(fvar);
end;
{-----}
procedure save_real(fnum : integer);
var
  dvar   : file of data_rec;
  j      : integer;
  tstr   : string[4];
  t_rec  : data_rec;

begin
  with t_rec do { build data header record attach to end of file }
  begin
    sens_loc.x := avg_count;      {-- sample count for meter --}
    sens_loc.y := volts;
    sens_loc.z := current;
    high_res  := watts;
    low_res   := velocity;
    avg_res   := air_temp;
    high      := atmos_pres;
    low       := box_hgt;
    average   := model_rotation;
  end;

```

```

str(fnum, tstr);
assign(dvar, 'C:\TP\HBOX\DATA\box' + tstr + '.rel');
rewrite(dvar);

for j := 0 to sensor_count do
begin
  write(dvar, data[j]);
end;
write(dvar, t_rec); { puts data header record at end of file }
close(dvar);
end;
{-----}

FUNCTION do_date: string;
var
  yr, mon, day, dow : word;
  tstr      : string;
  smstr     : string;

const
  months    : array[1..12] of string[5] = ('Jan.', 'Feb.', 'Mar.',
                                             'April', 'May', 'June', 'July', 'Aug.', 'Sept.',
                                             'Oct.', 'Nov.', 'Dec.');
  days      : array[0..6] of string[10] = ('Sunday', 'Monday',
                                             'Tuesday', 'Wednesday', 'Thursday', 'Friday',
                                             'Saturday');

begin
  GetDate(yr, mon, day, dow);
  str(day, smstr);
  tstr := days[dow] + '' + months[mon] + smstr;
  str(yr, smstr);
  do_date := tstr + '' + smstr;
end;
{-----}

function do_time : string;
var
  tstr, smstr      : string;
  hr, min, sec, hsec : word;

begin
  GetTime(hr, min, sec, hsec);
  str(hr,smstr);
  tstr := smstr + ':';
  str(min,smstr);
  if min < 10 then smstr := '0'+ smstr;
  tstr := tstr + smstr + ':';
  str(sec,smstr);
  if sec < 10 then smstr := '0'+ smstr;
  do_time := tstr + smstr;
end;
{-----}

procedure save_text(fnum : integer);
var
  tvar      : text;
  j         : integer;
  tstr      : string[4];

```

```

cable      : char;
gage       : byte;
po         : string[2];
date_string : string;
time_string : string;

begin
  str(fnum, tstr);
  assign(tvar, 'C:\TP\HBOX\DATA\box' + tstr + '.dat');
  rewrite(tvar);
  writeln(tvar,'Current date.....',date_stg);
  writeln(tvar,'Current time.....',time_stg);
  writeln(tvar,'Number of meter samples...',avg_count);
  writeln(tvar,'Input Voltage.....',volts:3:4);
  writeln(tvar,'Input Current.....',(current / 0.0960):3:4);
  writeln(tvar,'Total wattage.....',(volts * current / 0.096):3:4);
  writeln(tvar,'Air Stream Velocity.....',velocity:6:4);
  writeln(tvar,'Air stream Temprature....',air_temp:6:4);
  writeln(tvar,'Atmospheric pressure....',atmos_pres:4:2);
  writeln(tvar,'Box height.....',box_hgt:4:2);
  writeln(tvar,'Model Rotation C.C.W.....',model_rotation:5:2);
  writeln(tvar);

  writeln(tvar,'Cable  High Res  Low Res  Avg Res  Loc. X  Loc. Y  Loc. Z');
  writeln(tvar,'      High Temp  Low Temp  Avg Temp');
  writeln(tvar);

  for j := 0 to SENSOR_COUNT do
    begin
      cable := chr(j div 16 + 65);
      gage := j mod 16 + 1;
      with data[j] do
        begin
          if gage < 10 then po := '..' else po := ':';
          writeln(tvar,cable,'',gage,po,'.',high_res:3:4,'  ',low_res:3:4,'  ',avg_res:3:4,
                  ',sens_loc.x:5:2,'  ',sens_loc.y:5:2,'  ',sens_loc.z:5:2);
          writeln(tvar,'      ,high:3:4,'  ',low:3:4,'  ',average:3:4);

          writeln(tvar);
        end;
    end;
    close(tvar);
  end;

{-----}
procedure rotate_sensors;
var
  temp_point : point;
  j          : integer;

begin
  Writeln('Rotating sensor list 90 deg. Counter Clockwise...');
  for j := 0 to sensor_count do
    begin

```

```

temp_point := sensor_loc[j];
with sensor_loc[j] do
begin
  x := 25.0 - temp_point.y;
  y := temp_point.x;
  z := temp_point.z;
end;
end;
end;
{-----}

procedure init;
var
  ad_address : integer;

begin
  clrscr;
  date_stg := do_date;
  time_stg := do_time;
  writeln;
  file_count := 0;
  writeln('The date is.....',date_stg);
  writeln('The time is.....',time_stg);
  writeln;
  writeln('Data will be saved in the C:\TPHBOX\DATA directory');
  writeln;
  write('Enter air stream velocity in Ft/Min... ');
  readln(velocity);
  writeln;
  write('Enter voltage accross strips.....');
  readln(volts);
  writeln;
  write('Enter voltage across current shunt....');
  readln(current);
  writeln;
  write('Enter current file count.....');
  readln(file_count);
  writeln;
  write('Enter sample count.....');
  readln(avg_count);
  writeln;
  write('Enter box height in inches.....');
  readln(box_hgt);
  writeln;
  write('Enter atmospheric pressure in In/Hg....');
  readln(atmos_pres);
  writeln;
  write('Enter air stream temprature deg. C.....');
  readln(air_temp);
  writeln;
  write('Model rotation Counter Clockwise 0, 90, 180, 270 deg....');
  readln(model_rotation);

watts := volts * current / 0.0960;
fillchar(data, sizeof(data), 0); { clear main data array }

```

```

my_address := 21;      { make PC a controller at address 21 }
level      := 0;
initialize (my_address,level);

send_it(7, 'F2R2S3X'); {-- ohms 300 scale 6.5 digit --}

run_hi := 0.0;
run_low := 10000.0;

load_locations;        {-- get x,y,z sensor locations from data file }

if model_rotation > 0.0 then
begin
  if model_rotation > 1.0 then rotate_sensors;
  if model_rotation > 91.0 then rotate_sensors;
  if model_rotation > 181.0 then rotate_sensors;
end;
set_up_display;
end;

{-----}
procedure finish_screen;
begin
  clrscr;
  gotoxy(30,5); writeln('HOTBOX RUN ',file_count,' FINISHED...');
  gotoxy(30,10); writeln('Highest recorded temprature...',run_hi:5:3);
  gotoxy(30,12); writeln('Lowest recorded temprature....',run_low:5:3);
  gotoxy(1,20);
end;
{-----}
procedure main;
var
  j : byte;
  .
  .
  .
BEGIN
  init;
  for j := 0 to SENSOR_COUNT do
  begin
    if j in BAD_LIST then FILL_BAD_NODE(j) else get_data(j);
  end;
  save_real(file_count);
  save_text(file_count);
  finish_screen;
END;
{-----}
procedure scan_sensors(chnl : byte);
var
  j   : integer;
  temp : real;
  deg_f : extended;
  qwert : char;

begin
  my_address := 21;      { make PC a controller at address 21 }

```

```

level := 0;
initialize (my_address,level);
clrscr;
meter_msg('THIS IS IT',3000);
send_it(7,'F2R2S3X'); {-- ohms 300 scale 6.5 digit --}
avg_count := 5;

if chnl = 99 then
begin
  for j := 1 to sensor_count do
    begin
      select_channel(j);
      do_average;
      temp := 0.0;
      temp := read_meter(3);

      if (temp > 40.0) and (temp < 90.0) then
begin
        deg_f := convert(temp);
        writeln(j,'....',temp:6:4,' ',deg_f:6:3);
        writeln(fvar, j,' ',temp:6:4,' ',deg_f:6:3);

      end
      ELSE
begin
      WRITELN(j,'.....Bad sensor');
      WRITELN(fvar, J,' 0      0');
      end
    end;
  end;
else
begin
  select_channel(chnl);
  do_average;
  temp := 0.0;
  temp := read_meter(3);

  if (temp > 40.0) and (temp < 90.0) then
begin
  deg_f := convert(temp);
  writeln(j,'....',temp:6:4,' ',deg_f:6:3);
  writeln(fvar, j,' ',temp:6:4,' ',deg_f:6:3);
end
ELSE
begin
  WRITELN(J,'.....Bad sensor');
  WRITELN(fvar, J,' 0      0');
  end
end;
end;
{-----}
function Yes_no(x, y : integer; stuff : string): boolean;
var
  ch : char;

begin

```

```

gotoxy(x, y);
write(stuff + ' Y/N');
repeat
  ch := readkey;
  ch := uppercase(ch);
  until ch in ['Y', 'N'];
  if ch = 'Y' then Yes_no := true else Yes_no := false;
end;
{-----}
procedure main_test;
var
  go_on : boolean;
  ans : boolean;

  chk_num : byte;

begin
  assign(fvar, 'C:\TP\HBOX\DATA\tempscan.dat');
  rewrite(fvar);
  while go_on do
    begin
      clrscr;
      ans := true;
      ans := Yes_no(5, 5, 'Run scan <Y> or single sensor <N> ');
      writeln;
      if ans then Scan_sensors(99)
      else
        begin
          write('Enter sensor Number to test... ');
          readln(chk_num);
          Scan_sensors(chk_num);
        end;
      go_on := Yes_no(5, 10, 'Run this test again... ');
    end;
  close(fvar);
end;
{-----}

begin
  main_test;
end.

```

XIII(E). Equipment List:

1. Hewlett Packard, Model 3465A, Digital Multimeter
2. Micronta, Model 22-195A, Portable Digital Multimeter
3. Keithley, Model 196, System Digital Multimeter
4. General Electric, Custom Built, 500A, Direct Current Power Supply with Speed Variator
5. Lambda, Model LK352-FM-0180, 15A, 60V, Direct Current Power Supply
6. Hewlett Packard, Model 6215, 500mA, 30V, Direct Current Power Supply
7. IBM PC AT, 8088, Personal Computer
8. Texas Instruments, Model 4000E, 486DX2-50, Portable Computer
9. Custom Built, 80 Channel, Solid-State, Multiplexer Unit
10. Solomat, Model MPM500e, Hot-Wire Anemometer
11. Omega, Model HH21, Microprocessor Thermometer
12. Fisher, Permatch, Model 15-043A, Mercury Bulb Thermometer
13. Omega, Model OM-202, Thermocouple Data Logger
14. Delonghi, Model 5108, 1500W, Floor Heater
15. Joy, Model 38-26-1770AP, 40HP, Axivane Wind Tunnel Fan

XIII(F). Testing Data Tables and Figures

Table F-1

Example Test Log

Test Filename: 10-25_1.dat**Test Date:** 25 Oct 95**Test Performer:** Scott E. LeClair, (207)581-2123Initial Conditions:

Block Rotation: 0 degrees

Test Resistor Resistance: 0.1020 ohms

Hbox Continuity Check: initial = 10.99 ohms final = 10.24 ohms

Measurements Log:

Time	Sensor Temperatures ('F)			Air Temp	Air Speed	Resistor	Sensor #1	Remarks
	#1	#19	#36	(deg C)	(fpm)	volt. drop	temp diff	
1125	105.938	110.088	104.815	26.8	660	0.718	25.698	
1135	116.676	120.772	116.021	31.8	660	0.722	27.436	Adjusted Voltage
1145	124.790	127.210	125.129	33.6	660	0.725	32.310	Adjusted Voltage
1155	128.455	129.629	129.418	34.1	660	0.724	35.075	
1205	130.890	131.023	132.472	34.3	660	0.723	37.150	
1215	132.631	131.977	134.546	34.8	660	0.723	37.991	
1225	133.862	132.364	136.223	34.8	660	0.723	39.222	
1230	134.299	132.752	136.703	35.1	660	0.722	39.119	
1235	135.116	133.323	137.530	35.3	660	0.726	39.576	
1240	135.559	133.817	138.135	35.7	660	0.722	39.299	
1245	135.793	134.185	138.457	35.8	660	0.718	39.353	
1247	136.001	134.350	138.740	36	660	0.717	39.201	Created 10-25_1
1252	136.438	134.571	139.194	36.3	660	0.714	39.098	

Table F-2

Output Filename ==> d:\scottstu\thesis\data\10-25_1.cal

(Created from input file ==> a:10-25_1.dat)

Current Date: Wednesday, October 25, 1995

Current Time: 12:49 hrs

User Name: S.LeClair

Input Current ==> 7.03 amps
Model Rotation ==> 0.0 deg's
Airstream Velocity ==> 660.00 fpm
Airstream Temp ==> 96.8 deg F

Sensor Num	Resist (ohms)	Temp (deg 'F)
1	59.3419990	125.895821
2	60.3270000	129.629257
3	59.4129980	125.431953
4	59.1440010	122.335747
5	58.9840010	121.421486
6	60.3730010	130.265808
7	59.5299990	124.913368
8	59.1950000	122.856544
9	58.4990010	119.951431
10	58.7010000	119.628357
11	58.7570000	122.425362
12	58.6209980	121.923584
13	58.4980010	119.501663
14	58.4100000	118.018356
15	58.4080010	118.624222
16	58.0470010	115.186172
17	58.5449980	117.361847
18	58.3030010	117.432655
19	59.0810010	119.485710
20	58.1539990	116.411446
21	58.5099980	109.499313
22	58.1670000	116.929932
23	58.6160010	117.429764
24	58.2379990	118.670349
25	59.1110000	121.011345
26	58.1650010	116.811638
27	58.3759990	117.710960
28	57.4640010	109.781303
29	58.6679990	116.441269
30	0.0000000	0.000000
31	58.5870020	117.964058
32	0.0000000	0.000000
33	58.2620010	117.713097
34	58.9389990	120.385391
35	59.1609990	120.606346

Table F-2

36	59.7760010	129.968933
37	60.8860020	130.425415
38	59.3100010	122.693405
39	58.5330010	117.391602
40	59.3060000	119.369583
41	59.2160000	123.029381
42	59.0530010	119.637558
43	59.6120000	125.562263
44	0.0000000	0.000000
45	58.8839990	122.500580
46	60.4510000	129.377396
47	60.3849980	129.217529
48	59.1150020	119.314034
49	58.5830000	116.397888
50	59.7270010	121.911667
51	58.5190010	116.824615
52	0.0000000	-29.345400
53	0.0000000	0.000000
54	58.1689990	114.711082
55	58.6440010	113.502953
56	56.5999980	100.223976
57	58.7109990	117.217682
58	58.9580000	114.826462
59	58.8230020	117.836655
60	59.2690010	117.684235
61	58.6590000	114.320580
62	0.0000000	0.000000
63	0.0000000	0.000000
64	58.5040020	117.911537
65	0.0000000	0.000000
66	58.6150020	118.518623
67	59.3660010	123.078720
68	58.6959990	118.126419
69	0.0000000	0.000000
70	59.6110000	124.467644
71	58.0820010	118.933662
72	59.1910020	122.220741
73	58.7640000	121.192368
74	59.8219990	128.009689
75	60.3930020	129.256134
76	58.1310010	115.617897
77	59.7840000	126.135735
78	58.7249980	118.343826
79	59.5490000	125.188568

Table F-3

Test File: 10-25_1											
	airstream velocity =	660 fpm									
	airstream temp =	96.8 °F									
	model rotation =	0 deg (ccw)									
sensor#	x-value	y-value	temp (°F)	k,ss	gen	cond,1	cond,2	cond,b	rad	conv	h
0		0									
1		125.8958	26	1.814817	0	-0.065772	0.299006	0.165436	1.284603	1.588157	
2		129.6293	26	1.814817	0	-0.090833	0.5485	0.188531	0.986952	1.08141	
3		125.432	26	1.814817	-0.090833	-0.065065	0.268007	0.162597	1.228315	1.543171	
4		122.3357		1.814817							
5		121.4215		1.814817							
6		130.2658	26	1.814817	0	-0.115831	0.591039	0.192513	0.915434	0.983968	
7		124.9134	26	1.814817	-0.115831	-0.064701	0.233352	0.159431	1.241502	1.58851	
8		122.8565	26	1.814817	-0.065772	-0.062869	0.095901	0.146957	1.443318	1.99251	
9		119.9514	26	1.814817	-0.062869	-0.044145	-0.098239	0.129562	1.67648	2.604808	
10		119.6284	26	1.814817	-0.060529	-0.024015	-0.119829	0.127644	1.722457	2.71412	
11		122.4254	26	1.814817	-0.065065	-0.060529	0.067086	0.144359	1.477778	2.074409	
12		121.9236	26	1.814817	-0.00892	-0.052412	0.033554	0.141342	1.578589	2.260178	
13		119.5017	26	1.814817	-0.052412	-0.029761	-0.128296	0.126893	1.734046	2.74763	
14		118.0184									
15		118.6242									
16		115.1862									
17		117.3618									
18		117.4327									
19		119.4857									
20		116.4114									
21		109.4993									
22		116.9299									
23		117.4298									
24		118.6703									
25		121.0113									
26		116.8116									
27		117.7111									
28		109.7813									
29		116.4413									
30		0									
31		117.9641									
32		0									
33		117.7131	26	1.814817	0	0.041647	-0.110698	0.116337	1.850824	3.183479	
34		120.3854	26	1.814817	-0.017464	0.004782	0.136432	0.132144	1.533559	2.338905	
35		120.6063	26	1.814817	0.004782	0	-0.306216	0.133461	1.992353	3.010431	
36		129.9689	26	1.814817	0.015425	0.009879	0.319457	0.190655	1.330009	1.442375	
37		130.4254	26	1.814817	0.009879	-0.02268	0.494254	0.193514	1.114247	1.191981	
38		122.6934									
39		117.3916									
40		119.3696									
41		123.0294									
42		119.6376	26	1.814817	0.041647	0.128215	0.017908	0.127699	1.839072	2.896704	
43		125.5623	26	1.814817	0.128215	0	0.413838	0.163393	1.3658	1.708124	
44		0	0	0	0	0	0	0			
45		122.5006	26	1.814817	0	0	0.209235	0.144812	1.46077	2.044533	
46		129.3774	26	1.814817	-0.02268	-0.00346	0.424218	0.186959	1.177499	1.300168	
47		129.2175	26	1.814817	-0.00346	0	0.413535	0.185963	1.211859	1.344707	
48		119.314									
49		116.3979									
50		121.9117									
51		116.8246									
52		0									
53		0									
54		114.7111									
55		113.503									
56		100.224									
57		117.2177									

Table F-3

58		114.8265									
59		117.8367									
60		117.6842									
61		114.3206									
62		0									
63		0									
64		117.9115	26	1.814817	-0.044145	0	-0.234559	0.117504	1.887727	3.216434	
65		0									
66		118.5186	26	1.814817	-0.024015	0.098684	-0.193989	0.121079	1.962395	3.250195	
67		123.0787	26	1.814817	0.098684	0	0.110748	0.148298	1.654454	2.264675	
68		118.1264	26		-0.029761	0	-0.220199	0.118768	1.886487	3.181933	
69		0									
70		124.4676	26	1.814817	0	-0.119759	0.409236	0.156716	1.129105	1.46797	
71		118.9337	26	1.814817	-0.119759	0	0.039417	0.12353	1.53211	2.489958	
72		122.2207	26	1.814817	0	-0.022255	0.259082	0.143128	1.390352	1.967395	
73		121.1924	26	1.814817	-0.022255	0	0.190359	0.136961	1.465242	2.16078	
74		128.0097	26	1.814817	0	0.026974	0.188527	0.178458	1.474805	1.69981	
75		129.2561	26	1.814817	0.026974	0	0.729236	0.186203	0.926351	1.026678	
76		115.6179									
77		126.1357									
78		118.3438									
79		125.1886									

Table F-4

Cover Temperature Map (Test 10-25_1)		
	129.6293	130.2658
125.8958	125.432	124.9134
122.8565	122.4254	121.9236
119.9514	119.6284	119.5017
117.9115	118.5186	118.1264
0	123.0787	0
Average Surf T =	121.4237	

Table F-4

Cover Temperature Map (Test 10-25_1)		
	129.6293	130.2658
125.8958	125.432	124.9134
122.8565	122.4254	121.9236
119.9514	119.6284	119.5017
117.9115	118.5186	118.1264
0	123.0787	0
Average Surf T =	121.4237	

Table F-5

Cover Temp Difference Map (Test 10-25_1)					
	32.82926	33.46581			
29.09582	28.63195	28.11337			
26.05654	25.62536	25.12358			
23.15143	22.82836	22.70166			
21.11154	21.71862	21.32642			
-96.8	26.27872	-96.8			
Average Delta T =		24.62372			

Table F-6

Cover Surf Coeff Map (Test 10-25_1)		
1.588157	1.543171	1.58851
1.99251	2.074409	2.260178
2.604808	2.71412	2.74763
3.216434	3.250195	3.181933
Ave Surf Coeff. =	2.396838	

Table F-7

Front Surface Coeff Map (Test 10-25_1)					
1.46797	2.489958	0	3.183479	2.896704	1.708124
1.967395	2.16078	2.338905	3.010431	0	2.044533
1.69981	1.026678	1.442375	1.191981	1.300168	1.344707
Bottom					
Ave =	1.954625				

Temperature Distribution Surface Plot
Test: 10-25_1 (Left Half of Cover)

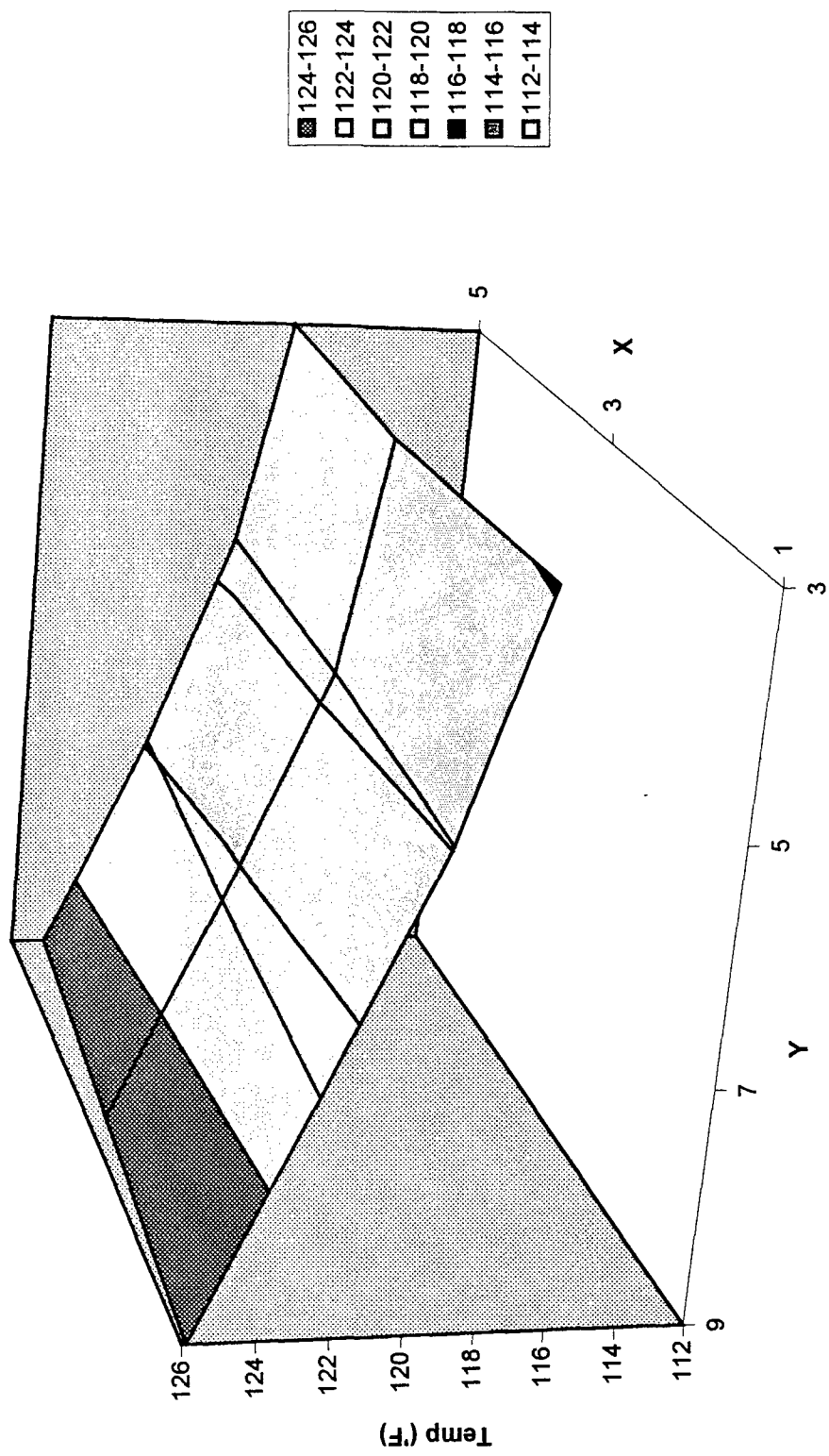


Figure F-1

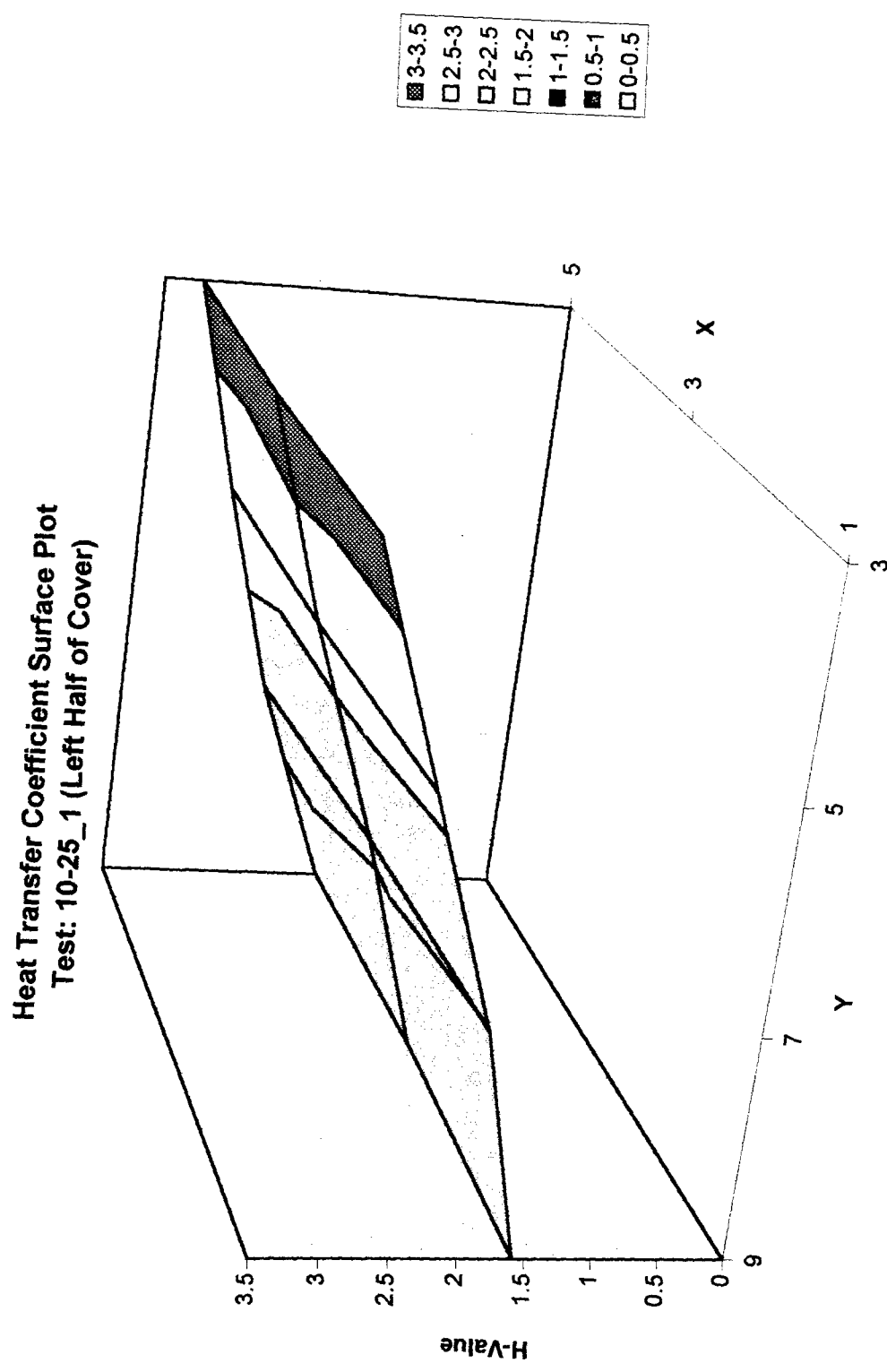


Figure F-2

Table F-8

Output Filename ==> d:\SCOTTSTU\THESIS\DATA\10-30_1.cal

(Created from input file ==> a:10-30_1.dat)

Current Date: Monday, October 30, 1995

Current Time: 11:29 hrs

User Name: S.LeClair

Input Current ==> 5.54 amps
Model Rotation ==> 0.0 deg's
Airstream Velocity ==> 455.00 fpm
Airstream Temp ==> 88.9 deg F

Sensor Num	Resist (ohms)	Temp (deg 'F)
1	56.7319980	108.395699
2	57.4199980	111.317490
3	56.9109990	108.608994
4	56.5690000	105.427475
5	56.4480020	104.609505
6	57.4259990	111.679329
7	56.8709980	107.696877
8	56.6629980	106.271767
9	56.2070010	104.111946
10	56.4010010	104.235191
11	56.3569980	106.698570
12	56.1800000	105.472801
13	56.1170010	103.133240
14	56.1139980	101.827515
15	55.9350010	101.654236
16	55.6749990	99.022591
17	56.0810010	100.661545
18	55.8019980	100.051041
19	56.5320010	102.026993
20	55.6199990	98.764374
21	55.9049990	92.529907
22	55.9070010	101.036621
23	56.3699990	102.027267
24	55.9370000	102.094444
25	56.6889990	104.343742
26	55.8160020	99.585144
27	55.9490010	101.018387
28	55.4720000	96.058647
29	56.5040020	101.846703
30	0.0000000	0.000000
31	56.3130000	101.808075
32	0.0000000	0.000000
33	55.8060000	100.073929
34	56.4160000	103.335075
35	56.4760020	102.911110

Table F-8

36	56.9790000	111.148766
37	57.7519990	110.494728
38	56.5919990	104.691292
39	56.0110020	100.340347
40	56.5740010	101.257156
41	56.3930020	103.958099
42	56.3909990	101.414330
43	56.6800000	106.050232
44	0.0000000	0.000000
45	56.1730000	103.664627
46	57.2980000	109.159279
47	57.3110010	109.173439
48	56.5470010	101.095573
49	56.2729990	100.117607
50	57.3390010	105.905663
51	56.3450010	101.110008
52	0.0000000	-29.345400
53	0.0000000	0.000000
54	56.0770000	100.106674
55	56.5029980	98.667519
56	55.0180020	89.233604
57	56.3960000	100.119743
58	56.5280000	98.269569
59	56.4690020	100.630821
60	56.7270010	100.021782
61	56.2949980	98.115417
62	0.0000000	0.000000
63	0.0000000	0.000000
64	56.1980020	102.135277
65	0.0000000	0.000000
66	56.1430020	101.410439
67	56.2990000	102.655022
68	56.0620000	100.370689
69	0.0000000	0.000000
70	56.7529980	105.905731
71	55.5870020	101.414879
72	56.4679990	104.299019
73	56.3200000	103.953178
74	57.0649990	110.011253
75	57.5929990	111.328598
76	55.8670010	100.417305
77	56.5680010	104.990761
78	56.1269990	100.969292
79	56.6469990	106.304451

Table F-9

Test File:		10-30_1									
airstream velocity =		455	fpm								
airstream temp =		88.9	'F								
model rotation =		0	deg (ccw)								
sensor#	x-value	y-value	temp ('F)	k,ss	gen	cond,1	cond,2	cond,b	rad	conv	h
0			0								
1			105.362	26	1.14465	0	-0.0432	0.24292	0.08675	0.77179	1.68648
2			108.447	26	1.14465	0	-0.07708	0.44911	0.10387	0.51459	0.94697
3			104.885	26	1.14465	0.07708	-0.04249	0.21108	0.08413	0.88404	1.98935
4			102.043		1.14465						
5			101.727		1.14465						
6			110.239	26	1.14465	0	-0.12192	0.56885	0.11395	0.33994	0.57304
7			104.605	26	1.14465	0.12192	-0.05304	0.19236	0.08259	0.93859	2.14977
8			103.365	26	1.14465	0.0432	-0.0322	0.10951	0.07581	0.97034	2.41298
9			101.878	26	1.14465	0.0322	0.0041	0.01008	0.06774	1.10313	3.05766
10			101.51	26	1.14465	0.03056	0.00511	-0.0145	0.06576	1.12906	3.22084
11			102.922	26	1.14465	0.04249	-0.03056	0.07988	0.0734	1.0033	2.57382
12			102.154	26	1.14465	-0.00241	-0.04049	0.02857	0.06924	1.00394	2.72465
13			100.283	26	1.14465	0.04049	0.01043	-0.09645	0.05916	1.23285	3.89578
14			100.88								
15			100.406								
16			99.5942								
17			100.471								
18			100.444								
19			101.785								
20			100.121								
21			93.879								
22			100.42								
23			100.177								
24			100.808								
25			102.119								
26			99.8367								
27			101.193								
28			93.8821								
29			99.7209								
30			0								
31			100.646								
32			0								
33			101.24	26	1.14465	0	0.02666	-0.04768	0.0643	1.1547	3.36584
34			102.513	26	1.14465	0.01476	0.00626	0.03732	0.07118	1.05717	2.79345
35			102.803	26	1.14465	-0.00626	0	-0.08428	0.07275	1.14992	2.97525
36			108.125	26	1.14465	-0.01484	0.0175	0.27142	0.10207	0.77382	1.44784
37			108.934	26	1.14465	-0.0175	-0.01567	0.36696	0.1066	0.6379	1.14538
38			105.869								
39			100.225								
40			101.954								
41			103.442								
42			102.473	26	1.14465	-0.02666	0.10942	0.03465	0.07096	1.12179	2.97309
43			107.529	26	1.14465	-0.10942	0	0.09547	0.09875	0.84102	1.62398
44			0	0	0	0	0	0	-0.35037	0.35037	-0.14177
45			103.973	26	1.14465	0	0	-0.14213	0.07913	1.20766	2.88202
46			108.21	26	1.14465	0.01567	-0.01021	0.31859	0.10255	0.72898	1.358
47			107.738	26	1.14465	0.01021	0	0.10947	0.09991	0.94548	1.80538
48			102.771								
49			98.9507								
50			104.263								
51			101.918								
52			-29.3454								
53			0								
54			100.016								
55			99.2478								
56			91.8581								
57			100.97								
58			99.9262								
59			102.009								
60			101.256								

Table F-9

61		100.21								
62		0								
63		0								
64		102.067	26	1.14465	-0.0041	0	0.02276	0.06877	1.04903	2.86584
65		0								
66		101.746	26	1.14465	-0.00511	0.12736	0.00127	0.06703	1.19861	3.35644
67		107.631	26	1.14465	-0.12736	0	0.39455	0.09931	0.52343	1.00522
68		100.765	26		-0.01043	0	-0.06424	0.06175	1.13671	3.44609
69		0								
70		107.483	26	1.14465	0	-0.1031	0.09241	0.09849	0.85066	1.64664
71		102.719	26	1.14465	0.1031	0	0.05106	0.0723	1.12439	2.92664
72		104.326	26	1.14465	0	-0.02448	-0.11853	0.08106	1.15765	2.69942
73		103.195	26	1.14465	0.02448	0	0.0829	0.07489	1.01134	2.54485
74		106.69	26	1.14465	0	0.01621	0.03946	0.09409	1.02732	2.07718
75		107.439	26	1.14465	-0.01621	0	0.36653	0.09825	0.66367	1.28769
76		99.0614								
77		104.881								
78		101.955								
79		104.064								

Table F-10

Cover Temperature Map (Test 10-30_1)		
	108.4471	110.2388
105.3616	104.8852	104.605
103.3653	102.9219	102.1542
101.8775	101.5097	100.2834
102.0671	101.7456	100.7653
0	107.6307	0
Average Surf T =	102.6285	

Table F-11

Cover Temp Difference Map (Test10-30_1)		
	19.54708	21.33884
16.46162	15.98519	15.70503
14.46525	14.02191	13.25418
12.9775	12.60967	11.38339
13.16712	12.84558	11.86533
-88.9	18.73069	-88.9
Average Delta T =		13.72848

Table F-12

Cover Surf Coeff Map (Test 10-30_1)		
1.686477	1.989347	2.149772
2.41298	2.573822	2.724653
3.057665	3.220844	3.895781
2.865839	3.356441	3.446093
Ave Surf Coeff. =	2.781643	

Table F-13

Front Surface Coeff Map (Test 10-30_1)					
1.646641	2.926839	0	3.365837	2.973091	1.623977
2.699416	2.544853	2.793454	2.975253	-0.14177	2.882019
2.077178	1.287687	1.447839	1.145375	1.357995	1.805382
Bottom					
Ave H =	2.222052				
StDev =	0.743511				

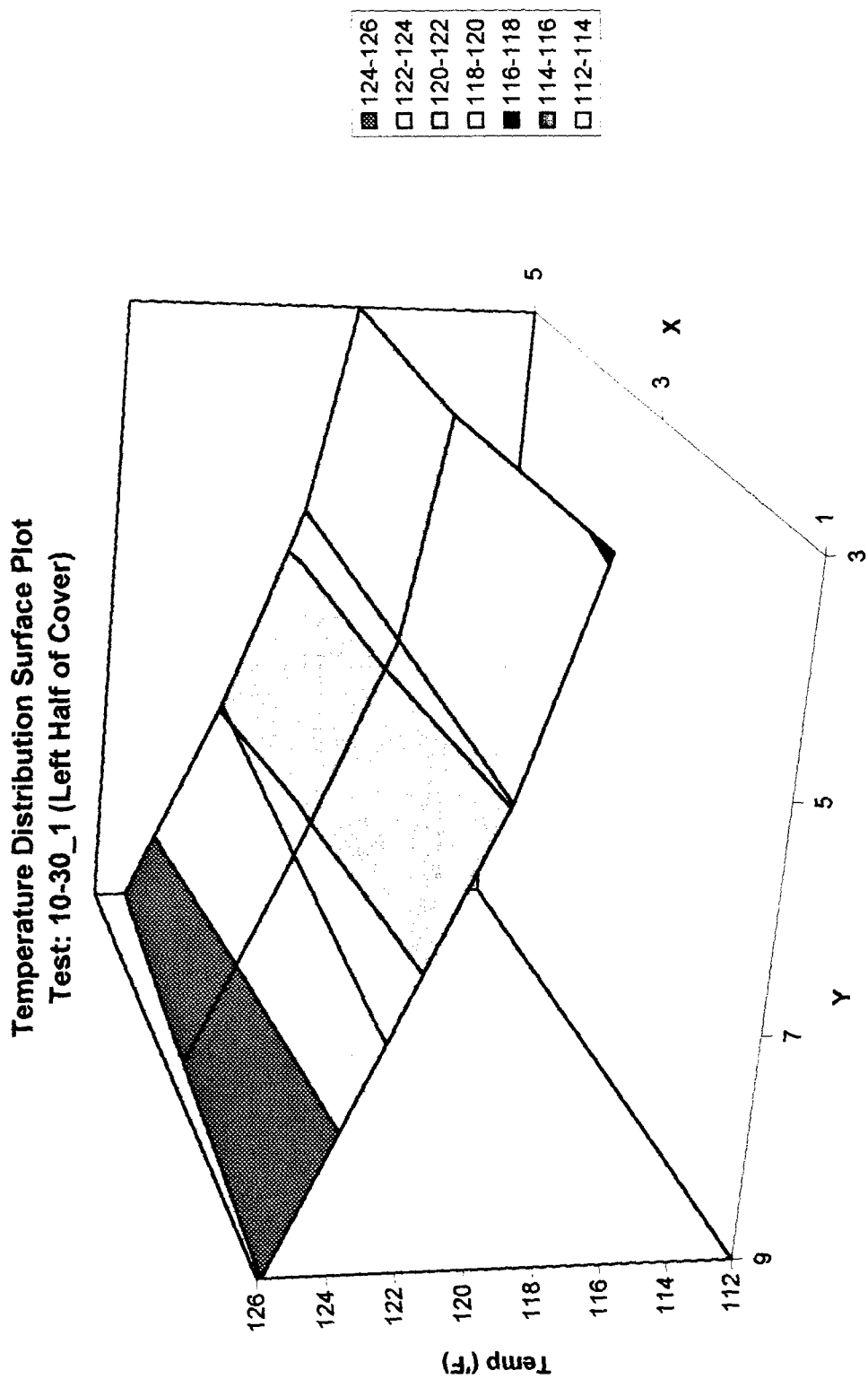


Figure F-3

Figure F-4

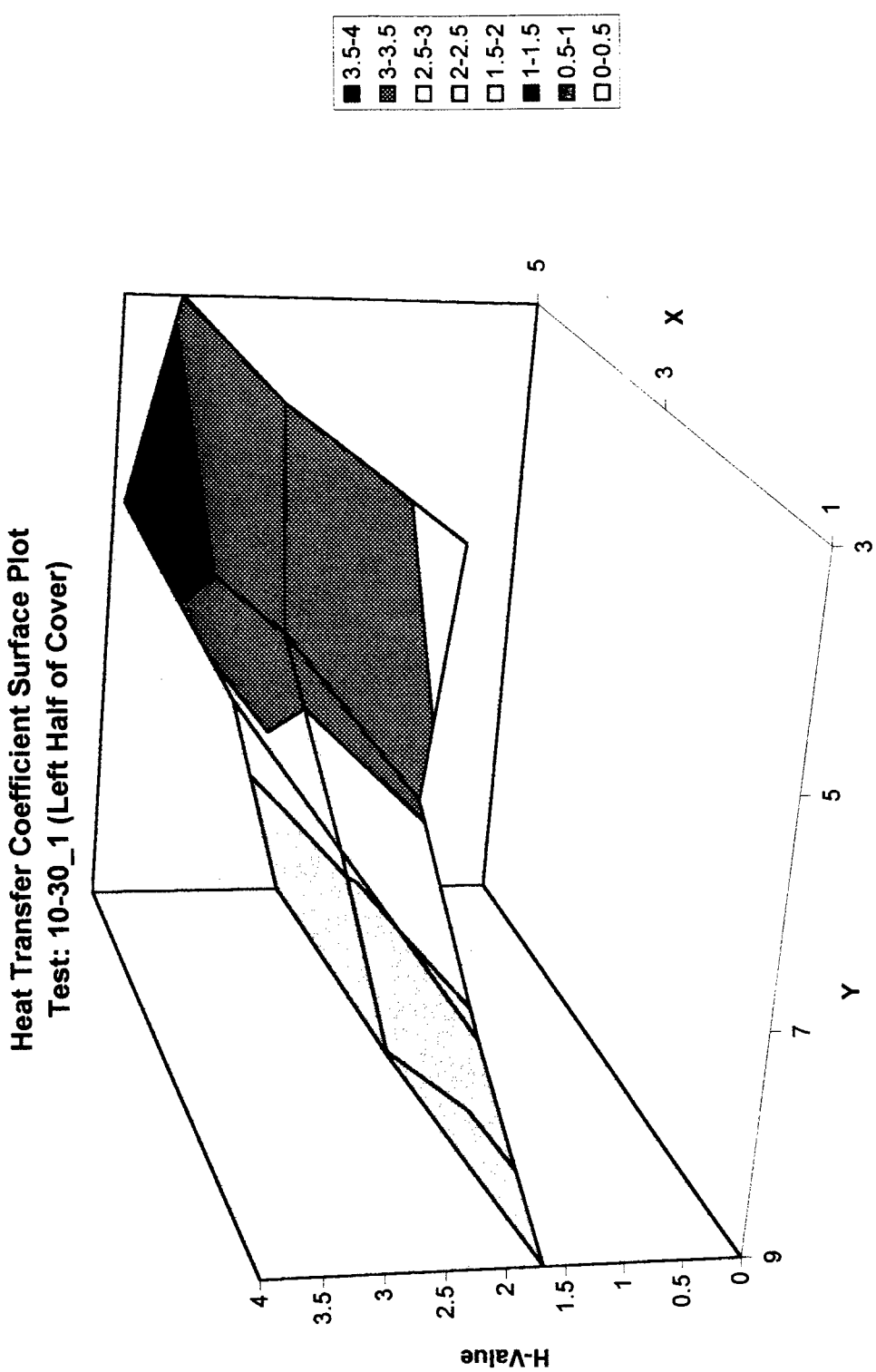


Table F-14

Output Filename ==> d:\scottstu\thesis\data\11-01_1a.cal

(Created from input file ==> a:11-01_1a.dat)

Current Date: Wednesday, November 1, 1995

Current Time: 17:43 hrs

User Name: S.LeClair

Input Current ==> 5.49 amps
Model Rotation ==> 90.0 deg's
Airstream Velocity ==> 455.00 fpm
Airstream Temp ==> 99.0 deg F

Sensor Num	Resist (ohms)	Temp (deg 'F)
1	57.3950000	113.075050
2	57.4990010	111.848618
3	57.4170000	112.176071
4	57.2430000	109.977951
5	57.3190000	110.514076
6	57.9830020	115.452942
7	57.7200010	113.422997
8	57.4860000	111.830864
9	57.2020000	111.108208
10	57.4939990	111.586395
11	57.1050000	111.751915
12	57.2560010	112.912140
13	57.5250020	112.849884
14	57.1710010	109.317421
15	57.2319980	110.596817
16	57.2290000	109.646515
17	57.6469990	111.314125
18	57.3499980	110.850197
19	58.1570010	113.197784
20	57.1129990	109.205299
21	57.5029980	102.981583
22	57.3349990	111.113129
23	57.7789990	111.721687
24	57.3790020	112.518028
25	58.1199990	114.408798
26	57.2999990	110.506386
27	57.4790000	111.579132
28	56.8759990	105.752991
29	57.9199980	111.424942
30	0.0000000	0.000000
31	57.7230000	111.860733
32	0.0000000	0.000000
33	57.7039990	113.736290
34	58.0670010	114.650513
35	58.4669990	116.237427

Table F-14

36	57.5330010	115.074982
37	58.7319980	117.056480
38	57.2160000	108.933098
39	57.5449980	110.752846
40	58.4259990	113.578201
41	57.1180000	108.986137
42	58.6209980	116.706703
43	59.4290010	124.421944
44	0.0000000	0.000000
45	58.7509990	121.645439
46	58.7480010	118.858459
47	59.5449980	123.989738
48	58.0690000	111.939285
49	58.3419990	114.712898
50	58.9510000	117.048088
51	57.8689990	112.155045
52	0.0000000	-29.345400
53	0.0000000	0.000000
54	57.6640010	111.208588
55	58.0280000	109.260864
56	56.6650010	100.672607
57	57.8820000	111.131432
58	58.0770000	108.861671
59	57.9840010	111.741730
60	58.3450010	111.305321
61	57.8170010	108.583458
62	0.0000000	0.000000
63	0.0000000	0.000000
64	57.5620000	111.502625
65	0.0000000	0.000000
66	57.5260010	111.023827
67	57.7260020	112.612846
68	57.8520010	112.477585
69	0.0000000	0.000000
70	58.4249990	117.161613
71	57.0019990	111.392799
72	58.1740000	115.793480
73	57.7570000	114.267845
74	57.3160020	111.718163
75	58.0200000	114.199776
76	56.6619990	105.786758
77	56.8200000	106.712830
78	57.4870000	110.110214
79	56.5280000	105.501915

Table F-15

Test File:		11-01_1a.cal									
		airstream velocity =	455	fpm			total wattage =	313.457			
		airstream temp =	98.96	'F							
		model rotation =	90	deg (ccw)							
sensor#	x-value	y-value	temp (°F)	k,ss	gen	cond,1	cond,2	cond,b	rad	conv	h
0			0								
1			113.075	26	1.12409	0	-0.02693	0.17114	0.07799	0.84803	2.16114
2			111.849	26	1.12409	0	0.00709	0.08918	0.07098	0.97101	2.71001
3			112.176	26	1.12409	0.00709	-0.00918	0.11107	0.07285	0.93808	2.55324
4			109.978		1.12409						
5			110.514		1.12409						
6			115.453	26	1.12409	0	-0.04393	0.33005	0.09171	0.6584	1.43597
7			113.423	26	1.12409	-0.04393	-0.01106	0.19439	0.07999	0.79472	1.97656
8			111.831	26	1.12409	-0.02693	-0.01564	0.088	0.07088	0.92264	2.57859
9			111.108	26	1.12409	-0.01564	0.00854	0.0397	0.06677	1.01051	2.99214
10			111.586	26	1.12409	-0.00358	-0.01217	0.07166	0.06949	0.96718	2.75539
11			111.752	26	1.12409	-0.00918	-0.00358	0.08272	0.07043	0.95817	2.69441
12			112.912	26	1.12409	0.0635	-0.00135	0.16026	0.07706	0.94892	2.4465
13			112.85	26	1.12409	-0.00135	-0.00806	0.15609	0.0767	0.88189	2.28386
14			109.317								
15			110.597								
16			109.647								
17			111.314								
18			110.85								
19			113.198								
20			109.205								
21			102.982								
22			111.113								
23			111.722								
24			112.518								
25			114.409								
26			110.506								
27			111.579								
28			105.753								
29			111.425								
30			0								
31			111.861								
32			0								
33			113.736	26	1.12409	0	0.06428	0.01056	0.08179	1.09601	2.66812
34			114.651	26	1.12409	0.00828	0.03434	0.30341	0.08706	0.77623	1.77955
35			116.237	26	1.12409	0.03434	0	0.71742	0.09628	0.34473	0.71772
36			115.075	26	1.12409	0.01894	0.04288	0.63974	0.08952	0.45665	1.01932
37			117.056	26	1.12409	0.04288	0.039	0.53932	0.10106	0.56559	1.12425
38			108.933								
39			110.753								
40			113.578								
41			108.986								
42			116.707	26	1.12409	0.06428	0.16696	0.20907	0.09902	1.04725	2.1227
43			124.422	26	1.12409	0.16696	0	0.72465	0.14501	0.42138	0.59531
44			0	0	0	0	0	0			
45			121.645	26	1.12409	0	0	0.53911	0.12825	0.45673	0.72422
46			118.858	26	1.12409	0.039	0.11104	0.65974	0.11166	0.50273	0.90881
47			123.99	26	1.12409	0.11104	0	1.00264	0.14239	0.0901	0.12949
48			111.839								
49			114.713								
50			117.048								
51			112.155								
52			-29.3454								
53			0								
54			111.209								
55			109.261								
56			100.673								
57			111.131								
58			108.862								
59			111.742								
60			111.305								

Table F-15

61		108.583								
62		0								
63		0								
64		111.503	26	1.12409	0.00854	0	0.06606	0.06901	0.99755	2.86088
65		0								
66		111.024	26	1.12409	-0.01217	0.03439	0.03407	0.06629	1.04594	3.11873
67		112.613	26	1.12409	0.03439	0	0.14025	0.07535	0.94287	2.4842
68		112.478	26		-0.00806	0	0.13122	0.07457	0.91024	2.42222
69		0								
70		117.162	26	1.12409	0	-0.12484	0.47122	0.10168	0.42635	0.84257
71		111.393	26	1.12409	-0.12484	0	0.08571	0.06839	0.84515	2.44522
72		115.793	26	1.12409	0	-0.03302	0.3798	0.09369	0.61759	1.31971
73		114.268	26	1.12409	-0.03302	0	0.27784	0.08485	0.72838	1.71158
74		111.718	26	1.12409	0	0.0537	0.41541	0.07024	0.69214	1.95146
75		114.2	26	1.12409	0.0537	0	0.27329	0.08446	0.82004	1.93558
76		105.787								
77		106.713								
78		110.11								
79		105.502								

Table F-16

Cover Temperature Map (Test 11-01_1a)						
115.4529	113.423	112.9121	112.8499	112.4776	0	
111.8486	112.1761	111.7519	111.5864	111.0238	112.6128	
0	113.0751	111.8309	111.1082	111.5026	0	
Average Surf T =		112.1431				

Table F-17

Cover Temp Difference Map (Test 11-01_1a)						
16.49294	14.463	13.95214	13.88988	13.51759	-98.96	
12.88862	13.21607	12.79192	12.6264	12.06383	13.65285	
-98.96	14.11505	12.87086	12.14821	12.54263	-98.96	
Average Delta T =		13.18313				

Table F-18

Cover Surf Coeff Map (Test 11-01_1a)					
	1.976562	2.446503	2.283858	2.422219	
	2.553242	2.69441	2.755394	3.118727	
	2.161139	2.578588	2.992143	2.860885	
Ave Surf Coeff. =	2.570306				

Table F-19

Side Surface Coeff Map (Test 11-01_1a)						
	0.842574	2.44522	0	2.668123	2.122695	0.595308
Air -->	1.319709	1.711579	1.77955	0.717725	0	0.724217
	1.951462	1.935577	1.019315	1.124245	0.908808	0.129487
Right Side						

Temperature Distribution Surface Plot
Test: 11-01_1a (Front Half of Cover)

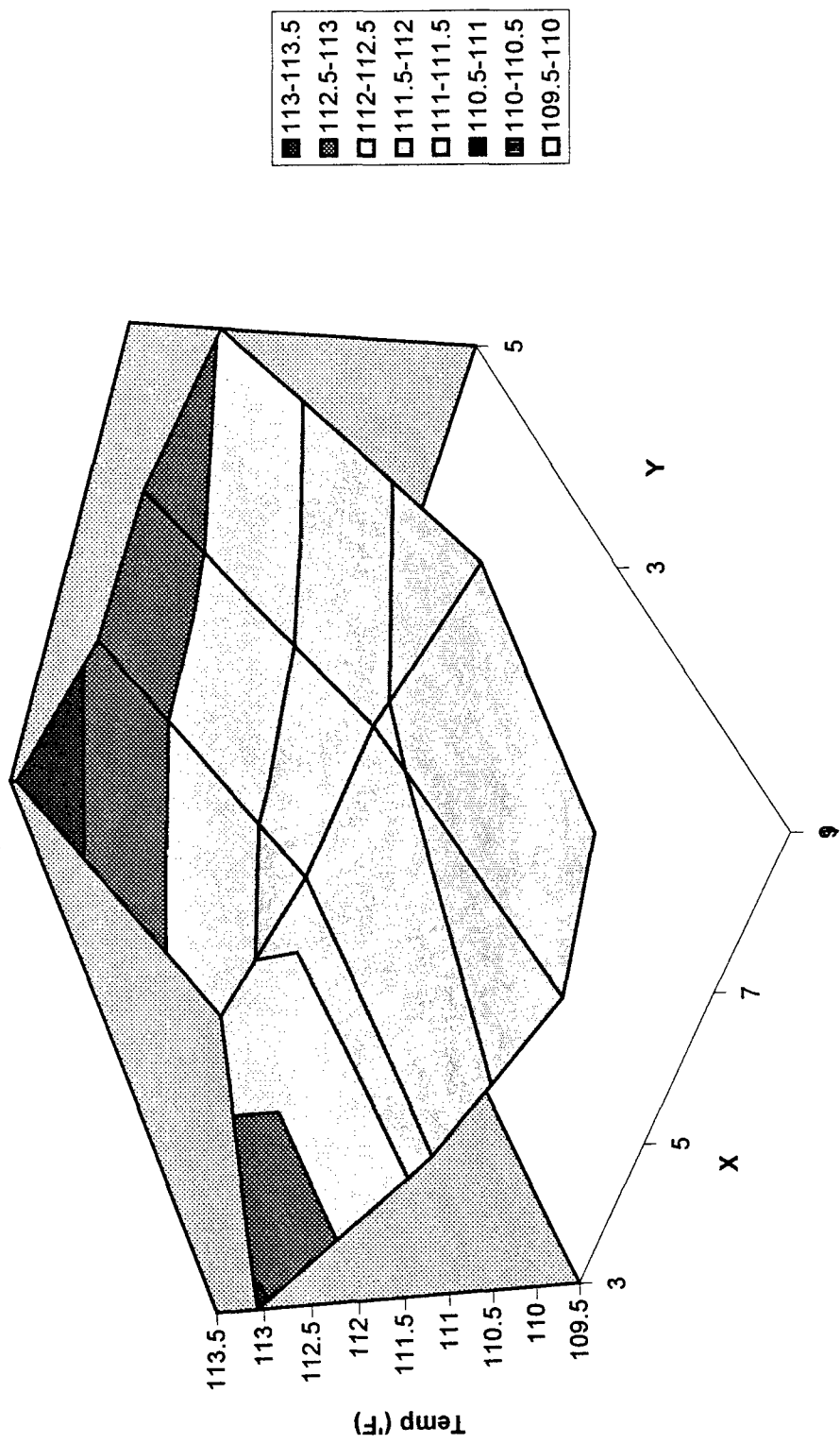


Figure F 5

Figure F-6

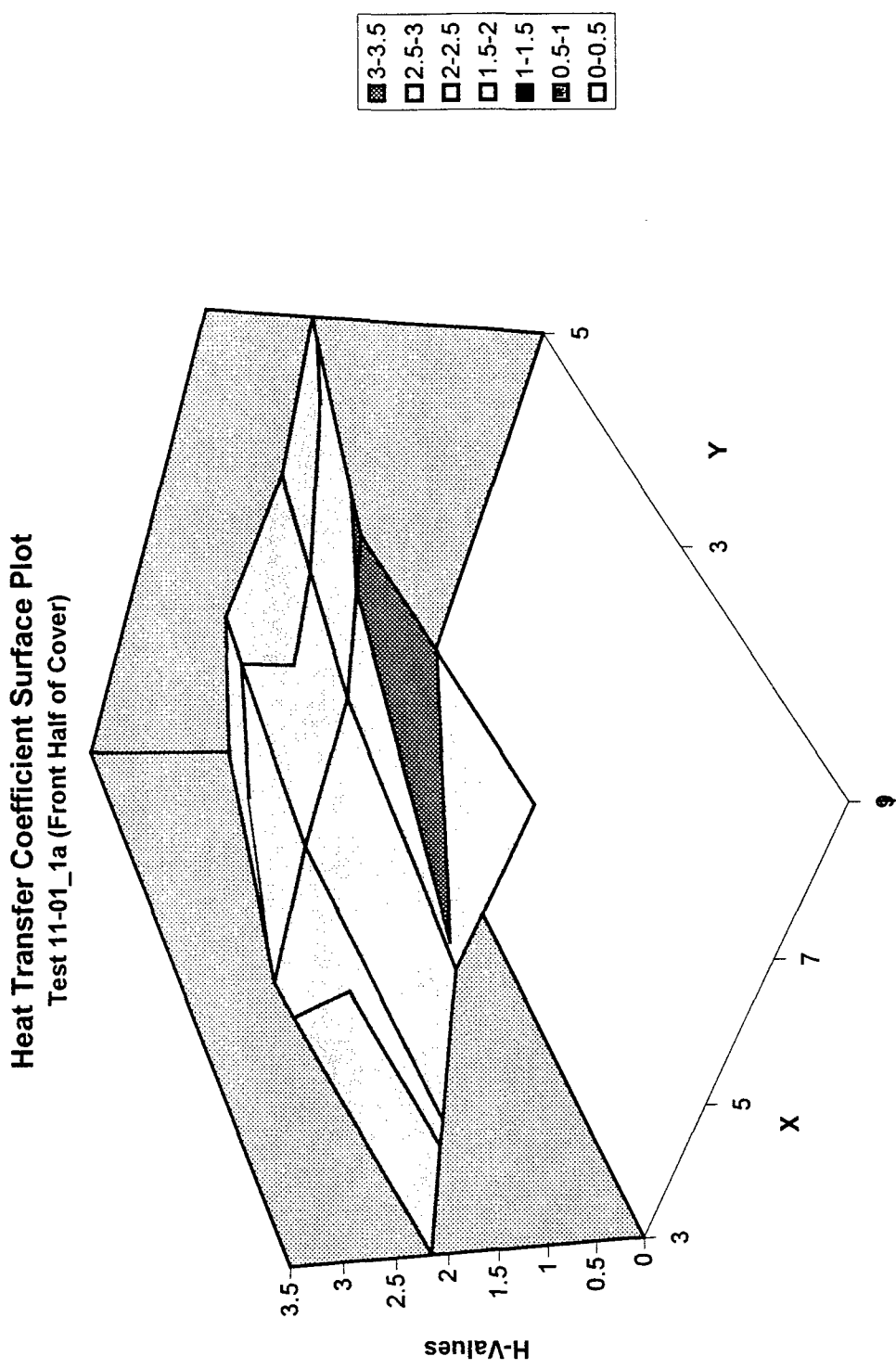


Table F-20

Output Filename ==> d:\scottstu\thesis\data\11-02_1.cal

(Created from input file ==> a:11-02_1.dat)

Current Date: Thursday, November 2, 1995

Current Time: 12:14 hrs

User Name: S.LeClair

Input Current ==> 5.45 amps

Model Rotation ==> 270.0 deg's

Airstream Velocity ==> 455.00 fpm

Airstream Temp ==> 94.3 deg F

Sensor Num	Resist (ohms)	Temp (deg 'F)
1	57.5330010	114.046219
2	57.5330010	112.076996
3	57.3689990	111.838547
4	57.2529980	110.046021
5	56.9739990	108.180008
6	57.4490010	111.835861
7	57.1800000	109.785393
8	57.8019980	113.955666
9	57.6269990	114.079842
10	57.5709990	112.101860
11	57.1390000	111.980034
12	56.7659990	109.532471
13	57.0490000	109.577484
14	57.4420010	111.228294
15	56.9630010	108.749420
16	56.4520000	104.351990
17	57.0639990	107.364235
18	56.5820010	105.508904
19	57.3930020	107.963913
20	56.3590010	103.948662
21	56.7280010	97.929451
22	56.8969990	108.034920
23	57.1419980	107.352737
24	56.7190020	107.762230
25	57.3950000	109.323685
26	56.5750010	105.186928
27	56.7370000	106.473541
28	56.2140010	101.195457
29	57.2360000	106.811485
30	0.0000000	0.000000
31	56.9599990	106.434822
32	0.0000000	0.000000
33	56.7840000	107.139854
34	57.5400010	111.054947
35	57.4300000	109.323433

Table F-20

36	57.7579990	116.664429
37	58.3800010	114.705116
38	57.9949990	114.198715
39	58.3829990	116.387161
40	57.3419990	106.389023
41	57.8940010	114.336548
42	57.2470020	107.316650
43	57.6290020	112.648979
44	0.0000000	0.000000
45	57.0750010	110.109222
46	57.8499980	112.865570
47	58.0149990	114.012642
48	58.5439990	115.296272
49	57.7509990	110.568993
50	58.1069980	111.232155
51	57.0970000	106.576790
52	0.0000000	-29.345400
53	0.0000000	0.000000
54	56.9259990	106.063858
55	57.2920000	104.164085
56	55.8880000	95.294388
57	57.0900000	105.278954
58	57.2649990	103.325691
59	57.2540020	106.404114
60	57.5019990	105.445007
61	57.0620000	103.407120
62	0.0000000	0.000000
63	0.0000000	0.000000
64	58.1160010	115.277893
65	0.0000000	0.000000
66	57.7770000	112.756630
67	57.9430010	114.116486
68	57.4090000	109.497826
69	0.0000000	0.000000
70	58.6660000	118.771255
71	57.0579990	111.785736
72	58.3160020	116.743492
73	57.6170010	113.268036
74	59.0280000	122.952530
75	58.8750000	119.919014
76	58.0779990	115.265633
77	57.8089980	113.439171
78	57.2789990	108.718498
79	57.8759990	114.550079

Table F-21

Test File: 11-02_1.cal										
	airstream velocity =	455 fpm					total wattage =	306.906		
	airstream temp =	94.28 °F								
	model rotation =	270 deg (ccw)								
sensor#	x-value	y-value	temp (°F)	k,ss	gen	cond,1	cond,2	cond,b	rad	conv
0			0							
1		114.046	26	1.10777	0	-0.00196	0.39202	0.10816	0.60562	1.10213
2		112.077	26	1.10777	0	-0.00516	0.26042	0.09687	0.74531	1.50642
3		111.839	26	1.10777	-0.00516	0.00306	0.24449	0.09551	0.76567	1.56858
4		110.046								
5		108.18								
6		111.836	26	1.10777	0	-0.04437	0.24431	0.0955	0.72358	1.48259
7		109.785	26	1.10777	-0.04437	-0.00547	0.10728	0.08388	0.86676	2.0108
8		113.956	26	1.10777	-0.00196	0.00269	0.38597	0.10764	0.61488	1.12413
9		114.08	26	1.10777	0.00269	0.02593	0.39427	0.10836	0.63375	1.15137
10		112.102	26	1.10777	0.00264	0.01417	0.26209	0.09702	0.76547	1.54501
11		111.98	26	1.10777	0.00306	0.00264	0.25394	0.09632	0.7632	1.55103
12		109.532	26	1.10777	-0.01111	0.00097	0.09038	0.08246	0.92479	2.18101
13		109.577	26	1.10777	0.00097	-0.00172	0.09339	0.08271	0.93092	2.189
14		111.228								
15		108.749								
16		104.352								
17		107.364								
18		105.509								
19		107.964								
20		103.949								
21		97.9295								
22		108.035								
23		107.353								
24		107.762								
25		109.324								
26		105.187								
27		106.474								
28		101.195								
29		106.811								
30		0								
31		106.435								
32		0								
33		107.14	26	1.10777	0	0.00383	0.05018	0.06908	0.99234	2.77575
34		111.055	26	1.10777	-0.04789	-0.03747	0.15614	0.09106	0.77521	1.66231
35		109.323	26	1.10777	-0.03747	0	-0.34928	0.08128	1.3383	3.20008
36		116.664	26	1.10777	-0.07043	-0.0424	0.1413	0.12336	0.73028	1.17354
37		114.705	26	1.10777	-0.0424	-0.03981	0.02463	0.11197	0.88896	1.56557
38		114.199								
39		116.387								
40		106.389								
41		114.337								
42		107.317	26	1.10777	0.00383	0.1154	0.06199	0.07006	1.09494	3.0212
43		112.649	26	1.10777	0.1154	0	0.41833	0.10014	0.70469	1.37996
44		0	0	0	0	0	0	0		
45		110.109	26	1.10777	0	0	0.24861	0.08571	0.77345	1.75763
46		112.866	26	1.10777	-0.03981	0.02482	-0.0983	0.10138	1.0897	2.10905
47		114.013	26	1.10777	0.02482	0	-0.02165	0.10797	1.04627	1.90727
48		115.296								
49		110.569								
50		111.232								
51		106.577								
52		-29.3454								
53		0								
54		106.064								
55		104.164								
56		95.2944								
57		105.279								
58		103.326								
59		106.404								
60		105.445								

Table F-21

61		103.407								
62		0								
63		0								
64		115.278	26	1.10777	0.02593	0	0.47433	0.11529	0.54408	0.93205
65		0								
66		112.757	26	1.10777	0.01417	0.02943	0.30584	0.10076	0.74477	1.44995
67		114.116	26	1.10777	0.02943	0	0.39672	0.10857	0.63191	1.1459
68		109.498	26		-0.00172	0	0.08807	0.08226	0.93572	2.2118
69		0								
70		118.771	26	1.10777	0	-0.15117	0.67179	0.13573	0.14907	0.21894
71		111.786	26	1.10777	-0.15117	0	0.20497	0.09521	0.65641	1.3488
72		116.743	26	1.10777	0	-0.07521	0.53629	0.12382	0.37245	0.59641
73		113.268	26	1.10777	-0.07521	0	0.30403	0.10369	0.62484	1.1837
74		122.953	26	1.10777	0	-0.06565	0.56151	0.1607	0.31991	0.40134
75		119.919	26	1.10777	-0.06565	0	0.7485	0.14253	0.15109	0.21198
76		115.266								
77		113.439								
78		108.718								
79		114.55								

Table F-22

Cover Temperature Map (Test 11-02_1)					
0	115.2779	114.0798	113.9557	114.0462	0
114.1165	112.7566	112.1019	111.98	111.8385	0
0	109.4978	109.5775	109.5325	109.7854	0
Ave Surf Temp =	112.0358				

Table F-23

Cover Temp Difference Map (Test 11-02_1)					
-94.28	20.99789	19.79984	19.67567	19.76622	-94.28
19.83649	18.47663	17.82186	17.70003	17.55855	17.797
-94.28	15.21783	15.29748	15.25247	15.50539	17.55586
Ave Delta Temp =	17.75582				

Table F-24

Cover Surf Coeff Map (Test 11-02_1)				
	0.932053	1.15137	1.124133	1.102131
	1.449947	1.545011	1.551028	1.568576
	2.211803	2.189005	2.181012	2.010802
Ave Surf Coeff =	1.584739			

Table F-25

Side Surface Coeff Map (Test 11-02_1)						
0.21894	1.348802	0	2.775752	3.0212	1.37996	
0.596413	1.183697	1.662305	3.200076	0	1.757631	<-- Air
0.401345	0.211978	1.173545	1.565568	2.109049	1.907268	
Left Side						
Ave =	1.532096					
StDev =	0.931547					

Temperature Distribution Surface Plot
Test: 11-02_1 (Front Half of Cover)

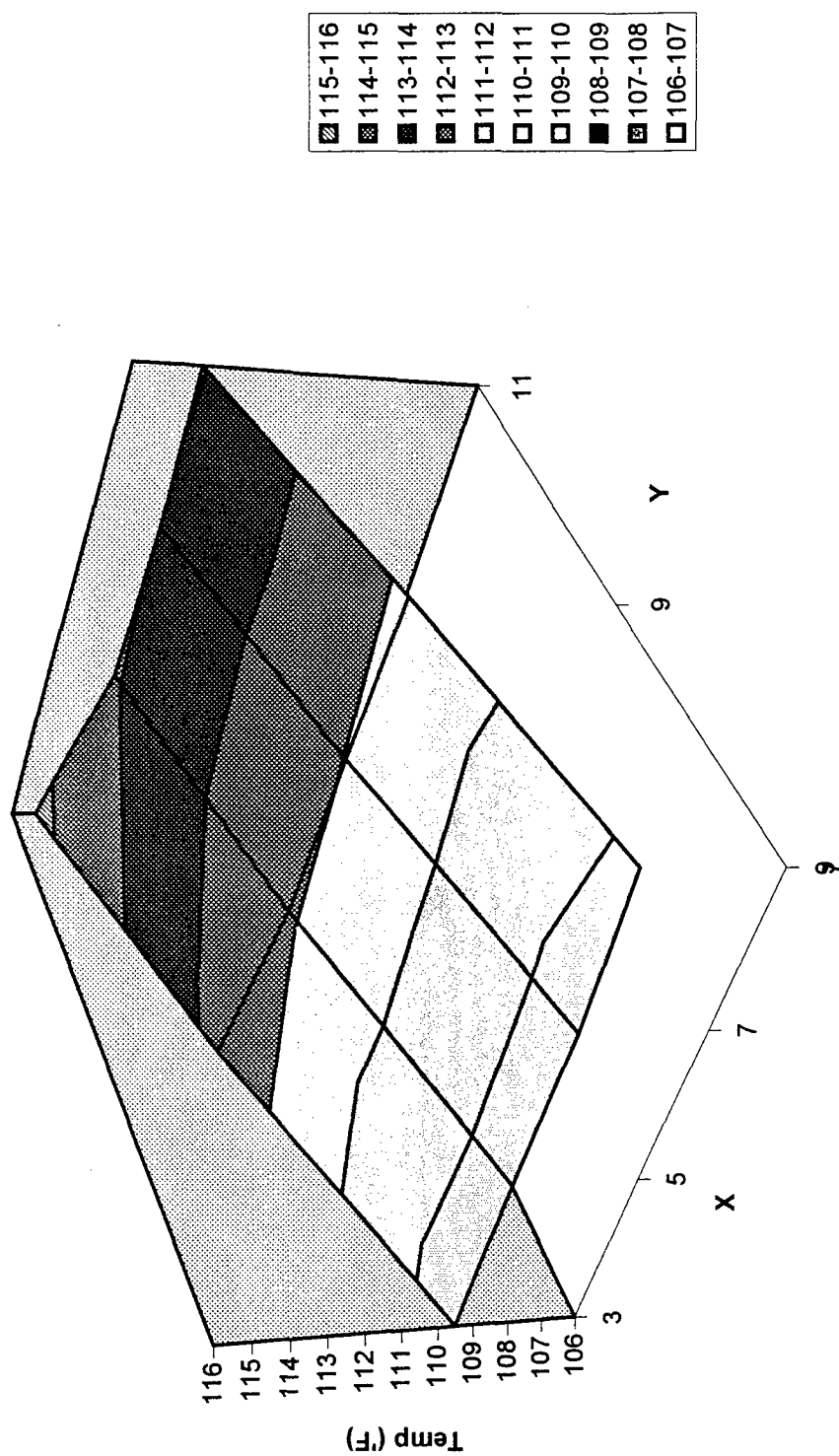


Figure F-7

Figure F-8

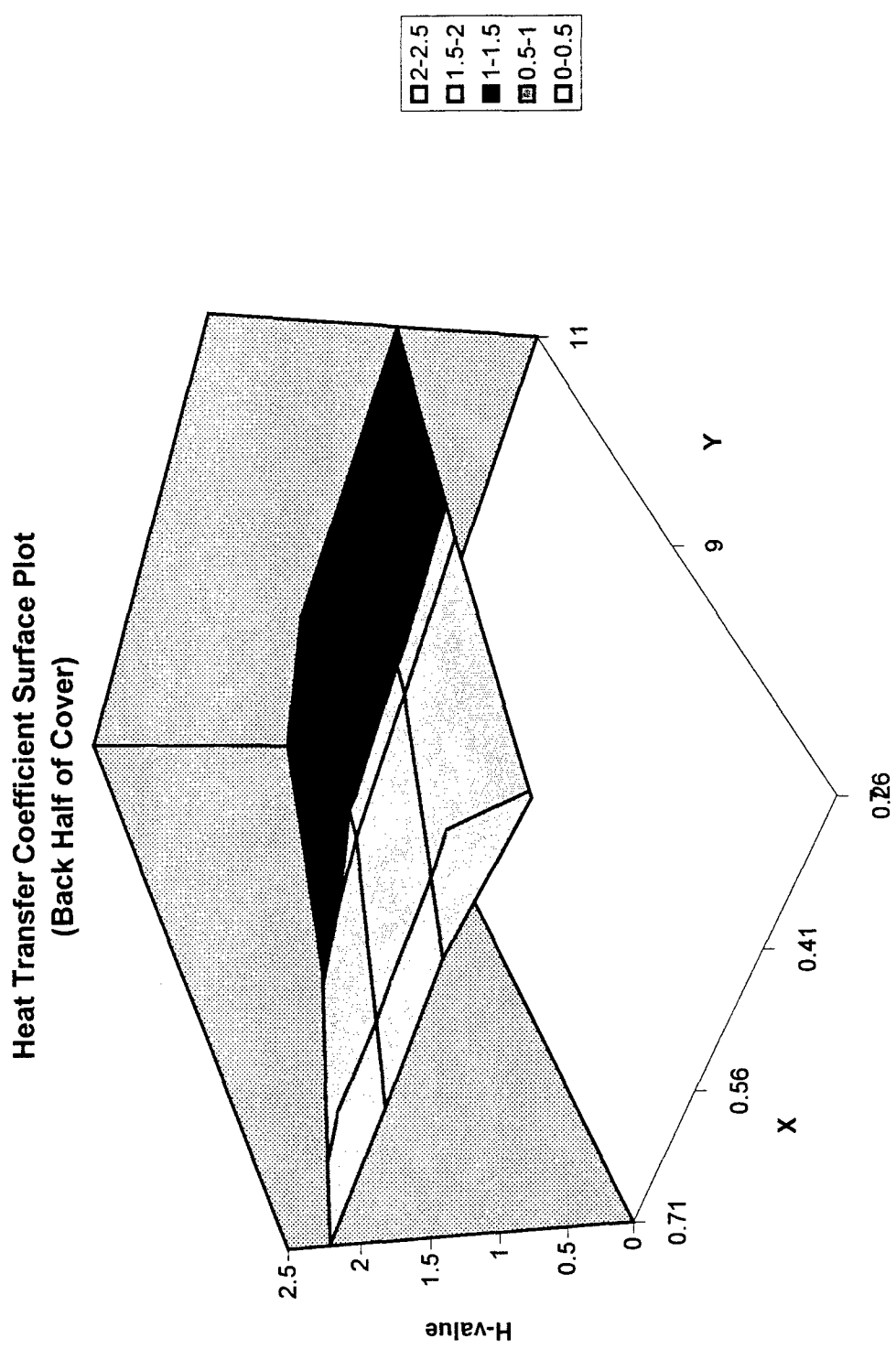


Table F-26

Output Filename ==> 11-13_1.cal

(Created from input file ==> a:11-13_1.dat)

Current Date: Monday, November 13, 1995

Current Time: 11:39 hrs

User Name: S.LeClair

Input Current ==> 5.43 amps
Model Rotation ==> 270.0 deg's
Airstream Velocity ==> 660.00 fpm
Airstream Temp ==> 89.6 deg F

Sensor Num	Resist (ohms)	Temp (deg 'F)
1	56.6189990	107.595520
2	56.6220020	105.932846
3	56.4660000	105.459435
4	56.5190010	105.089195
5	56.2230000	103.076584
6	56.5190010	105.498558
7	56.2430000	103.435867
8	56.8019980	107.212967
9	56.6819990	107.458168
10	56.5880010	105.497795
11	56.1590000	105.354919
12	55.8580020	103.233620
13	56.0200000	102.459290
14	56.7760010	106.525711
15	56.2120020	103.572021
16	55.6040000	98.534454
17	56.1059990	100.833466
18	55.7780000	99.882675
19	56.4370000	101.368874
20	55.6430020	98.926384
21	56.0000000	93.155853
22	55.8270000	100.468803
23	56.1170010	100.274551
24	55.7120020	100.457321
25	56.3540000	101.969887
26	55.7739980	99.274384
27	55.7760010	99.816826
28	55.2620010	94.598740
29	56.1629980	99.523140
30	0.0000000	0.000000
31	56.0369990	99.826775
32	0.0000000	0.000000
33	55.7509990	99.674683
34	56.3019980	102.547302
35	56.2280010	101.236069

Table F-26

36	56.3709980	106.820229
37	56.9700010	105.222015
38	56.5849990	104.643845
39	57.3050000	109.132072
40	56.4570010	100.472183
41	56.7840000	106.673607
42	56.2239990	100.257805
43	57.1720010	109.478210
44	0.0000000	0.000000
45	56.5560000	106.406540
46	56.6880000	105.044662
47	57.2120020	108.490097
48	57.5040020	107.929291
49	56.7470020	103.483223
50	56.8110010	102.225090
51	55.9889980	98.510056
52	0.0000000	-29.345400
53	0.0000000	0.000000
54	55.6269990	96.933929
55	56.0870020	95.755531
56	54.8520010	88.071442
57	56.1699980	98.433792
58	56.3870010	97.299194
59	56.2360000	98.909790
60	56.5660020	98.891037
61	55.9949990	96.036766
62	0.0000000	0.000000
63	0.0000000	0.000000
64	57.0919990	108.286461
65	0.0000000	0.000000
66	56.7140010	105.392220
67	57.0509990	107.916679
68	56.3699990	102.466698
69	0.0000000	0.000000
70	57.4690020	110.744080
71	55.9370000	103.893303
72	57.0379980	108.156723
73	56.4189990	104.667648
74	57.5470010	113.285568
75	57.3829990	109.912453
76	56.8470000	107.031151
77	56.4590000	104.244568
78	56.3340000	102.367249
79	56.7060010	106.702072

Table F-27

Test File:		11-13_1.cal									
airstream velocity =	660	fpm				total wattage =	307.23				
airstream temp =	89.6	'F									
model rotation =	270	deg (ccw)									
sensor#	x-value	y-value	temp (F)	k,ss	gen	cond,1	cond,2	cond,b	rad	conv	h
0			0								
1			107.5955	26	1.101757	0	-0.00828	0.301987	0.095585	0.695907	1.391047
2			105.9328	26	1.101757	0	-0.01024	0.190875	0.086363	0.814274	1.793345
3			105.4594	26	1.101757	0.010245	-0.00226	0.159239	0.083752	0.86675	1.965899
4			105.0892		1.101757				0.081714		
5			103.0766		1.101757				0.070709		
6			105.4986	26	1.101757	0	-0.04464	0.161853	0.083967	0.811298	1.8356
7			103.4359	26	1.101757	0.044638	-0.00438	0.02401	0.072665	1.045343	2.717739
8			107.213	26	1.101757	0.008279	0.005306	0.276422	0.093456	0.745464	1.522473
9			107.4582	26	1.101757	-0.00531	0.017925	0.292808	0.09482	0.726748	1.463868
10			105.4978	26	1.101757	-0.00309	-0.00228	0.161802	0.083963	0.850615	1.924648
11			105.3549	26	1.101757	0.002262	0.003092	0.152254	0.083176	0.87168	1.990198
12			103.2336	26	1.101757	0.040156	-0.01676	0.010494	0.071564	1.043098	2.752131
13			102.4593	26	1.101757	0.016757	0.00016	-0.04125	0.067357	1.092569	3.056237
14			106.5257						0.089642		
15			103.572						0.073407		
16			98.53445						0.046302		
17			100.8335						0.058582		
18			99.88268						0.053485		
19			101.3689						0.061463		
20			98.92638						0.048385		
21			93.15585						0.01816		
22			100.4688						0.056624		
23			100.2746						0.055582		
24			100.4573						0.056562		
25			101.9699						0.064707		
26			99.27438						0.050238		
27			99.81683						0.053133		
28			94.59874						0.025629		
29			99.52314						0.051564		
30			0						-0.35391		
31			99.82678						0.053186		
32			0						-0.35391		
33			99.67468	26	1.101757	0	0.012619	-0.05329	0.052373	1.115297	3.982121
34			102.5473	26	1.101757	0.045886	-0.02838	0.012032	0.067834	1.0394	2.887743
35			101.2361	26	1.101757	0.028376	0	-0.36528	0.060748	1.434662	4.435048
36			106.8202	26	1.101757	0.066918	-0.03459	0.007896	0.091275	1.034918	2.161833
37			105.222	26	1.101757	0.034586	-0.00384	-0.09701	0.082445	1.147066	2.641232
38			104.6438						0.079269		
39			109.1321						0.10418		
40			100.4722						0.056642		
41			106.6736						0.090461		
42			100.2578	26	1.101757	-0.01262	0.199536	-0.01433	0.055493	1.247508	4.21047
43			109.4782	26	1.101757	-0.19954	0	0.601845	0.106126	0.19425	0.351511
44			0	0	0	0	0	0	-0.35391	0.353906	-0.14208
45			106.4065	26	1.101757	0	0	0.396575	0.088982	0.6162	1.31886
46			105.0447	26	1.101757	0.003838	0.074562	-0.10886	0.08147	1.207544	2.812418
47			108.4901	26	1.101757	-0.07456	0	0.12139	0.10058	0.805224	1.533338
48			107.9293						0.097446		
49			103.4832						0.072923		
50			102.2251						0.066088		
51			98.51006						0.046172		
52			-29.3454						-0.43295		
53			0						-0.35391		
54			96.93393						0.037842		
55			95.75553						0.03166		

Table F-27

56			88.07144					-0.0077		
57			98.43379					0.045768		
58			97.29919					0.039766		
59			98.90979					0.048296		
60			98.89104					0.048197		
61			96.03677					0.033132		
62			0					-0.35391		
63			0					-0.35391		
64		108.2865	26	1.101757	-0.01792	0	0.34816	0.099441	0.636231	1.224737
65		0						-0.35391		
66		105.3922	26	1.101757	0.002285	0.054631	0.154747	0.083382	0.920544	2.096798
67		107.9167	26	1.101757	-0.05463	0	0.323449	0.097376	0.626301	1.229963
68		102.4667	26		-0.00016	0	-0.04076	0.067397	1.074956	3.005238
69		0						-0.35391		
70		110.7441	26	1.101757	0	-0.14826	0.559798	0.113272	0.280431	0.477082
71		103.8933	26	1.101757	0.148256	0	0.101981	0.075161	1.07287	2.700038
72		108.1567	26	1.101757	0	-0.07551	0.386893	0.098716	0.540642	1.048006
73		104.6676	26	1.101757	0.075506	0	0.153729	0.0794	0.944135	2.253947
74		113.2856	26	1.101757	0	-0.073	0.439955	0.127764	0.461042	0.700183
75		109.9125	26	1.101757	0.072997	0	0.504223	0.108572	0.561959	0.99517
76		107.0312								
77		104.2446								
78		102.3672								
79		106.7021								

Table F-28

Cover Temperature Map (Test 11-13_1)					
0	108.2865	107.4582	107.213	107.5955	0
107.9167	105.3922	105.4978	105.3549	105.4594	105.9328
0	102.4667	102.4593	103.2336	103.4359	105.4986
Ave Surf Temp =	105.3211				

Table F-29

Cover Temp Difference Map (Test 11-13_1)					
-89.6	18.68646	17.85817	17.61297	17.99552	-89.6
18.31668	15.79222	15.8978	15.75492	15.85944	16.33285
-89.6	12.8667	12.85929	13.63362	13.83587	15.89856
Ave Temp Diff =	15.72108				

Table F-30

Cover Surf Coeff Map (Test 11-13_1)					
	1.224737	1.463868	1.522473	1.391047	
	2.096798	1.924648	1.990198	1.965899	
	3.005238	3.056237	2.752131	2.717739	
Ave Surf Coeff =	2.092584				

Table F-31

Side Surface Coeff Map (Test 11-13_1)						
0.477082	2.700038	0	3.982121	4.21047	0.351511	
1.048006	2.253947	2.887743	4.435048	0	1.31886	<-- Air
0.700183	0.99517	2.161833	2.641232	2.812418	1.533338	
Left Side						
Ave =	2.029941					
StDev =	1.319471					

Temperature Distribution Surface Plot
Test: 11-13_1 (Back Half of Cover)

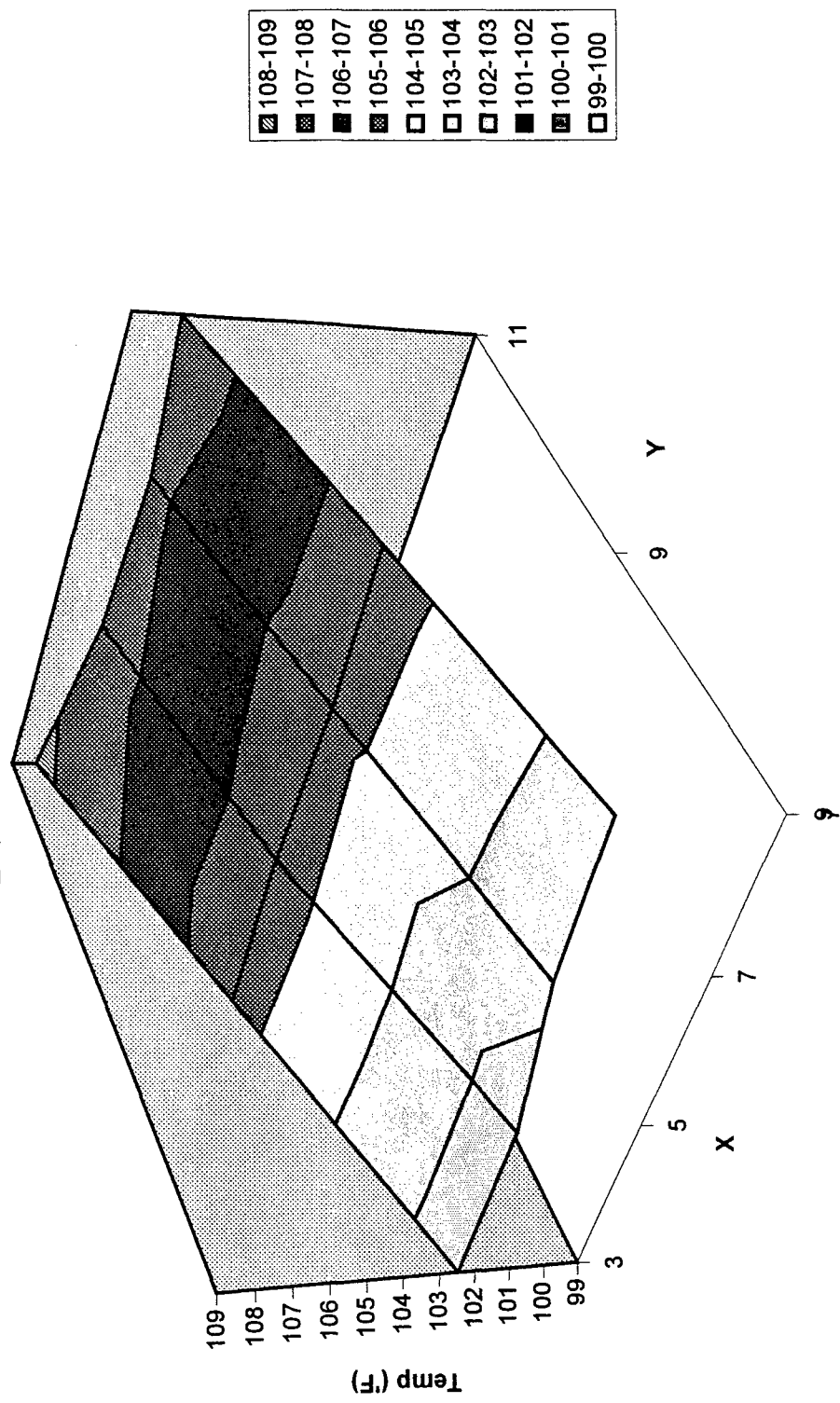


Figure F-9

Heat Transfer Coefficient Surface Plot
Test 11-13_1 (Back Half of Cover)

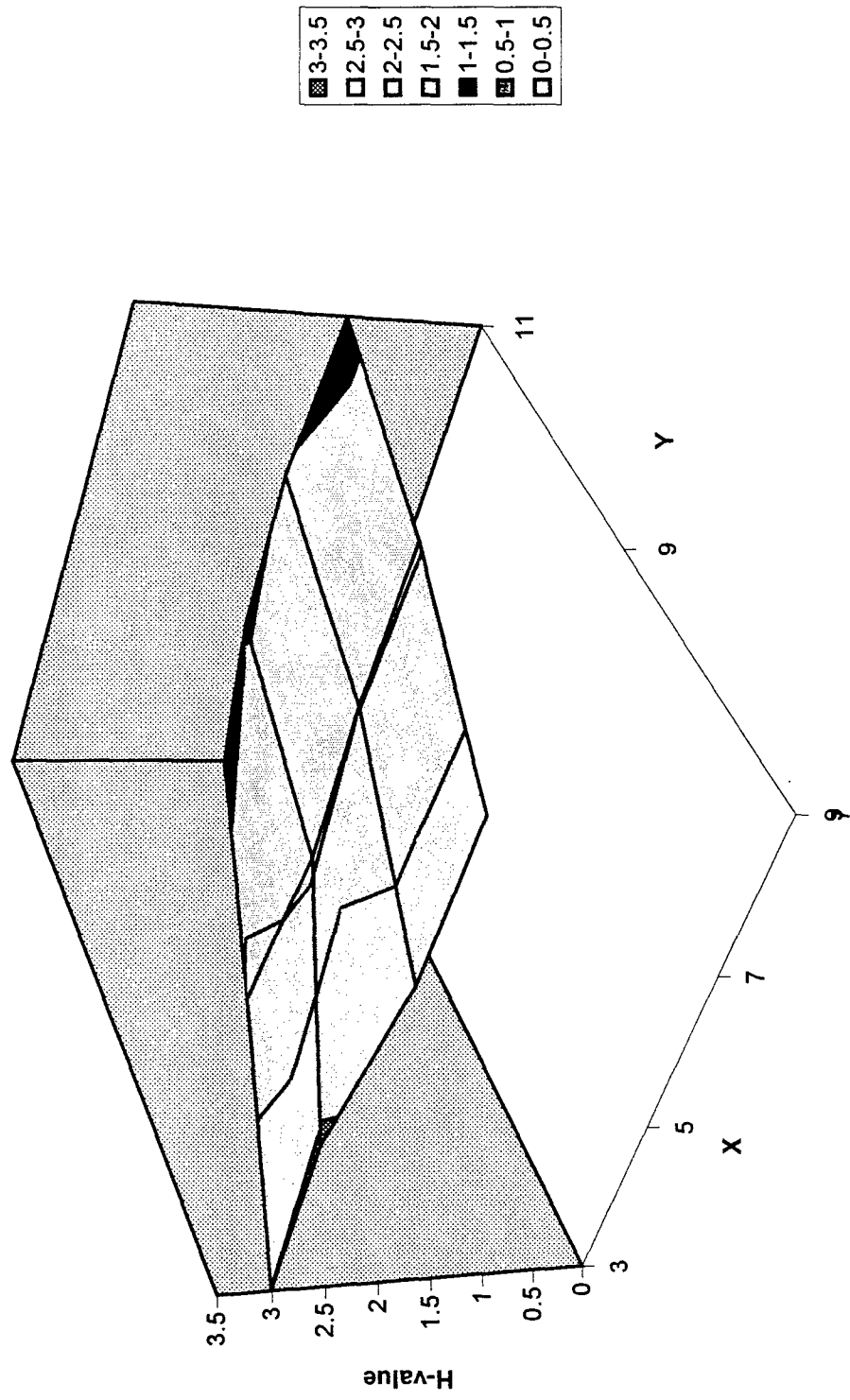


Figure F-10

Table F-32

Output Filename ==> d:\scottstu\thesis\data\11-14_1.cal

(Created from input file ==> a:11-14_1.dat)

Current Date: Tuesday, November 14, 1995

Current Time: 13:33 hrs

User Name: S.LeClair

Input Current ==> 5.42 amps
Model Rotation ==> 90.0 deg's
Airstream Velocity ==> 660.00 fpm
Airstream Temp ==> 84.4 deg F

Sensor Num	Resist (ohms)	Temp (deg 'F)
1	55.3209990	98.354103
2	55.1600000	95.977562
3	55.1580010	96.136787
4	55.1580010	95.820679
5	55.0989990	95.382561
6	55.5779990	99.038574
7	55.2319980	96.531151
8	55.4350010	97.906883
9	55.2739980	97.500084
10	55.1959990	96.057579
11	54.8429990	96.377365
12	54.8450010	96.153038
13	55.0519980	95.710159
14	55.2080000	95.355560
15	55.0509990	95.507278
16	54.8660010	93.439621
17	55.2160000	94.721420
18	55.0589980	94.819832
19	55.6689990	96.034416
20	54.9679990	94.165497
21	55.1990010	87.869759
22	54.9720000	94.377922
23	55.3230020	94.751373
24	55.0140000	95.359108
25	55.6399990	96.890259
26	55.1040000	94.298698
27	55.1040000	95.130287
28	54.4529990	88.954002
29	55.3979990	94.289093
30	0.0000000	0.000000
31	55.3960000	95.208878
32	0.0000000	0.000000
33	55.2130010	95.762543
34	55.4160000	96.407234
35	55.6619990	97.400978

Table F-32

36	55.0099980	97.054298
37	56.1160010	99.426552
38	55.0149990	93.876434
39	55.4770010	96.685463
40	55.9370000	96.975586
41	55.3069990	96.370361
42	56.0019990	98.718628
43	56.7620010	106.623009
44	0.0000000	0.000000
45	56.0400010	102.710487
46	56.2620010	102.159195
47	56.9580000	106.736145
48	56.2060010	98.647667
49	56.5420000	102.029831
50	56.1339990	97.482254
51	55.4140010	94.295403
52	0.0000000	-29.345400
53	0.0000000	0.000000
54	55.0280000	92.691658
55	55.5519980	91.996422
56	54.3680000	84.677879
57	55.5400010	93.716797
58	55.7140010	92.650581
59	55.6259990	94.388779
60	55.8800010	94.056015
61	55.4520000	92.261871
62	0.0000000	0.000000
63	0.0000000	0.000000
64	55.4070010	96.657143
65	0.0000000	0.000000
66	55.1759990	94.624718
67	55.4049990	96.358803
68	55.3209990	95.307526
69	0.0000000	0.000000
70	56.2439990	102.449165
71	54.6010020	94.395401
72	55.8030010	99.775475
73	55.3890000	97.206390
74	54.7960010	94.429184
75	55.4510000	96.776291
76	54.6479990	92.119255
77	54.6940000	92.071526
78	55.1530000	94.361778
79	54.4730000	91.519516

Table F-33

Test File:		11-14_1.cal									
airstream velocity =		660 fpm					total wattage =				
airstream temp =		84.38 °F					306.98				
model rotation =		90 deg (ccw)									
sensor#	x-value	y-value	temp (°F)	k,ss	gen	cond,1	cond,2	cond,b	rad	conv	h
0		0									
1		98.3541	26	1.10086	0	-0.00968	0.19858	0.07137	0.82123	2.11396	
2		95.9776	26	1.10086	0	0.00345	0.03976	0.05885	1.00569	3.11928	
3		96.1368	26	1.10086	-0.00345	0.00521	0.0504	0.05968	0.99253	3.03677	
4		95.8207		1.10086							
5		95.3826		1.10086							
6		99.0386	26	1.10086	0	-0.05426	0.24432	0.07501	0.72727	1.78467	
7		96.5312	26	1.10086	0.05426	-0.00818	0.07676	0.06175	1.00843	2.98527	
8		97.9069	26	1.10086	0.00968	-0.0088	0.16869	0.069	0.86404	2.29769	
9		97.5001	26	1.10086	0.0088	-0.01824	0.14151	0.06685	0.88306	2.42108	
10		96.0576	26	1.10086	0.00692	-0.03101	0.04511	0.05927	0.97239	2.99533	
11		96.3774	26	1.10086	-0.00521	-0.00692	0.06648	0.06094	0.96131	2.88225	
12		96.153	26	1.10086	-0.00719	-0.00958	0.05149	0.05977	0.97283	2.97236	
13		95.7102	26	1.10086	0.00958	-0.00871	0.02189	0.05745	1.02239	3.2459	
14		95.3556									
15		95.5073									
16		93.4396									
17		94.7214									
18		94.8198									
19		96.0344									
20		94.1655									
21		87.8698									
22		94.3779									
23		94.7514									
24		95.3591									
25		96.8903									
26		94.2987									
27		95.1303									
28		88.954									
29		94.2891									
30		0									
31		95.2089									
32		0									
33		95.7625	26	1.10086	0	0.06397	-0.08106	0.05772	1.18817	3.75487	
34		96.4072	26	1.10086	0.01729	0.02151	0.13669	0.0611	0.94187	2.81695	
35		97.401	26	1.10086	-0.02151	0	0.39304	0.06633	0.61998	1.71274	
36		97.0543	26	1.10086	-0.00602	0.05134	0.36987	0.0645	0.71181	2.02019	
37		99.4266	26	1.10086	-0.05134	0.05914	0.20424	0.07708	0.82735	1.97791	
38		93.8764									
39		96.6855									
40		96.9756									
41		96.3704									
42		98.7186	26	1.10086	-0.06397	0.17106	0.11648	0.07331	1.01816	2.55424	
43		106.623	26	1.10086	-0.17106	0	0.64471	0.11621	0.16889	0.27312	
44		0	0	0	0	0	0	0			
45		102.71	26	1.10086	0	0	0.38325	0.09475	0.62287	1.22223	
46		102.159	26	1.10086	-0.05914	0.09905	0.38685	0.09176	0.66216	1.3397	
47		106.736	26	1.10086	-0.09905	0	0.69271	0.11684	0.19226	0.30935	
48		98.6477									
49		102.03									
50		97.4823									
51		94.2954									
52		-29.3454									
53		0									
54		92.6917									
55		91.9964									
56		84.6779									
57		93.7168									
58		92.6506									
59		94.3888									
60		94.056									

Table F-33

61		92.2619								
62		0								
63		0								
64		96.6571	26	1.10086	0.01824	0	0.08518	0.06241	0.97151	2.84647
65		0								
66		94.6247	26	1.10086	0.03101	0.03753	-0.05064	0.05179	1.16825	4.10195
67		96.3588	26	1.10086	-0.03753	0	0.06524	0.06085	0.93725	2.81446
68		95.3075	26		0.00871	0	-0.00501	0.05535	1.05924	3.48681
69		0								
70		102.449	26	1.10086	0	-0.17429	0.54046	0.09333	0.29279	0.58286
71		94.3954	26	1.10086	0.17429	0	0.00225	0.0506	1.2223	4.39001
72		99.7755	26	1.10086	0	-0.0556	0.36178	0.07894	0.60454	1.4125
73		97.2064	26	1.10086	0.0556	0	0.1901	0.0653	0.90106	2.52698
74		94.4292	26	1.10086	0	0.05079	0.19444	0.05078	0.90643	3.24459
75		96.7763	26	1.10086	-0.05079	0	0.16135	0.06304	0.82567	2.39591
76		92.1193								
77		92.0715								
78		94.3618								
79		91.5195								

Table F-34

Cover Temperature Map (Test 11-14_1)					
99.03857	96.53115	96.15304	95.71016	95.30753	0
95.97756	96.13679	96.37737	96.05758	94.62472	96.3588
0	98.3541	97.90688	97.50008	96.65714	0
Average Surf T =	96.44304				

Table F-35

Cover Temp Difference Map (Test 11-14_1)					
14.65857	12.15115	11.77304	11.33016	10.92753	-84.38
11.59756	11.75679	11.99737	11.67758	10.24472	11.9788
-84.38	13.9741	13.52688	13.12008	12.27714	-84.38
Average Delta T =	12.06304				

Table F-36

Cover Surf Coeff Map (Test 11-14_1)					
	2.985273	2.972365	3.245901	3.486807	
	3.036773	2.882255	2.995333	4.101948	
	2.113958	2.297686	2.42108	2.846466	
Ave Surf Coeff. =	2.94882				

Table F-37

Side Surface Coeff Map (Test 11-14_1)						
	0.582864	4.390009	0	3.754873	2.55424	0.273124
Air -->	1.412504	2.526984	2.816949	1.712743	0	1.222297
	3.244593	2.395914	2.020192	1.977908	1.339702	0.309352
	Right Side					

Temperature Distribution Surface Plot
Test: 11-14_1 (Front Half of Cover)

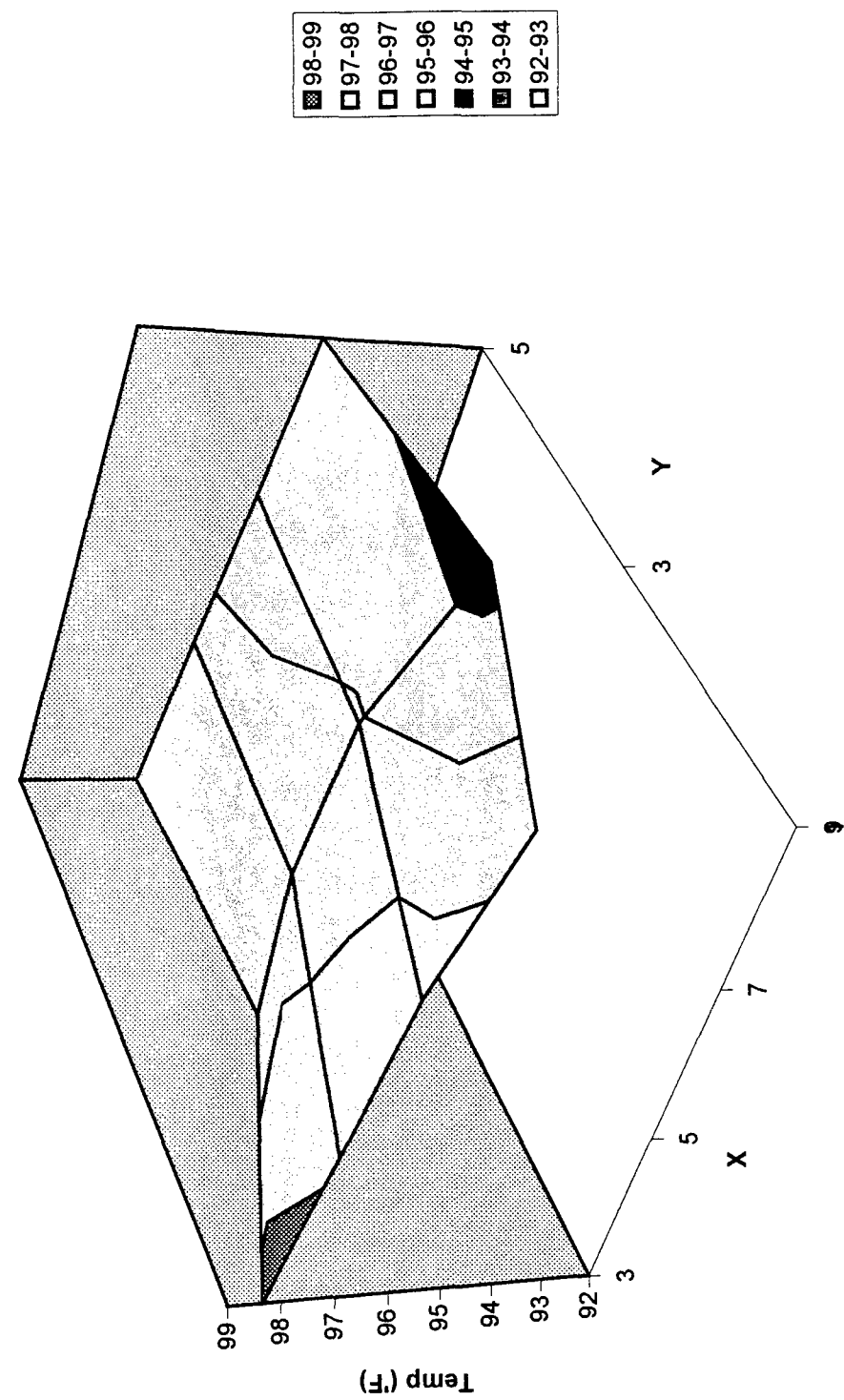


Figure F-11

Figure F-12

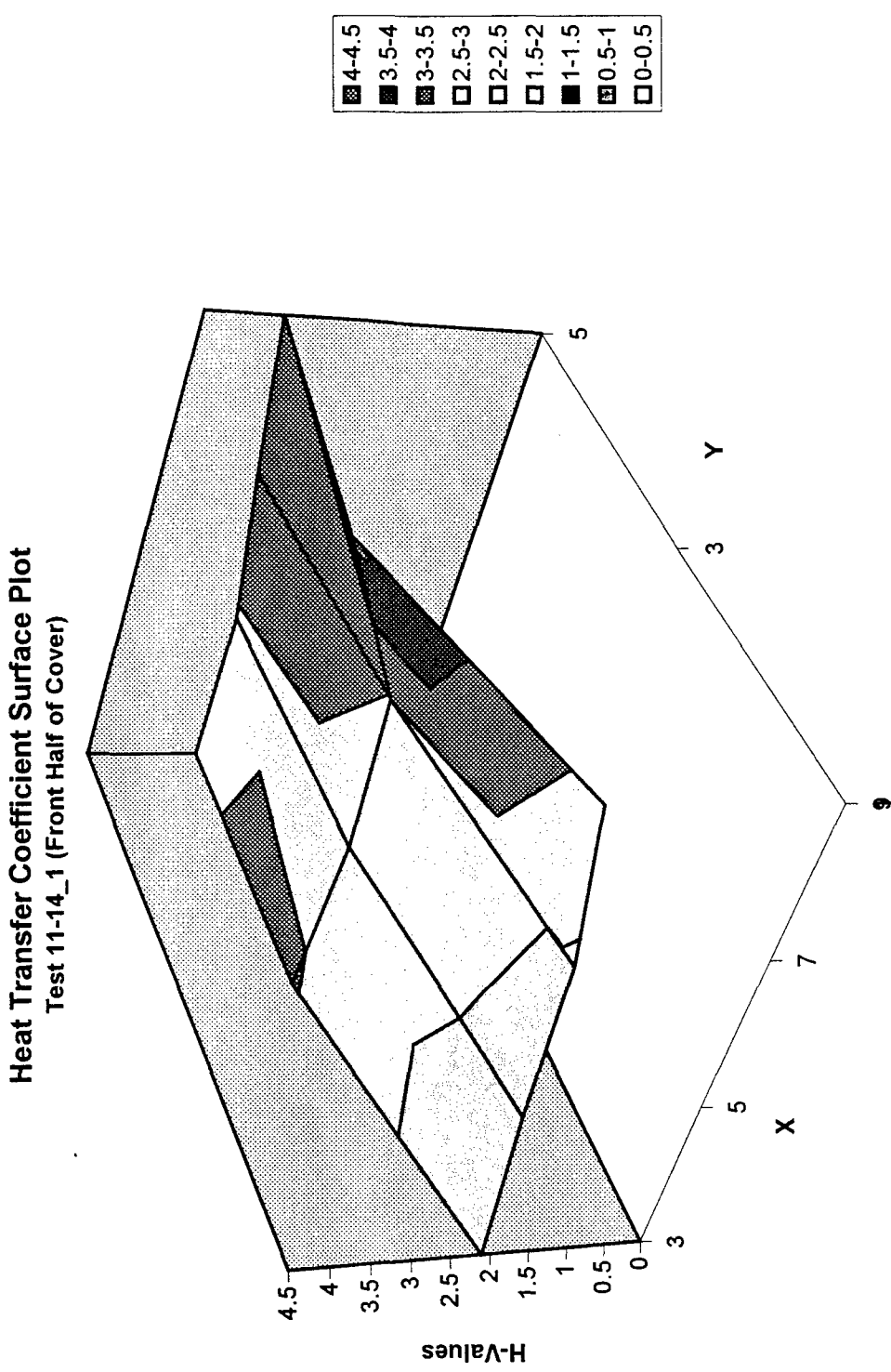


Table F-38

Output Filename ==> d:\scottstu\thesis\data\11-15_1.cal

(Created from input file ==> a:11-15_1.dat)

Current Date: Wednesday, November 15, 1995

Current Time: 13:24 hrs

User Name: S.LeClair

Input Current ==> 6.98 amps

Model Rotation ==> 90.0 deg's

Airstream Velocity ==> 1550.00 fpm

Airstream Temp ==> 79.2 deg F

Sensor Num	Resist (ohms)	Temp (deg 'F)
1	54.3940010	91.696251
2	54.0509990	88.348991
3	54.0480000	88.150032
4	53.5519980	84.755020
5	53.4000020	83.619675
6	54.4819980	91.452209
7	53.9879990	87.958763
8	54.4840010	91.372993
9	54.3639980	91.004723
10	54.0999980	88.550903
11	53.6559980	88.197205
12	53.7319980	88.306778
13	54.0200000	88.457169
14	54.0490000	87.008934
15	53.8340000	86.972153
16	54.3180010	89.638046
17	54.6819990	91.033089
18	54.5530010	91.239899
19	55.2439990	93.068092
20	54.3880000	90.054794
21	54.6360020	84.135345
22	54.3380010	89.833221
23	54.6110000	89.770035
24	54.4949990	91.551117
25	55.0210000	92.463516
26	54.5550000	90.202950
27	54.4389990	90.468338
28	53.5079990	82.312561
29	54.6180000	88.919350
30	0.0000000	0.000000
31	54.6930010	90.117241
32	0.0000000	0.000000
33	54.3730010	89.620003
34	54.4900020	89.944153
35	54.7439990	91.143021

Table F-38

36	54.2990000	91.910103
37	55.4030000	94.556938
38	54.6510010	91.360664
39	55.1800000	94.646088
40	54.8779980	89.811287
41	54.7060010	92.142899
42	55.1209980	92.581154
43	56.0140000	101.390266
44	0.0000000	0.000000
45	55.2449990	96.986740
46	55.4420010	96.577766
47	56.1419980	101.076279
48	55.9609990	96.884911
49	56.3349990	100.558891
50	55.5070000	93.067513
51	54.9800000	91.102028
52	0.0000000	-29.345400
53	0.0000000	0.000000
54	54.4570010	88.629456
55	55.0670010	88.574440
56	53.5910000	79.200317
57	54.9760020	89.474274
58	55.1349980	88.631859
59	55.2260020	91.413170
60	55.4710010	91.160652
61	54.9210010	88.555328
62	0.0000000	0.000000
63	0.0000000	0.000000
64	54.6170010	91.150253
65	0.0000000	0.000000
66	54.2729990	88.240929
67	54.4269980	89.419090
68	54.3330000	88.510452
69	0.0000000	0.000000
70	55.3489990	96.336136
71	53.6370010	87.479309
72	54.8480000	93.237610
73	54.4710010	90.505310
74	54.0330010	89.126648
75	54.6930010	91.566574
76	54.1520000	88.718536
77	54.1479990	88.271751
78	54.0359990	86.719864
79	53.7920000	86.835762

Table F-39

Test File: 11-15_1.cal											
	airstream velocity =	1550 fpm					total wattage =	511.56			
	airstream temp =	79.16 °F									
	model rotation =	90 deg (ccw)									
sensor#	x-value	y-value	temp (°F)	k,ss	gen	cond,1	cond,2	cond,b	rad	conv	h
0		0									
1		91.6963	26	1.8345	0	-0.007	0.53973	0.06198	1.2258	3.51727	
2		88.349	26	1.8345	0	-0.00431	0.31605	0.04501	1.46914	5.7511	
3		88.15	26	1.8345	-0.00431	0.00102	0.30275	0.04401	1.48446	5.93966	
4		84.755		1.8345							
5		83.6197		1.8345							
6		91.4522	26	1.8345	0	-0.0756	0.52342	0.06073	1.17475	3.43771	
7		87.9588	26	1.8345	-0.0756	0.00753	0.28997	0.04305	1.43341	5.8601	
8		91.373	26	1.8345	-0.007	-0.00797	0.51813	0.06033	1.24108	3.65539	
9		91.0047	26	1.8345	-0.00797	0.00315	0.49352	0.05845	1.27771	3.88029	
10		88.5509	26	1.8345	0.00765	-0.00671	0.32954	0.04603	1.45989	5.59199	
11		88.1972	26	1.8345	0.00102	0.00765	0.3059	0.04425	1.49303	5.94277	
12		88.3068	26	1.8345	0.07686	0.00325	0.31322	0.0448	1.5566	6.12158	
13		88.4572	26	1.8345	0.00325	0.00115	0.32327	0.04555	1.47008	5.68782	
14		87.0089									
15		86.9722									
16		89.638									
17		91.0331									
18		91.2399									
19		93.0681									
20		90.0548									
21		84.1353									
22		89.8332									
23		89.77									
24		91.5511									
25		92.4635									
26		90.203									
27		90.4683									
28		82.3126									
29		88.9194									
30		0									
31		90.1172									
32		0									
33		89.62	26	1.8345	0	0.06408	-0.01278	0.05142	1.85995	6.39624	
34		89.9442	26	1.8345	-0.01214	0.02594	0.21547	0.05306	1.57978	5.26944	
35		91.143	26	1.8345	0.02594	0	0.28784	0.05915	1.51345	4.54316	
36		91.9101	26	1.8345	0.00743	0.05728	0.3391	0.06307	1.49704	4.22352	
37		94.5569	26	1.8345	0.05728	0.04373	0.16132	0.07673	1.69746	3.96571	
38		91.3607									
39		94.6461									
40		89.8113									
41		92.1429									
42		92.5812	26	1.8345	0.06408	0.19064	0.1851	0.06652	1.8376	4.92512	
43		101.39	26	1.8345	0.19064	0	0.77379	0.1129	1.13846	1.84216	
44		0	0	0	0	0	0	0			
45		96.9867	26	1.8345	0	0	0.47951	0.08944	1.26555	2.55366	
46		96.5778	26	1.8345	0.04373	0.09735	0.29637	0.08729	1.59193	3.28766	
47		101.076	26	1.8345	0.09735	0	0.59699	0.1112	1.22366	2.0084	
48		96.8849									
49		100.559									
50		93.0675									
51		91.102									
52		-29.3454									
53		0									
54		88.6295									
55		88.5744									
56		79.2003									
57		89.4743									
58		88.6319									
59		91.4132									
60		91.1607									

Table F-39

61	88.5553								
62	0								
63	0								
64	91.1503	26	1.8345	0.00315	0	0.50325	0.05919	1.27522	3.8257
65	0								
66	88.2409	26	1.8345	-0.00671	0.0255	0.30882	0.04447	1.5	5.94177
67	89.4191	26	1.8345	0.0255	0	0.38756	0.0504	1.42204	4.98607
68	88.5105	26		0.00115	0	0.32684	0.04582	1.463	5.62816
69	0								
70	96.3361	26	1.8345	0	-0.19167	0.64263	0.08602	0.91419	1.91455
71	87.4793	26	1.8345	-0.19167	0	0.05075	0.04065	1.55143	6.70812
72	93.2376	26	1.8345	0	-0.05913	0.43556	0.0699	1.26992	3.2449
73	90.5053	26	1.8345	-0.05913	0	0.25297	0.05591	1.4665	4.64965
74	89.1266	26	1.8345	0	0.0528	0.15309	0.04893	1.68529	6.08247
75	91.5666	26	1.8345	0.0528	0	0.32389	0.06132	1.5021	4.35514
76	88.7185								
77	88.2718								
78	86.7199								
79	86.8358								

Table F-40

Cover Temperature Map (Test 11-15_1)					
91.45221	87.95876	88.30678	88.45717	88.51045	0
88.34899	88.15003	88.19721	88.5509	88.24093	89.41909
0	91.69625	91.37299	91.00472	91.15025	0
Average Surf T =	89.2997				

Table F-41

Cover Temp Difference Map (Test 11-15_1)						
12.29221	8.798763	9.146778	9.297169	9.350452	-79.16	
9.188991	8.990032	9.037205	9.390903	9.080929	10.25909	
-79.16	12.53625	12.21299	11.84472	11.99025	-79.16	
Average Delta T =	10.1397					

Table F-42

Cover Surf Coeff Map (Test 11-15_1)				
	5.860102	6.121578	5.687823	5.628162
	5.939661	5.942771	5.591993	5.941773
	3.51727	3.655385	3.880291	3.825701
Ave Surf Coeff. =	5.132709			

Table F-43

Side Surface Coeff Map (Test 11-15_1)						
	1.914552	6.708117	0	6.39624	4.925118	1.842159
Air -->	3.244899	4.649652	5.269443	4.54316	0	2.553665
	6.08247	4.355136	4.223525	3.965714	3.287664	2.008396
Right Side						

Temperature Distribution Surface Plot
Test: 11-15_1 (Font Half of Cover)

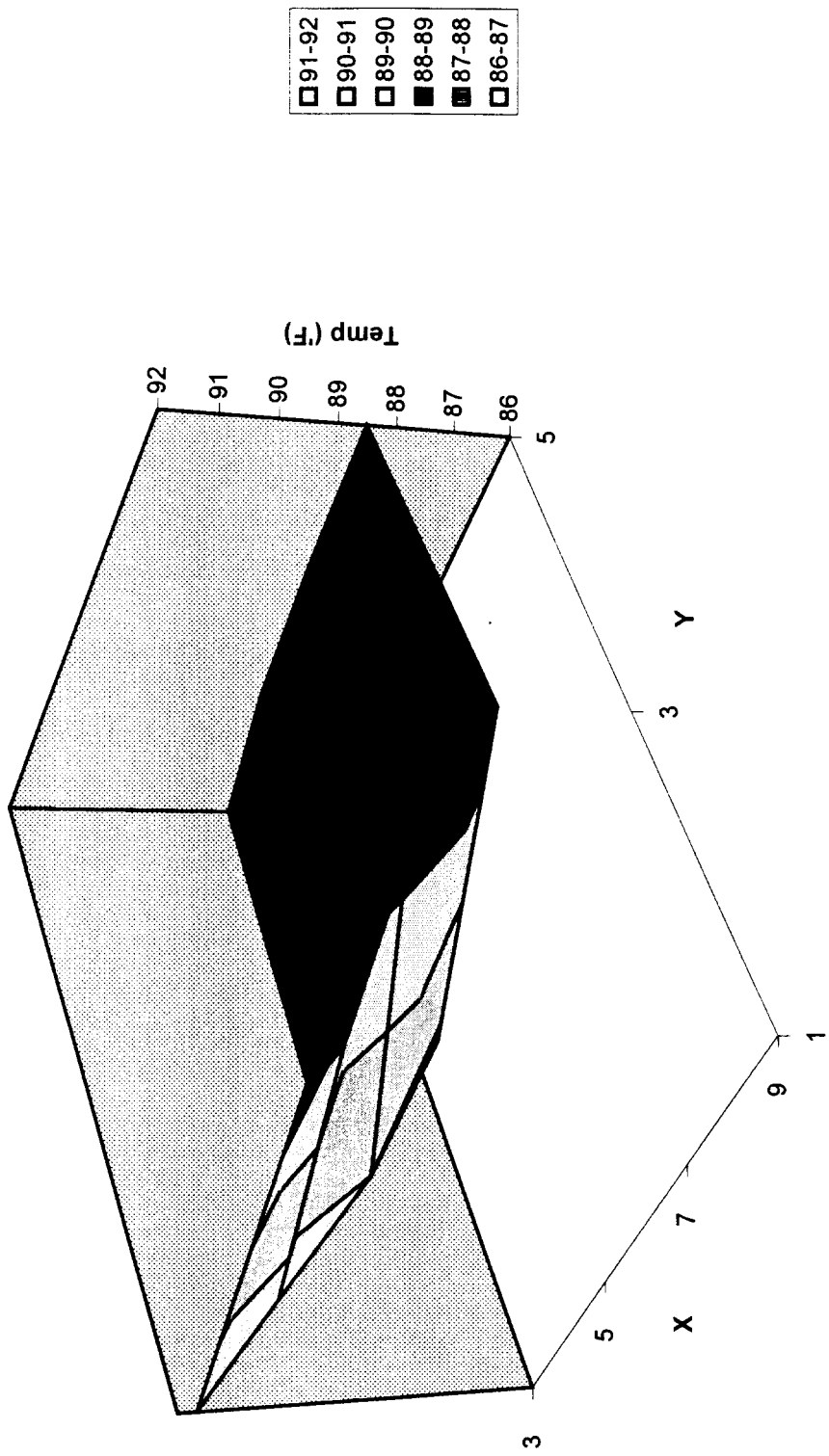


Figure F-13

Heat Transfer Coefficient Surface Plot
Test 11-15_1 (Front Half of Cover)

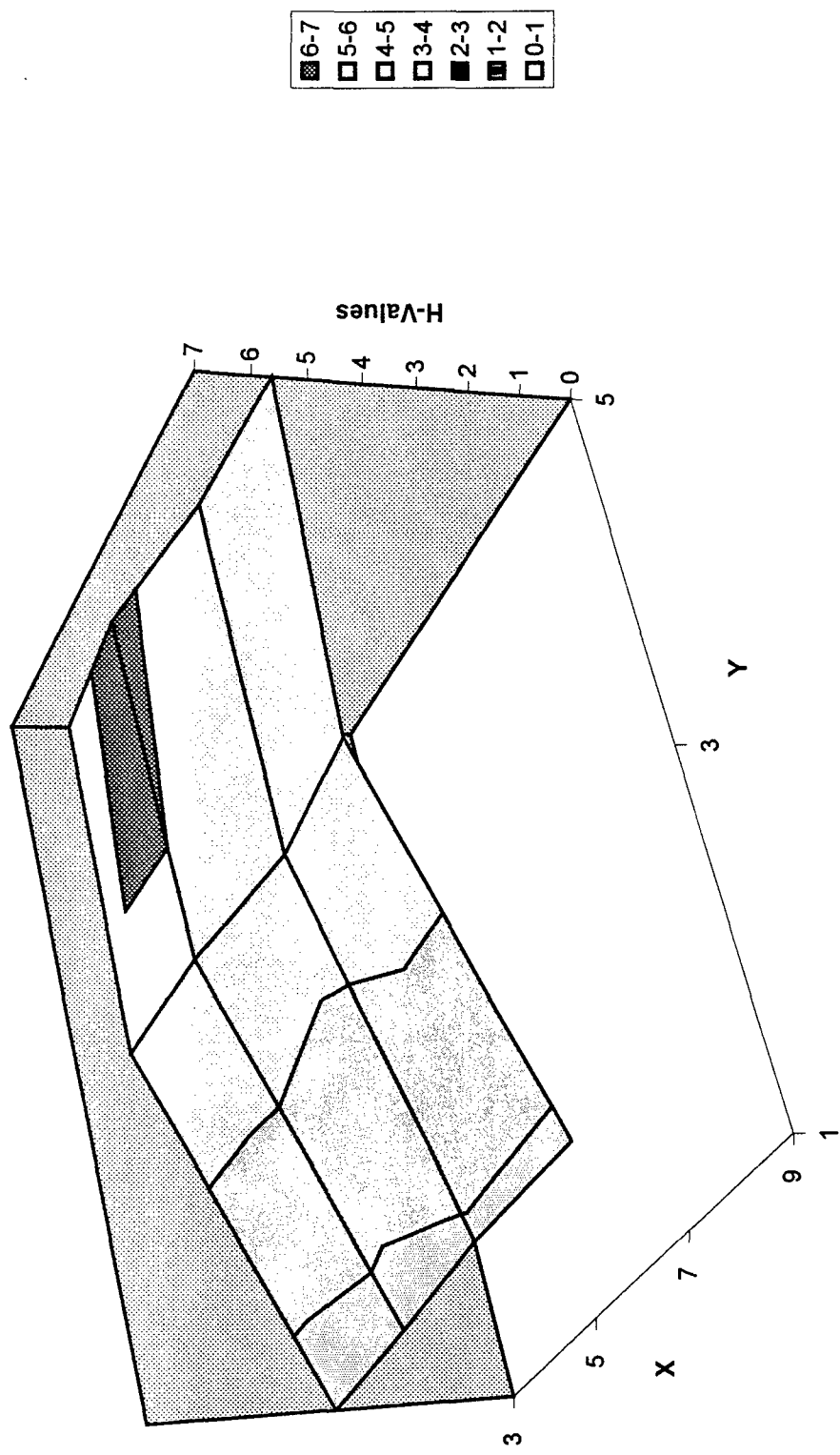


Figure F-14

Table F-44

Output Filename ==> d:\scottstu\thesis\data\11-21_.CAL

(Created from input file ==> a:11-21_1.dat)

Current Date: Tuesday, November 21, 1995

Current Time: 11:57 hrs

User Name: S.LeClair

Input Current ==> 6.92 amps
Model Rotation ==> 270.0 deg's
Airstream Velocity ==> 1550.00 fpm
Airstream Temp ==> 79.7 deg F

Sensor Num	Resist (ohms)	Temp (deg 'F)
1	54.8709980	95.128212
2	54.9599990	94.607315
3	54.7729990	93.375175
4	54.5340000	91.538315
5	54.2350010	89.420158
6	54.9370000	94.609230
7	54.4860000	91.400101
8	55.0340000	95.157761
9	54.9129980	94.929161
10	54.7900010	93.284058
11	54.4039990	93.360428
12	54.1240010	91.078194
13	54.2570000	90.128143
14	54.8610000	92.864403
15	54.2270010	89.736839
16	54.4039990	90.235008
17	54.8510020	92.201714
18	54.6600000	91.997543
19	55.3429990	93.760445
20	54.4830020	90.729828
21	54.6990010	84.553658
22	54.5210000	91.146843
23	54.7820010	90.969147
24	54.5980000	92.307571
25	55.1390000	93.309204
26	54.6339990	90.793747
27	54.5420000	91.192062
28	53.6600000	83.384865
29	54.7519990	89.843933
30	0.0000000	0.000000
31	54.7879980	90.806831
32	0.0000000	0.000000
33	54.1520000	87.997375
34	54.5719990	90.517654
35	54.4560010	89.170723

Table F-44

36	54.6829990	94.692177
37	55.2850000	93.747604
38	55.2900010	95.772224
39	55.8300020	99.103477
40	54.3530010	86.236923
41	55.1040000	94.944374
42	54.4840010	88.117538
43	55.1629980	95.397797
44	0.0000000	0.000000
45	54.7700000	93.549400
46	54.9949990	93.519554
47	55.5359990	96.849617
48	55.8720020	96.244102
49	55.7050020	96.069214
50	55.6010020	93.730209
51	55.0789990	91.831688
52	0.0000000	-29.345400
53	0.0000000	0.000000
54	54.5260010	89.120827
55	55.1220020	88.963425
56	53.6559980	79.659630
57	55.0810010	90.265427
58	55.2070010	89.133003
59	55.3390010	92.254868
60	55.5810010	91.940216
61	55.0359990	89.358589
62	0.0000000	0.000000
63	0.0000000	0.000000
64	55.2560010	95.607094
65	0.0000000	0.000000
66	54.9850010	93.278778
67	55.3600010	96.040306
68	54.5960010	90.325172
69	0.0000000	0.000000
70	55.6959990	98.711212
71	54.3110010	92.319695
72	55.1500020	95.310646
73	54.7120020	92.268631
74	55.7529980	101.035950
75	55.5910000	97.734398
76	55.6570010	98.993652
77	55.2949980	96.236465
78	54.4210010	89.361610
79	55.0079990	95.181580

Table F-45

Test File: 11-21_1.cal											
	airstream velocity =	1550 fpm								total wattage =	
	airstream temp =	79.7 °F									
	model rotation =	270 deg (ccw)									
sensor#	x-value	y-value	temp (°F)	k,ss	gen	cond,1	cond,2	cond,b	rad	conv	h
0		0									
1		95.1282	26	1.76019	0	0.00064	0.38145	0.07712	1.30225	3.03623	
2		94.6073	26	1.76019	0	-0.02666	0.34664	0.07441	1.31247	3.16698	
3		93.3752	26	1.76019	-0.02666	-0.00032	0.2643	0.06803	1.40087	3.68487	
4		91.5383		1.76019							
5		89.4202		1.76019							
6		94.6092	26	1.76019	0	-0.06945	0.34677	0.07442	1.26955	3.06302	
7		91.4001	26	1.76019	-0.06945	-0.00697	0.13231	0.05788	1.49357	4.5919	
8		95.1578	26	1.76019	0.00064	-0.00495	0.38343	0.07727	1.29518	3.01397	
9		94.9292	26	1.76019	-0.00495	0.01467	0.36815	0.07608	1.32568	3.13125	
10		93.2841	26	1.76019	-0.00165	-0.00011	0.25821	0.06756	1.43265	3.79373	
11		93.3604	26	1.76019	-0.00032	-0.00165	0.26332	0.06795	1.42695	3.7575	
12		91.0782	26	1.76019	-0.00996	-0.02056	0.1108	0.05624	1.56263	4.94011	
13		90.1281	26	1.76019	-0.02056	0.00426	0.04731	0.05141	1.64517	5.6749	
14		92.8644									
15		89.7368									
16		90.235									
17		92.2017									
18		91.9975									
19		93.7604									
20		90.7298									
21		84.5537									
22		91.1468									
23		90.9691									
24		92.3076									
25		93.3092									
26		90.7937									
27		91.1921									
28		83.3849									
29		89.8439									
30		0									
31		90.8068									
32		0									
33		87.9974	26	1.76019	0	0.0026	0.11765	0.04066	1.60448	6.95581	
34		90.5177	26	1.76019	-0.03789	-0.02915	0.07725	0.05339	1.5625	5.19569	
35		89.1707	26	1.76019	-0.02915	0	-0.40169	0.04657	2.08616	7.92354	
36		94.6922	26	1.76019	-0.06584	-0.02044	-0.03271	0.07485	1.63176	3.91515	
37		93.7476	26	1.76019	-0.02044	-0.00494	-0.07998	0.06995	1.74484	4.46794	
38		95.7722									
39		99.1035									
40		86.2369									
41		94.9444									
42		88.1175	26	1.76019	0.0026	0.15755	0.12568	0.04127	1.75339	7.49289	
43		95.3978	26	1.76019	0.15755	0	0.61219	0.07853	1.22702	2.81169	
44		0	0	0	0	0	0	0			
45		93.5494	26	1.76019	0	0	0.48867	0.06893	1.20259	3.1235	
46		93.5196	26	1.76019	-0.00494	0.07206	-0.09522	0.06877	1.85376	4.82519	
47		96.8496	26	1.76019	0.07206	0	0.12732	0.08613	1.6188	3.39542	
48		96.2441									
49		96.0692									
50		93.7302									
51		91.8317									
52		-29.3454									
53		0									
54		89.1208									
55		88.9634									
56		79.6596									
57		90.2654									
58		89.133									
59		92.2549									
60		91.9402									

Table F-45

61	89.3586								
62	0								
63	0								
64	95.6071	26	1.76019	0.01467	0	0.41345	0.07962	1.28178	2.89854
65	0								
66	93.2788	26	1.76019	-0.00011	0.05976	0.25786	0.06753	1.49444	3.9589
67	96.0403	26	1.76019	0.05976	0	0.4424	0.08189	1.29566	2.85224
68	90.3252	26		0.00426	0	0.06048	0.05241	1.65156	5.59131
69	0								
70	98.7112	26	1.76019	0	-0.13832	0.62481	0.09598	0.90109	1.70495
71	92.3197	26	1.76019	-0.13832	0	0.19768	0.06259	1.3616	3.8811
72	95.3106	26	1.76019	0	-0.06583	0.39756	0.07807	1.21873	2.80828
73	92.2686	26	1.76019	-0.06583	0	0.19427	0.06233	1.43776	4.11484
74	101.036	26	1.76019	0	-0.07145	0.39123	0.10841	1.1891	2.00476
75	97.7344	26	1.76019	-0.07145	0	0.55953	0.0908	1.03841	2.07121
76	98.9937								
77	96.2365								
78	89.3616								
79	95.1816								

Table F-46

Cover Temperature Map (Test 11-21_1)						
0	95.60709	94.92916	95.15776	95.12821	0	
96.04031	93.27878	93.28406	93.36043	93.37518	94.60732	
0	90.32517	90.12814	91.07819	91.4001	94.60923	
Ave Surf Temp =	93.08769					

Table F-47

Cover Temp Difference Map (Test 11-21_1)						
-79.7	15.90709	15.22916	15.45776	15.42821	-79.7	
16.34031	13.57878	13.58406	13.66043	13.67518	14.90732	
-79.7	10.62517	10.42814	11.37819	11.7001	14.90923	
Ave Delta Temp =	13.38769					

Table F-48

Cover Surf Coeff Map (Test 11-21_1)				
	1.478477	1.669633	1.672944	1.575492
	2.269926	2.12222	2.16339	2.102989
	3.188462	3.144814	2.722879	2.668363
Ave Surf Coeff =	2.231632			

Table F-49

Side Surface Coeff Map (Test 11-21_1)					
1.704955	3.8811	5.418	6.955811	7.492893	2.811688
2.808284	4.114837	5.195686	7.923542	6.159	3.123501 <-- Air
2.004762	2.071205	3.915146	4.46794	4.825194	3.395416
Left Side					
Ave =	4.168248				
StDev =	1.917933				

Figure F-15

Temperature Distribution Surface Plot
Test: 11-21_1 (Back Half of Cover)

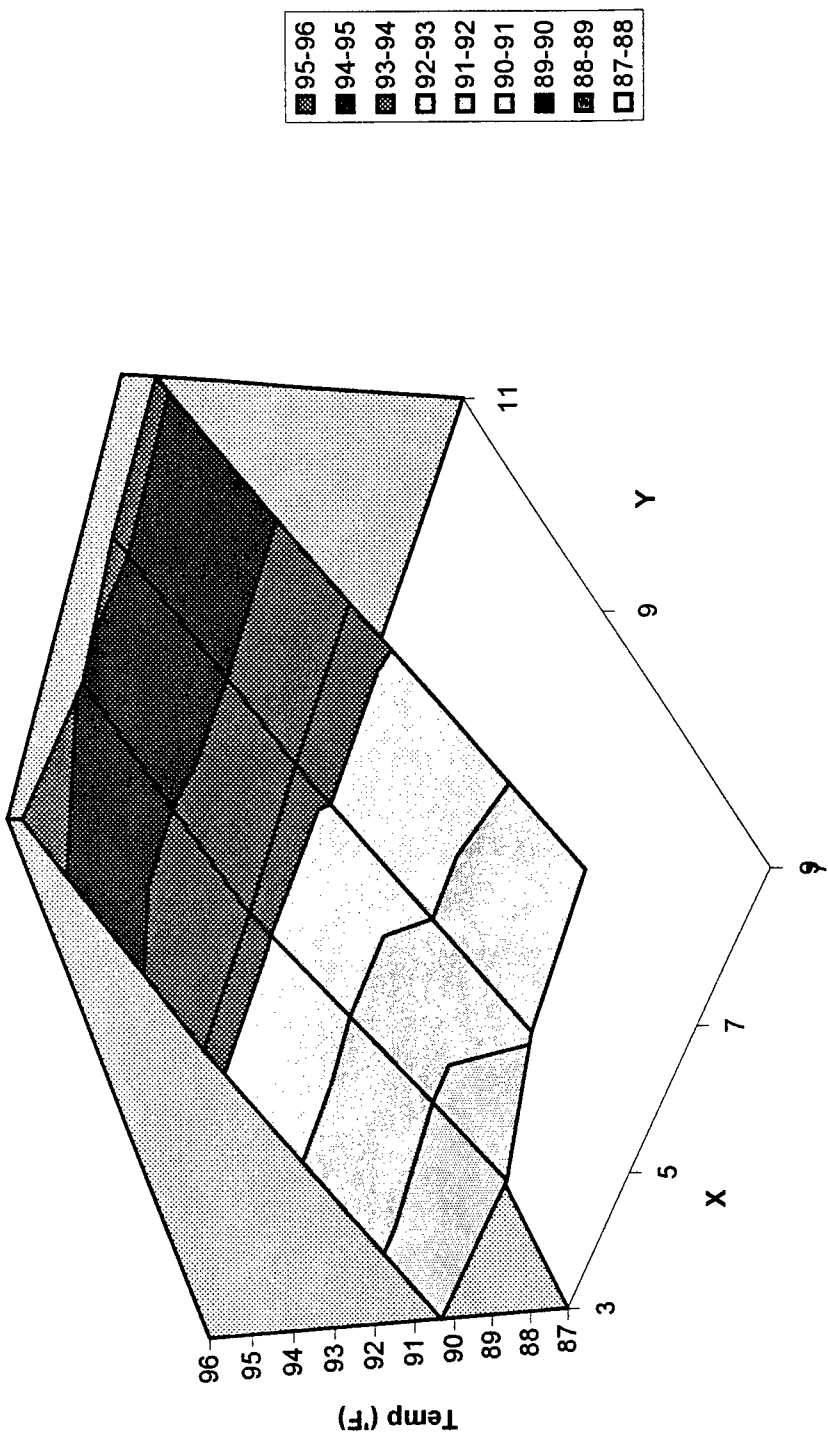


Figure F-16

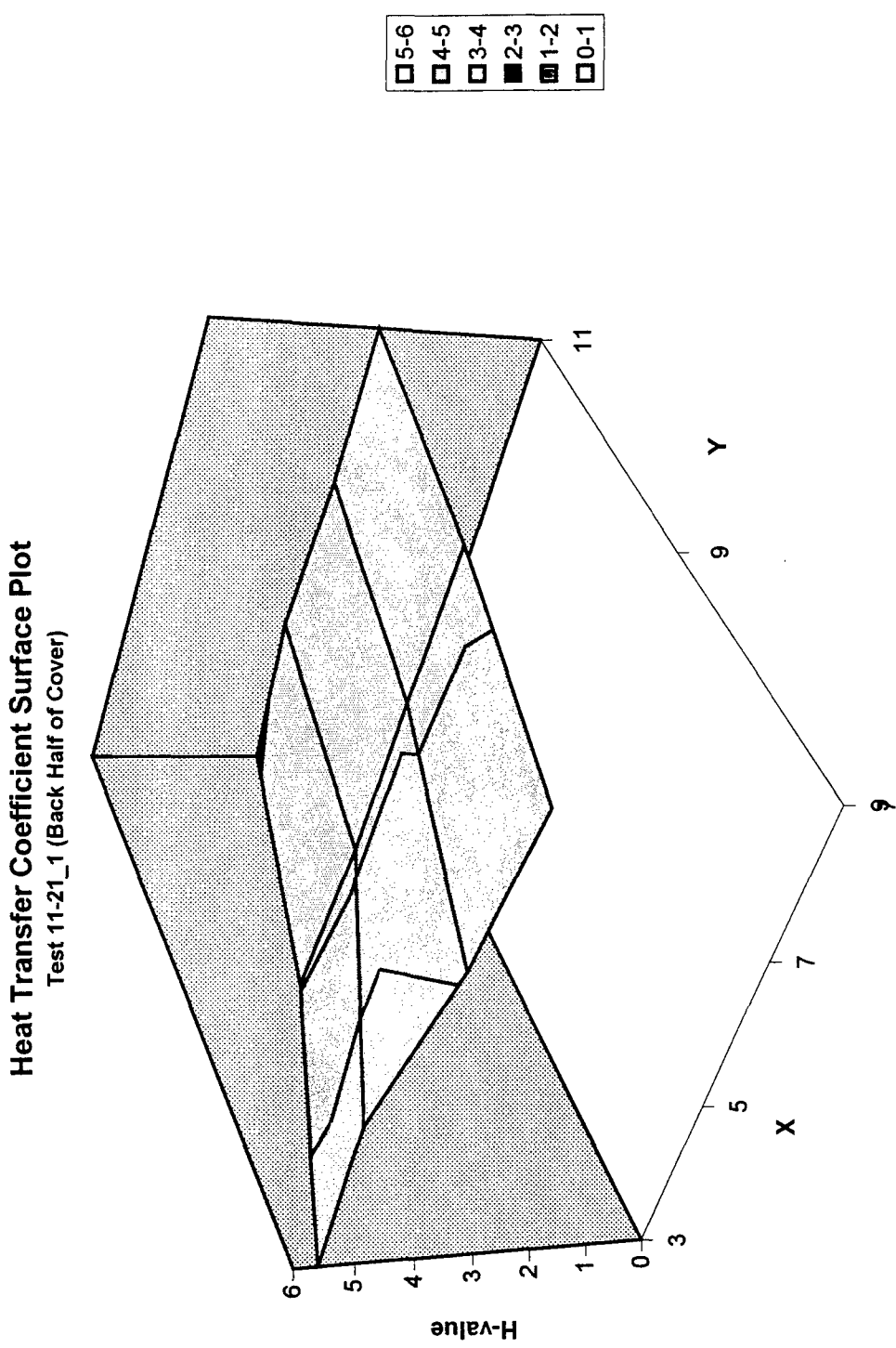


Table F-50

Output Filename ==> d:\scottstu\thesis\data\12-11_1.dat

(Created from input file ==> a:12-11_1.dat)

Current Date: Monday, December 11, 1995

Current Time: 11:53 hrs

User Name: S.LeClair

Input Current ==> 4.22 amps
Model Rotation ==> 90.0 deg's
Airstream Velocity ==> 660.00 fpm
Airstream Temp ==> 87.4 deg F

Sensor Num	Resist (ohms)	Temp (deg 'F)
1	54.6740000	93.712013
2	54.6220020	92.285843
3	54.5420000	91.712730
4	54.4650000	91.062843
5	54.3660010	90.326454
6	54.8499980	94.006386
7	54.5379980	91.759033
8	54.7519990	93.219734
9	54.6020010	92.707779
10	54.5499990	91.640594
11	54.1720010	91.762482
12	54.1699980	91.402657
13	54.3899990	91.064186
14	54.5779990	90.828484
15	54.3520010	90.614677
16	54.5379980	91.165863
17	54.7589990	91.565720
18	54.5950010	91.537781
19	55.1780010	92.606880
20	54.6310010	91.779648
21	54.9230000	86.041550
22	54.6020010	91.727753
23	54.8610000	91.521675
24	54.5670010	92.080406
25	55.0239980	92.485428
26	54.7120020	91.375443
27	54.7140010	92.400040
28	54.2599980	87.601646
29	54.9259990	91.043053
30	0.0000000	0.000000
31	54.9269980	91.815186
32	0.0000000	0.000000
33	54.7820010	92.616554
34	54.8470000	92.441765
35	55.0589980	93.295761

Table F-50

36	54.7570000	95.227867
37	55.6559980	96.287903
38	54.8440020	92.695518
39	54.9420010	93.008484
40	55.3120000	92.755196
41	54.9770010	94.051384
42	55.4170000	94.648354
43	55.7820010	99.760574
44	0.0000000	0.000000
45	55.1850010	96.553345
46	55.5219990	97.124283
47	55.8139990	98.791306
48	55.4760020	93.386009
49	55.3890000	93.807915
50	55.6339990	93.963028
51	55.1710010	92.508415
52	0.0000000	-29.345400
53	0.0000000	0.000000
54	54.8340000	91.314095
55	55.3890000	90.847847
56	54.5289990	85.807999
57	55.2690010	91.680756
58	55.5000000	91.167374
59	55.3689990	92.478416
60	55.5900000	92.004364
61	55.2869990	91.111450
62	0.0000000	0.000000
63	0.0000000	0.000000
64	54.8180010	92.554932
65	0.0000000	0.000000
66	54.7490010	91.611702
67	54.9360010	93.037369
68	54.7980000	91.716919
69	0.0000000	0.000000
70	55.3069990	96.048431
71	54.2280010	91.725403
72	55.1090010	95.029625
73	54.8139990	93.014313
74	54.6489980	93.410316
75	55.0040020	93.707611
76	54.3779980	90.269341
77	54.5369990	90.981339
78	54.7039990	91.298134
79	54.3349990	90.571915

Table F-51

Test File: 12-11_1.cal											
	airstream velocity =	660 fpm									
	airstream temp =	87.44°F									
	model rotation =	90 deg (ccw)									
sensor#	x-value	y-value	temp (F)	k,ss	gen	cond,1	cond,2	cond,b	rad	conv	h
0			0								
1			93.712	26	0.67822	0	-0.01065	0.22625	0.03189	0.40943	2.34815
2			92.2858	26	0.67822	0	-0.0124	0.13094	0.02454	0.51033	3.78826
3			91.7127	26	0.67822	-0.0124	0.00108	0.09264	0.02161	0.55265	4.65262
4			91.0628		0.67822						
5			90.3265		0.67822						
6			94.0064	26	0.67822	0	-0.04863	0.24592	0.03342	0.35025	1.91871
7			91.759	26	0.67822	-0.04863	-0.00771	0.09573	0.02184	0.50429	4.20004
8			93.2197	26	0.67822	-0.01065	-0.01108	0.19335	0.02935	0.43379	2.69977
9			92.7078	26	0.67822	-0.01108	-0.00331	0.15914	0.02671	0.47798	3.26394
10			91.6406	26	0.67822	-0.00264	-0.00063	0.08782	0.02124	0.5659	4.846
11			91.7625	26	0.67822	0.00108	-0.00264	0.09597	0.02186	0.55883	4.65054
12			91.4027	26	0.67822	0.00735	-0.00732	0.07192	0.02002	0.58631	5.32224
13			91.0642	26	0.67822	-0.00732	0.01413	0.0493	0.0183	0.61743	6.12815
14			90.8285								
15			90.6147								
16			91.1659								
17			91.5657								
18			91.5378								
19			92.6069								
20			91.7796								
21			86.0416								
22			91.7278								
23			91.5217								
24			92.0804								
25			92.4854								
26			91.3754								
27			92.4								
28			87.6016								
29			91.0431								
30			0								
31			91.8152								
32			0								
33			92.6166								
34			92.4418								
35			93.2958								
36			95.2279								
37			96.2879								
38			92.6955								
39			93.0085								
40			92.7552								
41			94.0514								
42			94.6484								
43			99.7606								
44			0								
45			96.5533								
46			97.1243								
47			98.7913								
48			93.386								
49			93.8079								
50			93.963								
51			92.5084								
52			-29.3454								
53			0								
54			91.3141								
55			90.8478								
56			85.808								
57			91.6808								
58			91.1674								
59			92.4784								
60			92.0044								

Table F-51

61		91.1115							
62		0							
63		0							
64		92.5549	26	0.67822	-0.00331	0	0.14892	0.02593	0.50006
65		0							
66		91.6117	26	0.67822	-0.00063	0.03085	0.08589	0.02109	0.60147
67		93.0374	26	0.67822	0.04047	0	0.18116	0.02841	0.50912
68		91.7169	26	0.67822	0.01413	0	0.09292	0.02163	0.5778
69		0							
70		96.0484							
71		91.7254							
72		95.0296							
73		93.0143							
74		93.4103							
75		93.7076							
76		90.2693							
77		90.9813							
78		91.2981							
79		90.5719							

Table F-52

Cover Temperature Map (Test 12-11_1)						
94.00639	91.75903	91.40266	91.06419	91.71692	0	
92.28584	91.71273	91.76248	91.64059	91.6117	93.03737	
0	93.71201	93.21973	92.70778	92.55493	0	
Ave Surf Temp =	92.07206					

Table F-53

Cover Surf Coeff Map (Test 12-11_1)				
	4.200036	5.322239	6.128151	4.859585
	4.652616	4.650539	4.846	5.18626
	2.348153	2.699769	3.263937	3.516746
Ave Surf Coeff. =	4.306169			

Table F-54

Cover Surf Coeff Map (Test 12-11_1)				
	4.200036	5.322239	6.128151	4.859585
	4.652616	4.650539	4.846	5.18626
	2.348153	2.699769	3.263937	3.516746
Ave Surf Coeff. =	4.306169			
Stand Dev =	1.132091			

Temperature Distribution Surface Plot
Test: 12-11_1 (Front Half of Cover)

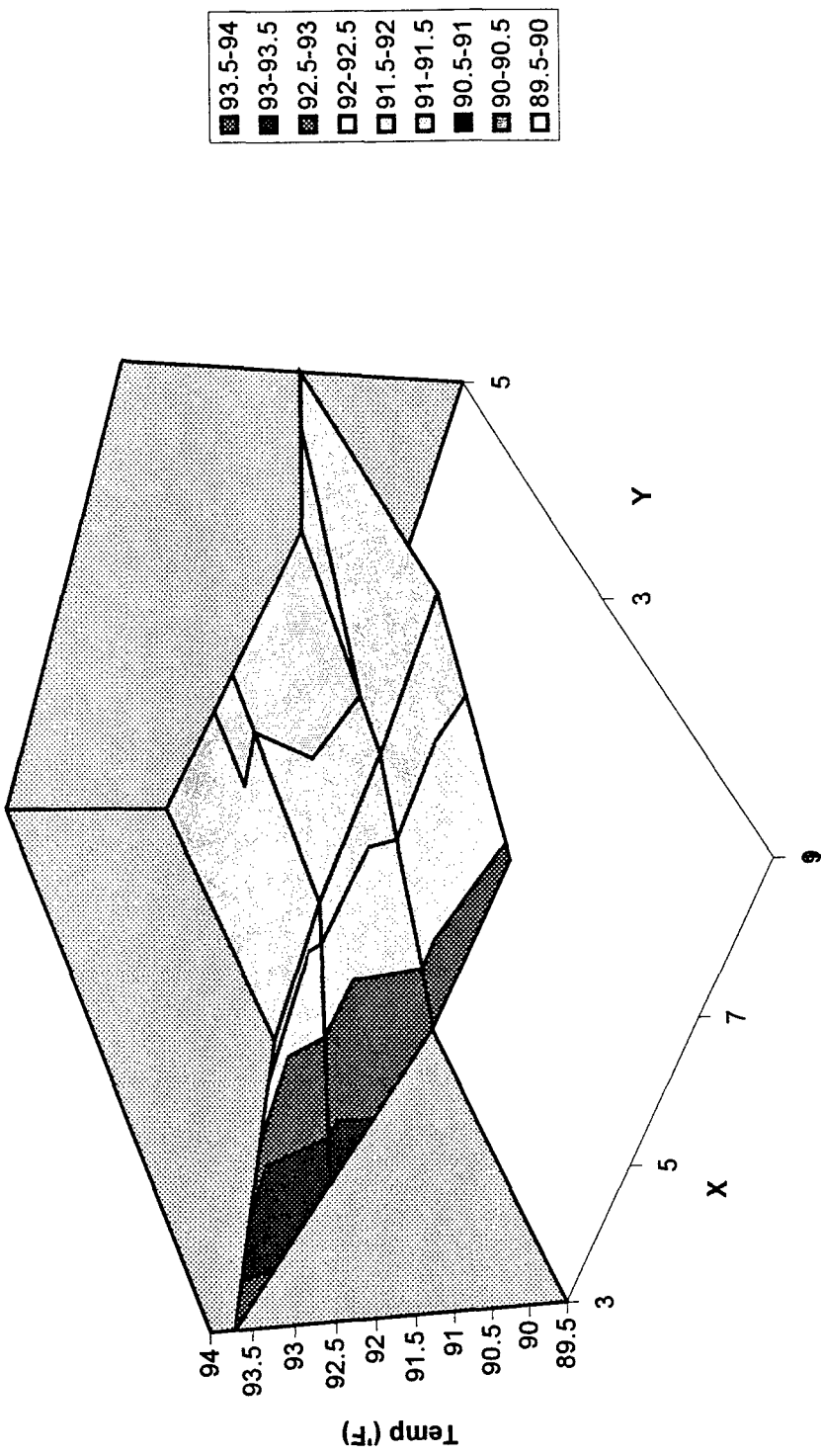


Figure F-17

Figure F-18

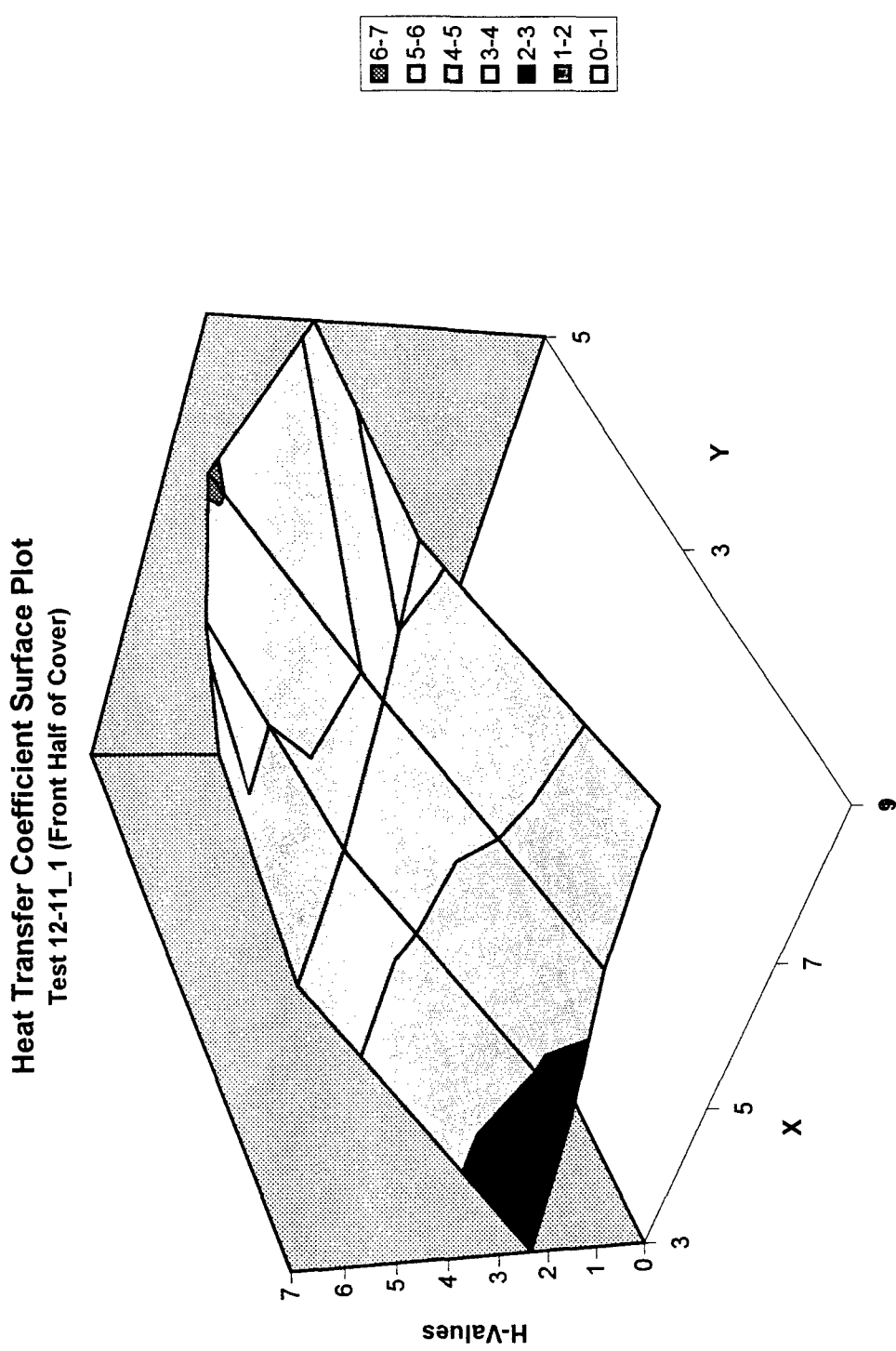


Table F-55

Output Filename ==> d:\scottstu\thesis\data\12-12_1.cal

(Created from input file ==> a:12-12_1.dat)

Current Date: Tuesday, December 12, 1995

Current Time: 15: 9 hrs

User Name: S.LeClair

Input Current ==> 7.02 amps
Model Rotation ==> 90.0 deg's
Airstream Velocity ==> 660.00 fpm
Airstream Temp ==> 91.8 deg F

Sensor Num	Resist (ohms)	Temp (deg 'F)
1	58.4550020	120.320312
2	58.0680010	115.663948
3	57.9119990	115.652199
4	58.3470000	117.379150
5	58.1710010	116.250427
6	58.5740010	119.438080
7	58.0859990	115.879890
8	58.5709990	119.104492
9	58.1390000	117.646027
10	57.9290010	114.493477
11	57.6670000	115.528580
12	57.6670000	115.737091
13	57.8250010	114.907036
14	58.0810010	115.715881
15	57.9459990	115.479813
16	57.6050000	112.198158
17	57.9399990	113.291710
18	57.7439990	113.577507
19	58.4949990	115.503853
20	57.6259990	112.764091
21	58.1170010	106.962105
22	57.6170010	113.088455
23	57.9780010	113.082184
24	57.5740010	113.919037
25	58.2920000	115.611595
26	57.5670010	112.457497
27	57.7509990	113.443474
28	56.5810010	103.725525
29	57.9529990	111.646881
30	0.0000000	0.000000
31	57.9570010	113.517731
32	0.0000000	0.000000
33	58.0429990	116.155167
34	58.3709980	116.717468
35	58.8759990	118.949219

Table F-55

36	58.8790020	124.092422
37	60.4170000	127.534523
38	59.2050020	122.032700
39	59.7640000	125.076782
40	59.4609990	120.222626
41	59.7379990	126.342064
42	59.2490010	120.689857
43	60.6329990	131.894760
44	0.0000000	0.000000
45	59.6889990	127.652672
46	60.9290010	132.326736
47	61.5530010	136.427383
48	60.5390010	128.390610
49	60.9269980	131.525421
50	59.2690010	119.228920
51	58.2480010	114.881104
52	0.0000000	-29.345400
53	0.0000000	0.000000
54	57.7099990	111.527489
55	58.2490010	110.784393
56	56.2550010	97.838760
57	58.1500020	113.104126
58	58.4840010	111.622757
59	58.4140010	114.870171
60	58.7420010	114.051727
61	58.2330020	111.422646
62	0.0000000	0.000000
63	0.0000000	0.000000
64	58.3709980	117.009521
65	0.0000000	0.000000
66	57.9290010	113.805145
67	58.1790010	115.750130
68	58.2529980	115.166611
69	0.0000000	0.000000
70	59.7449990	125.285988
71	57.1980020	112.766441
72	59.4070010	123.558586
73	58.3359990	118.390816
74	58.3919980	118.993965
75	59.0709990	121.041100
76	57.9010010	114.086891
77	58.3190000	116.887543
78	58.1199990	114.330154
79	58.4049990	118.074379

Table F-56

Test File: 12-12_1.cal											
	airstream velocity =	660 fpm									
	airstream temp =	91.76 °F									
	model rotation =	90 deg (ccw)									
sensor#	x-value	y-value	temp (°F)	k,ss	gen	cond,1	cond,2	cond,b	rad	conv	h
0			0								
1			120.32	26	1.80966	0	-0.02631	0.27198	0.1579	1.35346	1.70466
2			115.664	26	1.80966	0	-0.00025	-0.03919	0.13051	1.71808	2.58541
3			115.652	26	1.80966	-0.00025	-0.00268	-0.03998	0.13044	1.71626	2.58394
4			117.379		1.80966						
5			116.25		1.80966						
6			119.438	26	1.80966	0	-0.077	0.21302	0.15266	1.36697	1.77655
7			115.88	26	1.80966	-0.077	-0.00309	-0.02476	0.13177	1.62256	2.4198
8			119.104	26	1.80966	-0.02631	-0.03156	0.19073	0.15069	1.41037	1.85531
9			117.646	26	1.80966	-0.03156	-0.01377	0.09326	0.14209	1.52896	2.12465
10			114.493	26	1.80966	-0.0224	-0.0149	-0.11741	0.12373	1.76604	2.79441
11			115.529	26	1.80966	-0.00268	-0.0224	-0.04824	0.12973	1.70309	2.57745
12			115.737	26	1.80966	-0.03554	-0.01796	-0.0343	0.13094	1.65953	2.48967
13			114.907	26	1.80966	-0.01796	0.00562	-0.08977	0.12612	1.76096	2.73659
14			115.716								
15			115.48								
16			112.198								
17			113.292								
18			113.578								
19			115.504								
20			112.764								
21			106.962								
22			113.088								
23			113.082								
24			113.919								
25			115.612								
26			112.457								
27			113.443								
28			103.726								
29			111.647								
30			0								
31			113.518								
32			0								
33			116.155								
34			116.717								
35			118.949								
36			124.092								
37			127.535								
38			122.033								
39			125.077								
40			120.223								
41			126.342								
42			120.69								
43			131.895								
44			0								
45			127.653								
46			132.327								
47			136.427								
48			128.391								
49			131.525								
50			119.229								
51			114.881								
52			-29.3454								
53			0								
54			111.527								
55			110.784								
56			97.8388								
57			113.104								
58			111.623								
59			114.87								
60			114.052								

Table F-56

61		111.423								
62		0								
63		0								
64		117.01	26	1.80966	-0.01377	0	0.05073	0.13836	1.60679	2.28909
65		0								
66		113.805	26	1.80966	-0.0149	0.04209	-0.16341	0.11976	1.8805	3.06843
67		115.75	26	1.80966	0.08932	0	-0.03343	0.13101	1.8014	2.70104
68		115.167	26	1.80966	0.00562	0	-0.07243	0.12763	1.76008	2.70488
69		0								
70		125.286								
71		112.766								
72		123.559								
73		118.391								
74		118.994								
75		121.041								
76		114.087								
77		116.888								
78		114.33								
79		118.074								

Table F-57

Cover Surf Coeff Map (Test 12-12_1)				
2.419803	2.489674	2.736593	2.704881	
2.583939	2.577451	2.79441	3.068426	
1.704662	1.855313	2.124649	2.289086	
Ave Surf Coeff. =	2.445741			

Table F-58

Cover Temp Difference Map (Test 12-12_1)					
27.67808	24.11989	23.97709	23.14704	23.40661	-91.76
23.90395	23.8922	23.76858	22.73348	22.04515	23.99013
-91.76	28.56031	27.34449	25.88603	25.24952	-91.76
Average Delta T =	24.51087				

Table F-59

Cover Surf Coeff Map (Test 12-12_1)				
	2.419803	2.489674	2.736593	2.704881
	2.583939	2.577451	2.79441	3.068426
	1.704662	1.855313	2.124649	2.289086
Ave Surf Coeff. =	2.445741			
Stan Dev =	0.396066			

Temperature Distribution Surface Plot
Test: 12-12_1 (Front Half of Cover)

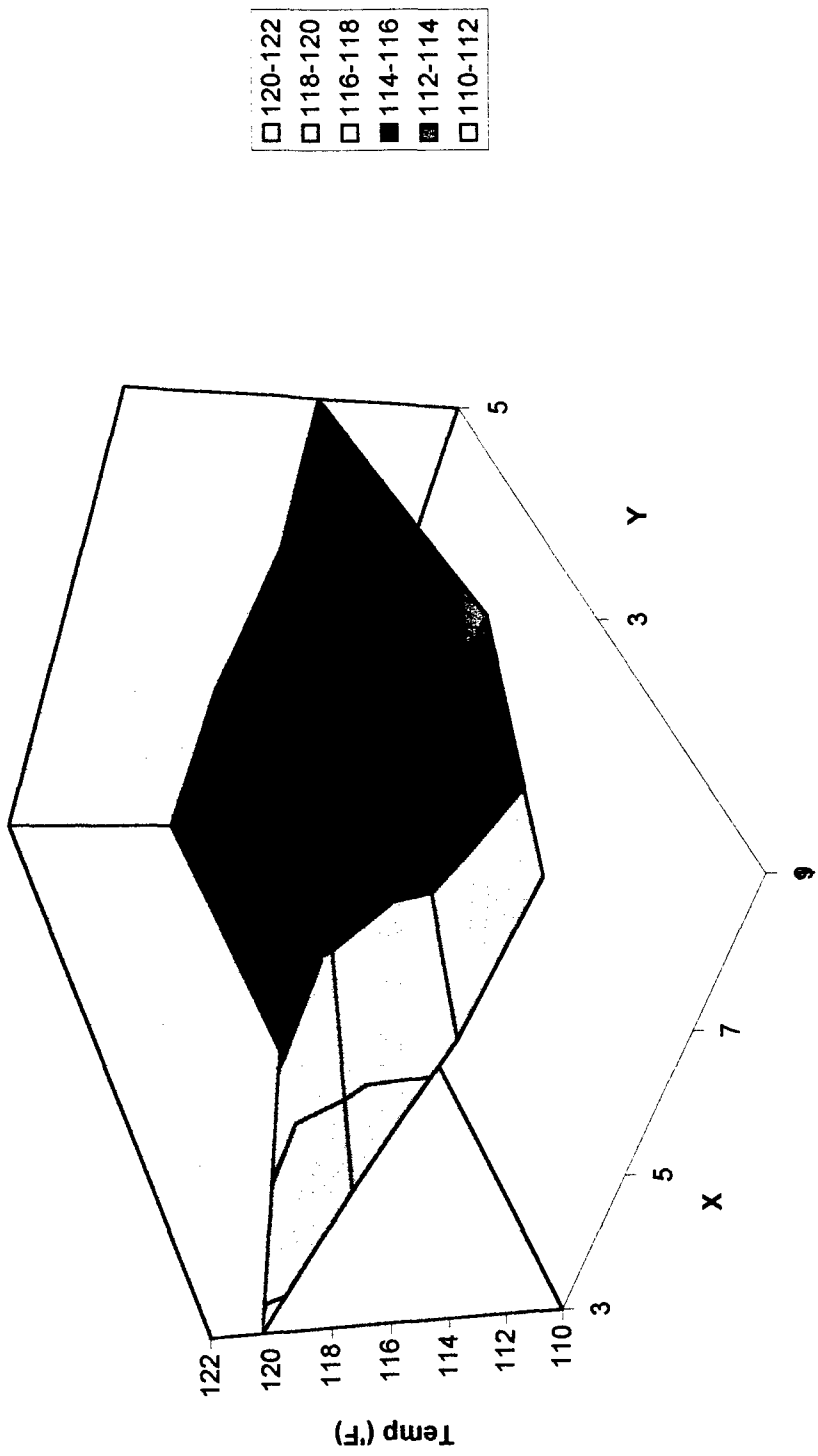


Figure F-19

Heat Transfer Coefficient Surface Plot
Test 12-12_1 (Front Half of Cover)

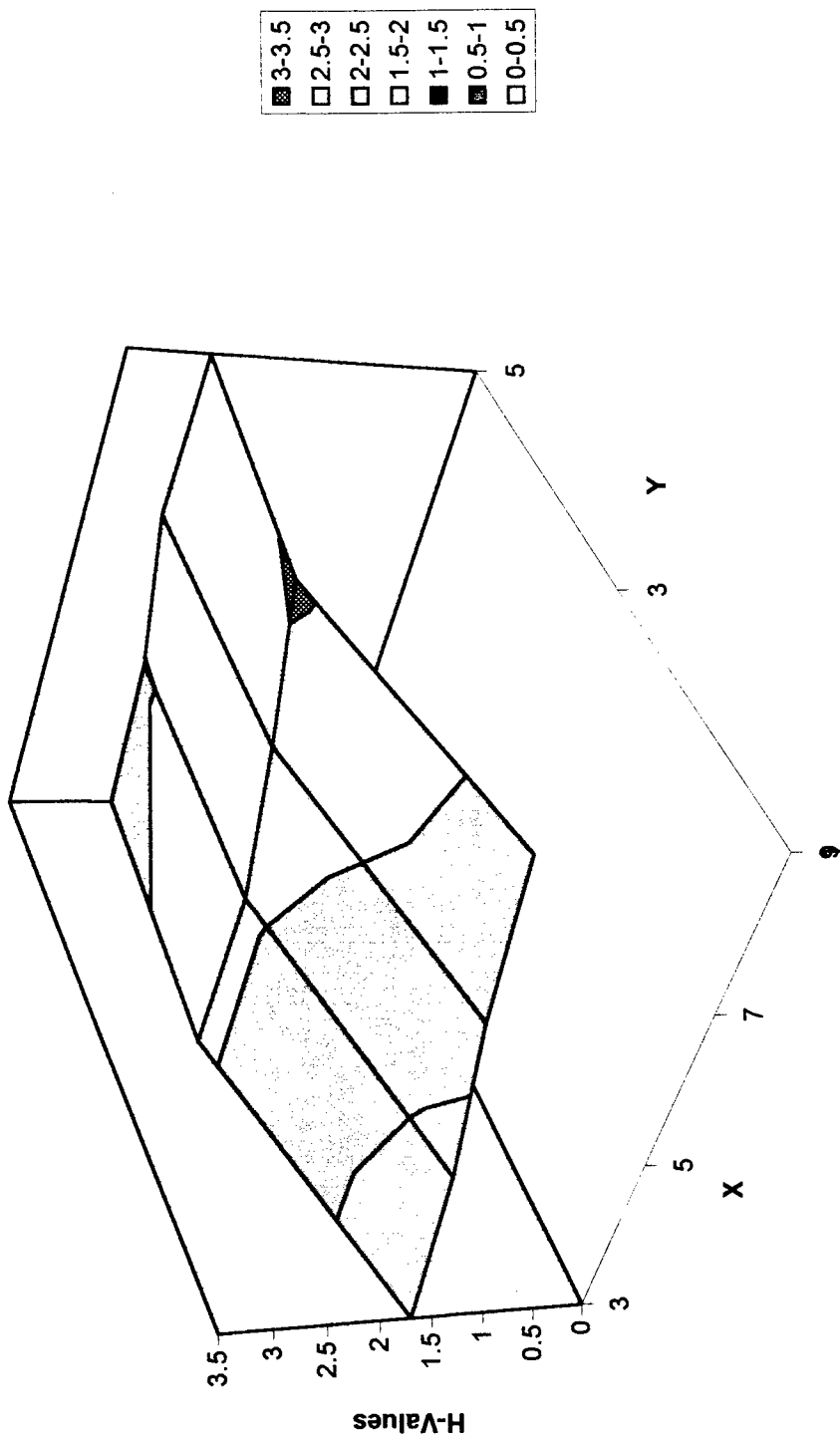


Figure F-20

Table F-60

Output Filename ==> d:\scottstu\thesis\data\12-14_1.cal

(Created from input file ==> a:12-14_1.dat)

Current Date: Thursday, December 14, 1995

Current Time: 14:18 hrs

User Name: S.LeClair

Input Current ==> 3.43 amps
Model Rotation ==> 90.0 deg's
Airstream Velocity ==> 0.00 fpm
Airstream Temp ==> 71.6 deg F

Sensor Num	Resist (ohms)	Temp (deg 'F)
1	56.5660020	107.220650
2	56.8699990	107.610054
3	56.8130000	107.916389
4	56.6800000	106.178375
5	56.6819990	106.199196
6	57.0760000	109.299667
7	56.9450000	108.197487
8	56.6510010	106.189919
9	56.5530010	106.551109
10	57.0340000	108.500877
11	56.5449980	107.971062
12	56.4900020	107.622040
13	56.7130010	107.260384
14	56.8720020	107.205818
15	56.7649990	107.387337
16	55.7290000	99.394508
17	55.9230000	99.579414
18	55.7220000	99.488739
19	56.2560010	100.114716
20	55.4570010	97.617363
21	55.7370000	91.423866
22	55.5340000	98.386459
23	56.0719990	99.962486
24	55.5849990	99.531906
25	56.2750020	101.409012
26	55.5250020	97.427994
27	55.7610020	99.712051
28	55.6240010	97.112839
29	57.0880010	105.810120
30	0.0000000	0.000000
31	56.3919980	102.373688
32	0.0000000	0.000000
33	56.8790020	107.823471
34	57.3839990	109.986824
35	57.4949990	109.758354

Table F-60

36	57.7770000	116.797798
37	58.6220020	116.322723
38	56.9990010	107.460121
39	56.9980010	107.054832
40	57.6720010	108.584251
41	57.8230020	113.848679
42	57.5859990	109.643585
43	57.8520010	114.192215
44	0.0000000	0.000000
45	57.1450000	110.606743
46	58.1390000	114.799339
47	57.9949990	113.875336
48	57.4650000	107.651016
49	57.5569990	109.204536
50	58.8390010	116.278191
51	56.6590000	103.396942
52	0.0000000	-29.345400
53	0.0000000	0.000000
54	57.2750020	108.500092
55	56.8079990	100.797211
56	56.2389980	97.727676
57	56.6800000	102.234093
58	57.0320010	101.730751
59	56.6030010	101.618515
60	56.7809980	100.400146
61	56.3909990	98.779823
62	0.0000000	0.000000
63	0.0000000	0.000000
64	57.2809980	109.581444
65	0.0000000	0.000000
66	57.3860020	110.055054
67	57.7200010	112.570595
68	57.2370000	108.338051
69	0.0000000	0.000000
70	57.8190000	113.099213
71	56.6790010	109.125534
72	57.4580000	110.988922
73	57.1679990	110.054596
74	57.7480010	114.646873
75	58.2190020	115.533981
76	56.2340010	102.900887
77	56.5740010	105.032036
78	57.1310010	107.726807
79	57.5149990	112.136192

Table F-61

Test File:		12-14_1.cal									
		airstream velocity =	0 fpm			total wattage =	126.355				
		airstream temp =	71.6 °F								
		model rotation =	90 deg (ccw)								
sensor#	x-value	y-value	temp (°F)	k,ss	gen	cond,1	cond,2	cond,b	rad	conv	h
0			0								
1			107.221	26	0.45312	0	-0.02231	0.06826	0.00504	0.35751	0.36103
2			107.61	26	0.45312	0	0.00663	0.09428	0.00513	0.36034	0.35995
3			107.916	26	0.45312	0.00663	0.00118	0.11475	0.00521	0.34097	0.33773
4			106.178		0.45312						
5			106.199		0.45312						
6			109.3	26	0.45312	0	-0.02385	0.20719	0.00554	0.21653	0.2066
7			108.197	26	0.45312	-0.02385	-0.01245	0.13354	0.00527	0.278	0.27325
8			106.19	26	0.45312	-0.02231	0.00782	-0.00062	0.0048	0.43445	0.4518
9			106.551	26	0.45312	0.00782	0.06558	0.02352	0.00488	0.49811	0.51265
10			108.501	26	0.45312	0.01147	0.03363	0.15381	0.00535	0.33906	0.33052
11			107.971	26	0.45312	0.00118	0.01147	0.11841	0.00522	0.34214	0.33838
12			107.622	26	0.45312	0.03124	-0.00783	0.09508	0.00514	0.37632	0.37579
13			107.26	26	0.45312	-0.00783	0.02332	0.07092	0.00505	0.39265	0.39607
14			107.206								
15			107.387								
16			99.3945								
17			99.5794								
18			99.4887								
19			100.115								
20			97.6174								
21			91.4239								
22			98.3865								
23			99.9625								
24			99.5319								
25			101.409								
26			97.428								
27			99.7121								
28			97.1128								
29			105.81								
30			0								
31			102.374								
32			0								
33			107.823								
34			109.987								
35			109.758								
36			116.798								
37			116.323								
38			107.46								
39			107.055								
40			108.584								
41			113.849								
42			109.644								
43			114.192								
44			0								
45			110.607								
46			114.799								
47			113.875								
48			107.651								
49			109.205								
50			116.278								
51			103.397								
52			-29.3454								
53			0								
54			108.5								
55			100.797								
56			97.7277								
57			102.234								
58			101.731								
59			101.619								
60			100.4								

Table F-61

61	98.7798								
62	0								
63	0								
64	109.581	26	0.45312	0.06558	0	0.22603	0.00561	0.28706	0.27187
65	0								
66	110.055	26	0.45312	0.03363	0.05444	0.25768	0.00573	0.27779	0.25984
67	112.571	26	0.45312	0.23458	0	0.42578	0.00639	0.25553	0.22435
68	108.338	26	0.45312	0.02332	0	0.14293	0.00531	0.3282	0.32135
69	0								
70	113.099								
71	109.126								
72	110.989								
73	110.055								
74	114.647								
75	115.534								
76	102.901								
77	105.032								
78	107.727								
79	112.136								

Table F-62

Cover Temperature Map (Test 12-14_1)					
109.2997	108.1975	107.622	107.2604	108.3381	0
107.6101	107.9164	107.9711	108.5009	110.0551	112.5706
0	107.2207	106.1899	106.5511	109.5814	0
Average Surf T =		107.9504			

Table F-63

Cover Temp Difference Map (Test 12-14_1)						
37.69967	36.59749	36.02204	35.66038	36.73805	-71.6	
36.01005	36.31639	36.37106	36.90088	38.45505	40.9706	
-71.6	35.62065	34.58992	34.95111	37.98144	-71.6	
Average Delta T =	36.35037					

Table F-64

Cover Surf Coeff Map (Test 12-14_1)				
	0.273247	0.375787	0.396073	0.321353
	0.337733	0.338382	0.330518	0.259843
	0.361033	0.451799	0.512653	0.271869
Ave Surf Coeff. =	0.352524			
Standard Dev =	0.074627			

Temperature Distribution Surface Plot
Test: 12-14_1 (Front Half of Cover)

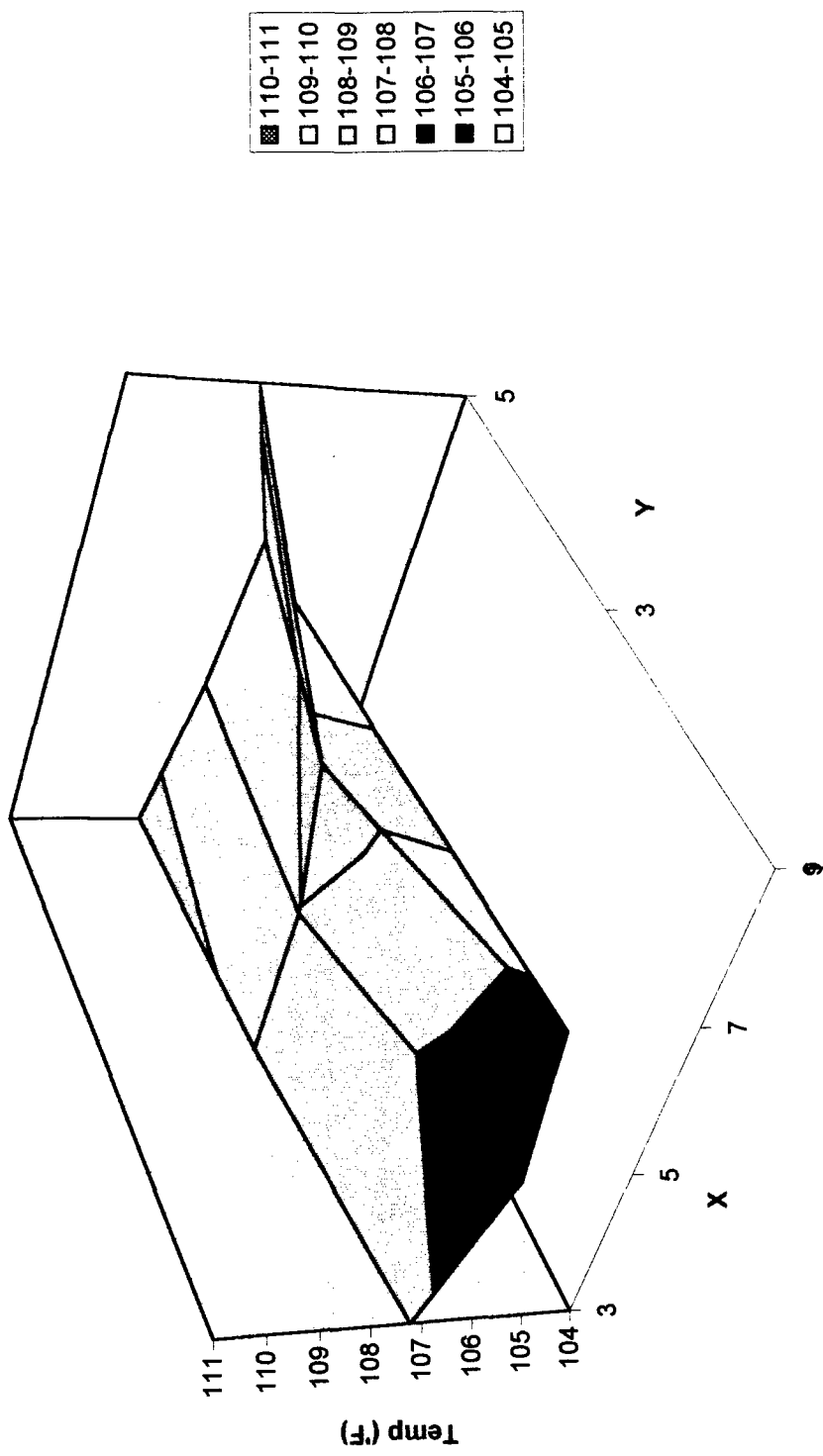


Figure F-21

Figure F-22

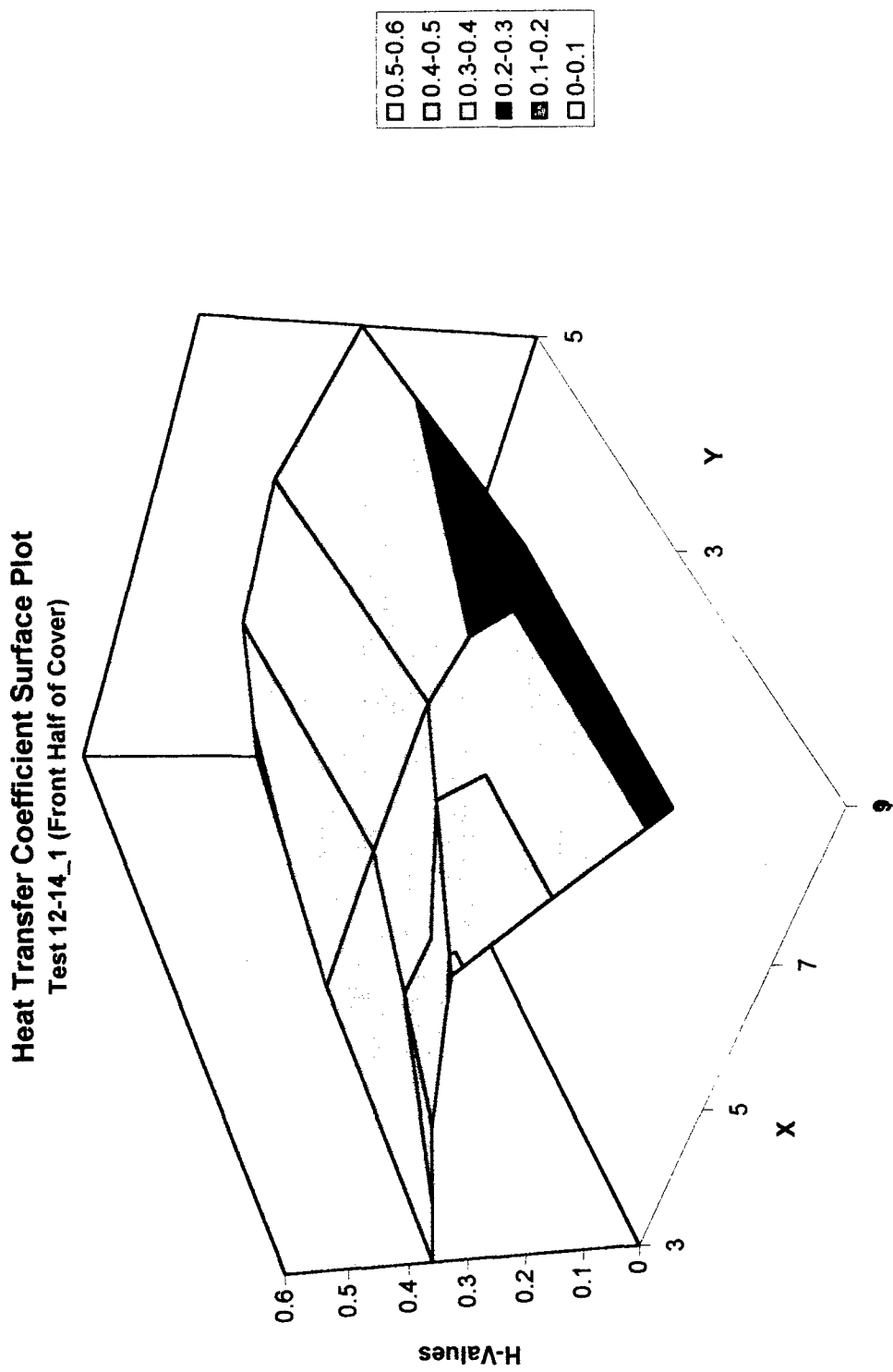


Table F-65

Output Filename ==> d:\scottstu\thesis\data\12-14_2a.cal

(Created from input file ==> a:12-14_2.dat)

Current Date: Thursday, December 14, 1995

Current Time: 16:58 hrs

User Name: S.LeClair

Input Current ==> 2.21 amps
Model Rotation ==> 90.0 deg's
Airstream Velocity ==> 0.00 fpm
Airstream Temp ==> 70.5 deg F

Sensor Num	Resist (ohms)	Temp (deg 'F)
1	53.6829990	86.555420
2	53.8470000	86.938927
3	53.8480000	86.703461
4	53.7820010	86.347946
5	53.7830010	86.284935
6	53.9809990	87.963104
7	53.8480000	86.989006
8	53.7599980	86.365822
9	53.7640000	86.695900
10	53.9000020	87.173531
11	53.4570010	86.819023
12	53.4539990	86.336380
13	53.7099990	86.266304
14	54.0309980	86.879494
15	53.8349990	86.979622
16	53.0439990	80.733177
17	53.2700000	81.205292
18	53.1769980	81.430428
19	53.6600000	81.925125
20	53.1530000	81.238281
21	53.3489990	75.534172
22	53.0180020	80.299416
23	53.3699990	81.018234
24	53.1699980	81.755295
25	53.6740000	82.754494
26	53.3139990	80.877670
27	53.4039990	83.163803
28	53.1839980	80.025276
29	53.9910010	84.578316
30	0.0000000	0.000000
31	53.9900020	84.996834
32	0.0000000	0.000000
33	54.0320010	87.115250
34	54.2500000	88.260963
35	54.3310010	88.313385

Table F-65

36	54.2690010	91.692947
37	54.8750000	90.932274
38	53.9900020	86.774078
39	53.9420010	86.093117
40	54.5070000	87.286316
41	54.3880000	89.898071
42	54.3349990	87.070045
43	54.3370020	89.543655
44	0.0000000	0.000000
45	54.0180020	88.081062
46	54.3960000	89.404938
47	54.4739990	89.392891
48	54.4850010	86.193085
49	54.4420010	86.998749
50	55.0550000	89.870972
51	54.0989990	84.584694
52	0.0000000	-29.345400
53	0.0000000	0.000000
54	54.2360000	87.052307
55	54.2360000	82.681328
56	53.7809980	80.543007
57	54.0849990	82.732750
58	54.1870000	82.011658
59	54.0250020	82.420204
60	54.1580010	81.802658
61	53.8559990	81.071747
62	0.0000000	0.000000
63	0.0000000	0.000000
64	54.1160010	87.640160
65	0.0000000	0.000000
66	54.2070010	87.773247
67	54.4259990	89.411514
68	54.1189990	87.031593
69	0.0000000	0.000000
70	54.2599980	88.840263
71	53.6790010	87.780815
72	54.1110000	88.158318
73	54.1539990	88.179100
74	54.1500020	89.941528
75	54.5089990	90.297501
76	53.4129980	83.628395
77	53.6870000	85.049881
78	54.1810000	87.715729
79	54.1259990	89.135902

Table F-66

Test File: 12-14_2.cal											
	airstream velocity =	0 fpm					total wattage =	52.065			
	airstream temp =	70.5 °F									
	model rotation =	90 deg (ccw)									
sensor#	x-value	y-value	temp (°F)	k,ss	gen	cond,1	cond,2	cond,b	rad	conv	h
0			0								
1			86.5554	26	0.18671	0	-0.0041	0.01808	0.0015	0.16304	0.36527
2			86.9389	26	0.18671	0	-0.0051	0.0437	0.00154	0.13637	0.29839
3			86.7035	26	0.18671	-0.0051	0.0025	0.02797	0.00151	0.15463	0.34328
4			86.3479		0.18671						
5			86.2849		0.18671						
6			87.9631	26	0.18671	0	-0.02108	0.11215	0.00167	0.05181	0.10672
7			86.989	26	0.18671	-0.02108	-0.01412	0.04705	0.00155	0.10291	0.22449
8			86.3658	26	0.18671	-0.0041	0.00714	0.00541	0.00147	0.18287	0.41461
9			86.6959	26	0.18671	0.00714	0.02043	0.02746	0.00151	0.18531	0.41158
10			87.1735	26	0.18671	0.00767	0.01298	0.05938	0.00157	0.14641	0.31585
11			86.819	26	0.18671	0.0025	0.00767	0.03569	0.00153	0.15966	0.35194
12			86.3364	26	0.18671	-0.00025	-0.00152	0.00344	0.00147	0.18004	0.40894
13			86.2663	26	0.18671	-0.00152	0.01656	-0.00125	0.00146	0.20154	0.45982
14			86.8795								
15			86.9796								
16			80.7332								
17			81.2053								
18			81.4304								
19			81.9251								
20			81.2383								
21			75.5342								
22			80.2994								
23			81.0182								
24			81.7553								
25			82.7545								
26			80.8777								
27			83.1638								
28			80.0253								
29			84.5783								
30			0								
31			84.9968								
32			0								
33			87.1153								
34			88.261								
35			88.3134								
36			91.6929								
37			90.9323								
38			86.7741								
39			86.0931								
40			87.2863								
41			89.8981								
42			87.07								
43			89.5437								
44			0								
45			88.0811								
46			89.4049								
47			89.3929								
48			86.1931								
49			86.9987								
50			89.871								
51			84.5847								
52			-29.3454								
53			0								
54			87.0523								
55			82.6813								
56			80.543								
57			82.7328								
58			82.0117								
59			82.4202								
60			81.8027								

Table F-66

61		81.0717							
62		0							
63		0							
64		87.6402	26	0.18671	0.02043	0	0.09057	0.00163	0.11495
65		0							0.24123
66		87.7732	26	0.18671	0.01298	0.03545	0.09946	0.00165	0.13403
67		89.4115	26	0.18671	0.16014	0	0.20894	0.00187	0.13604
68		87.0316	26	0.18671	0.01656	0	0.0499	0.00156	0.15182
69		0							
70		88.8403							
71		87.7808							
72		88.1583							
73		88.1791							
74		89.9415							
75		90.2975							
76		83.6284							
77		85.0499							
78		87.7157							
79		89.1359							

Table F-67

Cover Temperature Map (Test 12-14_2)					
87.9631	86.98901	86.33638	86.26663	87.03159	0
86.93893	86.70346	86.81902	87.17353	87.77325	89.41151
0	86.55542	86.36582	86.6959	87.64016	0
Average Surf T =	86.86249				

Table F-68

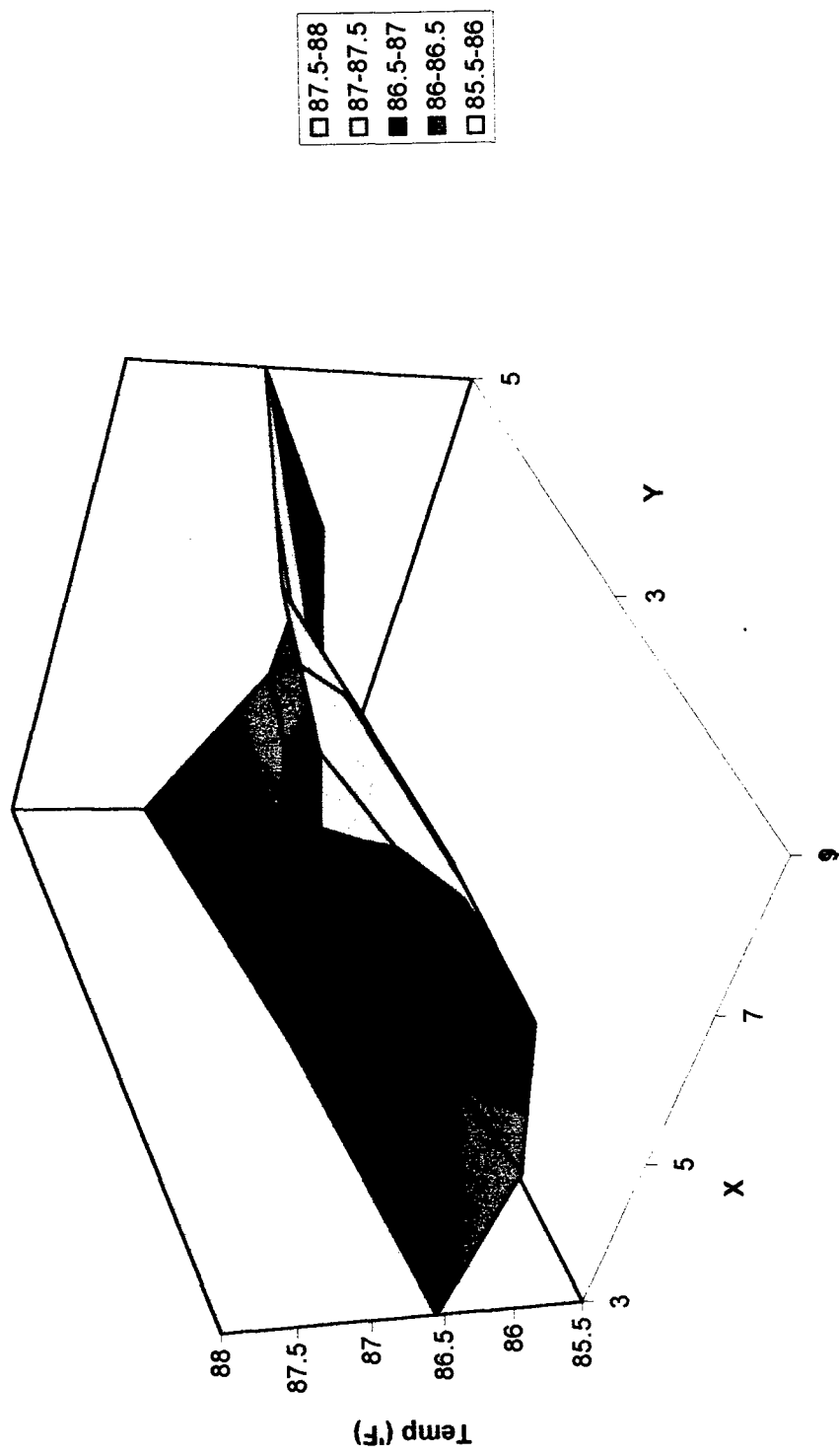
Cover Surf Coeff Map (Test 12-14_2)				
	0.224492	0.40894	0.459818	0.330345
	0.343279	0.351937	0.315852	0.279121
	0.365272	0.414611	0.411577	0.241233
Ave Surf Coeff. =	0.34554			
Standard Dev =	0.072427			

Table F-69

Cover Surf Coeff Map (Test 12-14_2)				
	0.224492	0.40894	0.459818	0.330345
	0.343279	0.351937	0.315852	0.279121
	0.365272	0.414611	0.411577	0.241233
Ave Surf Coeff. =	0.34554			
Standard Dev =	0.072427			

Figure F-23

Temperature Distribution Surface Plot
Test: 12-14_2 (Front Half of Cover)



Heat Transfer Coefficient Surface Plot
Test 12-14_2 (Front Half of Cover)

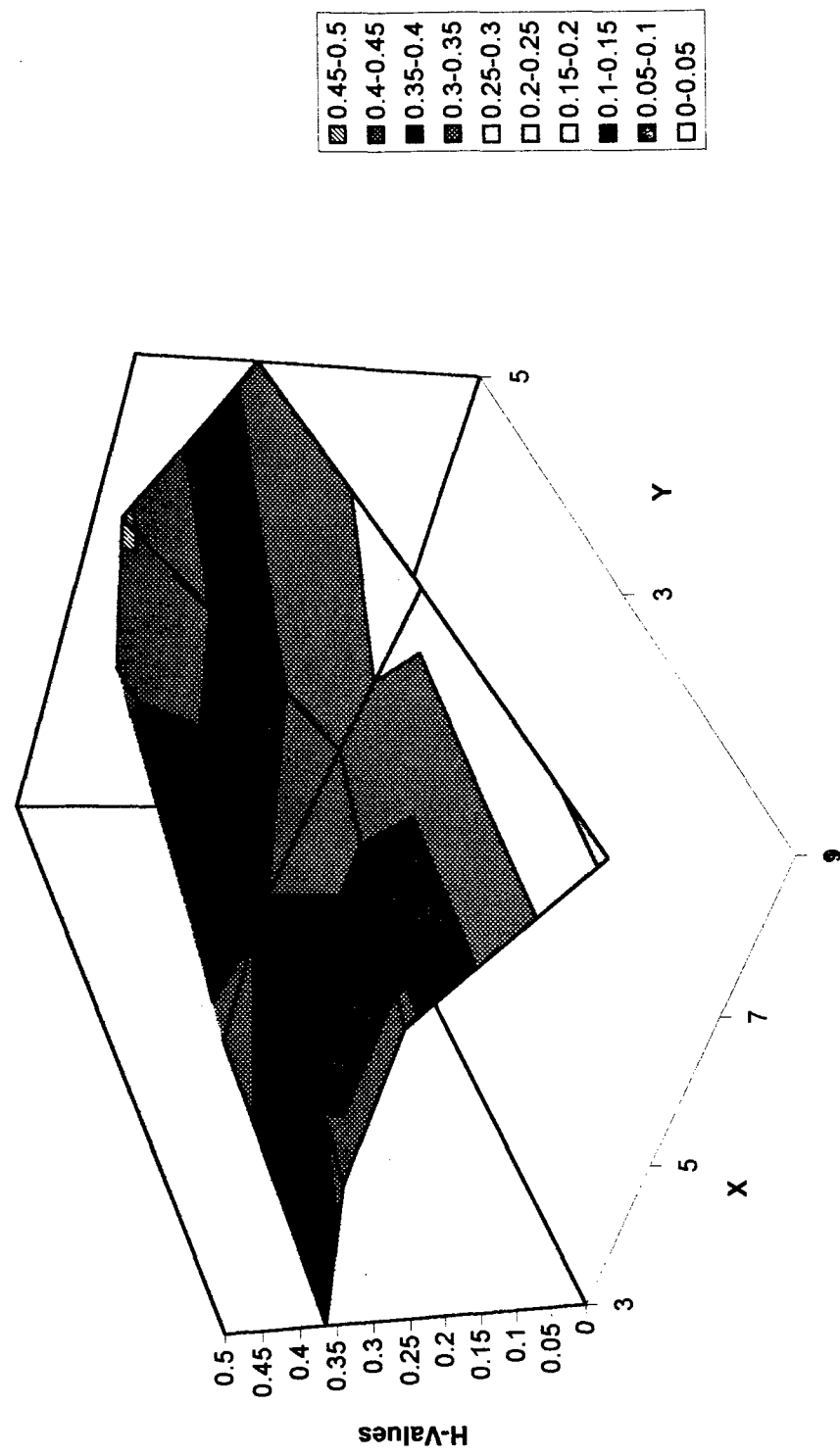


Figure F-24

Table F-70

Output Filename ==> c:\scottstu\thesis\data\01-31_1.cal

(Created from input file ==> a:\thesis\data\01-31_1.dat)

Current Date: Wednesday, January 31, 1996

Current Time: 12: 9 hrs

User Name: S.LeClair

Input Current ==> 5.42 amps
Model Rotation ==> 0.0 deg's
Airstream Velocity ==> 660.00 fpm
Airstream Temp ==> 89.8 deg F

Sensor Num	Resist (ohms)	Temp (deg 'F)
1	56.3040010	105.361618
2	56.9939990	108.447075
3	56.3849980	104.885193
4	56.0700000	102.042633
5	56.0250020	101.726608
6	57.2140010	110.238838
7	56.4150010	104.605026
8	56.2350010	103.365250
9	55.8909990	101.877502
10	55.9980010	101.509666
11	55.8009990	102.921906
12	55.7029990	102.154182
13	55.7070010	100.283386
14	55.9809990	100.879753
15	55.7550010	100.406288
16	55.7579990	99.594200
17	56.0530010	100.470642
18	55.8580020	100.443893
19	56.4970020	101.785141
20	55.8130000	100.120934
21	56.1100010	93.879036
22	55.8200000	100.419670
23	56.1030010	100.177299
24	55.7599980	100.807579
25	56.3750000	102.118866
26	55.8499980	99.836723
27	55.9739990	101.192635
28	55.1590000	93.882103
29	56.1920010	99.720894
30	0.0000000	0.000000
31	56.1510010	100.645859
32	0.0000000	0.000000
33	55.9669990	101.240425
34	56.2970010	102.513199
35	56.4599990	102.802643

Table F-70

36	56.5540010	108.125298
37	57.5200000	108.933800
38	56.7649990	105.869049
39	55.9939990	100.224663
40	56.6780010	101.953979
41	56.3190000	103.442284
42	56.5439990	102.472511
43	56.8919980	107.528633
44	0.0000000	0.000000
45	56.2160000	103.973091
46	57.1570010	108.209671
47	57.1030010	107.738098
48	56.7809980	102.770737
49	56.1090010	98.950729
50	57.1030010	104.263000
51	56.4560010	101.918488
52	0.0000000	-29.345400
53	0.0000000	0.000000
54	56.0639990	100.015564
55	56.5859990	99.247757
56	55.3940010	91.858093
57	56.5099980	100.969627
58	56.7690010	99.926216
59	56.6559980	102.008560
60	56.9030000	101.255821
61	56.5980000	100.210091
62	0.0000000	0.000000
63	0.0000000	0.000000
64	56.1880000	102.067116
65	0.0000000	0.000000
66	56.1910020	101.745583
67	57.0099980	107.630692
68	56.1199990	100.765327
69	0.0000000	0.000000
70	56.9860000	107.482811
71	55.7710000	102.718857
72	56.4720000	104.326286
73	56.2150000	103.195236
74	56.5779990	106.690430
75	57.0169980	107.439445
76	55.6670000	99.061394
77	56.5519980	104.880684
78	56.2729990	101.954742
79	56.3149990	104.063805

Table F-71

Test File:		01-31_1									
airstream velocity =		660 fpm									
airstream temp =		89.78 °F									
model rotation =		0 deg (ccw)									
sensor#	x-value	y-value	temp (°F)	K,ss	gen	cond,1	cond,2	cond,b	rad	conv	h
0		0									
1		105.362	26	1.1093	0	-0.0432	0.24292	0.0823	0.74088	1.71036	
2		108.447	26	1.1093	0	-0.07708	0.44911	0.09943	0.48368	0.93205	
3		104.885	26	1.1093	0.07708	-0.04249	0.21108	0.07968	0.85313	2.03163	
4		102.043		1.1093							
5		101.727		1.1093							
6		110.239	26	1.1093	0	-0.12192	0.56885	0.1095	0.30903	0.54334	
7		104.605	26	1.1093	0.12192	-0.05304	0.19236	0.07815	0.90768	2.20238	
8		103.365	26	1.1093	0.0432	-0.0322	0.10951	0.07137	0.93943	2.48744	
9		101.878	26	1.1093	0.0322	0.0041	0.01008	0.0633	1.07222	3.18817	
10		101.51	26	1.1093	0.03056	0.00511	-0.0145	0.06131	1.09815	3.36769	
11		102.922	26	1.1093	0.04249	-0.03056	0.07988	0.06896	0.97239	2.66156	
12		102.154	26	1.1093	-0.00241	-0.04049	0.02857	0.06479	0.97303	2.82856	
13		100.283	26	1.1093	0.04049	0.01043	-0.09645	0.05472	1.20194	4.11632	
14		100.88									
15		100.406									
16		99.5942									
17		100.471									
18		100.444									
19		101.785									
20		100.121									
21		93.879									
22		100.42									
23		100.177									
24		100.808									
25		102.119									
26		99.8367									
27		101.193									
28		93.8821									
29		99.7209									
30		0									
31		100.646									
32		0									
33		101.24	26	1.1093	0	0.02666	-0.04768	0.05986	1.12379	3.52727	
34		102.513	26	1.1093	0.01476	0.00626	0.03732	0.06674	1.02626	2.89919	
35		102.803	26	1.1093	-0.00626	0	-0.08428	0.06831	1.119	3.09092	
36		108.125	26	1.1093	-0.01484	0.0175	0.27142	0.09763	0.74291	1.45668	
37		108.934	26	1.1093	-0.0175	-0.01567	0.36698	0.10216	0.60699	1.13995	
38		105.869									
39		100.225									
40		101.954									
41		103.442									
42		102.473	26	1.1093	-0.02666	0.10942	0.03465	0.06652	1.09088	3.09162	
43		107.529	26	1.1093	-0.10942	0	0.09547	0.0943	0.81011	1.64185	
44		0	0	0	0	0	0	0			
45		103.973	26	1.1093	0	0	-0.14213	0.07469	1.17675	2.98237	
46		108.21	26	1.1093	0.01567	-0.01021	0.31859	0.0981	0.69807	1.36251	
47		107.738	26	1.1093	0.01021	0	0.10947	0.09547	0.91457	1.83193	
48		102.771									
49		98.9507									
50		104.263									
51		101.918									
52		-29.3454									
53		0									
54		100.016									
55		99.2478									
56		91.8581									
57		100.97									
58		99.9262									
59		102.009									
60		101.256									

Table F-71

61	100.21								
62	0								
63	0								
64	102.067	26	1.1093	-0.0041	0	0.02276	0.06432	1.01812	2.9806
65	0								
66	101.746	26	1.1093	-0.00511	0.12736	0.00127	0.06258	1.1677	3.51036
67	107.631	26	1.1093	-0.12736	0	0.39455	0.09487	0.49252	0.99248
68	100.765	26		-0.01043	0	-0.06424	0.0573	1.1058	3.62093
69	0								
70	107.483	26	1.1093	0	-0.1031	0.09241	0.09405	0.81975	1.66569
71	102.719	26	1.1093	0.1031	0	0.05106	0.06785	1.09348	3.03996
72	104.326	26	1.1093	0	-0.02448	-0.11853	0.07662	1.12674	2.78628
73	103.195	26	1.1093	0.02448	0	0.0829	0.07044	0.98043	2.6289
74	106.69	26	1.1093	0	0.01621	0.03946	0.08964	0.99641	2.11952
75	107.439	26	1.1093	-0.01621	0	0.36653	0.0938	0.63276	1.28889
76	99.0614								
77	104.881								
78	101.955								
79	104.064								

Table F-72

Cover Temperature Map (Test 01-31_1)		
	108.4471	110.2388
105.3616	104.8852	104.605
103.3653	102.9219	102.1542
101.8775	101.5097	100.2834
102.0671	101.7456	100.7653
0	107.6307	0
Average Surf T =		102.6285

Table F-73

Cover Temp Difference Map (Test 01-31_1)		
	18.66708	20.45884
15.58162	15.10519	14.82503
13.58525	13.14191	12.37418
12.0975	11.72967	10.50339
12.28712	11.96558	10.98533
-89.78	17.85069	-89.78
Average Delta T =		12.84848

Table F-74

Cover Surf Coeff Map (Test 01-31_1)		
1.710364	2.031632	2.202379
2.487438	2.661561	2.828563
3.188174	3.367689	4.116318
2.980596	3.510363	3.620931
Ave Surf Coeff. =	2.892167	

Table F-75

Front Surface Coeff Map (Test 01-31_1)					
1.665686	3.039965	0	3.527265	3.091619	1.641848
2.786282	2.628904	2.899189	3.090922	0	2.982369
2.119519	1.288891	1.45668	1.139947	1.362506	1.831934
Bottom					
Ave H =	2.284596				
StDev =	0.796525				

Temperature Distribution Surface Plot
Test: 01-31_1 (Left Half of Cover)

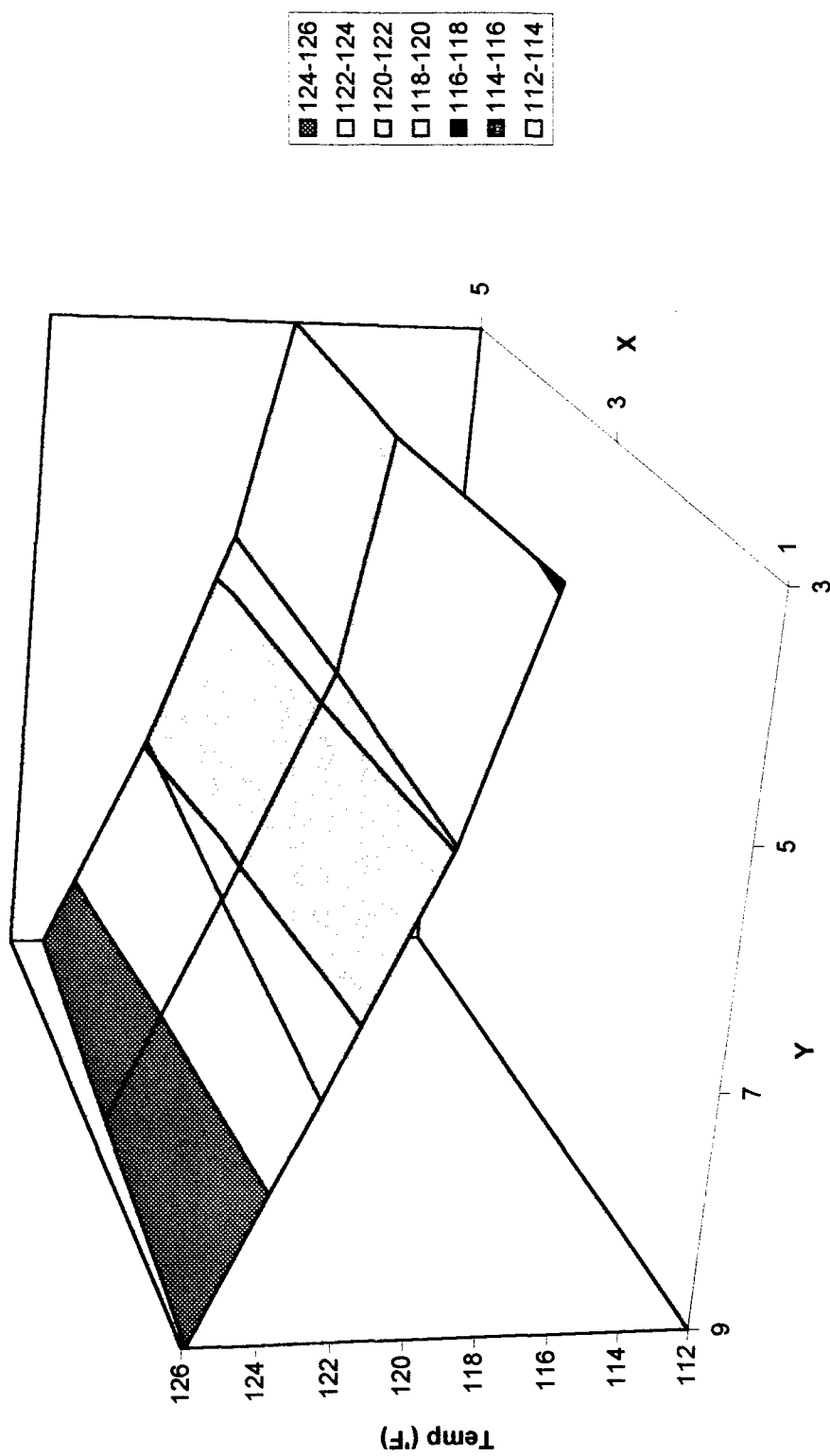


Figure F-25

Heat Transfer Coefficient Surface Plot
Test: 01-31_1 (Left Half of Cover)

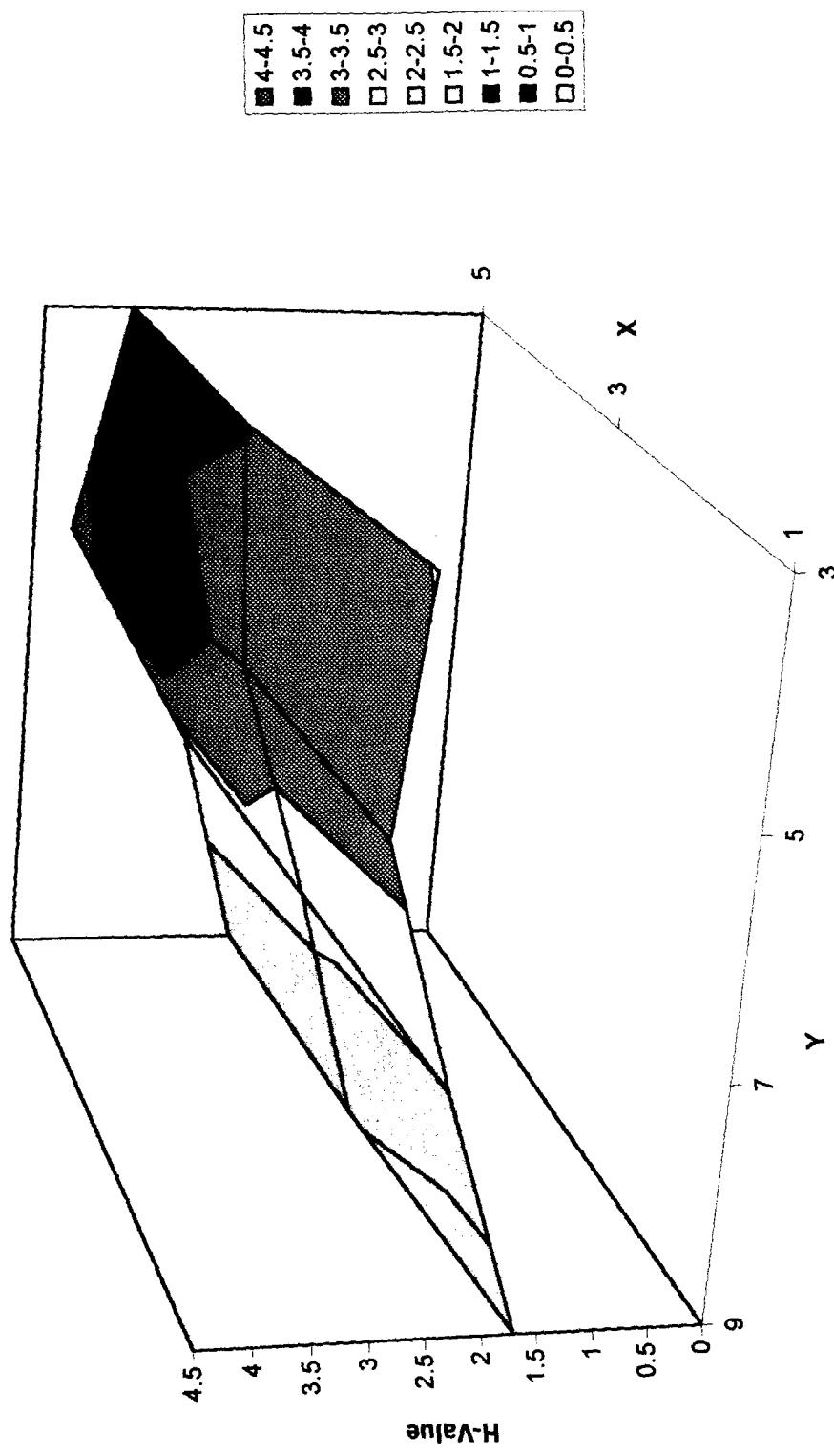


Figure F-26

Table F-76

Output Filename ==> c:\scottstu\thesis\data\02-01_1.cal

(Created from input file ==> c:\scottstu\thesis\data\02-01_1.dat)

Current Date: Thursday, February 1, 1996

Current Time: 14: 5 hrs

User Name: S.LeClair

Input Current ==> 5.42 amps
Model Rotation ==> 180.0 deg's
Airstream Velocity ==> 660.00 fpm
Airstream Temp ==> 89.4 deg F

Sensor Num	Resist (ohms)	Temp (deg 'F)
1	55.3930020	98.869278
2	56.1590000	102.792168
3	55.5989990	99.290726
4	55.6430020	99.135353
5	55.5900000	98.752243
6	56.4370000	104.936958
7	55.6650010	99.494957
8	55.7690010	100.190117
9	56.0000000	102.649536
10	56.1150020	102.301659
11	55.3829990	100.072403
12	55.3260000	99.521988
13	55.8260000	101.111389
14	56.4590000	104.279175
15	56.0820010	102.672867
16	55.6339990	98.740486
17	55.9150010	99.524574
18	55.7190020	99.468239
19	56.4049990	101.147362
20	55.7109990	99.404854
21	56.1160010	93.918541
22	55.6479990	99.197784
23	55.9269980	98.955742
24	55.6489980	99.998535
25	56.2379990	101.147202
26	55.7309990	98.955643
27	55.8270000	100.170662
28	55.0009990	92.781052
29	55.9850010	98.308243
30	0.0000000	0.000000
31	55.9870000	99.467033
32	0.0000000	0.000000
33	57.4459990	111.891739
34	57.5369990	111.033630
35	57.6339990	110.687660

Table F-76

36	57.1339990	112.248810
37	57.9860000	112.066147
38	57.9860000	114.137558
39	58.1349980	114.723267
40	57.8919980	110.044273
41	57.2980000	110.230515
42	58.5579990	116.279160
43	60.1430020	128.862793
44	0.0000000	0.000000
45	58.8800010	122.474266
46	58.0719990	114.351227
47	59.1580010	121.568321
48	58.8030010	117.121124
49	58.5940020	116.474731
50	57.0149990	103.649025
51	56.3559990	101.189964
52	0.0000000	-29.345400
53	0.0000000	0.000000
54	55.9710010	99.360405
55	56.4850010	98.542183
56	55.2529980	90.874313
57	56.3660010	99.896332
58	56.6069980	98.813263
59	56.4980010	100.844101
60	56.7589990	100.245758
61	56.4129980	98.931496
62	0.0000000	0.000000
63	0.0000000	0.000000
64	56.7579990	105.993614
65	0.0000000	0.000000
66	56.6740000	105.114204
67	57.4129980	110.438629
68	56.5379980	103.607590
69	0.0000000	0.000000
70	60.3520010	128.980667
71	57.6740000	116.092781
72	59.5620000	124.517410
73	57.8340000	114.817360
74	59.7579990	127.603386
75	58.4389990	117.006866
76	59.0980000	121.871880
77	57.9640010	114.489136
78	57.4580000	109.916458
79	56.8349990	107.571404

Table F-77

Test File: 02-01_1											
	airstream velocity =	660 fpm					total wattage =	312.565			
	airstream temp =	89.4 °F									
	model rotation =	180 deg (ccw)					Side Int Temp =	117 °F			
sensor#	x-value	y-value	temp (°F)	k,ss	gen	cond,1	cond,2	cond,b	rad	conv	h
0			0								
1			98.8693	26	1.12089	0	0.02858	0.00782	0.04909	1.09256	4.15034
2			102.792	26	1.12089	0	-0.07577	0.26998	0.07017	0.70496	1.89353
3			99.2907	26	1.12089	0.07577	0.01692	0.03599	0.05134	1.12626	4.09605
4			99.1354		1.12089						
5			98.7522		1.12089						
6			104.937	26	1.12089	0	-0.11777	0.41331	0.08189	0.50793	1.17595
7			99.495	26	1.12089	0.11777	0.00058	0.04963	0.05242	1.13718	4.05211
8			100.19	26	1.12089	-0.02858	0.05322	0.09609	0.05614	0.9933	3.31138
9			102.65	26	1.12089	-0.05322	0.07237	0.26044	0.0694	0.81019	2.19959
10			102.302	26	1.12089	-0.04824	0.06087	0.2372	0.06751	0.8288	2.31079
11			100.072	26	1.12089	-0.01692	0.04824	0.08822	0.05551	1.00848	3.39908
12			99.522	26	1.12089	-0.00837	0.0344	0.05144	0.05257	1.04291	3.70626
13			101.111	26	1.12089	-0.0344	0.05402	0.15765	0.06109	0.92177	2.83119
14			104.279								
15			102.673								
16			98.7405								
17			99.5246								
18			99.4682								
19			101.147								
20			99.4049								
21			93.9185								
22			99.1978								
23			98.9557								
24			99.9985								
25			101.147								
26			98.9556								
27			100.171								
28			92.7811								
29			98.3082								
30			0								
31			99.467								
32			0								
33			111.892	26	1.12089	0	0.09495	0.12346	0.1208	0.97157	1.55384
34			111.034	26	1.12089	0.08188	-0.00749	0.07466	0.11592	1.0047	1.67057
35			110.688	26	1.12089	0.00749	0	0.20825	0.11396	0.80616	1.36223
36			112.249	26	1.12089	0.10297	-0.00395	0.31258	0.12284	0.78449	1.23503
37			112.066	26	1.12089	0.00395	0.04945	0.12267	0.12118	0.92983	1.47563
38			114.138								
39			114.723								
40			110.044								
41			110.231								
42			116.279	26	1.12089	-0.09495	0.27232	0.41666	0.14609	0.73551	0.9843
43			128.863	26	1.12089	-0.27232	0	0.79275	0.22119	-0.16609	0.15139
44			0	0	0	0	0	0			
45			122.474	26	1.12089	0	0	0.36583	0.1828	0.57226	0.62238
46			114.351	26	1.12089	-0.04945	0.15618	0.27537	0.13491	0.81734	1.17832
47			121.568	26	1.12089	-0.15618	0	0.30529	0.17736	0.48206	0.53905
48			117.121								
49			116.475								
50			103.649								
51			101.19								
52			-29.3454								
53			0								
54			99.3604								
55			98.5422								
56			90.8743								
57			99.8963								
58			98.8133								
59			100.844								
60			100.246								

Table F-77

61		98.9315								
62		0								
63		0								
64		105.994	26	1.12089	-0.07237	0	0.48392	0.08771	0.47689	1.0338
65		0								
66		105.114	26	1.12089	-0.06087	0.11522	0.42515	0.08286	0.66723	1.52736
67		110.439	26	1.12089	-0.11522	0	0.78097	0.11255	0.11214	0.19174
68		103.608	26		-0.05402	0	0.32447	0.07461	0.66779	1.69073
69		0								
70		128.981	26	1.12089	0	-0.2789	0.80063	0.22264	-0.18128	0.16475
71		116.093	26	1.12089	0.2789	0	0.41274	0.14501	0.84204	1.13473
72		124.517	26	1.12089	0	-0.20992	0.50237	0.19517	0.21344	0.21863
73		114.817	26	1.12089	0.20992	0	0.32751	0.1376	0.86569	1.22514
74		127.603	26	1.12089	0	-0.22932	0.70859	0.21409	-0.03111	0.02929
75		117.007	26	1.12089	0.22932	0	0.47383	0.15034	0.72603	0.946
76		121.872								
77		114.489								
78		109.916								
79		107.571								

Table F-78

Cover Temperature Map (Test 02-01_1)					
		0	110.4386	0	
		103.6076	105.1142	105.9936	
		101.1114	102.3017	102.6495	
		99.52199	100.0724	100.1901	
		99.49496	99.29073	98.86928	
		104.937	102.7922		
Average Surf T =	101.5181				

Table F-79

Cover Temp Difference Map (Test 02-01_1)					
			-89.4	21.03863	-89.4
			14.20759	15.7142	16.59361
			11.71139	12.90166	13.24954
			10.12199	10.6724	10.79012
			10.09496	9.890726	9.469278
			15.53696	13.39217	-89.4
Average Delta T =	12.11812				

Table F-80

Cover Surf Coeff Map (Test 02-01_1)			
		1.690729 1.527359	1.033796
		2.831195 2.310787	2.199586
		3.706258 3.399079	3.311379
		4.052114 4.096046	4.150338
Ave Surf Coeff. =	2.859056		

Table F-81

Rear Surface Coeff Map (Test 02-01_1)					
0.16475	1.134733	1.34	1.553843	0.984299	0.151392
0.218629	1.225143	1.670565	1.362228	0.991	0.622382
0.029294	0.946003	1.23503	1.475635	1.178324	0.539047
Bottom					
Ave H =	0.905706				

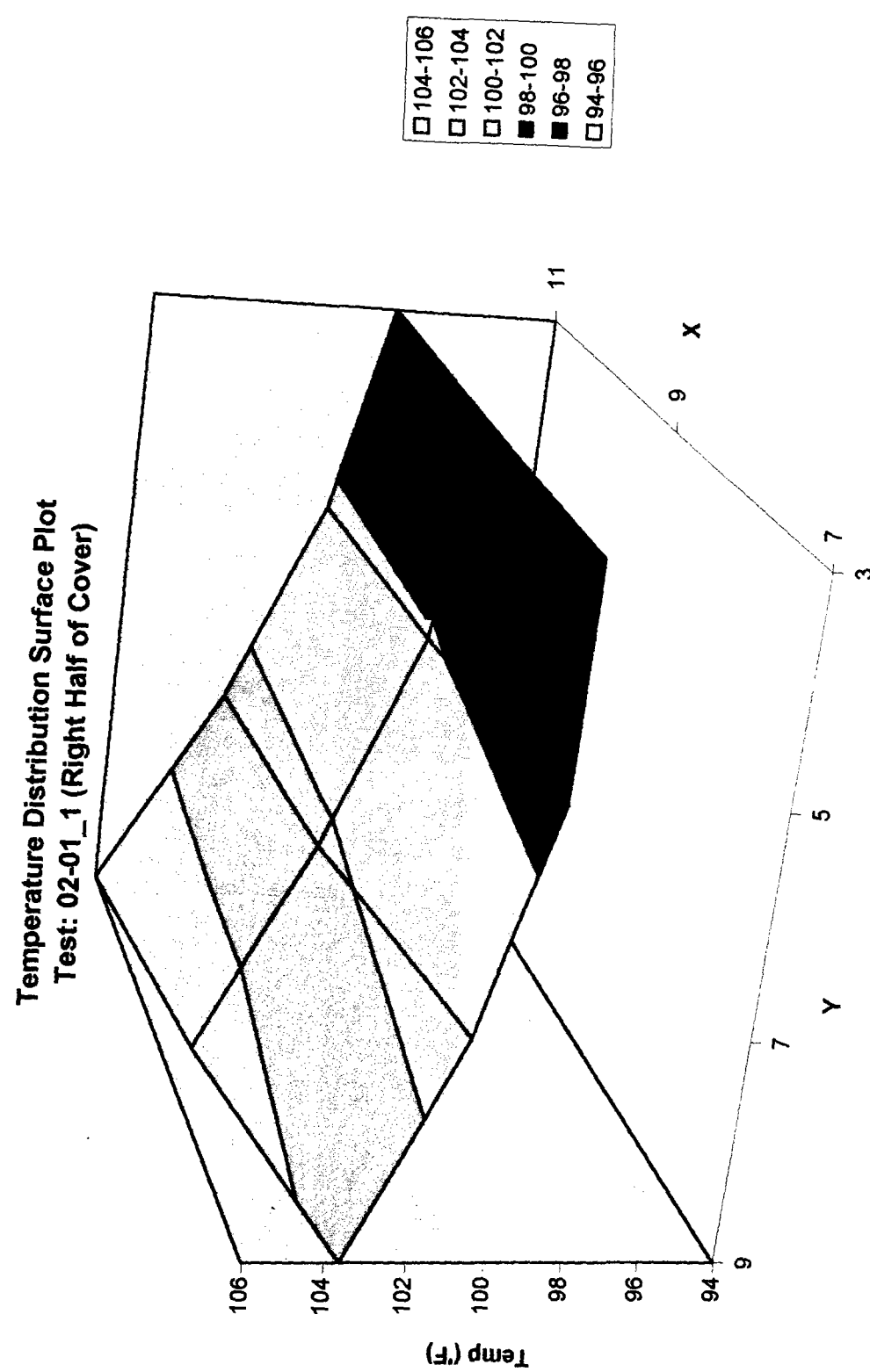


Figure F-27

**Heat Transfer Coefficient Surface Plot
Test: 02-01_1 (Right Half of Cover)**

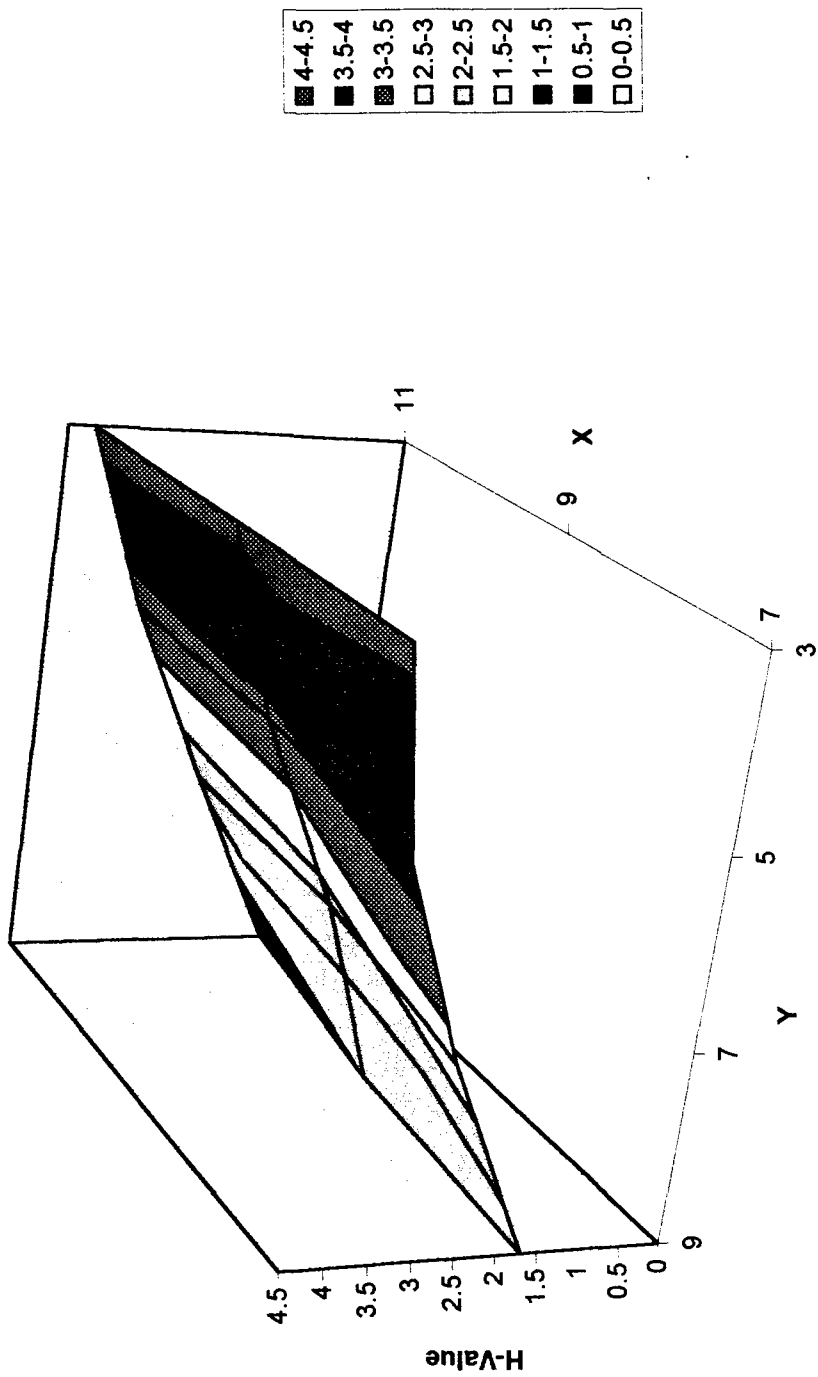


Figure F-28

Table F-82

Output Filename ==> c:\scottstu\thesis\data\02-21_1.cal

(Created from input file ==> c:\scottstu\thesis\data\02-21_1.dat)

Current Date: Wednesday, February 21, 1996

Current Time: 21:45 hrs

User Name: S.LeClair

Input Current ==> 4.22 amps
Model Rotation ==> 270.0 deg's
Airstream Velocity ==> 660.00 fpm
Airstream Temp ==> 92.3 deg F

Sensor Num	Resist (ohms)	Temp (deg 'F)
1	55.7260020	101.247871
2	55.8969990	101.010208
3	55.6810000	99.875931
4	55.6460000	99.156303
5	55.4459990	97.764999
6	55.9280010	101.446793
7	55.5369990	98.619667
8	55.8540000	100.770370
9	55.7700000	101.021622
10	55.7210010	99.630402
11	55.3139990	99.601501
12	55.0999980	97.940315
13	55.3190000	97.576897
14	55.8870010	100.209518
15	55.4590000	98.349838
16	55.3390010	96.708679
17	55.6520000	97.721008
18	55.3289990	96.724739
19	55.9650000	98.094360
20	55.3340000	96.750069
21	55.6250000	90.685501
22	55.4939990	98.101463
23	55.7480010	97.712814
24	55.3069990	97.503136
25	55.8489990	98.380081
26	55.4339980	96.752960
27	55.4830020	97.776085
28	55.0919990	93.415703
29	55.7809980	96.913483
30	0.0000000	0.000000
31	55.6360020	96.940033
32	0.0000000	0.000000
33	55.4510000	97.495567
34	55.7589990	98.789711
35	55.7599980	98.066406

Table F-82

36	55.6380000	101.573524
37	56.3550000	101.052551
38	55.9770010	100.489563
39	56.2509990	101.977959
40	56.0639990	97.831070
41	55.9290010	100.723557
42	55.9329990	98.238708
43	56.5950010	105.456932
44	0.0000000	0.000000
45	55.9720000	102.222908
46	55.9770010	100.223343
47	56.6189990	104.388947
48	56.5130000	100.851662
49	55.9329990	97.696037
50	56.4980010	100.035591
51	55.9630010	98.319756
52	0.0000000	-29.345400
53	0.0000000	0.000000
54	55.6549990	97.131348
55	56.2050020	96.583206
56	55.3620000	91.634850
57	56.0369990	97.439957
58	56.2970010	96.678886
59	56.1300010	98.125107
60	56.3849980	97.617867
61	56.0779990	96.612511
62	0.0000000	0.000000
63	0.0000000	0.000000
64	56.2410010	102.432396
65	0.0000000	0.000000
66	56.0260010	100.591454
67	56.4339980	103.601845
68	55.7869990	98.495094
69	0.0000000	0.000000
70	56.5480000	104.514496
71	55.4370000	100.350357
72	56.0999980	101.799217
73	55.7929990	100.140060
74	56.2719990	104.597740
75	56.3610000	102.988235
76	55.6780010	99.136436
77	55.6139980	98.438004
78	55.8390010	99.020271
79	55.6250000	99.386314

Table F-83

Test File: 02-21_1.cal										
airstream velocity =	660	fpm				total wattage =				194.25
airstream temp =	92.3	'F								
model rotation =	270	deg (ccw)				Side Int Temp =				103.9 'F
sensor#	x-value	y-value	temp ('F)	k,ss	gen	cond,1	cond,2	cond,b	rad	conv
0			0							
1			101.248	26	0.6966	0	-0.01033	0.23275	0.04705	0.40646
2			101.01	26	0.6966	0	-0.02455	0.21687	0.04578	0.40941
3			99.8759	26	0.6966	0.02455	-0.00594	0.14107	0.03969	0.53445
4			99.1563		0.6966					
5			97.765		0.6966					
6			101.447	26	0.6966	0	-0.06118	0.24604	0.04813	0.34125
7			98.6197	26	0.6966	0.06118	-0.0147	0.05711	0.033	0.65297
8			100.77	26	0.6966	0.01033	0.00544	0.20084	0.04449	0.46704
9			101.022	26	0.6966	-0.00544	0.03053	0.21763	0.04584	0.45823
10			99.6304	26	0.6966	-0.00063	0.0208	0.12466	0.03838	0.55373
11			99.6015	26	0.6966	0.00594	0.00063	0.12273	0.03823	0.54221
12			97.9403	26	0.6966	0.02631	-0.00786	0.01172	0.0294	0.67394
13			97.5769	26	0.6966	0.00786	0.01987	-0.01257	0.02747	0.70943
14			100.21							
15			98.3498							
16			96.7087							
17			97.721							
18			96.7247							
19			98.0944							
20			96.7501							
21			90.6855							
22			98.1015							
23			97.7128							
24			97.5031							
25			98.3801							
26			96.753							
27			97.7761							
28			93.4157							
29			96.9135							
30			0							
31			96.94							
32			0							
33			97.4956	26	0.6966	0	0.01608	-0.02242	0.02705	0.70806
34			98.7897	26	0.6966	0.02922	-0.01565	-0.01541	0.0339	0.69168
35			98.0664	26	0.6966	0.01565	0	-0.08821	0.03006	0.77039
36			101.574	26	0.6966	0.03062	-0.01127	0.14616	0.04881	0.52097
37			101.053	26	0.6966	0.01127	-0.01794	0.02199	0.046	0.62194
38			100.49							
39			101.978							
40			97.8311							
41			100.724							
42			98.2387	26	0.6966	-0.01608	0.15621	0.02724	0.03098	0.77851
43			105.457	26	0.6966	-0.15621	0	0.10404	0.06998	0.36637
44			0	0	0	0	0	0		
45			102.223	26	0.6966	0	0	-0.11207	0.05232	0.75635
46			100.223	26	0.6966	0.01794	0.09015	-0.03343	0.04155	0.79657
47			104.389	26	0.6966	-0.09015	0	0.03267	0.06412	0.50966
48			100.852							
49			97.696							
50			100.036							
51			98.3198							
52			-29.3454							
53			0							
54			97.1313							
55			96.5832							
56			91.6349							
57			97.44							
58			96.6789							
59			98.1251							
60			97.6179							

Table F-83

61		96.6125							
62		0							
63		0							
64		102.432	26	0.6966	-0.03053	0	0.31191	0.05345	0.30071 1.06755
65		0							
66		100.591	26	0.6966	-0.0208	0.06515	0.18888	0.04352	0.50854 2.20623
67		103.602	26	0.6966	-0.06515	0	0.39006	0.05981	0.18158 0.57793
68		98.4951	26		-0.01987	0	0.04879	0.03234	0.5956 3.45831
69		0							
70		104.514	26	0.6966	0	-0.09011	0.04106	0.0648	0.50062 1.4743
71		100.35	26	0.6966	0.09011	0	0.08889	0.04223	0.6556 2.92939
72		101.799	26	0.6966	0	-0.03591	-0.14039	0.05003	0.75105 2.84406
73		100.114	26	0.6966	0.03591	0	0.07483	0.04111	0.61657 2.82889
74		104.598	26	0.6966	0	-0.03483	0.04663	0.06526	0.54988 1.60842
75		102.988	26	0.6966	0.03483	0	0.26517	0.05647	0.40979 1.37915
76		99.1364							
77		98.438							
78		99.0203							
79		99.3863							

Table F-84

Cover Temperature Map (Test 02-21_1)					
0	102.4324	101.0216	100.7704	101.2479	0
103.6018	100.5915	99.6304	99.6015	99.87593	101.0102
0	98.49509	97.5769	97.94032	98.61967	101.4468
Ave Surf Temp =	99.81696				

Table F-85

Cover Temp Difference Map (Test 02-21_1)					
-92.3	10.1324	8.721622	8.47037	8.947871	-92.3
11.30185	8.291454	7.330402	7.301501	7.575931	8.710208
-92.3	6.195094	5.276897	5.640315	6.319667	9.146793
Ave Temp Diff =	7.51696				

Table F-86

Cover Surf Coeff Map (Test 02-21_1)				
	1.067546	1.889895	1.983405	1.634013
	2.206226	2.717238	2.671228	2.53761
	3.458312	4.835997	4.298052	3.716652
Ave Surf Coeff =	2.751348			

Table F-87

Side Surface Coeff Map (Test 02-21_1)					
1.474297	2.92939	0	4.902192	4.715481	1.001649
2.844062	2.828894	3.833826	4.80577	0	2.741838 <-- Air
1.608418	1.379153	2.020785	2.556051	3.616341	1.516526
Left Side					
Ave =	2.633804				
StDev =	1.280981				

Figure F-29

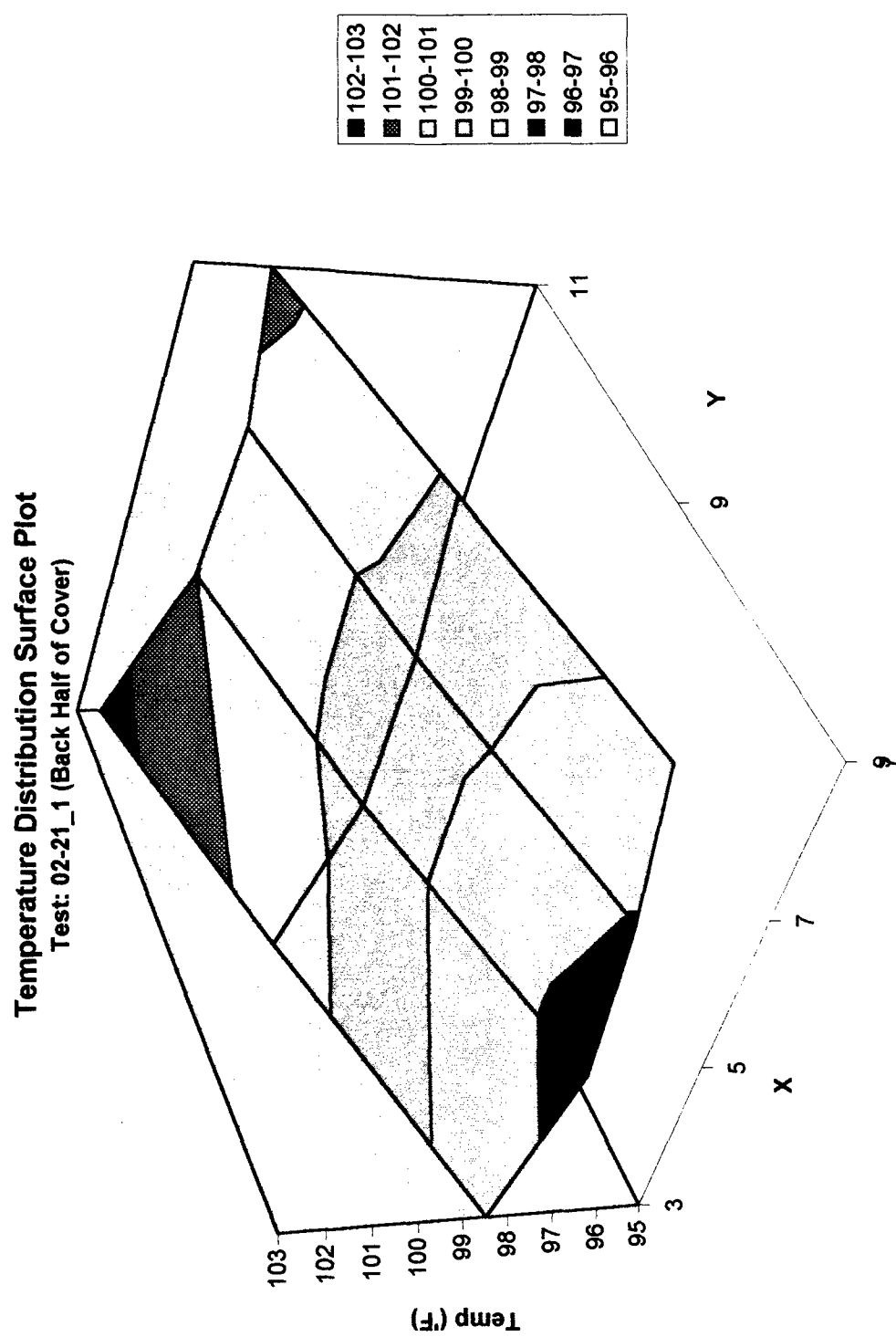


Figure F-30

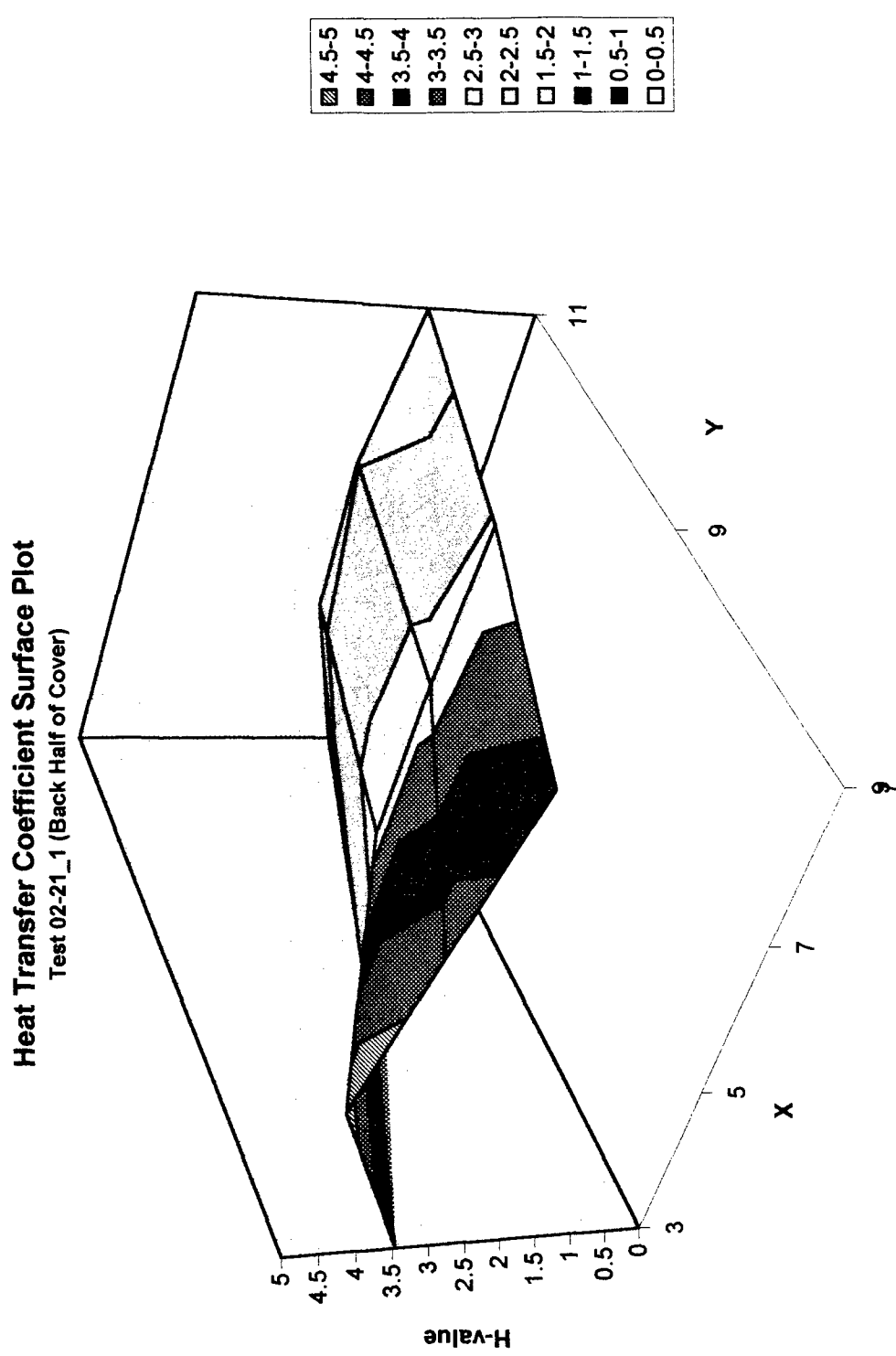


Table F-88

Output Filename ==> a:\data\02-27_1.cal

(Created from input file ==> a:\data\02-27_1.dat)

Current Date: Tuesday, February 27, 1996

Current Time: 15:30 hrs

User Name: S.LeClair

Input Current ==> 6.96 amps
Model Rotation ==> 270.0 deg's
Airstream Velocity ==> 660.00 fpm
Airstream Temp ==> 95.0 deg F

Sensor Num	Resist (ohms)	Temp (deg 'F)
1	59.5929990	127.467300
2	59.6730000	125.701073
3	59.2179990	124.197441
4	59.3730010	123.730583
5	58.9039990	120.919548
6	59.6230010	125.736137
7	58.8769990	120.933968
8	59.8470000	126.819580
9	59.6290020	127.078674
10	59.4210010	123.944435
11	58.9930000	123.863617
12	58.4240000	120.693550
13	58.6180000	120.098091
14	59.5760000	125.487602
15	58.8260000	121.160255
16	57.8559990	113.896088
17	58.5400010	117.328079
18	58.0219990	115.496445
19	58.9240000	118.420944
20	57.9850010	115.246063
21	58.4879990	109.357513
22	58.4090000	118.614807
23	58.6670000	117.776039
24	58.0009990	116.977287
25	58.8510020	119.505951
26	57.9660000	115.364815
27	58.2050020	116.545746
28	57.0730020	107.105347
29	58.5429990	115.605042
30	0.0000000	0.000000
31	58.3380010	116.209648
32	0.0000000	0.000000
33	57.9500010	115.491615
34	58.7999990	119.626526
35	58.7370000	118.029289

Table F-88

36	59.4889980	128.093323
37	60.1590000	125.940300
38	60.2579990	128.634811
39	60.7640000	131.300247
40	59.0530010	117.708382
41	60.1129990	128.712997
42	58.6290020	116.761223
43	60.3289990	130.014969
44	0.0000000	0.000000
45	59.5630000	126.848129
46	59.9080010	126.013634
47	60.8019980	131.799255
48	60.5229990	128.286774
49	59.0320010	119.526398
50	59.6870000	121.669289
51	58.3930020	115.921547
52	0.0000000	-29.345400
53	0.0000000	0.000000
54	58.0770000	114.074371
55	58.4119990	111.907051
56	56.5099980	99.602303
57	58.4080010	114.998528
58	58.6250000	112.577156
59	58.6110000	116.300377
60	58.9240000	115.308586
61	58.4800000	113.103943
62	0.0000000	0.000000
63	0.0000000	0.000000
64	60.1460000	128.004959
65	0.0000000	0.000000
66	59.4620020	123.759453
67	60.0810010	127.493385
68	58.8960000	119.459389
69	0.0000000	0.000000
70	60.6780010	130.957291
71	58.5260010	121.682343
72	59.9360010	126.824844
73	58.9679990	122.527390
74	61.0040020	135.477493
75	60.7519990	131.471848
76	59.5270000	124.539833
77	59.2249980	122.659500
78	58.8989980	119.494896
79	59.6959990	126.097694

Table F-89

Test File:		02-27_1.cal									
		airstream velocity =	660	fpm				total wattage =	506.329		
		airstream temp =	95	'F							
		model rotation =	270	deg (ccw)				Side Int Temp =	127.2	'F	
sensor#	x-value	y-value	temp (F)	k,ss	gen	cond,1	cond,2	cond,b	rad	conv	h
0			0								
1			127.467	26	1.81575	0	-0.01402	0.43757	0.18452	1.17964	1.30695
2			125.701	26	1.81575	0	-0.03254	0.31953	0.17366	1.29001	1.51145
3			124.197	26	1.81575	0.03254	-0.00722	0.21905	0.16449	1.45751	1.79566
4			123.731		1.81575						
5			120.92		1.81575						
6			125.736	26	1.81575	0	-0.10392	0.32188	0.17388	1.21607	1.42319
7			120.934	26	1.81575	0.10392	-0.0052	0.00096	0.14484	1.76866	2.45319
8			126.82	26	1.81575	0.01402	0.00561	0.39428	0.18053	1.26056	1.42503
9			127.079	26	1.81575	-0.00561	0.02005	0.4116	0.18213	1.23646	1.3865
10			123.944	26	1.81575	-0.00175	-0.004	0.20214	0.16296	1.44489	1.79566
11			123.864	26	1.81575	0.00722	0.00175	0.19674	0.16247	1.46551	1.82638
12			120.694	26	1.81575	0.06572	-0.01289	-0.0151	0.1434	1.74028	2.43641
13			120.098	26	1.81575	0.01289	-0.01382	-0.0549	0.13985	1.72985	2.47927
14			125.488								
15			121.16								
16			113.896								
17			117.328								
18			115.496								
19			118.421								
20			115.246								
21			109.358								
22			118.615								
23			117.776								
24			116.977								
25			119.506								
26			115.365								
27			116.546								
28			107.105								
29			115.605								
30			0								
31			116.21								
32			0								
33			115.492	26	1.81575	0	0.02748	-0.14814	0.11278	1.87858	3.29768
34			119.627	26	1.81575	0.06278	-0.03457	0.0088	0.13705	1.69811	2.48037
35			118.029	26	1.81575	0.03457	0	-0.53919	0.12762	2.26188	3.53301
36			128.093	26	1.81575	0.07311	-0.04659	0.13336	0.1884	1.52051	1.65274
37			125.94	26	1.81575	0.04659	0.00159	-0.18529	0.17513	1.87409	2.17882
38			128.635								
39			131.3								
40			117.708								
41			128.713								
42			116.761	26	1.81575	-0.02748	0.28682	-0.0633	0.12018	2.01821	3.33609
43			130.015	26	1.81575	-0.28682	0	0.18812	0.20036	1.14045	1.17159
44			0	0	0	0	0	0			
45			126.848	26	1.81575	0	0	-0.02351	0.18071	1.65855	1.87327
46			126.014	26	1.81575	-0.00159	0.1252	-0.18039	0.17558	1.94418	2.25496
47			131.799	26	1.81575	-0.1252	0	0.30735	0.21158	1.17161	1.14524
48			128.287								
49			119.526								
50			121.669								
51			115.922								
52			-29.3454								
53			0								
54			114.074								
55			111.907								
56			99.6023								
57			114.999								
58			112.577								
59			116.3								
60			115.309								

Table F-89

61		113.104									
62		0									
63		0									
64		128.005	26	1.81575	-0.02005	0	0.4735	0.18785	1.13435	1.2363	
65		0									
66		123.759	26	1.81575	0.004	0.0808	0.18978	0.16184	1.54893	1.93735	
67		127.493	26	1.81575	-0.0808	0	0.43931	0.18469	1.11095	1.22985	
68		119.459	26		0.01382	0	-0.09758	0.13606	1.79108	2.63406	
69		0									
70		130.957	26	1.81575	0	-0.20072	0.25109	0.20627	1.15767	1.15812	
71		121.682	26	1.81575	0.20072	0	0.14618	0.14932	1.72097	2.32008	
72		126.825	26	1.81575	0	-0.093	-0.02507	0.18056	1.56725	1.77145	
73		122.527	26	1.81575	0.093	0	0.20265	0.15439	1.5517	2.02767	
74		135.477	26	1.81575	0	-0.08669	0.55316	0.23502	0.94088	0.83613	
75		131.472	26	1.81575	0.08669	0	0.80038	0.20951	0.89253	0.88028	
76		124.54									
77		122.66									
78		119.495									
79		126.098									

Table F-90

Cover Temperature Map (Test 02-27_1)						
0	128.005	127.0787	126.8196	127.4673	0	
127.4934	123.7595	123.9444	123.8636	124.1974	125.7011	
0	119.4594	120.0981	120.6936	120.934	125.7361	
Ave Surf Temp =	123.86					

Table F-91

Cover Temp Difference Map (Test 02-27_1)						
-95	33.00496	32.07867	31.81958	32.4673	-95	
32.49339	28.75945	28.94444	28.86362	29.19744	30.70107	
-95	24.45939	25.09809	25.69355	25.93397	30.73614	
Ave Temp Diff =	28.86004					

Table F-92

Cover Surf Coeff Map (Test 02-27_1)				
	1.236302	1.3865	1.425029	1.306947
	1.937348	1.795664	1.826385	1.795657
	2.634057	2.479265	2.436414	2.453193
Ave Surf Coeff =	1.89273			

Table F-93

Side Surface Coeff Map (Test 02-27_1)						
1.158115	2.320083	0	3.297676	3.336088	1.171591	
1.771447	2.027672	2.480373	3.533006	0	1.873273	<-- Air
0.836132	0.880283	1.652735	2.178816	2.254955	1.145244	
Left Side						
Ave =	1.877499					
StDev =	0.863042					

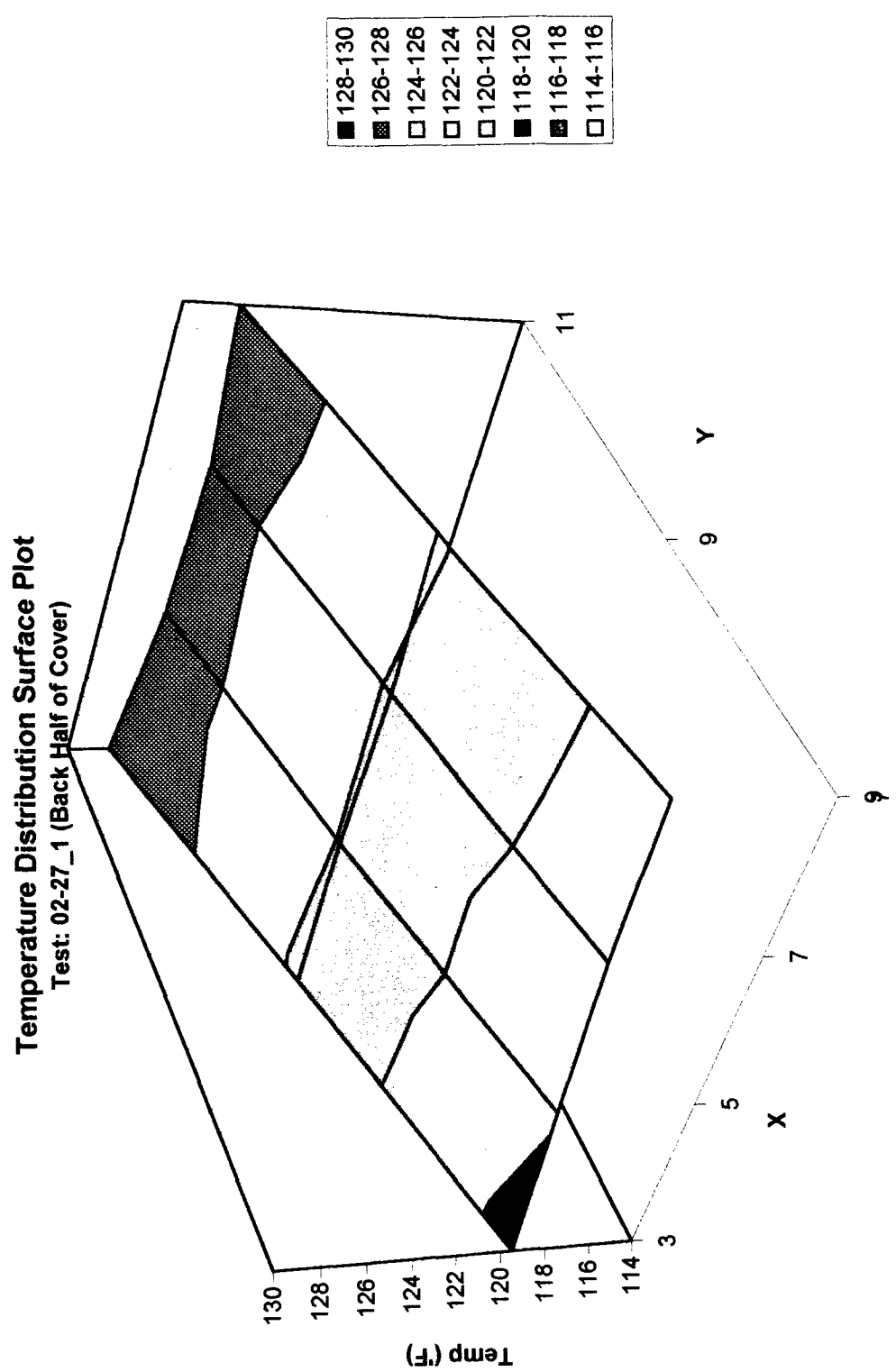
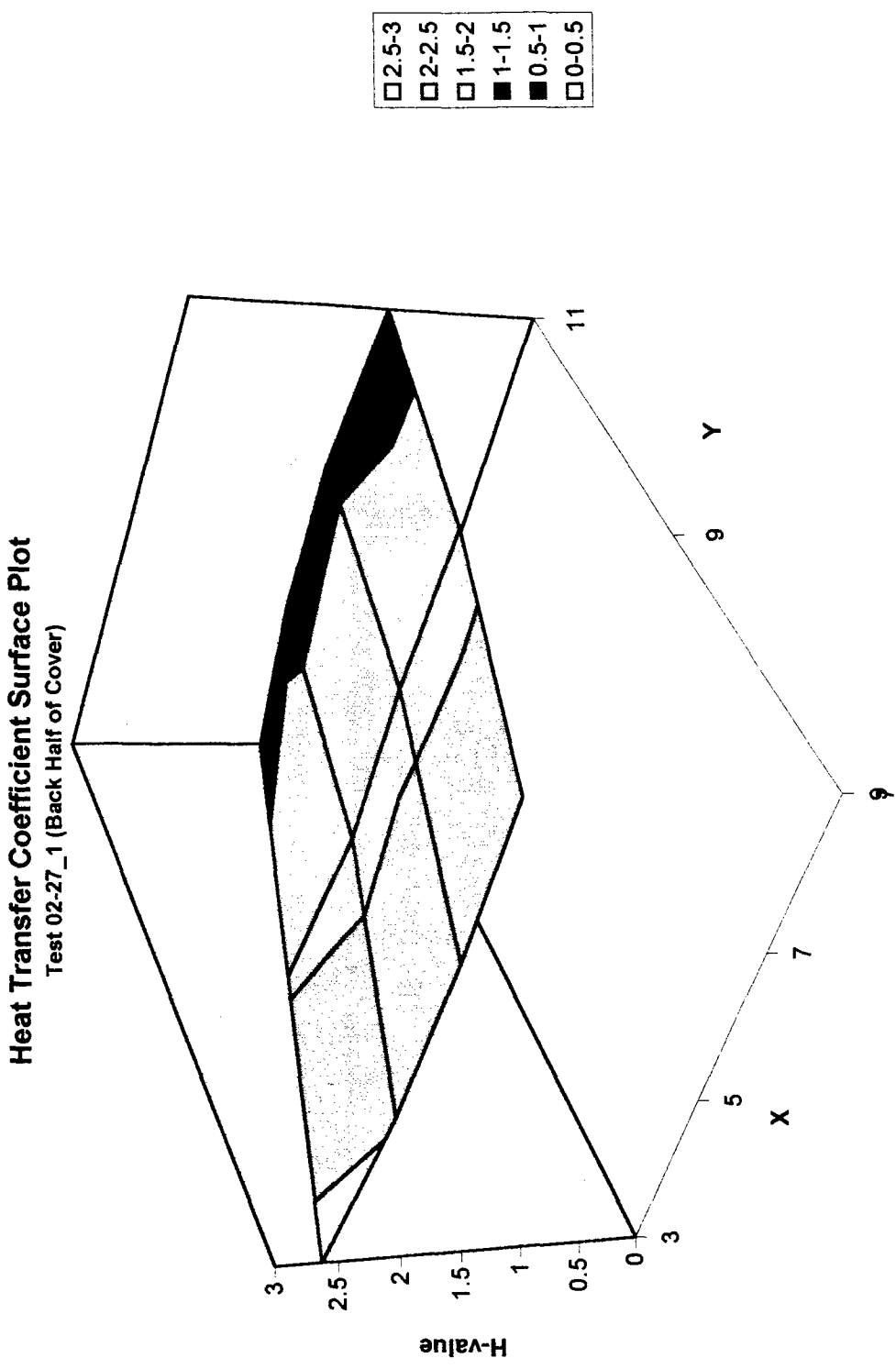


Figure F-31

Figure F-32



XIII(G). Flow Visualization Test Modification:

The overall purpose of flow visualization testing is to create a means by which an invisible flow can be seen or recorded in its naturally occurring state. One frequently used method is outlined in Langston and Boyle (1982). This method consists of spraying wintergreen oil on the surface of a previously ink-dotted test sheet and then starting the flow to be investigated. Portions of the ink dots will dissolve into the oil film, which is being dragged by the viscous forces of the flow directly adjacent to it. The result is the production of an ink trail on the test sheet, indicating the local surface flow direction. If the ink dots are placed in a consistent pattern over the entire surface of the test specimen, the flow visualization test will result in a tangible, two-dimensional representation of the specimens surface flow field.

The purpose of the wintergreen oil in these tests is to dissolve portions of the ink, for directional marking on the test sheet. For this to happen accurately, the oil must interact with the surface flow (via viscous forces) but not change the directional nature of the flow field. The Langston and Boyle method accomplishes this task well for relatively strong, warm temperature flow fields. This type of environment allows the oil to move relatively quickly on the test sheet, and volatilize fast enough to produce a dry test sheet within a reasonable time period. The high speed flows are only minimally effected by the viscous drag difference of the flow-to-oil interface versus the flow-to-surface interface. In this experiment, however, the lower Reynold's number flow fields, particularly the 455 foot per minute freestream flow, are relatively weak, and temperatures are only 25-30 degrees Fahrenheit above room temperature. This scenario, when tested with an un-modified Langston and Boyle's method, results in substantial changes to the surface flow field as a result of the flow-to-oil interface. An illustration of this change can be seen by viewing flow visualization figures G-1 and

Un-Modified Flow Visualization

$N_{Re} = 15030$, Freestream Velocity = 455 FPM

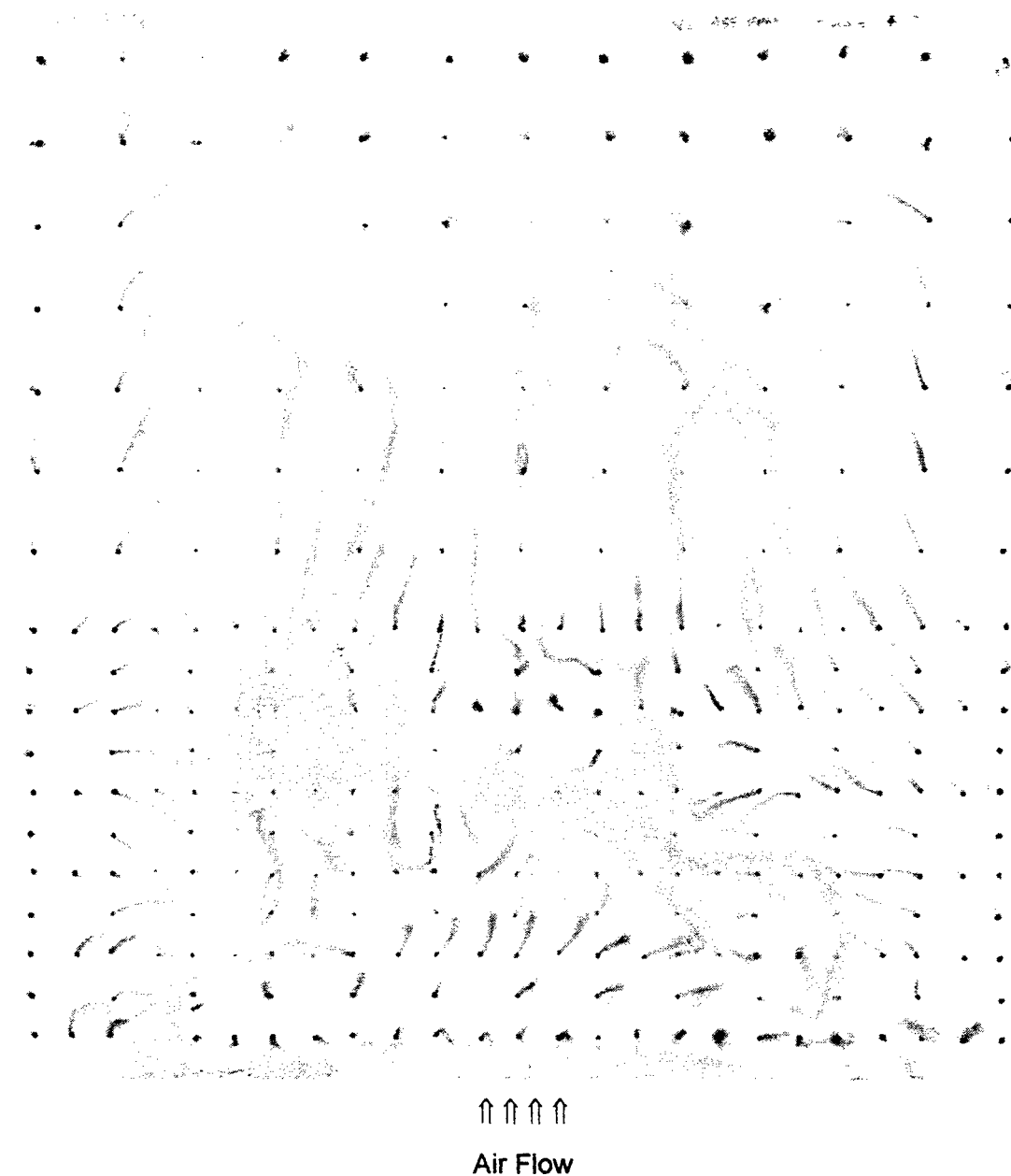
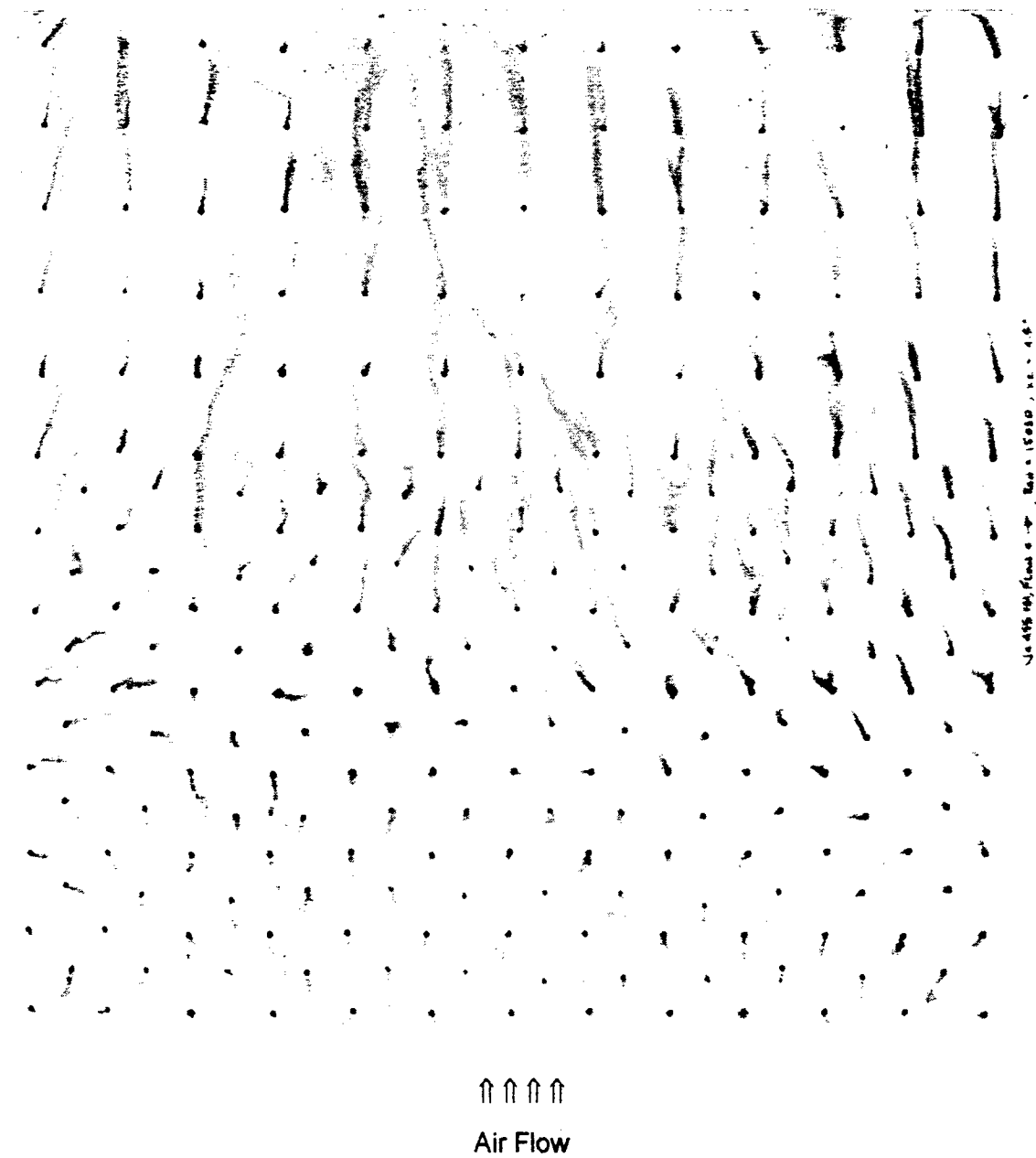


Figure G-1

Modified Flow Visualization

$N_{Re} = 15030$, Freestream Velocity = 455 FPM



↑↑↑↑

Air Flow

Figure G-2

G-2. The differences between the two, which are intended to represent the identical surface flow field, are significant. Figure G-1, the un-modified test, shows a highly inconsistent, almost incomprehensible flow field structure. Numerous areas of recirculation are shown, and there is no evidence of any axial or longitudinal symmetry. On the other hand, Figure G-2, the modified test, shows a highly symmetric, easily distinguishable flow field. The front portion of the sheet shows an inverted U-shaped reattachment line, with corresponding upstream reverse flow velocity vectors. Behind the separation zone, lies an area of relatively weak flow, minimally converging from the sheet edges towards the streamwise centerline.

The difference between the procedures used to conduct the two tests is the thinning of the wintergreen oil with oil-base paint thinner in a one part thinner, to two parts oil, concentration. All other testing procedures are identical. The substantial difference in the results of the two tests is attributed to the fact that the un-thinned oil fails to volatilize quickly enough for the relatively weak surface flow, and therefore pools. The pools of oil are massive enough to cause a disturbance in the surface flow field velocity structure. As the pools move slowly, mostly due now only to the effects of gravity, the surface flow field structure undergoes continuous change. As a final result, the test sheet produced, is more a representation of numerous random, unsteady surface flow fields, than the actual flow field it was intended to represent.

It is speculated that the modification made in this flow visualization testing could be studied in and of itself, to produce a more detailed procedure for adjusting the wintergreen oil and thinner solution to maximize its accuracy as a function of the flow field under investigation.

XIV. Biography of Author:

Scott Edmund LeClair was born in Lewiston [REDACTED]. He received his high school education at Lewiston High School in Lewiston, Maine.

Scott entered the University of Maine at Orono in September 1987, and graduated with distinction in May of 1991 with a Bachelor of Science in Mechanical Engineering. While an undergraduate at the University of Maine, he was a four-year contract cadet with the United States' Air Force Reserve Officer's Training Corps. Upon graduation, he was commissioned as a second lieutenant in the active duty Air Force, and assigned duty as a mechanical design engineer for the 93rd Civil Engineering Squadron, Castle Air Force Base, California.

In August of 1994, Scott was selected for admission into the Air Force Institute of Technology's Civilian Institute Programs, to complete his Master's work in preparation for a new assignment as a professor of mechanical engineering design, at the Air Force Institute of Technology, Wright-Patterson Air Force Base, Ohio.

In September of 1994, Scott was accepted into the Mechanical Engineering graduate program at the University of Maine. He is a candidate for the Master of Science Degree in Mechanical Engineering from the University of Maine, in May, 1996.